ADVERSE REACTIONS TO BIOMATERIALS: STATE OF THE ART IN BIOMATERIAL RISK ASSESSMENT, IMMUNOMODULATION AND *IN VITRO* MODELS FOR BIOMATERIAL TESTING

EDITED BY: Nihal Engin Vrana, Amir M. Ghaemmaghami and Pinar Zorlutuna
PUBLISHED IN: Frontiers in Bioengineering and Biotechnology

frontiers Research Topics

ISSN 1664-8714
ISBN 978-2-88945-822-6
DOI 10.3389/978-2-88945-822-6

About Frontiers

Frontiers is more than just an open-access publisher of scholarly articles: it is a pioneering approach to the world of academia, radically improving the way scholarly research is managed. The grand vision of Frontiers is a world where all people have an equal opportunity to seek, share and generate knowledge. Frontiers provides immediate and permanent online open access to all its publications, but this alone is not enough to realize our grand goals.

Frontiers Journal Series

The Frontiers Journal Series is a multi-tier and interdisciplinary set of open-access, online journals, promising a paradigm shift from the current review, selection and dissemination processes in academic publishing. All Frontiers journals are driven by researchers for researchers; therefore, they constitute a service to the scholarly community. At the same time, the Frontiers Journal Series operates on a revolutionary invention, the tiered publishing system, initially addressing specific communities of scholars, and gradually climbing up to broader public understanding, thus serving the interests of the lay society, too.

Dedication to Quality

Each Frontiers article is a landmark of the highest quality, thanks to genuinely collaborative interactions between authors and review editors, who include some of the world's best academicians. Research must be certified by peers before entering a stream of knowledge that may eventually reach the public - and shape society; therefore, Frontiers only applies the most rigorous and unbiased reviews.
Frontiers revolutionizes research publishing by freely delivering the most outstanding research, evaluated with no bias from both the academic and social point of view. By applying the most advanced information technologies, Frontiers is catapulting scholarly publishing into a new generation.

What are Frontiers Research Topics?

Frontiers Research Topics are very popular trademarks of the Frontiers Journals Series: they are collections of at least ten articles, all centered on a particular subject. With their unique mix of varied contributions from Original Research to Review Articles, Frontiers Research Topics unify the most influential researchers, the latest key findings and historical advances in a hot research area! Find out more on how to host your own Frontiers Research Topic or contribute to one as an author by contacting the Frontiers Editorial Office: researchtopics@frontiersin.org

ADVERSE REACTIONS TO BIOMATERIALS: STATE OF THE ART IN BIOMATERIAL RISK ASSESSMENT, IMMUNOMODULATION AND *IN VITRO* MODELS FOR BIOMATERIAL TESTING

Topic Editors:
Nihal Engin Vrana, Protip Medical, France
Amir M. Ghaemmaghami, University of Nottingham, United Kingdom
Pinar Zorlutuna, University of Notre Dame, United States

Nanoparticles and Nanocarries: The shape, surface chemistry and structure of nanobiomaterials will determine how the immune system will react to them.

Image: GiroScience/Shutterstock.com.

Adverse immune reactions to biomaterials are important bottlenecks for translation of novel biomaterials for clinical use. Moreover, recent advances in high throughput biomaterial discovery and synthetic biology, while providing exciting new venues, also significantly increases potential risks related to the *in vivo* reactions to these new materials. For example, the novel materials might have unintended biological activities due to their natural building blocks.

In this perspective, biomaterial field needs i) better understanding of cell/biomaterial interactions at systems level; ii) development of new analysis and testing tools for advanced risk assessment iii) tools and technologies for modulating reactions to biomaterials and iv) advanced *in vitro* models for understanding and testing of reactions to biomaterials.

In the following collection of articles you will find examples of such systems,together with comprehensive reviews of current developments in *in vitro* model systems. The collection also contains articles that elucidate the immune reaction to biomaterials *in vitro* and *in vitro*.

Citation: Vrana, N. E., Ghaemmaghami, A. M., Zorlutuna, P., eds. (2019). Adverse Reactions to Biomaterials: State of the Art in Biomaterial Risk Assessment, Immunomodulation and *In Vitro* Models for Biomaterial Testing. Lausanne: Frontiers Media.
doi: 10.3389/978-2-88945-822-6

Table of Contents

SECTION 3
SIMULATION AND BIOMATERIAL TESTING

frontiers in Bioengineering and Biotechnology

EDITORIAL
published: 11 February 2019
doi: 10.3389/fbioe.2019.00015

Editorial: Adverse Reactions to Biomaterials: State of the Art in Biomaterial Risk Assessment, Immunomodulation and *in vitro* Models for Biomaterial Testing

Nihal Engin Vrana[1,2*], *Amir M. Ghaemmaghami*[3] and *Pinar Zorlutuna*[4,5]

[1] Protip Medical, Strasbourg, France, [2] Faculté de Chirurgie Dentaire, Université de Strasbourg, Fédération de Médecine Translationnelle de Strasbourg, Fédération de Recherche Matériaux et Nanosciences Grand Est, Strasbourg, France, [3] Immunology and Immuno-Bioengineering Group, Faculty of Medicine and Health Sciences, School of Life Science, University of Nottingham, Nottingham, United Kingdom, [4] Bioengineering Graduate Program, University of Notre Dame, Notre Dame, IN, United States, [5] Department of Aerospace and Mechanical Engineering, University of Notre Dame, Notre Dame, IN, United States

Keywords: biomaterials, immunomodulation, *in vitro* models, risk assessment, adverse reactions

Editorial on the Research Topic

Adverse Reactions to Biomaterials: State of the Art in Biomaterial Risk Assessment, Immunomodulation and *in vitro* Models for Biomaterial Testing

OPEN ACCESS

Edited and reviewed by:
Hasan Uludag,
University of Alberta, Canada

***Correspondence:**
Nihal Engin Vrana
e.vrana@protipmedical.com

Specialty section:
This article was submitted to Biomaterials, a section of the journal Frontiers in Bioengineering and Biotechnology

Received: *27 December 2018*
Accepted: *21 January 2019*
Published: *11 February 2019*

Citation:
Vrana NE, Ghaemmaghami AM and Zorlutuna P (2019) Editorial: Adverse Reactions to Biomaterials: State of the Art in Biomaterial Risk Assessment, Immunomodulation and in vitro Models for Biomaterial Testing. Front. Bioeng. Biotechnol. 7:15. doi: 10.3389/fbioe.2019.00015

The recent advances in polymer chemistry (an ever increasing number of new polymers or derivatives of existing polymers with new properties) (Liu et al., 2018), materials science (metamaterials specifically designed for a given application, hybrid materials and highly controlled composite structures at nano/micro levels, materiomics) (Kowalski et al., 2018), biotechnology (new gene editing technologies for facilitating natural biomaterial production, accelerated rate of discovery, and isolation of functional natural biomaterials) (Sakar and Baker, 2018) and manufacturing techniques (3D printing, bioprinting, controlled self-assembly methods) (Nagarajan et al., 2018) have provided a significant boost in our capabilities to offer new solutions for debilitating chronic diseases in the form of implantable devices and regenerative medicine products. However, this rapid expansion in the biomaterials toolkit unfortunately comes at a cost; a considerable increased risk of adverse reactions to implanted biomaterials which includes allergies, chronic inflammation, susceptibility to infection, collateral tissue damage, and loss of functionality due to immune reactions. Moreover, the highly personalized nature of immune reactions needs to be taken into account while assessing the use of new biomaterials. These concerns have created a general reticence in the medical device industry for the utilization of novel biomaterials and complex, multi-material structures which significantly hinders the advances in the field and also decelerates the introduction of new and potentially transformative technologies to the healthcare system.

The potential ways out of this conundrum are (i) to improve our capacities in the risk assessment of biomaterials by developing novel *in vitro* testing systems which can provide more relevant and in-depth information about cell/tissue/organ-biomaterial interactions, preferably in a personalized manner (i.e., using patients' own cells); (ii) to develop new technologies to control the interface between the implanted materials and the host tissues where immune reactions can be either attenuated or directed toward expected outcomes (immunomodulation and integration)

(iii) to achieve systems level understanding of personalized response to biomaterials using the recent advances in high throughput analysis methods available (immunoprofiling).

Being actively involved in the development of such technologies (Ellis et al., 2017; Rostam et al., 2017; Kubon et al., 2018), our motivation for this research topic was to bring together a group of high quality articles that provide insights on responses to biomaterials, immunomodulation and *in vitro* model systems. The review articles in the topic cover: skin substitutes with immunomodulatory components and skin models with their use in biomaterial assessment (Savoji et al.), haemocompatibility of biomaterials and the analyses of interactions of biomaterials with human blood (Weber et al.), liver- and lung-on-a-chip systems for biomaterial testing and related *in silico* models (Nikolic et al.), and an overview of production and development of a medical grade biomaterial and its derivatives using Hyaluronic acid as an example (Huerta-Ángeles et al). The original research articles in the research topic covered different aspects of immune reaction and immunomodulation such as: the effect of photocrosslinked Gelatin hydrogels on Tumor Necrosis Factor Alpha (TNF-α) secretion by primary human mononuclear cells and underlying mechanisms (Donaldson et al.), the incorporation of macrophages for immune assisted tissue engineering within hydrogel structures in co-culture and tri-culture configurations (Barthes et al.), the multinucleated giant cell induction by collagen based membranes *in vivo* and its potential ramifications (Al-Maawi et al). The upcoming, materiomics-based biomaterial selection methodologies were represented by the detection of distinct biomaterial topographies that can be used for Fibroblastic Reticular Cell differentiation by TopoChip system (Vasilevich et al.), whereas utilization of an advanced biomechanical testing system that can mimic natural loading conditions in the articular cartilage was used to demonstrate the potential ways to optimize polymeric composite scaffold mechanical properties for better integration (Gasik et al). Finally, as an example of a potential parameter to compare biomaterial properties and evaluate coatings for decision-making purposes, a methodology based on zeta potential measurements was presented (Ferraris et al.).

The key to better harness the innovations in biomaterial and biomedical device fields is to establish the necessary methodologies and model systems for their risk assessment, validation, and testing. Recent success and ongoing efforts in developing technologies for immune engineering, personalized biomaterials and personalized *in vitro* testing platforms will bring forth the solutions that can improve the quality of life and life expectancy even further in twenty-first century.

AUTHOR CONTRIBUTIONS

NV, AG, and PZ equally contributed to the preparation of the manuscript. The submitted version is revised and confirmed by all authors.

FUNDING

This project has received funding from the European Union's Horizon 2020 research and innovation programme under grant agreement No 760921 (PANBioRA). NSF award nos. 1611083 and 1651385, and NIH award no. 1 R01 HL141909-01A1.

REFERENCES

Ellis, B. W., Acun, A., Can, U. I., and Zorlutuna, P. (2017). Human iPSC-derived myocardium-on-chip with capillary-like flow for personalized medicine. *Biomicrofluidics* 11:024105. doi: 10.1063/1.4978468

Kowalski, P. S., Bhattacharya, C., Afewerki, S., and Langer, R. (2018). Smart biomaterials: recent advances and future directions. *ACS Biomater. Sci. Eng.* 4, 3809–3817. doi: 10.1021/acsbiomaterials.8b00889

Kubon, M., Hartmann, H., Moschallski, M., Burkhardt, C., Link, G., Werner, S., et al. (2018). Multimodal chemosensor-based, real-time biomaterial/cell interface monitoring. *Adv. Biosyst.* 2:1700236. doi: 10.1002/adbi.201700236

Liu, Z., Tang, M., Zhao, J., Chai, R., and Kang, J. (2018). Looking into the future: toward advanced 3D biomaterials for stem-cell-based regenerative medicine. *Adv. Mater.* 30:1705388. doi: 10.1002/adma.201705388

Nagarajan, N., Dupret-Bories, A., Karabulut, E., Zorlutuna, P., and Vrana, N. E. (2018). Enabling personalized implant and controllable biosystem development through 3D printing. *Biotechnol. Adv.* 36, 521–533. doi: 10.1016/j.biotechadv.2018.02.004

Rostam, H. M., Reynolds, P. M., Alexander, M. R., Gadegaard, N., and Ghaemmaghami, A. M. (2017). Image based machine learning for identification of macrophage subsets. *Sci. Rep.* 7:3521. doi: 10.1038/s41598-017-03780-z

Sakar, M. S., and Baker, B. M. (2018). Engineering control over 3D morphogenesis by tissue origami. *Dev. Cell* 44, 131–132. doi: 10.1016/j.devcel.2018.01.005

Conflict of Interest Statement: The authors declare that the research was conducted in the absence of any commercial or financial relationships that could be construed as a potential conflict of interest.

frontiers in Bioengineering and Biotechnology

REVIEW
published: 16 July 2018
doi: 10.3389/fbioe.2018.00099

Blood-Contacting Biomaterials: *In Vitro* Evaluation of the Hemocompatibility

*Marbod Weber, Heidrun Steinle, Sonia Golombek, Ludmilla Hann, Christian Schlensak, Hans P. Wendel and Meltem Avci-Adali**

Department of Thoracic and Cardiovascular Surgery, University Hospital Tübingen, Tübingen, Germany

Hemocompatibility of blood-contacting biomaterials is one of the most important criteria for their successful *in vivo* applicability. Thus, extensive *in vitro* analyses according to ISO 10993-4 are required prior to clinical applications. In this review, we summarize essential aspects regarding the evaluation of the hemocompatibility of biomaterials and the required *in vitro* analyses for determining the blood compatibility. Static, agitated, or shear flow models are used to perform hemocompatibility studies. Before and after the incubation of the test material with fresh human blood, hemolysis, cell counts, and the activation of platelets, leukocytes, coagulation and complement system are analyzed. Furthermore, the surface of biomaterials are evaluated concerning attachment of blood cells, adsorption of proteins, and generation of thrombus and fibrin networks.

Keywords: hemocompatibility, blood contact, biomaterials, coagulation, complement system

OPEN ACCESS

Edited by:
Nihal Engin Vrana,
Protip Medical, France

Reviewed by:
Giovann Vozzi,
Università degli Studi di Pisa, Italy
Elif Vardar,
Centre Hospitalier Universitaire Vaudois (CHUV), Switzerland

****Correspondence:***
Meltem Avci-Adali
meltem.avci-adali@uni-tuebingen.de

Specialty section:
This article was submitted to Biomaterials, a section of the journal Frontiers in Bioengineering and Biotechnology

Received: *12 May 2018*
Accepted: *26 June 2018*
Published: *16 July 2018*

Citation:
Weber M, Steinle H, Golombek S, Hann L, Schlensak C, Wendel HP and Avci-Adali M (2018) Blood-Contacting Biomaterials: In Vitro Evaluation of the Hemocompatibility. Front. Bioeng. Biotechnol. 6:99. doi: 10.3389/fbioe.2018.00099

INTRODUCTION

Hemocompatibility is one of the major criteria, which limit the clinical applicability of blood-contacting biomaterials. These materials come in close contact with blood, which is a complex "organ," comprising of 55% plasma, 44% erythrocytes, and 1% leukocytes and platelets. Thus, adverse interactions between newly developed materials and blood should be extensively analyzed to prevent activation and destruction of blood components. The initially adsorbed protein layer on the biomaterial surface mainly triggers the adverse reactions, such as the activation of coagulation via intrinsic pathway, the activation of leukocytes, which results in inflammation, and the adhesion and activation of platelets (Liu et al., 2014). As a result, the number of blood cells can decrease and a thrombus can be formed.

Thus, the applied blood-contacting biomaterials should not adversely interact with any blood components and activate or destruct blood components. Erythrocytes are the most abundant blood cells with 4–6 $\times$ 10^6 cells/μl and they are important for the transport of oxygen (O_2) from the lung to all tissues and cells and carbon dioxide (CO_2) from tissues back to the lung. Since erythrocytes are the most rigid cells in the blood, they are sensitive to rupture and hemolysis due to shear stress and changes in osmotic pressure. Blood platelets are the smallest (1–3 μm) and the second abundant cell type in the blood with 1.5–3.5 $\times$ 10^5 cells/μl, which can rapidly recognize foreign surfaces and initiate blood coagulation. Furthermore, human blood contains 4.3–10 $\times$ 10^3 leukocytes/μl, such as granulocytes, lymphocytes, monocytes, dendritic and natural killer cells. Monocytes account for 1–6% of all leukocytes and neutrophil granulocytes are the most abundant leukocytes in the blood, comprising 50–70% of all leukocytes. These immune cells are belonging to the innate immune system and they can be rapidly activated upon recognition of

a foreign invader such as a pathogen or a foreign material. Furthermore, blood plasma contains high amounts of plasma proteins, such as albumin, coagulation factors, and immunoglobulins.

Catheters, guidewires, dialyzer, oxygenators (artificial lungs), heart-supporting systems, cardiac pacemaker, vascular grafts, stents, heart valves, micro-, and nanoparticles are widely used medical devices and materials coming in direct contact with blood. Prior to clinical application, the hemocompatibility of blood-contacting medical materials have to be analyzed and therefore, a guidance is developed by the International Organization for Standardization (ISO 10993-4) (International Organization for Standardization, 2000). According this guideline, five different categories, thrombosis, coagulation, platelets, hematology, and immunology (complement system and leukocytes), are indicated for hemocompatibility evaluation. The devices are divided into three categories concerning blood contact: (1) Externally communicating devices with indirect blood contact, e.g., cannulas and blood collection sets; (2) Externally communicating devices with direct blood contact, e.g., catheters and hemodialysis equipment; (3) Implant devices, e.g., heart valves, stents, and vascular grafts. So far, several studies were performed according ISO-10993-4 to evaluate various blood contacting devices and materials, such as stents (Sinn et al., 2011; Stang et al., 2014), catheters with a noble metal alloy coating (Vafa Homann et al., 2016), poly(2-dimethylamino-ethylmethacrylate) (PDMAEMA) (Cerda-Cristerna et al., 2011), and DNA hydrogels (Stoll et al., 2017). To perform hemocompatibility analysis, static, agitated, or shear flow *in vitro* models are used for the incubation of blood with the biomaterial. Before and after the incubation of biomaterials with fresh human blood, the activation markers regarding hemocompatibility are analyzed (**Figure 1**).

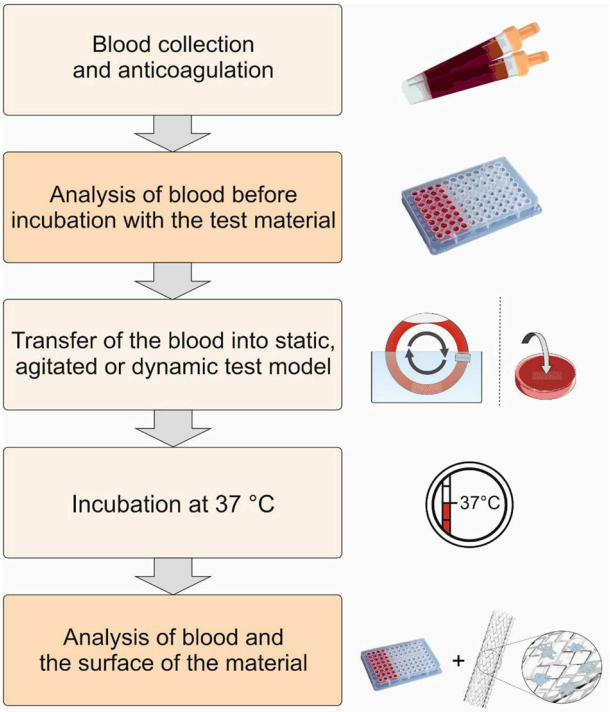

FIGURE 1 | Schematic representation of the procedure for the evaluation of the hemocompatibility of biomaterials. First, fresh human blood is collected and anticoagulated with low dose heparin. Thereafter, the test material is incubated at 37°C using static, agitated, or dynamic test models with the blood. The activation markers in the blood are analyzed before and after the incubation with the test material. Furthermore, the surface of the biomaterial is analyzed to determine the interaction of blood cells and proteins with the biomaterial surface.

INCUBATION OF BIOMATERIALS WITH HUMAN BLOOD

Using fresh human blood and adequate *in vitro* models, the hemocompatibility of blood-contacting biomaterials can be studied accurately. Compared to *in vivo* animal models, *in vitro* models allow the analysis under well controllable conditions such as blood flow, anticoagulation and eliminate disturbing factors related to flow obstruction, surgery, and tissue effects (van Oeveren, 2013). Furthermore, the blood contact is more intense and products generated due to reaction of the blood components to the biomaterial are not cleared. Moreover, using *in vitro* models, different devices can be analyzed under the same conditions, which enable the direct comparison of outcomes. Thereby, positive controls, which show a poor hemocompatibility, such as glass (Ferrer et al., 2013), devices or biomaterials, which are already on the market with a comparable surface area, and negative controls without test material should be simultaneously tested to be able to evaluate the hemocompatibility.

The quality of collected blood is extremely important to enable standardized hemocompatibility analysis. The *in vitro* analysis should be performed with fresh blood from healthy subjects (Blok et al., 2016). Blok et al. demonstrated that the stationary storage of blood over 4 h at room temperature affects the platelet function and activity of leukocytes. Thus, experiments should be started within 4 h after the blood collection. However, the faster the experiments are started, the better it is. Peripheral blood should be collected from healthy non-smoker, non-pregnant subjects free of medication (particularly drugs affecting the hemostasis, such as aspirin, oral contraceptives, and nonsteroidal anti-inflammatory drugs). Moreover, atraumatic blood collection by minimizing venostasis during blood withdrawal and the use of 21-gauge needles is required to minimize activation of platelets and the coagulation cascade during collection (Braune et al., 2013).

Furthermore, prior to starting hemocompatibility analyses, unreacted monomers, intermediate- or by-products, solvents, and unwanted chemical residues should be removed by appropriate washing and cleaning procedures from generated biomaterials to eliminate an unwanted influence on blood components. Depending on biomaterial, device, and production technique, different washing and cleaning procedures with different solutions are required, for example ethanol can be removed by evaporation or washing with PBS (Punet et al.,

2015), NaCl, or water and unreacted methacrylic anhydride and by-products can be eliminated by dialysis (Xiao et al., 2011; Camci-Unal et al., 2013). Additionally, endotoxin content should be determined to exclude material-unrelated activation of platelets and blood cells due to presence of endotoxins (Watanabe et al., 2003; Kälsch et al., 2007; Schrottmaier et al., 2016). Furthermore, a process called depyrogenation can be applied to remove endotoxins from biomaterials (Li and Boraschi, 2016). For example by using detergents (e.g., Triton X-114) and a two-phase extraction method, endotoxins can be eliminated (Zhang et al., 2015). After the addition of the detergent to the sample, endotoxins are incorporated into micelles via non-polar interactions of the surfactant end groups and alkyl chains of lipid A, which is the most conserved part of endotoxins (Magalhães et al., 2007). The increase of temperature leads to the formation of a water phase (micelle-poor) and a micelle-rich phase. Thereby, endotoxins remained in the micelle-rich phase (bottom-phase) can be removed.

Static Blood Incubation Models

In static blood incubation models, test materials are incubated with blood or platelet-rich plasma (PRP) without flow conditions (Mohan et al., 2013). Therefore, container, such as well plates or tubes, can be used to incubate the material with a certain blood or PRP volume. It is a very simple and rapid method to determine the hemocompatibility of biomaterials, especially the thrombogenicity. However, this method provides only rudimentary results regarding hemocompatibility. Thereby, major limitations can be the cell sedimentation and the big blood-air interface, which can lead to a protein aggregation and result in platelet activation (Haycox and Ratner, 1993).

Agitated Blood Incubation Models

In agitated blood incubation models, flat incubation chambers with top and bottom surfaces made of the test material are completely filled with blood and incubated on a shaker or overhead rotator without directed flow (Streller et al., 2003). Furthermore, the container filled with the blood can be rotated to prevent the sedimentation of the test material, such as nanoparticles (Maitz et al., 2017). Using these models, the blood-air contact is almost excluded and cell sedimentation is reduced.

Shear Flow Models

Flat-plate flow chambers (Van Kruchten et al., 2012), parallel-plate and cone-platelet viscometer (Lackner et al., 2012), and tubular systems such as the "Chandler loop" (McClung et al., 2007; Krajewski et al., 2013; Stang et al., 2014) and the roller pump closed-loop (Podias et al., 1995; Wang et al., 2001) systems are some of *in vitro* shear flow models. In these models, vascular blood flow is mimicked to simulate the dynamic interaction between the biomaterial and whole blood (Sanak and Wegrzyn, 2010). In flat-plate flow chambers, blood flows over a flat piece of biomaterial and in parallel-plate viscometers, blood is filled between two plates made of the biomaterial to be tested and one of the plates is rotated relative to the other (Sukavaneshvar, 2017). In Chandler loop, a circular conduit made of the biomaterial or coated with the biomaterial, is filled with fresh human blood with air bubble to allow the blood mixture and rotated in a water bath with 37°C to stimulate blood circulation. In modified versions of the Chandler loop, small materials, such as stents are inserted in tubings and then filled with blood (Müller et al., 2012). Since the Chandler loop is partially filled with air, the device circulates through an air-liquid interface. Thus, this method can lead to the denaturation of proteins at the air-liquid interface (Thorsen et al., 1993; Ritz-Timme et al., 1997) and the detachment of adhered blood cells. Therefore, roller pump closed-loop test systems were also used instead of Chandler loop. Hereby, the blood flow is realized by using a pump. However, due to use of a pump even with lowest pumping rates a slight destruction of erythrocytes (hemolysis) can occur. Van Oeveren and colleagues analyzed additionally to the Chandler loop and roller pump model, the Hemobile model (Van Oeveren et al., 2012) regarding intrinsic damage of blood components and activation of platelets. Hemobile model has a one-way ball valve to ensure unidirectional flow and the tubing contains no air, and there is no mechanical device compressing the tubing. Thus, using this model, less blood trauma was induced compared to Chandler-Loop and roller pump model.

However, the main limitation of these *in vitro* models is the lack of an endothelium in the circulating system. The endothelium produces cytokines, anti-thrombotic components and expresses adhesion molecules for thrombocytes, monocytes, and neutrophils and plays an important role in interaction between the circulating blood and injured vessel wall. Therefore, in a recent study, Nordling et al. used a novel blood endothelial cell chamber model to study the interactions between human whole blood and endothelium (Nordling et al., 2014). There, the blood contacting surface of incubation chambers were seeded with human umbilical vein endothelial cells (HUVECs). Furthermore, a relatively new field for the examination of platelet and coagulation activation is the use of microfluidics (Kent et al., 2010; Onasoga-Jarvis et al., 2013, 2014; Kovach et al., 2014; Zhu et al., 2015; Nagy et al., 2017). Using microfluidic flow devices platelet and coagulation activation can be determined at the same time and under defined, physiological or pathological (stenotic) wall shear rates. Due to the small size of microfluidic devices, only small amounts of blood are required. Furthermore, the combination with fluorescence microscopy allows the real-time optical imaging of platelet adhesion and formation of fibrin fibers (Westein et al., 2012; Zhu et al., 2015).

ANALYSIS OF HEMOCOMPATIBILITY

Using the described *in vitro* models, various information regarding hemocompatibility (**Figure 2**) can be obtained: (1) Changes of platelets, erythrocytes and leukocytes, (2) Generation of activation products in plasma, (3) Deposition of proteins and cells on the material surface. Thus, blood and surface of biomaterials are analyzed before and after the incubation. In **Table 1**, test categories for the hemocompatibility analysis of biomaterials are summarized and in the following, the required analyses for the evaluation of hemocompatibility are described.

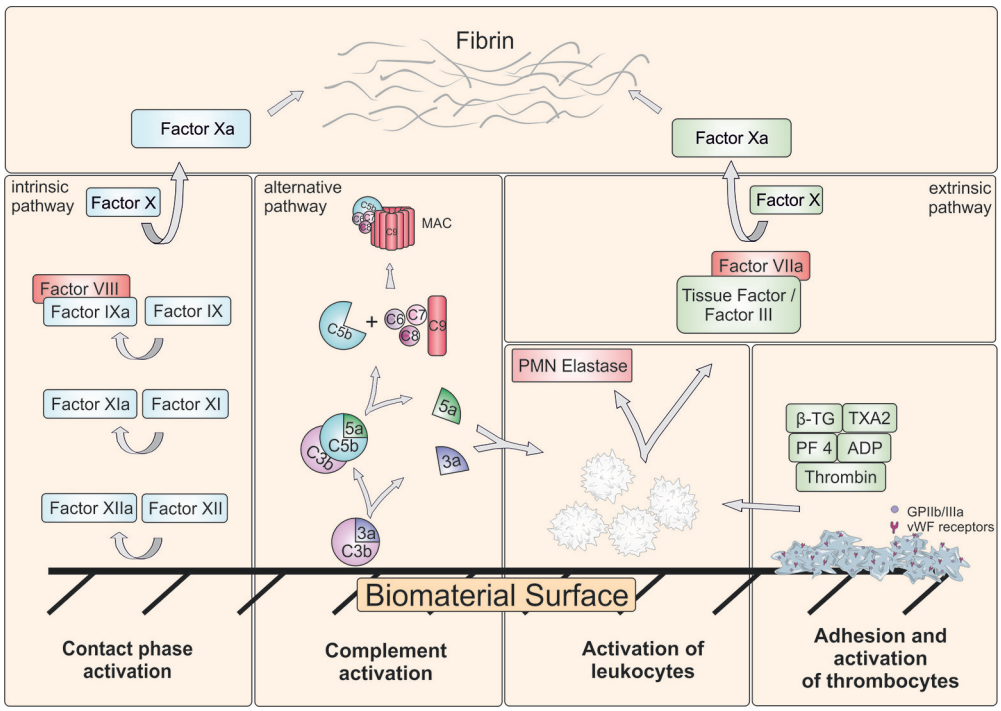

FIGURE 2 | Schematic representation of major reactions in blood induced by biomaterial surface**.** Besides complement system, intrinsic and extrinsic coagulation pathway can be activated. Coagulation activation results in generation of a fibrin network. Furthermore, platelets can adhere and aggregate on the surface. The adhesion and activation of leukocytes can lead to the release of polymorphonuclear (PMN) elastase and tissue factor (TF) and result in activation of extrinsic pathway. ADP, Adenosine diphosphate; β-TG, β-Thromboglobulin; GPIIb/IIIa, Glycoprotein IIb/IIIa; MAC, Membrane attack complex; PF4, Platelet factor 4; TXA2, Thromboxane A2; vWF, von Willebrand factor.

DETERMINATION OF BLOOD CELL NUMBERS AND HEMOLYSIS

The number of erythrocytes, leukocytes, and platelets is measured before and after the incubation of blood with biomaterial using a hematology analyzer, which uses electrical impedance. A decrease of the platelet count over time indicates a thrombogenic material. Furthermore, the rupture of erythrocytes, called hemolysis, is accompanied by the release of hemoglobin. Thus, an increased concentration of free hemoglobin in the plasma is a direct indicator of erythrocytes destruction. The damage of erythrocytes can lead to the reduced oxygen transport to tissues and organs *in vivo* and increased levels of free hemoglobin can induce toxicity or alter the kidney function (Qian et al., 2010). Additionally, microvesicles derived from erythrocytes can promote the thrombus formation in a tissue factor (TF)-dependent manner (Biró et al., 2003). Thus, hemolysis can be analyzed after direct or indirect blood contact. In direct analysis, blood is incubated with the biomaterial and in indirect testing blood is incubated with biomaterial extract (Kuhbier et al., 2017). Hemolysis can be detected by using a photometric colorimetric test (cyanmethemoglobin method) (Stadie, 1920). Thereby, the free amount of hemoglobin in plasma is examined after the addition of cyanmethemoglobin (CMH) reagent, e.g., Drabkin's reagent, which rapidly converts hemoglobin to the cyanoderivate (Neun and Dobrovolskaia, 2011). The absorption of CMH is measured at 540 nm using a photometer. Depending on hemolysis, materials can be classified in three different categories: Materials resulting in over 5% hemolysis are classified hemolytic, between 5 and 2% as slightly hemolytic, and below 2% as nonhemolytic (Totea et al., 2014).

COAGULATION ACTIVATION

The interaction of plasma proteins with artificial surfaces triggers intrinsic coagulation pathway by contact activation. The contact-phase system consists of three serine proteinases, factor XII, factor XI, and plasma prekallikrein (PK), and the nonenzymatic cofactor high molecular weight kininogen (HMWK) and it is also called as plasma kallikrein-kinin system (Wu, 2015). The contact of blood with artificial, negatively charged surfaces, such as kaolin, glass, collagen, silica, or dextran sulfate, leads to the conversion of Factor XII to the active enzyme Factor XIIa. Factor XIIa converts PK into active kallikrein and HMWK into bradykinin. Besides coagulation, kallikrein and bradykinin promote inflammation (Long et al., 2016). Kallikrein can directly activate neutrophils (Wachtfogel et al., 1995) and bradykinin can stimulate the release of nitric oxide (Bae et al., 2003), TNFα, and IL-1 (Tiffany and Burch, 1989). Factor XIIa activates Factor XI to XIa and in the following step, Factor IX is converted by Factor

TABLE 1 | Summary of test categories for the hemocompatibility analysis of biomaterials.

Test category	Parameter	Test principle
Complement System	C3a, C5a, Bb, C4d, C5b-9	ELISA
Coagulation	Factor XIIa, TAT, F1 + 2, free active thrombin, FPA, aPTT	ELISA, Optical density, Viscoelasticity
Fibrinolysis	D-Dimers	Immunoturbidimetry, LPIA, ELISA
Platelets	β-TG, PF4, number of platelets,	ELISA, Cell Counter,
	P-selectin, activated GPIIb/IIIa	FACS
Hemolysis	Number of erythrocytes,	Cell Counter
	Hemoglobin	Colorimetric Assay
Leukocyte Activation	PMN elastase, ROS detection, CD11b expression	ELISA, fluorimetric or spectrophotometric methods, FACS
Surface Analysis	Platelet adhesion, aggregation, leukocyte adhesion	SEM, Fluorescence microscopy
	Plasma protein adsorption	ELISA, Western Blot

aPTT, activated partial thromboplastin time; β-TG, β-Thromboglobulin; C3a, Complement factor 3a; C5a, Complement factor 5a; C4d, Complement factor 4d; Bb, complement factor Bb; ELISA, Enzyme-linked Immunosorbent Assay; FACS, Fluorescence-activated cell sorting; FPA, fibrinopeptide A; F1+2, Prothrombin fragment 1+2; LPIA, Latex photometric immunoassay; PF4, Platelet factor 4; TAT, thrombin-antithrombin III complex; PMN elastase, Polymorphonuclear elastase; ROS, Reactive oxygen species; SEM, Scanning electron microscopy.

XIa to IXa, which then activates factor X. The conversion of factor X into factor Xa is the first common step in the coagulation cascade between the intrinsic and extrinsic pathways (Millar et al., 2016). In addition, the activation of complement system can lead to the generation of TF by monocytes, which can result in activation of extrinsic pathway (Kappelmayer et al., 1993). Factor Xa converts prothrombin to thrombin, which hydrolyses fibrinogen into fibrin and leads to the subsequent clot formation.

The activation of coagulation system is screened by detection of FXIIa (Basu et al., 2017), prothrombin fragment 1 + 2 (F1 + 2) (Maitz et al., 2017; Sperling et al., 2017), which is released during thrombin formation, free active thrombin (Müller et al., 2011), fibrinopeptide A (FPA) (Peckham et al., 1997), partial thromboplastin time (PTT), or thrombin-antithrombin III complex (TAT). Furthermore, the degradation product of fibrin, D-dimer, can be detected by ELISA to determine the activation of fibrinolysis (Sperling et al., 2017). Antithrombin III inhibits thrombin by forming a TAT complex. Thus, this complex reflects a functional state of the coagulation system and can be quantified using ELISA. PTT assay measures the clotting time from the activation of Factor XII to the formation of a stable fibrin clot. To detect PTT, citrated platelet-poor plasma is incubated at 37°C with the test material for 15, 30, or 60 min. The addition of PTT reagent (cephalin) followed by the addition of calcium chloride solution inactivates the anticoagulant and initiates clot formation and this time is recorded to obtain the activated PTT (aPTT). A shortened clotting time indicates an activation of the intrinsic and common pathways of coagulation by the test material. Untreated plasma is used as negative control and latex or black rubber as positive control.

ACTIVATION OF COMPLEMENT SYSTEM

Complement system consists of more than 30 proteins circulating in the blood and present as membrane-associated proteins (Dunkelberger and Song, 2010). In response to the recognition of foreign surface structures, complement factors are sequentially activated in an enzyme cascade via three different pathways: classical, alternative, and mannose binding lectin (MBL) pathway. All of these pathways lead to the generation of a C3 convertase, which cleaves C3 into a large fragment C3b, which acts as an opsonin and a small fragment C3a, which is an anapylatoxin that promotes inflammation. Afterwards, C5 convertase is generated, which cleaves C5 in C5a, which is an anapylatoxin, and C5b that binds to the foreign surface and initiates the generation of terminal lysis complex (C5b-9, TCC), which is also called membrane attack complex (MAC). As a result, microorganisms are eliminated by lysis, opsonization and triggering a series of inflammatory reactions.

The contact of the artificial surface with blood leads to an immediate adsorption of serum proteins, e.g., fibrinogen, albumin, and immunoglobulin G (IgG), to the surface of the material (Wetterö et al., 2000) and it results in a kinetic competition between the proteins on the material surface, which is called the Vroman effect (Vroman et al., 1980). During the first minutes, abundant proteins, such as fibrinogen, adsorb and they are progressively displaced by less abundant proteins with a higher affinity for the surface, such as HMWK, Factor XII, and plasminogen (Ballet et al., 2010). Especially, the complement protein C3 and IgG can readily bind to hydrophobic surfaces and lead to the activation of complement system. Thereby, the following conformational changes on the blood-contacting surface are considered as initial trigger for the complement activation via the alternative or classical pathway (Gorbet and Sefton, 2004; Andersson et al., 2005; Nilsson et al., 2007). Different biomaterial surfaces show different complement activating properties, for example, hydrophobic surfaces can lead to an increased complement activation compared to hydrophilic surfaces (Nilsson et al., 2007).

The generated complement activation products lead to the increased expression of P-selectin, which is an important mediator of neutrophil recruitment and platelet accumulation (Sukavaneshvar, 2017). Compared to C3a and C4a, the produced C5a is the most powerful anaphylatoxin. It can increase the permeability of blood vessels, attract and activate neutrophil granulocytes and monocytes to stimulate phagocytosis. C5a stimulates endothelial cells to increasingly express cytokines, chemokines and cell adhesion molecules, such as E-selectin (Newton and Dixit, 2012). Furthermore, it can bind to mast cells and increase inflammation. Moreover, C5a is able to trigger the release of TF from neutrophils and monocytes, which can initiate coagulation cascade (Ikeda et al., 1997; Ritis et al., 2006;

Kourtzelis et al., 2010). Thus, there is a close cross-talk between the complement system and the coagulation pathway mediated by the generated C5a (Oikonomopoulou et al., 2010).

Therefore, the analysis of complement activation is a highly relevant criterion in the legislation for testing biomaterials intended for blood contact. According to ISO 10993-4 (International Organization for Standardization, 2000), the complement activation can be analyzed by detection of C3a, C5a, Bb, iC3b, C4d, C3-, or C5-convertase, and the C5b-9 complex in whole blood, as well as the 50% complement hemolytic activity (CH50) (Costabile, 2010). Most frequently, the concentration of anaphylatoxins C3a and C5a as well as the C5b-9 complex is determined using ELISA (Kopp et al., 2002; Sperling et al., 2007; Engberg et al., 2011). Furthermore, in a recent study, Endgberg and colleagues proposed that the ratio between the binding of C4 and its inhibitor C4BP should be considered as a predictor for the evaluation of the hemocompatibility (Engberg et al., 2015).

PLATELET ACTIVATION

Platelets are present in large quantities in the blood and under physiological conditions, they circulate in a quiescent state for 7–10 days. The adhesion and activation of platelets is prevented by an healthy endothelial monolayer, which acts as a barrier between blood and tissues and has antithrombogenic properties by the release of e.g., nitric oxide (NO) and prostaglandin I_2 (PGI_2) (Brass et al., 2013; Golebiewska and Poole, 2015; Frohlich, 2016). The damage of endothelium leads to the exposure of the underlying subendothelial collagen to the blood. In addition, damaged endothelial cells secrete von Willebrand factor (vWF), which can bind to the collagen in the exposed subendothelial layer and mediate the adhesion of circulating platelets (Yau et al., 2015) to form a seal at the damaged area.

The exposure of biomaterial to the blood can result in an undesired activation of platelets and consequently lead to thrombotic complications. Thus, the analysis of platelet activation is an important part of hemocompatibility tests. The contact of blood with foreign surfaces immediately leads to the adsorption of plasma proteins, especially fibrinogen, immunoglobulins, fibronectin, vitronectin, Factor XI and XII, vWF, HMWK, and PK to the biomaterial surface (Long et al., 2016). Particularly, fibrinogen, vWF, fibronectin, and vitronectin induce the adhesion of platelets via interaction with the most frequent integrin receptor $\alpha_{IIb}\beta_3$ glycoprotein IIb/IIIa (GPIIb/IIIa) on the surface of platelets and lead to the activation of platelets. Subsequently, platelets release bioactive molecules from their alpha and dense granules. Each platelet contains ∼50–80 alpha granules and ∼3–6 dense granules (Fitch-Tewfik and Flaumenhaft, 2013). The dense granules contain proaggregatory factors such as adenosine diphosphate (ADP), adenosine triphosphate (ATP), histamine, serotonin [5-hydroxytryptamine (5-HT)], polyphosphates, and bivalent cations Mg^{2+} and Ca^{2+} (Meyers et al., 1982). ADP can activate neighboring platelets via binding to two different purinergic receptors on platelets, known as $P2Y_1$ and $P2Y_{12}$ (Wijeyeratne and Heptinstall, 2011). These platelets can activate further platelets passing by and lead to the adhesion and aggregation of neighbored platelets. Finally, the thrombi is stabilized by fibrin. Alpha granules contain hemostatic proteins, such as vWF, fibrinogen, Factor V, Factor IX, and plasminogen, chemokines (e.g., platelet factor 4 (PF4), SDF-1α), and growth factors (e.g., VEGF, PDGF). Furthermore, large amounts of β-thromboglobulin (β-TG) are released from alpha granules after the activation of platelets, which lead to leukocyte recruitment (Brandt et al., 2000; Frohlich, 2016). In addition, alpha granules also contain integral membrane protein P-selectin, which is translocated to the plasma membrane after the activation of platelets (Frenette et al., 2000). P-selectin glycoprotein ligand-1 (PSGL-1) expressed on leukocytes can interact with P-selectin and lead to the activation of neutrophils (Sreeramkumar et al., 2014). Furthermore, the released polyphosphates can activate Factor XII and lead to the initiation of the intrinsic coagulation pathway (Müller et al., 2009).

The activation of platelets can be determined according to ISO 10993-4 by measuring released contents from alpha granules, such as β-TG or PF4 using ELISA (Mayer et al., 2009; Teligui et al., 2016; Stoll et al., 2017) and detection of P-selectin (CD62P) or activated GPIIb/IIIa receptor with PAC-1 antibody using flow cytometry (Theoret et al., 2011; van Velzen et al., 2012).

ACTIVATION OF LEUKOCYTES

Besides coagulation, complement, and platelet activation, the activation of leukocytes and the occurrence of respiratory burst can be analyzed to evaluate biomaterial-induced inflammatory response. Thus, the generation of reactive oxygen species (ROS) and the release of PMN elastase are the mainly determined parameters for leukocytes activation. The activation of leukocytes leads to a respiratory burst (Dahlgren and Karlsson, 1999), which is the result of an enhanced oxygen metabolism, and results in generation of ROS (superoxide anion (O_2^-), hydrogen peroxide (H_2O_2), hydroxyl radical ($HO^\bullet$) and singlet oxygen ($^1O_2$). Thus, the ROS generation can be detected (Roesslein et al., 2013) using chemiluminogenic (Nygren et al., 2000) or fluorogenic substances (Ferrer et al., 2013). Furthermore, the release of elastase from PMN granulocytes, especially from neutrophils, can be quantified by ELISA (Zimmermann et al., 2007). Additionally, PMN elastase activity can also be measured by the proteolytic cleavage of a synthetic substrate and the release of a fluorophore, which can be easily quantified by fluorescence (Gramegna et al., 2017).

The activation of leukocytes leads to the increased expression of CD11b on the cell surface via translocation of the CD11b from intracellular granules to the plasma membrane. Thus, the detection of CD11b expression on the surface of leukocytes using fluorescence-activated cell sorting (FACS) can give additional information on activation of leukocytes (Gorbet et al., 1999). Furthermore, the production of neutrophil extracellular traps (NETs) is a recently described mechanism of neutrophils for host defense (Brinkmann et al., 2004; Delgado-Rizo et al., 2017). During NETosis, the nuclear material is released in form of a meshwork of chromatin by activated neutrophils to the

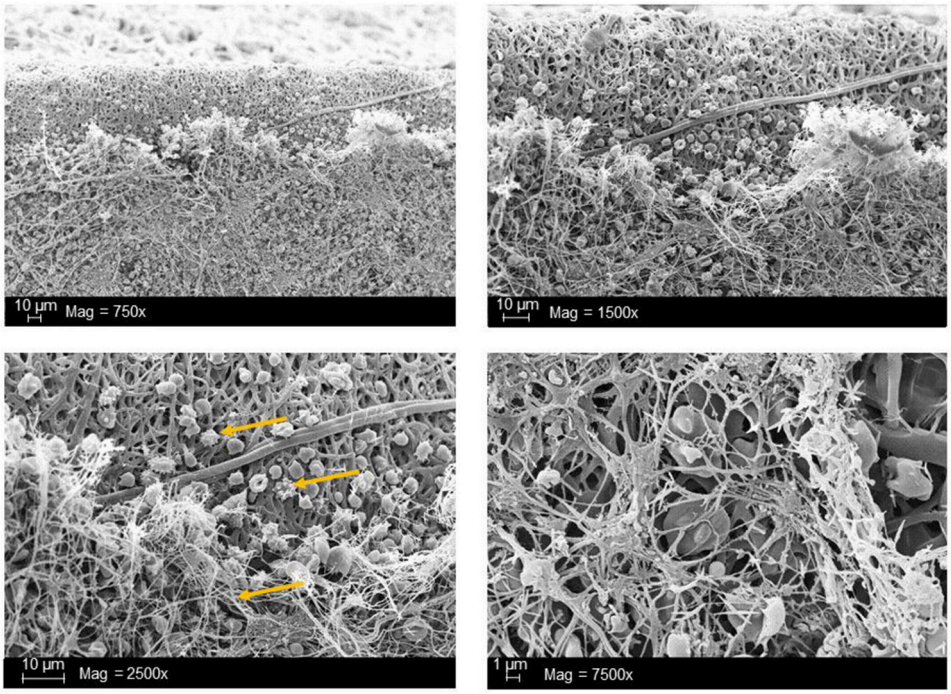

FIGURE 3 | Scanning electron microscopic (SEM) analysis of synthetic vascular graft surface after the blood contact. Arrows indicate the adhered platelets as well as the resulting 3D-fibrin meshes due to activation of blood coagulation. The analyses were performed in our working group and the data has not been published before.

extracellular space (Noubouossie et al., 2017). Several proteins adhere to the NETs, such as histones and components with antimicrobial activity, e.g., elastase and myeloperoxide (Delgado-Rizo et al., 2017). Besides the ability to trap bacteria, NETs ability to promote thrombosis was demonstrated in animal models (Brill et al., 2012).

ANALYSIS OF BIOMATERIAL SURFACES

The adsorption of proteins to the surface of biomaterials is the initial step directly after the blood contact. Subsequently, adhered proteins initiate the adhesion and activation of platelets on the surface. These platelets can further activate neighbored platelets and at the last step the thrombi are stabilized by the generation of a fibrin network.

The activation of platelets is a very fast process of ∼180 ms (van Oeveren, 2013) and different morphological appearance of platelets can be detected on material surfaces depending on varying states of activation: (1) unactivated platelets: round, discoid shaped without pseudopodia, (2) partially activated platelets: dendritic with early pseudopodia, (3) moderately activated platelets: spread-dendritic with irreversible long-dendritic extensions, (4) fully activated platelets: fully spread (Park et al., 1990).

The adhesion and activation of platelets lead to a cytoskeletal rearrangement and therefore to a morphological change of platelets on the biomaterial surface with extensive formation of pseudopodia. Afterwards, the spreading of platelets and the release of vasoconstrictive substances, such as thromboxane and PDGF, as well as contents of stored granules occur. Finally, the aggregation of platelets and the generation of a fibrin network can be analyzed using scanning electron microscopy (SEM) (Zhang et al., 2017) (**Figure 3**). Thus, in several studies, the surface thrombogenicity of biomaterials was examined by characterization of cell morphology and spreading using SEM (Balasubramanian and Slack, 2001; Aguilar et al., 2002). Furthermore, using fluorescently labeled antibodies against specific receptors, the adhered cells and the cell density can be detected using fluorescence and confocal microscopy (Nguyen et al., 2016). In recent years, microgravimetric analyses using quartz crystal microbalance (QCM) were also applied to investigate the platelet adhesion and activation (Sinn et al., 2010; Fatisson et al., 2011; Kunze et al., 2014). Moreover, Hanson and colleagues used surface plasmon resonance (SPR) based flow chamber device to detect platelet-surface interactions and blood coagulation (Hansson et al., 2007). Furthermore, Zhao et al. (2011) used SEM and transmission electron microscopy (TEM) to investigate the effect of different sizes of nanoparticles on hemolysis and the mechanism behind the lysis of red blood cells. The group demonstrated that a small proportion of small type of mesoporous silica nanoparticles (MSNs) adsorbed to the surface of erythrocytes without any alteration of cell membrane or morphology. In contrast, the adsorption of large type MSNs to the erythrocytes induced a strong local membrane deformation and resulted in internalization of particles and hemolysis.

CONCLUSION

The interaction of biomaterials with blood leads to cellular as well as humoral reactions, which can result in an unwanted inflammation and activation of coagulation and/or fibrinolysis. Thus, the development of biomaterials with an improved hemocompatibility increases the tolerability and minimizes unwanted side effects, such as thrombus formation. Therefore, during the development of new blood-contacting medical devices, not only the mechanical and chemical characteristics should play an important role, but also the hemocompatibility. Furthermore, to prove the safety and reliability of new products, hemocompatibility analyses should include appropriate references and follow the ISO 10993-4 standard.

AUTHOR CONTRIBUTIONS

MA-A is the corresponding author of this work. She developed the outline with HW and CS edited the paper. MW and MA-A wrote the manuscript. HS, SG, and LH revised the manuscript.

REFERENCES

Aguilar, M. R., Rodríguez, G., Fernández, M., Gallardo, A., and San Román, J. (2002). Polymeric active coatings with functionality in vascular applications. *J. Mater. Sci. Mater. Med.* 13, 1099–1104. doi: 10.1023/A:1021100916920

Andersson, J., Ekdahl, K. N., Lambris, J. D., and Nilsson, B. (2005). Binding of C3 fragments on top of adsorbed plasma proteins during complement activation on a model biomaterial surface. *Biomaterials* 26, 1477–1485. doi: 10.1016/j.biomaterials.2004.05.011

Bae, S. W., Kim, H. S., Cha, Y. N., Park, Y. S., Jo, S. A., and Jo, I. (2003). Rapid increase in endothelial nitric oxide production by bradykinin is mediated by protein kinase A signaling pathway. *Biochem. Biophys. Res. Commun.* 306, 981–987. doi: 10.1016/S0006-291X(03)01086-6

Balasubramanian, V., and Slack, S. M. (2001). Effects of fibrinogen residence time and shear rate on the morphology and procoagulant activity of human platelets adherent to polymeric biomaterials. *ASAIO J.* 47, 354–360. doi: 10.1097/00002480-200107000-00012

Ballet, T., Boulange, L., Brechet, Y., Bruckert, F., and Weidenhaupt, M. (2010). Protein conformational changes induced by adsorption onto material surfaces: an important issue for biomedical applications of material science. *Bull. Pol. Acad. Sci. Tech. Sci.* 58, 303–313. doi: 10.2478/v10175-010-0028-0

Basu, A., Hong, J., and Ferraz, N. (2017). Hemocompatibility of Ca(2+) -crosslinked nanocellulose hydrogels: toward efficient management of hemostasis. *Macromol. Biosci.* 17. doi: 10.1002/mabi.201700236

Biró, E. K., Sturk-Maquelin, Vogel, G., Meuleman, D., Smit, M., Hack, C., et al. (2003). Human cell-derived microparticles promote thrombus formation *in vivo* in a tissue factor-dependent manner. *J. Thromb. Haemost.* 1, 2561–2568. doi: 10.1046/j.1538-7836.2003.00456.x

Blok, L. J. S., Engels, G. E., and van Oeveren, W. (2016). *In vitro* hemocompatibility testing: the importance of fresh blood. *Biointerphases* 11:029802. doi: 10.1116/1.4941850

Brandt, E., Petersen, F., Ludwig, A., Ehlert, J. E., Bock, L., and Flad, H. D. (2000). The beta-thromboglobulins and platelet factor 4: blood platelet-derived CXC chemokines with divergent roles in early neutrophil regulation. *J. Leukoc. Biol.* 67, 471–478. doi: 10.1002/jlb.67.4.471

Brass, L. F., Tomaiuolo, M., and Stalker, T. J. (2013). Harnessing the platelet signaling network to produce an optimal hemostatic response. *Hematol. Oncol. Clin. North Am.* 27, 381–409. doi: 10.1016/j.hoc.2013.02.002

Braune, S., Grunze, M., Straub, A., and Jung, F. (2013). Are there sufficient standards for the *in vitro* hemocompatibility testing of biomaterials?. *Biointerphases* 8:33. doi: 10.1186/1559-4106-8-33

Brill, A., Fuchs, T., Savchenko, A., Thomas, G., Martinod, K., De Meyer, S., et al. (2012). Neutrophil extracellular traps promote deep vein thrombosis in mice. *J. Thromb. Haemost.* 10, 136–144. doi: 10.1111/j.1538-7836.2011.04544.x

Brinkmann, V., Reichard, U., Goosmann, C., Fauler, B., Uhlemann, Y., Weiss, D. S., et al. (2004) Neutrophil extracellular traps kill bacteria. *Science* 303, 1532–1535. doi: 10.1126/science.1092385

Camci-Unal, G., Cuttica, D., Annabi, N., Demarchi, D., and Khademhosseini, A. (2013). Synthesis and characterization of hybrid hyaluronic acid-gelatin hydrogels. *Biomacromolecules* 14, 1085–1092. doi: 10.1021/bm3019856

Cerda-Cristerna, B. I., Flores, H., Pozos-Guillén, A., Pérez, E., Sevrin, C., and Grandfils, C. (2011). Hemocompatibility assessment of poly (2-dimethylamino ethylmethacrylate)(PDMAEMA)-based polymers. *J. Control. Release* 153, 269–277. doi: 10.1016/j.jconrel.2011.04.016

Costabile, M. (2010). Measuring the 50% haemolytic complement (CH50) activity of serum. *J. Vis. Exp.* 37:1923. doi: 10.3791/1923

Dahlgren, C., and Karlsson, A. (1999). Respiratory burst in human neutrophils. *J. Immunol. Methods.* 232, 3–14.

Delgado-Rizo, V., Martínez-Guzmán, M. A., Iñiguez-Gutierrez, L., García-Orozco, A., Alvarado-Navarro, A., and Fafutis-Morris, M. (2017). Neutrophil extracellular traps and its implications in inflammation: an overview. *Front. Immunol.* 8:81. doi: 10.3389/fimmu.2017.00081

Dunkelberger, J. R., and Song, W.-C. (2010). Complement and its role in innate and adaptive immune responses. *Cell Res.* 20, 34–50. doi: 10.1038/cr.2009.139.

Engberg, A. E., Nilsson, P. H., Huang, S., Fromell, K., Hamad, O. A., Mollnes, T. E., et al. (2015). Prediction of inflammatory responses induced by biomaterials in contact with human blood using protein fingerprint from plasma. *Biomaterials* 36, 55–65. doi: 10.1016/j.biomaterials.2014.09.011

Engberg, A. E., Rosengren-Holmberg, J. P., Chen, H., Nilsson, B., Lambris, J. D., Nicholls, I. A., et al. (2011). Blood protein-polymer adsorption: implications for understanding complement-mediated hemoincompatibility. *J. Biomed. Mater. Res. A* 97, 74–84. doi: 10.1002/jbm.a.33030

Fatisson, J., Mansouri, S., Yacoub, D., Merhi, Y., and Tabrizian, M. (2011). Determination of surface-induced platelet activation by applying time-dependency dissipation factor versus frequency using quartz crystal microbalance with dissipation. *J. R. Soc. Interface* 8, 988–997. doi: 10.1098/rsif.2010.0617

Ferrer, M. C., Eckmann, U. N., Composto, R. J., and Eckmann, D. M. (2013). Hemocompatibility and biocompatibility of antibacterial biomimetic hybrid films. *Toxicol. Appl. Pharmacol.* 272, 703–712. doi: 10.1016/j.taap.2013.07.023

Fitch-Tewfik, J. L., and Flaumenhaft, R. (2013). Platelet granule exocytosis: a comparison with chromaffin cells. *Front. Endocrinol. (Lausanne)* 4:77. doi: 10.3389/fendo.2013.00077

Frenette, P. S., Denis, C. V., Weiss, L., Jurk, K., Subbarao, S., Kehrel, B., et al. (2000). P-Selectin glycoprotein ligand 1 (PSGL-1) is expressed on platelets and can mediate platelet-endothelial interactions *in vivo*. *J. Exp. Med.* 191, 1413–22. doi: 10.1084/jem.191.8.1413

Frohlich, E. (2016). Action of nanoparticles on platelet activation and plasmatic coagulation, *Curr. Med. Chem.* 23, 408–430. doi: 10.2174/0929867323666160106151428

Golebiewska, E. M., and Poole, A. W. (2015). Platelet secretion: from haemostasis to wound healing and beyond. *Blood Rev.* 29, 153–162. doi: 10.1016/j.blre.2014.10.003

Gorbet, M. B., and Sefton, M. V (2004). Biomaterial-associated thrombosis: roles of coagulation factors, complement, platelets and leukocytes. *Biomaterials* 25, 5681–703. doi: 10.1016/j.biomaterials.2004.01.023

Gorbet, M., Yeo, E., and Sefton, M. (1999). Flow cytometric study of *in vitro* neutrophil activation by biomaterials. *J. Biomed. Mater. Res. A* 44, 289–297.

Gramegna, A., Amati, F., Terranova, L., Sotgiu, G., Tarsia, P., Miglietta, D., et al. (2017). Neutrophil elastase in bronchiectasis. *Respir. Res.* 18:211. doi: 10.1186/s12931-017-0691-x

Hansson, K. M., Johansen, K., Wetterö, J., Klenkar, G., Benesch, J., Lundström, I., et al. (2007). Surface plasmon resonance detection of blood coagulation and platelet adhesion under venous and arterial shear conditions. *Biosens. Bioelectron.* 23, 261–268. doi: 10.1016/j.bios.2007.04.009

Haycox, C. L., and Ratner, B. D (1993). *In vitro* platelet interactions in whole human blood exposed to biomaterial surfaces: insights on blood compatibility. *J. Biomed. Mater. Res. A* 27, 1181–1193.

International Organization for Standardization (2000). *Biological Evaluation of Medical Devices*. Available online at https://www.iso.org/standard/63448.html (Accessed April 23, 2018).

Ikeda, K., Nagasawa, K., Horiuchi, T., Tsuru, T., Nishizaka, H., and Niho, Y. (1997). C5a induces tissue factor activity on endothelial cells. *Thromb. Haemost.* 77, 394–398.

Kälsch, T., Elmas, E., Nguyen, X. D., Suvajac, N., Klüter, H., Borggrefe, M. et al. (2007). Endotoxin-induced effects on platelets and monocytes in an *in vivo* model of inflammation. *Basic Res. Cardiol.* 102, 460–466. doi: 10.1007/s00395-007-0667-y

Kappelmayer, J., Bernabei, A., Edmunds, L. H., Edgington, T. S., and Colman, R. W. (1993). Tissue factor is expressed on monocytes during simulated extracorporeal circulation. *Circ. Res.* 72, 1075–1081.

Kent, N. J., Basabe-Desmonts, L., Meade, G., MacCraith, B. D., Corcoran, B. G., Kenny, D., et al. (2010). Microfluidic device to study arterial shear-mediated platelet-surface interactions in whole blood: reduced sample volumes and well-characterised protein surfaces. *Biomed. Microdevices* 12, 987–1000. doi: 10.1007/s10544-010-9453-y.

Kopp, R., Mottaghy, K., and Kirschfink, M. (2002). Mechanism of complement activation during extracorporeal blood-biomaterial interaction: effects of heparin coated and uncoated surfaces. *ASAIO J.* 48, 598–605. doi: 10.1097/00002480-200211000-00005

Kourtzelis, I., Markiewski, M. M., Doumas, M., Rafail, S., Kambas, K., Mitroulis, I., et al. (2010). Complement anaphylatoxin C5a contributes to hemodialysis-associated thrombosis. *Blood* 116, 631–639. doi: 10.1182/blood-2010-01-264051

Kovach, K. M., Capadona, J. R., Gupta, A. S., and Potkay, J. A. (2014). The effects of PEG-based surface modification of PDMS microchannels on long-term hemocompatibility. *J. Biomed. Mater. Res. A* 102, 4195–4205. doi: 10.1002/jbm.a.35090

Krajewski, S., Prucek, R., Panacek, A., Avci-Adali, M., Nolte, A., Straub, A., et al. (2013). Hemocompatibility evaluation of different silver nanoparticle concentrations employing a modified Chandler-loop *in vitro* assay on human blood. *Acta Biomater.* 9, 7460–7468. doi: 10.1016/j.actbio.2013.03.016

Kuhbier, J., Coger, V., Mueller, J., Liebsch, C., Schlottmann, F., Bucan, V., et al. (2017). Influence of direct or indirect contact for the cytotoxicity and blood compatibility of spider silk. *J. Mater. Sci. Mater. Med.* 28:127. doi: 10.1007/s10856-017-5936-1

Kunze, A., Hesse, C., and Svedhem, S. (2014). Real-time monitoring of surface-confined platelet activation on Tio2. *Colloids Surf. B Biointerfaces* 116, 446–451. doi: 10.1016/j.colsurfb.2014.01.025

Lackner, J. M., Waldhauser, W., Hartmann, P., Bruckert, F., Weidenhaupt, M., Major, R., et al. (2012). Hemocompatibility of inorganic physical vapor deposition (PVD) coatings on thermoplastic polyurethane polymers. *J. Funct. Biomater.* 3, 283–297. doi: 10.3390/jfb3020283.

Li, Y., and Boraschi, D. (2016). Endotoxin contamination: a key element in the interpretation of nanosafety studies. *Nanomedicine* 11, 269–287. doi: 10.2217/nnm.15.196

Liu, X., Yuan, L., Li, D., Tang, Z., Wang, Y., Chen, G., et al. (2014). Blood compatible materials: state of the art. *J. Mater. Chem. B* 2, 5718–5738. doi: 10.1039/C4TB00881B

Long, A. T., Kenne, E., Jung, R., Fuchs, T. A., and Renné, T. (2016). Contact system revisited: an interface between inflammation, coagulation, and innate immunity. *J. Thromb. Haemost.* 14, 427–437. doi: 10.1111/jth.13235

Magalhães, P. O., Lopes, A. M., Mazzola, P. G., Rangel-Yagui, C., Penna, T., and Pessoa, A. Jr. (2007). Methods of endotoxin removal from biological preparations: a review. *J. Pharm. Pharm. Sci.* 10, 388–404.

Maitz, M. F., Sperling, C., Wongpinyochit, T., Herklotz, M., Werner, C., and Seib, F. P. (2017). Biocompatibility assessment of silk nanoparticles: hemocompatibility and internalization by human blood cells. *Nanomedicine* 13, 2633–2642. doi: 10.1016/j.nano.2017.07.012

Mayer, A., Vadon, M., Rinner, B., Novak, A., Wintersteiger, R., and Frohlich, E. (2009). The role of nanoparticle size in hemocompatibility. *Toxicology* 258, 139–147. doi: 10.1016/j.tox.2009.01.015

McClung, W. G., Babcock, D., and Brash, J. (2007). Fibrinolytic properties of lysine-derivatized polyethylene in contact with flowing whole blood (Chandler loop model). *J. Biomed. Mater. Res. A* 81, 644–651. doi: 10.1002/jbm.a.31018

Meyers, K. M., Holmsen, H., and Seachord, C. L. (1982). Comparative study of platelet dense granule constituents. *Am. J. Physiol.* 243, R454–R461.

Millar, J. E., Fanning, J. P., McDonald, C. I., McAuley, D. F., and Fraser, J. F. (2016). The inflammatory response to extracorporeal membrane oxygenation (ECMO): a review of the pathophysiology. *Crit. Care* 20:387. doi: 10.1186/s13054-016-1570-4

Mohan, C. C., Chennazhi, K. P., and Menon, D. (2013). *In vitro* hemocompatibility and vascular endothelial cell functionality on titania nanostructures under static and dynamic conditions for improved coronary stenting applications. *Acta Biomater.* 9, 9568–9577. doi: 10.1016/j.actbio.2013.08.023

Müller, F., Mutch, N. J., Schenk, W. A., Smith, S. A., Esterl, L., Spronk, H. M., et al. (2009). Platelet polyphosphates are proinflammatory and procoagulant mediators *in vivo*. *Cell* 139, 1143–1156. doi: 10.1016/j.cell.2009.11.001

Müller, J., Becher, T., Braunstein, J., Berdel, P., Gravius, S., Rohrbach, F., et al. (2011). Profiling of active thrombin in human blood by supramolecular complexes. *Angew. Chem. Int. Ed. Engl.* 50, 6075–6078. doi: 10.1002/anie.201007032

Müller, M., Krolitzki, B., and Glasmacher, B. (2012). Dynamic *in vitro* hemocompatibility testing–improving the signal to noise ratio. *Biomed. Eng.* 57, 549–552. doi: 10.1515/bmt-2012-4211

Nagy, M., Heemskerk, J. W., and Swieringa, F. (2017). Use of microfluidics to assess the platelet-based control of coagulation. *Platelets* 28, 441–448. doi: 10.1080/09537104.2017.1293809

Neun, B. W., and Dobrovolskaia, M. A. (2011). "Method for analysis of nanoparticle hemolytic properties *in vitro*," in *Characterization of Nanoparticles Intended for Drug Delivery* (Humana Press), 215–224. doi: 10.1007/978-1-60327-198-1

Newton, K., and Dixit, V. M. (2012). Signaling in innate immunity and inflammation. *Cold Spring Harb. Perspect. Biol.* 4:*a*006049. doi: 10.1101/cshperspect.a006049.

Nilsson, B., Ekdahl, K. N., Mollnes, T. E., and Lambris, J. D. (2007). The role of complement in biomaterial-induced inflammation. *Mol. Immunol.* 44, 82–94. doi: 10.1016/j.molimm.2006.06.020

Nguyen, T.-H., Palankar, V.-R., Bui, C., Medvedev, N., Greinacher, A., and Delcea, M. (2016). Rupture forces among human blood platelets at different degrees of activation. *Sci. Rep.* 6:25402. doi: 10.1038/srep25402

Nordling, S., Nilsson, B.,and Magnusson, P. U (2014). A novel in vitro model for studying the interactions between human whole blood and endothelium. *J. Vis. Exp.* 96:e52112. doi: 10.3791/52112

Noubouossie, D. F., Whelihan, M. F.,Yu, Y.-B., Sparkenbaugh, E., Pawlinski, R., and Key, N. (2017). *In vitro* activation of coagulation by human neutrophil DNA and histone proteins but not neutrophil extracellular traps. *Blood* 129, 1021–1029. doi: 10.1182/blood-2016-06-722298

Nygren, H., Braide, M., and Karlsson, C. (2000). Different kinetics of the respiratory burst response in granulocytes, induced by serum from blood coagulated in contact with polymer materials. *Biomaterials* 21, 173–182. doi: 10.1016/S0142-9612(99)00146-5

Oikonomopoulou, K., Ricklin, D., Ward, P. A., and Lambris, J. D. (2010). Interactions between coagulation and complement—their role in inflammation. *Semin. immunopathol.* 34, 151–165. doi: 10.1007/s00281-011-0280-x.

Onasoga-Jarvis, A., Puls, T., O'brien, S., Kuang, L., Liang, H., and Neeves, K. (2014). Thrombin generation and fibrin formation under flow on biomimetic tissue factor-rich surfaces. *J. Thromb. Haemost.* 12, 373–382. doi: 10.1111/jth.12491

Onasoga-Jarvis, A. A., Leiderman, K., Fogelson, A. L., Wang, M., Manco-Johnson, M. J., Di Paola, J. A., et al. (2013). The effect of factor VIII deficiencies and replacement and bypass therapies on thrombus formation under venous flow

conditions in microfluidic and computational models. *PLoS ONE* 8:*e*78732. doi: 10.1371/journal.pone.0078732

Park, K., Mao, F., and Park, H. (1990). Morphological characterization of surface-induced platelet activation. *Biomaterials* 11, 24–31.

Peckham, S. M., Turitto, V. T., Glantz, J., Puryear, H., and Slack, S. (1997). Hemocompatibility studies of surface-treated polyurethane-based chronic indwelling catheters. *J. Biomater. Sci.* 8, 847–858.

Podias, A., Groth, T., and Missirlis, Y. (1995). The effect of shear rate on the adhesion/activation of human platelets in flow through a closed-loop polymeric tubular system. *J. Biomater. Sci.* 6, 399–410.

Punet, X., Mauchauffé, R., Rodríguez-Cabello, J. C., Alonso, M., Engel, E., and Mateos-Timoneda, M. A. (2015). Biomolecular functionalization for enhanced cell–material interactions of poly (methyl methacrylate) surfaces. *Regen. Biomater.* 2, 167–175. doi: 10.1093/rb/rbv014

Qian, Q., Nath, K. A., Wu, Y., Daoud, T. M., and Sethi, S. (2010). Hemolysis and acute kidney failure. *Am. J. Kidney Dis.* 56, 780–784. doi: 10.1053/j.ajkd.2010.03.025

Ritis, K., Doumas, M., Mastellos, D., Micheli, A., Giaglis, S., Magotti, P., et al. (2006). A novel C5a receptor-tissue factor cross-talk in neutrophils links innate immunity to coagulation pathways. *J. Immunol.* 177, 4794–4802. doi: 10.4049/jimmunol.177.7.4794

Ritz-Timme, S., Eckelt, N., Schmidtke, E., and Thomsen, H. (1997). Genesis and diagnostic value of leukocyte and platelet accumulations around "air bubbles" in blood after venous air embolism. *Int. J. Leg. Med.* 111, 22–26.

Roesslein, M., Hirsch, C., Kaiser, J.-P., Krug, H. F., and Wick, P. (2013). Comparability of *in vitro* tests for bioactive nanoparticles: a common assay to detect reactive oxygen species as an example. *Int. J. Mol. Sci.* 14, 24320–24337. doi: 10.3390/ijms141224320

Sanak, M, Jakieła, B., and Wegrzyn, W. (2010). Assessment of hemocompatibility of materials with arterial blood flow by platelet functional tests. *Bull. Polish Acad. Sci. Tech. Sci.* 58, 317–322. doi: 10.2478/v10175-010-0029-z

Schrottmaier, W. C., Kral, J. B., Zeitlinger, M., Salzmann, M., Jilma, B., and Assinger, A. (2016). Platelet activation at the onset of human endotoxemia is undetectable *in vivo*. *Platelets* 27, 479–483. doi: 10.3109/09537104.2015

Sinn, S., Müller, L., Drechsel, H., Wandel, M., Northoff, H., Ziemer, G., et al. (2010). Platelet aggregation monitoring with a newly developed quartz crystal microbalance system as an alternative to optical platelet aggregometry. *Analyst* 135, 2930–2938. doi: 10.1039/c0an00474j

Sinn, S., Scheuermann, T., Deichelbohrer, S., Ziemer, G., and Wendel, H. P. (2011). A novel *in vitro* model for preclinical testing of the hemocompatibility of intravascular stents according to ISO 10993-4. *J. Mater. Sci. Mater. Med.* 22, 1521–1528. doi: 10.1007/s10856-011-4335-2

Sperling, C., Maitz, M. F., Grasso, S., Werner, C., and Kanse, S. M. (2017). A positively charged surface triggers coagulation activation through factor VII activating protease (FSAP). *ACS Appl. Mater. Interfaces* 9, 40107–40116. doi: 10.1021/acsami.7b14281

Sperling, C., Maitz, M. F., Talkenberger, S., Gouzy, M. F., Groth, T., and Werner, C. (2007). *In vitro* blood reactivity to hydroxylated and non-hydroxylated polymer surfaces. *Biomaterials* 28, 3617–3625. doi: 10.1016/j.biomaterials.2007.04.041

Sreeramkumar, V., Adrover, J. M., Ballesteros, I., Cuartero, M. I., Rossaint, J., Bilbao, I., et al. (2014) Neutrophils scan for activated platelets to initiate inflammation. *Science* 346, 1234–1238. doi: 10.1126/science.1256478

Stadie, W. C (1920). A method for the determination of methaemoglobin in the blood. *J. Biol. Chem.* 41, 237–241.

Stang, K., Krajewski, S., Neumann, B., Kurz, J., Post, M., Stoppelkamp, S., et al. (2014). Hemocompatibility testing according to ISO 10993-4: discrimination between pyrogen-and device-induced hemostatic activation. *Mater. Sci. Eng. C* 42, 422–428. doi: 10.1016/j.msec.2014.05.070

Stoll, H., Steinle, H., Stang, K., Kunnakattu, S., Scheideler, L., Neumann, B., et al. (2017). Generation of Large-Scale DNA Hydrogels with excellent blood and cell compatibility. *Macromol. Biosci.* 17: 1600252. doi: 10.1002/mabi.201600252.

Streller, U., Sperling, C., Hübner, J., Hanke, R., and Werner, C. (2003). Design and evaluation of novel blood incubation systems for in vitro hemocompatibility assessment of planar solid surfaces. *J. Biomed. Mater. Res. B Appl. Biomater.* 66, 379–390. doi: 10.1002/jbm.b.10016

Sukavaneshvar, S. (2017). Device thrombosis and pre-clinical blood flow models for assessing antithrombogenic efficacy of drug-device combinations. *Adv. Drug Deliv. Rev.* 112, 24–34. doi: 10.1016/j.addr.2016.07.009

Teligui, L., Dalmayrac, E., Corbeau, J. J., Bouquet, E., Godon, A., Denomme, A. S., et al. (2016). *Ex vivo* simulation of cardiopulmonary bypass with human blood for hemocompatibility testing. *Perfusion* 31, 376–83. doi: 10.1177/0267659115599454

Théorêt, J. F., Yacoub, D., Hachem, A., Gillis, M. A., and Merhi, Y. (2011). P-selectin ligation induces platelet activation and enhances microaggregate and thrombus formation. *Thromb. Res.* 128, 243–50. doi: 10.1016/j.thromres.2011.04.018.

Thorsen, T., Klausen, H., Lie, R., and Holmsen, H. (1993) Bubble-induced aggregation of platelets: effects of gas species, proteins, and decompression. *Undersea Hyperb. Med.* 20, 101–119.

Tiffany, C. W., and Burch, R. M. (1989). Bradykinin stimulates tumor necrosis factor and interleukin-1 release from macrophages. *FEBS Lett.* 247, 189–192.

Totea, G., Ionita, D., Demetrescu, I., and Mitache, M. (2014). *In vitro* hemocompatibility and corrosion behavior of new Zr-binary alloys in whole human blood. *Open Chem.* 12, 796–803. doi: 10.2478/s11532-014-0535-1

Vafa Homann, M., Johansson, D., Wallen, H., and Sanchez, J. (2016). Improved *ex vivo* blood compatibility of central venous catheter with noble metal alloy coating. *J. Biomed. Mater. Res. B Appl. Biomater.* 104, 1359–1365. doi: 10.1002/jbm.b.33403

Van Kruchten, R., Cosemans, J. M., and Heemskerk, J. W. (2012). Measurement of whole blood thrombus formation using parallel-plate flow chambers–a practical guide. *Platelets* 23, 229–242. doi: 10.3109/09537104.2011.630848

van Oeveren, W. (2013). Obstacles in haemocompatibility testing. *Scientifica* 2013:392584. doi: 10.1155/2013/392584

Van Oeveren, W., Tielliu, I. F., and De Hart, J. (2012). Comparison of modified chandler, roller pump, and ball valve circulation models for *in vitro* testing in high blood flow conditions: application in thrombogenicity testing of different materials for vascular applications. *Int. J. Biomater.* 2012:673163. doi: 10.1155/2012/673163

van Velzen, J. F., Laros-van Gorkom, Pop, G. A., and van Heerde, W. L. (2012). Multicolor flow cytometry for evaluation of platelet surface antigens and activation markers. *Thromb. Res.* 130,92–98. doi: 10.1016/j.thromres.2012.02.041

Vroman, L., Adams, A. L, Fischer, G. C., and Munoz, P. C. (1980). Interaction of high molecular weight kininogen, factor XII, and fibrinogen in plasma at interfaces. *Blood* 55, 156–159.

Wachtfogel, Y. T., Hack, C. E., Nuijens, J., Kettner, C., Reilly, T. M., Knabb, R. M., et al. (1995). Selective kallikrein inhibitors alter human neutrophil elastase release during extracorporeal circulation. *Am. J. Physiol.* 268, H1352–H1357.

Wang, D.-A., Ji, J., Gao, C.-Y., Yu, G.-H., and Feng, L.-X. (2001) Surface coating of stearyl poly (ethylene oxide) coupling-polymer on polyurethane guiding catheters with poly (ether urethane) film-building additive for biomedical applications. *Biomaterials* 22, 1549–1562. doi: 10.1016/S0142-9612(00)00311-2

Watanabe, J., Marathe, G. K., Neilsen, P. O., Weyrich, A. S., Harrison, K. A., Murphy, R. C., et al. (2003). Endotoxins stimulate neutrophil adhesion followed by synthesis and release of platelet-activating factor in microparticles. *J. Biol. Chem.* 278, 33161–33168. doi: 10.1074/jbc.M305321200

Westein, E., de Witt, S., Lamers, M., Cosemans, J. M., and Heemskerk, J. W. (2012). Monitoring *in vitro* thrombus formation with novel microfluidic devices. *Platelets* 23, 501–509. doi: 10.3109/09537104.2012.709653

Wetterö, J., Bengtsson, T., and Tengvall, P. (2000). Complement activation on immunoglobulin G-coated hydrophobic surfaces enhances the release of oxygen radicals from neutrophils through an actin-dependent mechanism. *J. Biomed. Mater. Res.* 51, 742–751. doi: 10.1002/1097-4636(20000915)51:4<742::AID-JBM24>3.0.CO;2-D

Wijeyeratne, Y. D., and Heptinstall, S. (2011). Anti-platelet therapy: ADP receptor antagonists. *Br. J. Clin. Pharmacol.* 72, 647–57. doi: 10.1111/j.1365-2125.2011.03999.x

Wu, Y. (2015). Contact pathway of coagulation and inflammation. *Thromb. J.* 13:17. doi: 10.1186/s12959-015-0048-y

Xiao, W., He, J., Nichol, J. W., Wang, L., Hutson, C. B., Wang, B., et al. (2011). Synthesis and characterization of photocrosslinkable gelatin and silk fibroin interpenetrating polymer network hydrogels. *Acta Biomater.* 7, 2384–2393. doi: 10.1016/j.actbio.2011.01.016

Yau, J. W., Teoh, H., and Verma, S. (2015). Endothelial cell control of thrombosis. *BMC Cardiovasc. Disord.* 15:130. doi: 10.1186/s12872-015-0124-z

Zhang, J., Zhu, C., Fan, D., Ma, X., Mi, Y., and Xue, W. (2015). A two-step protocol to remove endotoxins from human-like collagen. *Sep. Sci. Technol.* 50, 993–1001. doi: 10.1080/01496395.2014.978467

Zhang, L., Casey, B., Galanakis, D. K., Marmorat, C., Skoog, S., Vorvolakos, K., et al. (2017). The influence of surface chemistry on adsorbed fibrinogen conformation, orientation, fiber formation and platelet adhesion. *Acta Biomater.* 54, 164–174. doi: 10.1016/j.actbio.2017.03.002

Zhao, Y., Sun, X., Zhang, G., Trewyn, B. G., Slowing, I. I., and Lin, V. S. (2011). Interaction of mesoporous silica nanoparticles with human red blood cell membranes: size and surface effects. *ACS Nano* 5, 1366–1375. doi: 10.1021/nn103077k

Zhu, S., Herbig, B. A., Li, R., Colace, T. V., Muthard, R. W., Neeves, K. B., et al. (2015). In microfluidico: recreating *in vivo* hemodynamics using miniaturized devices. *Biorheology* 52, 303–318. doi: 10.3233/BIR-15065

Zimmermann, A. K., Weber, N., Aebert, H., Ziemer, G., and Wendel, H. (2007). Effect of biopassive and bioactive surface-coatings on the hemocompatibility of membrane oxygenators. *J. Biomed. Mater. Res. B Appl. Biomater.* 80, 433–439. doi: 10.1002/jbm.b.30614

Conflict of Interest Statement: The authors declare that the research was conducted in the absence of any commercial or financial relationships that could be construed as a potential conflict of interest.

frontiers in Bioengineering and Biotechnology

REVIEW
published: 26 July 2018
doi: 10.3389/fbioe.2018.00086

Skin Tissue Substitutes and Biomaterial Risk Assessment and Testing

Houman Savoji[1,2], *Brent Godau*[3,4,5], *Mohsen Sheikh Hassani*[6] *and Mohsen Akbari*[3,4,5]*

[1] Institute of Biomaterials and Biomedical Engineering, University of Toronto, Toronto, ON, Canada, [2] Toronto General Research Institute, University Health Network, University of Toronto, Toronto, ON, Canada, [3] Laboratory for Innovations in Microengineering (LiME), Department of Mechanical Engineering, University of Victoria, Victoria, BC, Canada, [4] Center for Biomedical Research, University of Victoria, Victoria, BC, Canada, [5] Centre for Advanced Materials and Related Technology, University of Victoria, Victoria, BC, Canada, [6] Department of Systems and Computer Engineering, Carleton University, Ottawa, ON, Canada

Tremendous progress has been made over the past few decades to develop skin substitutes for the management of acute and chronic wounds. With the advent of tissue engineering and the ability to combine advanced manufacturing technologies with biomaterials and cell culture systems, more biomimetic tissue constructs have been emerged. Synthetic and natural biomaterials are the main constituents of these skin-like constructs, which play a significant role in tissue grafting, the body's immune response, and the healing process. The act of implanting biomaterials into the human body is subject to the body's immune response, and the complex nature of the immune system involves many different cell types and biological processes that will ultimately determine the success of a skin graft. As such, a large body of recent studies has been focused on the evaluation of the performance and risk assessment of these substitutes. This review summarizes the past and present advances in *in vitro*, *in vivo* and clinical applications of tissue-engineered skins. We discuss the role of immunomodulatory biomaterials and biomaterials risk assessment in skin tissue engineering. We will finally offer a roadmap for regulating tissue engineered skin substitutes.

Keywords: wound healing, skin substitutes, biomaterials, immunomodulation, regulatory pathway

OPEN ACCESS

Edited by:
Nihal Engin Vrana, Protip Medical, France

Reviewed by:
Sangamesh G. Kumbar, University of Connecticut Health Center, United States
Julien Georges Didier Barthès, Protip Medical, France
Meltem Avci-Adali, Universitätsklinikum Tübingen, Universität Tübingen, Germany

***Correspondence:**
Mohsen Akbari
makbari@uvic.ca

Specialty section:
This article was submitted to Biomaterials, a section of the journal Frontiers in Bioengineering and Biotechnology

Received: *12 March 2018*
Accepted: *05 June 2018*
Published: *26 July 2018*

Citation:
Savoji H, Godau B, Hassani MS and Akbari M (2018) Skin Tissue Substitutes and Biomaterial Risk Assessment and Testing. Front. Bioeng. Biotechnol. 6:86. doi: 10.3389/fbioe.2018.00086

INTRODUCTION

Skin is the largest organ in the human body and any damage to this living organ has dramatic and significant consequences which may lead to mortality, hospitalization or long-term morbidity (Korrapati et al., 2016). Tissue engineering is a promising and interdisciplinary active area of research in biomedical engineering that provides and investigates the application of novel biomaterials for the reconstruction of diseased or damaged tissues and organs (Chua et al., 2016). Tissue engineered skin substitutes provide new therapy potentials for treatment of acute and chronic skin wounds. Several important characteristic factors such as tunable physical, morphological and mechanical properties, suitable permeability, biocompatibility, non-toxicity and non-inflammatory; among others, need to be carefully considered in the fabrication of a functional skin substitute (Albanna and Holmes IV, 2016). In addition, a skin substitute should be able to replicate the gradients of various growth factors, cytokines, enzymes and pharmacological agents *in vivo* to promote optimal restoration and regeneration of full thickness wounds (Chua et al., 2016). For this purpose, scientists have used natural and synthetic polymers to mimic the

natural extracellular matrix (ECM) and recapitulate the structure and function of the envisaged tissues (Korrapati et al., 2016).

Although recent advances in skin tissue engineering have offered potential to significantly improve the clinical outcome in wound healing of both acute and chronic wounds, there are still some deficiencies that need to be addressed to provide substitutes with painless healing process and encourage the formation of vascular, neural and lymphatic networks, hair follicles, sebaceous and sweat glands (Pereira et al., 2013). Therefore, the ultimate goal of these efforts in skin tissue engineering is to fabricate a complex scar-free skin substitute that can be transplanted in large quantities in only one surgical intervention with a minimum chance of rejection by the host's body.

This review will summarize the advances in the engineering of skin substitutes both *in vitro* and *in vivo*. We further discuss the role of immunomodulatory biomaterials and biomaterials risk assessment in skin tissue engineering. We will then offer a roadmap for biomaterial selection, risk assessment and testing of skin substitutes. Finally, we will discuss prospects for further progress in skin regeneration in the future.

SKIN ANATOMY AND PHYSIOLOGY

The skin is the largest organ of the human body, serving as an interface between the body and the surrounding environment. The primary function of this complex organ is to protect the internal organs against external insults such as pathogens, as well as thermal, mechanical and chemical hazards (Groeber et al., 2011). The skin is composed of different cells and multiple anatomically distinct layers, commonly classified into three main compartments; epidermis, dermis and subcutaneous tissue (hypodermis) (**Figure 1**). The epidermis is a dynamic, continuously self-renewing multilayered epithelium, mainly composed of keratinocytes. These keratinocytes have the ability to differentiate and undergo structural and compositional changes, leading to the synthesis and expression of a variety of structural proteins and lipids, therefore playing a vital role in skin function (Bouwstra et al., 2003). The epidermis can be subdivided into stratum corneum, stratum lucidum (only in some parts), stratum granulosum, stratum spinosum and stratum germinativum. The uppermost layer of the epidermis, the stratum corneum (SC), is a 10–20 μm thick layer of enucleated dead cells (corneocytes) embedded in a lipid matrix (Groen et al., 2011; Flaten et al., 2015). The lipid matrix, which mainly consists of ceramides, cholesterol and free fatty acids, is considered to play a central role in the barrier functionality of skin against absorption of components and water loss (Hatta et al., 2006; Masukawa et al., 2008). The epidermis is connected to its adjacent layer, the dermis, via the basal membrane. Hair follicles, sweat glands, shafts and nerves are all embedded in this sub-layer (Bouwstra and Ponec, 2006). The dermis is around 1–2 mm thick and provides mechanical support for the skin as well as the elastic properties due to the high amount of elastin in this layer. The dermis itself is comprised of a loosely arranged collagen fiber upper papillary layer and a dense collagen fiber reticular layer (Mathes et al., 2014). The hypodermis is the final sub-layer, which functions as the skin's shock-absorber and the body's heat insulator, and is mainly comprised of fibroblasts and adipocytes (Mathes et al., 2014).

ETIOLOGY, PATHOLOGY AND PATHOPHYSIOLOGY OF WOUNDS

The skin covers about 3,000 square inches of the body surface and weighs around one-sixth of the entire body, thus it is the most exposed organ in the body to external hazards (Flora, 2002). Skin injuries are breaks in the skin tissue caused by surgical procedures, genetic irregularities and physical and chemical traumas. These wounds can also be divided into the following categories based on the depth of damage; epidermal, superficial partial-thickness, deep partial-thickness and full-thickness skin wounds (Papini, 2004). Epidermal and partial-thickness level wounds are normally regenerated using the skin's self-healing functions. However, in deep partial-thickness and full-thickness skin wounds, self-healing is not possible since the skin's epithelial regenerative elements are completely destroyed (Blanpain et al., 2004; Tumbar, 2006).

Wound healing occurs in four concurring phases; hemostasis, inflammation, cell proliferation and remodeling (**Figure 2**) (Hu et al., 2014). Upon the infliction of the injury, the skin rapidly responds with a series of actions. Platelets stimulate the inflammatory response by releasing proteins and growth factors. The site of the injury immediately recruits immune cells into the wound, where the accumulation of the platelets results in blood coagulation to prevent blood loss (Midwood et al., 2004). Fibroblasts enter the wound site and generate new tissue matrix from fibronectin and collagen (Groeber et al., 2011). Subsequently, keratinocyte re-epithelialization and the revascularization of the damaged area occurs via endothelial cells, while concurrently fibroblasts differentiate into myofibroblasts to close the wound by shrinking the matrix (Midwood et al., 2004; Groeber et al., 2011). Finally, cells undergo apoptosis which results in scar tissue formation. This process gives the skin its remarkable regeneration capacity and enables it to maintain homeostasis in response to a variety of disturbances throughout our lifetime. This self-repair capability is in large due to the presence of epidermal stem cells in different compartments of the skin such as inter-follicular compartments and epidermal appendages (Mathes et al., 2014).

TISSUE-ENGINEERED HUMAN SKIN EQUIVALENTS

The first milestone in skin tissue engineering was the in-lab culture of keratinocytes in 1966 (MacNeil, 2007). This led to the development of cultured epithelial autografts (CEAs), which consisted of small sheets containing two or three layers of cells (Vignesh, 1981; Gallico et al., 1984). The next important step was the design and *in vivo* evaluation of a dermo-epidermal skin substitute in human namely Apligraf®, which was made of human allogeneic fibroblasts and keratinocytes (Bell et al.,

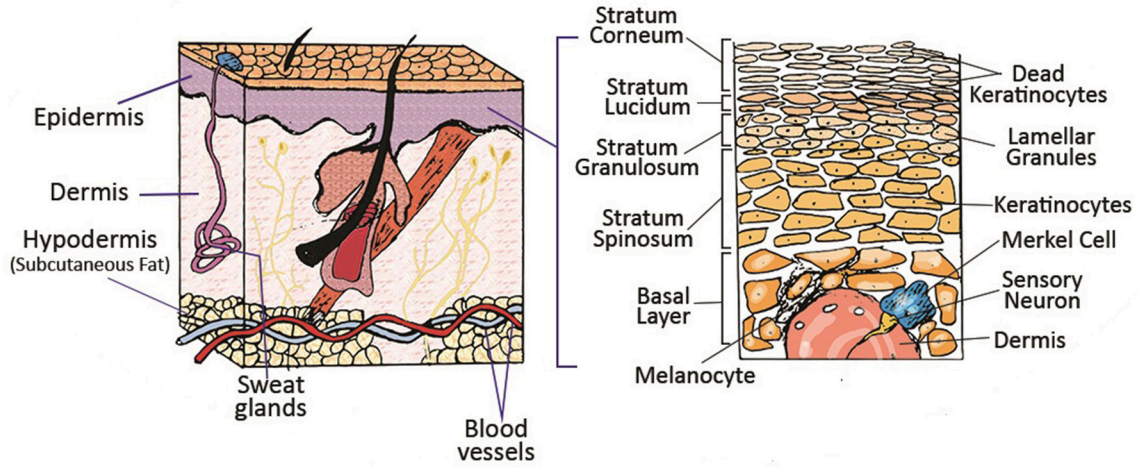

FIGURE 1 | Schematic of different layers of skin and its appendages. Reprinted with permission from Mohammadi et al. (2016). Copyright 2018, John Wiley & Sons.

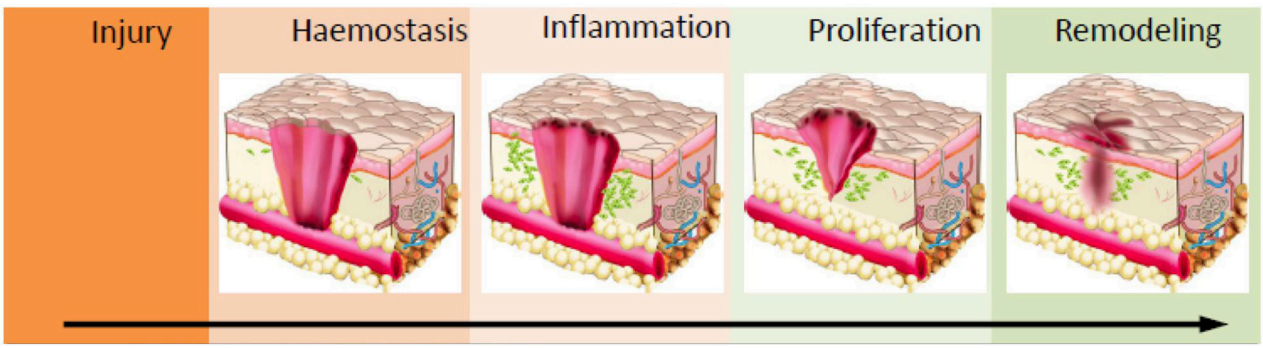

FIGURE 2 | Schematic of the wound healing process. Haemostasis via coagulation and clot formation occurs at the wounded site followed by immune cells infiltration and inflammation to clean up the site of injured tissue. This prevents infection and triggers granulation. In the proliferation phase, fibroblast, epithelial cells, keratinocytes and endothelial cells will migrate and proliferate into wounds to deposit ECM proteins and other biomolecules which enables wound closure. Ultimately, in the maturation/remodelling phase, ECM deposition and clearance controls the development of scar formation. Reprinted with permission from Lin et al. (2018). Copyright 2018, MDPI.

1981). Later on, attempts were made to develop a skin substitute similar to Apligraf® by using human autologous keratinocytes and fibroblasts in bovine collagen and were applied to extensive burns and ulcers (MacNeil, 2007).

In 1981, another practical and major step in the tissue engineering of the skin was reported by designing a dermal substitute named Integra™, which comprised bovine collagen and shark chondroitin sulfate with a silicone membrane, acting as a temporary barrier. Practically, Integra™ was grafted to the wound site leading to formation of blood vessels. Then, the silicone barrier was removed and replaced with a layer of autologous cells (Burke et al., 1981). Several commercialized models have been marketed for permanent and temporary use in clinics during the last several decades. They are usually comprised from two compartments; biodegradable material as scaffolds (natural or synthetic polymers) which are used to support cell attachment, and cells which could be autologous, allogenic or xenogeneic. These commercially available skin substitutes are categorized into three main products namely, epidermal, dermal and dermo-epidermal substitutes. In this section, we briefly discuss some of these substitutes and their pros and cons in wound repair and regeneration.

EPIDERMAL SUBSTITUTES

Inspired by CEAs, these substitutes have a small stratified sheet of cells (i.e., autologous keratinocytes which are grown in the presence of murine fibroblast). *In vitro* culture of autologous cells is performed by skin biopsy (approximately 2–5 cm^2). Single keratinocytes are extracted and cultured to form colonies (Gallico et al., 1984). The single colonies come together to form stratified epithelial layers and eventually these layers are delivered

to the wound site. This process takes 3–4 weeks upon the patient's arrival at the clinic. Epicel®, Epidex™ and Myskin™ are some of the examples of these substitutes (Wood et al., 2006). Despite the shortcomings of these products, they have still been applied for patients with extensive burns/wounds (Atiyeh and Costagliola, 2007). Epicel® is prepared using autologous keratinocytes which form the CEA sheets 15 days after skin biopsy (Vacher, 2003), whereas Epidex™ is cultured from keratinocytes obtained from the outer root sheath of scalp hair follicles (Tausche et al., 2003). Myskin™ is made up of a surface coated silicon substrate, covered with sub-confluent autologous keratinocytes which improves handling application and decreases the cell culture time. This product was reported to treat diabetic foot ulcers and superficial burns (Moustafa et al., 2007). The main disadvantages of epidermal substitutes are their long preparation time, poor keratinocyte attachment, difficult handling due to the thin cellular layers, poor mechanical stability, scarring and their high production costs (Atiyeh and Costagliola, 2007).

In another approach [i.e., ReCell®, (CellSpray)], the suspended cultured autologous keratinocytes are directly sprayed onto the wound site. This method showed faster formation of the epidermis layer in *in vivo* wound models but human application remains controversial (Navarro et al., 2000). The advantages of this approach include accelerated healing, minimizing scar formation, eliminating tissue rejection and re-introducing pigmentation to the skin. However, use of different scaffolds (fibrin matrix, silicon, etc.) has definite effects on shortening the fabrication process of epidermal substitutes and increasing the surface area of CEAs (Ronfard et al., 2000).

DERMAL SUBSTITUTES

Engineered dermal substitutes provide appropriate configuration and surface area for an effective epidermal engraftment. Several *in vitro* and clinical trials have shown successful engraftment of cultured autologous keratinocytes when applied to the dermal or neo-dermal bed (Hansbrough et al., 1993; Wood et al., 2006; Pham et al., 2007). Most of the dermal substitutes contain a matrix without incorporating cells and are applied permanently to the wound bed (Wood et al., 2006; Pham et al., 2007). Some currently commercially available dermal substitutes are AlloDerm®, Dermagraft®, Integra™, and Matriderm®; among others. AlloDerm® is an acellular human dermis which is produced by the removal of the epidermis and extraction of fibroblasts from the dermis while the collagen bundles or the basement membrane remains unchanged (Shakespeare, 2005). This product does not cause immunogenic response due to its acellular structure.

Dermagraft® is an engineered dermal substitute which contains cryopreserved human fibroblast cells derived from newborn foreskin tissue. The human neonatal fibroblasts are seeded onto a biodegradable polyglactin mesh scaffold. The fibroblasts proliferate to fill the pores of this scaffold and release human dermal collagen, matrix proteins, growth factors and cytokines to form a 3D human dermal substitute containing metabolically active living cells. Dermagraft® does not include macrophages, lymphocytes, blood vessels or hair follicles. It can promote re-epithelialization in the restoration of the dermal bed and wound healing especially in diabetic and venous ulcers (Gentzkow et al., 1996). Cost and antigenic response are the main disadvantages of this graft (Gentzkow et al., 1996).

Integra™ is the first approved tissue engineered product by the U.S. Food and Drug Administration (FDA) to regenerate dermis. This substitute consists of a porous matrix of cross-linked bovine type I tendon collagen, shark chondroitin-6-sulfate glycosaminoglycan and a semi-permeable polysiloxane. The semi-permeable silicone membrane controls water vapor loss, provides a flexible anti-bacterial support for the wound surface and promotes enhanced mechanical strength for the substitute. On the other hand, the collagen-glycosaminoglycan biodegradable matrix provides a scaffold for cellular invasion/infiltration and capillary growth (i.e., vascularization). Once applied, the infiltration of fibroblasts into the scaffold is inhibited, resulting in neo-dermis formation. After the completion of vascularization and neo-dermis formation (approximately 15–20 days), the silicone layer is peeled off and the wound can be closed permanently with an epidermal substitute. Integra™ provides patients with several promising advantages including long shelf life, simple handling, comfortability for various anatomical sites, excellent performance in deep donor sites, low risks of immunogenic response and disease transmission and reduced rates of contraction and scarring. It could be applied for a wide range of treatments including full-thickness burns, chronic ulcer and full-thickness non-thermal skin wound management; among others (Bello et al., 2001).

Matriderm® was designed as a 3D matrix consisting of collagen matrix coated with an elastin hydrolysate from the ligament, similar to the structure of the human dermis. The collagen matrix acts as a supportive structure for the growth of living cells and blood vessels. The elastin component promotes the stability and elasticity of the regenerating tissue. During the healing process, fibroblasts produce their own ECM, and the scaffold is resorbed. Matriderm® possesses more elastic properties similar to that of natural skin and can be applied in a single stage process which eventually reduces scar formation and wound contraction (Ryssel et al., 2008).

DERMO-EPIDERMAL SUBSTITUTES

Dermo-epidemal substitutes (composite skin substitutes) are comprised of two layers including keratinocytes on fibroblast-containing dermal substitutes. The cells could be autologous and allogeneic skin cells (i.e., keratinocytes and fibroblasts), which are integrated into scaffolds. However, using allogeneic skin cells is controversial due to the host body rejection. They are the most advanced skin substitutes which faithfully mimic both epidermal and dermal layers. Providing growth factors, cytokines

and ECM for host cells, initiating/regulating wound healing and effective pain relief are the advantages of these products. Although they can mimic the normal skin, they suffer from various shortcomings such as high costs, short shelf life and chance of tissue rejection by the host body (Shevchenko et al., 2010).

Apligraf® consists of two layers; the lower dermal layer contains bovine type I collagen and allogeneic neonatal fibroblasts, which produce additional matrix proteins. The upper epidermal layer is made of allogeneic neonatal keratinocytes. These layers form a substitute similar to normal human skin. It promotes transferring ECM components, cytokines and growth factors to the wound bed. Due to the short survival of the allogeneic cells (1–2 months), it can be applied as a temporary wound dress rather than permanent skin substitute (Griffiths et al., 2004). It is the FDA approved composite substitute to heal both diabetic foot ulcers and venous leg ulcers. Some efforts have been made to solve the shortcomings of using allogeneic cells by means of autologous cells but further clinical studies need to be done to confirm these results (Hernon et al., 2007).

OrCel® is a bilayered cellular matrix similar to Apligraf® in which normal human neonatal foreskin allogeneic epidermal keratinocytes and dermal fibroblasts are cultured in two separate layers into a Type I bovine collagen sponge. Donor dermal fibroblasts are cultured on and within the porous sponge side of the collagen matrix while keratinocytes, from the same donor, are cultured on the coated, non-porous side of the collagen matrix. OrCel® is comprised of an absorbable biocompatible matrix which has been shown to contain the cytokines and growth factors that are all suitable for host cell migration and wound healing. The extracellular secretion of cytokines and growth factors by the seeded cells is the main key factor to promote wound healing. It is applied for permanent skin replacement in severe burn patients. The clinical trials for this substitute demonstrated less scar formation and a shorter healing time when compared with the acellular bioactive wound dressing (Biobrane-L) (MacNeil, 2007).

EMERGING FABRICATION STRATEGIES FOR SKIN TISSUE ENGINEERING

Scaffolds are the backbones of any tissue-engineered skin substitute. They provide a platform for cells during the healing process. The structure, morphology, surface topography and mechanical elasticity of scaffolds play a crucial role in cell metabolic activities (e.g., cell-adhesion, -proliferation, -growth, and -differentiation) for successful neovascularization and complete wound repair. Traditional methods such as solvent casting/particulate leaching, freeze-drying (lyophilization), gas foaming, electrospinning, micro-patterning and micro-molding have been widely used for the fabrication of bioengineered tissue substitutes (Ma et al., 2003; Savoji et al., 2014a, 2016; Thadavirul et al., 2014; Limongi et al., 2015; Monteiro et al., 2015; Poursamar et al., 2015; Hadjizadeh et al., 2016; Ng et al., 2016; Mahmoudi et al., 2017). Recently, advanced biofabrication strategies such as three-dimensional (3D) bioprinting and biotextile have emerged as powerful tools that enable exquisite control over the micro and cytostructure of the bioengineering skin tissues (Akbari et al., 2016; Mirani et al., 2017; Pedde et al., 2017). In this section, we will focus on electrospinning, 3D bioprinting and biotextile as the three most popular biofabrication strategies for creating bioengineered skins substitutes.

3D bioprinting refers to the layer-by-layer deposition of biomaterials, bioactive molecules and living cells, on a 3D controllable platform (Pedde et al., 2017). The fabrication of 3D structures with complex geometries by 3D printing have been recently used in tissue engineering of the skin (Ng et al., 2016). The precise positioning with spatial control of bioactive substances enabled bioengineers to fabricate functional skin constructs with structural, biological and mechanical properties that are similar to those of the native skin (Pedde et al., 2017). The commonly used technologies for 3D printing and patterning of biological materials are inkjet, micro-extrusion, laser-assisted and microfluidic printing (Huang et al., 2017; Pedde et al., 2017; Hakimi et al., 2018). The selection of appropriate materials for use in 3D printing and their performance in a particular application depends on several factors including printability, biocompatibility, degradation kinetics and by-products, and structural and mechanical properties (Pedde et al., 2017). For example, 3D bioprinting was used to fabricate dermo-epidermal substitutes by printing a mixture of primary human dermal fibroblasts in a printable ECM-like bioink which were then seeded by primary human dermal keratinocytes (Rimann et al., 2016). The printed substitutes resulted in the formation of two-layer constructs containing distinct dermal and epidermal layers, suggesting the feasibility of 3D printed skin grafts. However, a fully stratified epidermis was not accomplished. (Rimann et al., 2016). 3D printing has also been utilized to fabricate full thickness skin constructs containing skin appendages (e.g., sweat gland; Huang et al., 2016). Mouse epidermal progenitor cells and suitable growth factors were encapsulated in gelatin and sodium alginate mixture as a bioink. The results revealed the successful differentiation of progenitor cells to sweat gland cells inside the ECM-like 3D printed structure. *In vivo* study in a small animal model (e.g., mice with severely burned paws) showed full regeneration of the functional sweat glands in animals (**Figure 3**). More recently, a handheld skin microfluidic-based printer was developed for *in situ* printing of biomaterial and skin tissue sheets containing dermal and epidermal cells embedded in different biomaterials (alginate, fibrin, collagen type I and hyaluronic acid) (Hakimi et al., 2018). *In vivo* results on a porcine full thickness wound model showed the feasibility of using this device for *in situ* biopolymer sheet deposition in a clinically relevant setting (Hakimi et al., 2018). H&E staining on healed wounds showed that both treated and control wounds formed complete granulation tissue, and displayed comparable levels of collagen deposition and cellularity (**Figure 4**; Hakimi et al., 2018).

Scaffolds/patches that mimic mechanical and morphological properties of native tissue, and that possess similar 3D fibrous structure and porosity, can be produced by a versatile electrospinning technique which has remarkably high controllability to tune the fibers architecture. Those fibrous

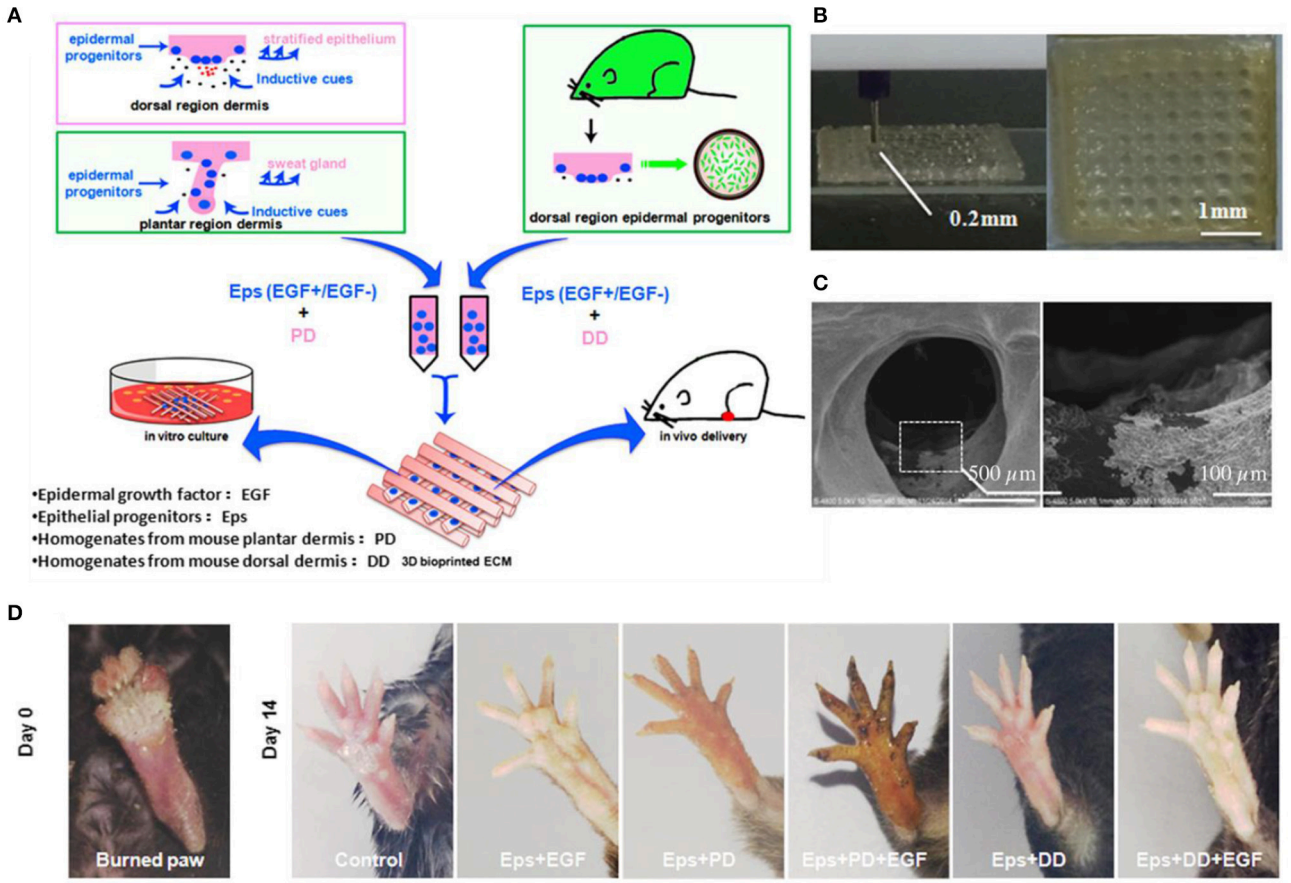

FIGURE 3 | 3D bioprinted scaffolds to direct the differentiation of epithelial progenitors for sweat gland regeneration. **(A)** Schematic of the printing process with epidermal progenitors and ECM incorporated in composite hydrogels. **(B)** Fabricated scaffold and **(C)** scanning electron microscopy (SEM) image of epidermal progenitor cells attached and spread out into the scaffold pores. **(D)** Iodine/starch-based sweat test on paws of mice at day 14 after surgery. Reprinted with permission from Huang et al. (2016). Copyright 2016, Elsevier.

structures undergo long periods of incubation because manual cell seeding is not uniform and cell infiltration is not complete over the entire depth of the scaffold (Savoji et al., 2014a, 2016; Hadjizadeh et al., 2016). Therefore, a novel approach has been investigated to spin cells-polymer solution in a single step, so called cell-electrospinning (Townsend-Nicholson and Jayasinghe, 2006). This fact could advantageously be used for regenerating 3D skin constructs by integrating autologous cells with these robust, tissue-engineered patches. Although there are several studies that have reported the high viability of the cells in a high electric field (Sampson et al., 2014), more investigation is needed to shed light on the precise assessment of cellular genetic change.

Another novel, easy and quick concept in wound healing is *in situ* electrospinning to fabricate suitable substitutes with or without encapsulated cells directly on the wounds. For example, a handheld portable electrospinning device for *in situ* electrospinning has been designed (**Figure 5**; Xu et al., 2015). The *in vitro* and *in vivo* results confirmed the antibacterial properties of the mesoporous silica nanoparticles dispersed in polycaprolactone (PCL) electrospun fibrous mats. Significant improvement of *in vivo* wound closure and re-epithelialization was observed 4 weeks after *in situ* treatment (Dong et al., 2016).

Biotextiles technologies including weaving, knitting, braiding and embroidering have also been investigated in skin tissue engineering applications to address the issues with permeability, mechanical strength and elasticity (Tamayol et al., 2013; Akbari et al., 2016). Various skin patches with significant permeability using natural and synthetic hydrogels have been reported with tunable structural, mechanical and biological properties (Grover and Tomar, 2016; Lu et al., 2017). For example, skin patches using collagen-laden poly(lactic-co-glycolic acid) and poly(lactic acid-co-caprolactone) incorporated with growth factors and bioactive molecules among others have shown promising outcomes in wound healing and regeneration (Townsend-Nicholson and Jayasinghe, 2006).

In addition to these emerging technologies which are combined with biochemical and biophysical cues in the skin substitutes' matrices (Xiao et al., 2017), commercially available therapies are still being used in clinics for treatment of diabetic

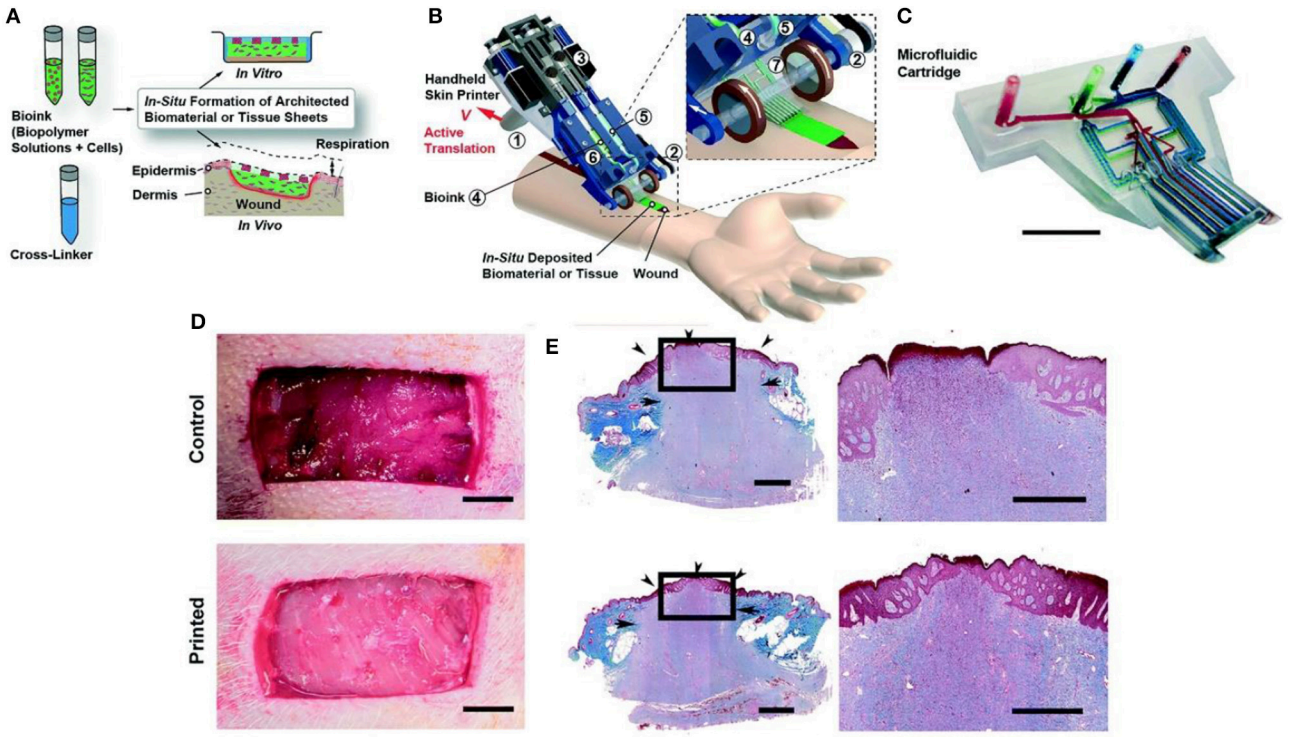

FIGURE 4 | Handheld skin microfluidic printer. **(A)** Schematic diagram illustrating working principle of handheld bioprinter. Bioinks (green) containing hydrogels and cells, and a cross-linker solution (blue) are prepared. **(B)** Schematic image of handheld bioprinter. **(C)** Image of 3D printed microfluidic cartridge. Scale bar 10 mm. **(D)** Control wound and in situ printed of biomaterial sheet. **(E)** Granulation tissue formation and re-epithelialization confirmed by trichrome staining. Arrows indicate the border between newly formed granulation tissue and intact skin. Arrowheads mark epithelialized area. Arrowhead at the center of treated wound shows complete re-epithelialization, while central arrowhead in control wound shows non re-epithelialized zone at wound center. Scale bars 10 mm **(C, D)**, 1 mm (**E** right), and 2 mm (**E** left). Reprinted with permission from Hakimi et al., 2018. Copyright 2018, Royal Society of Chemistry.

wounds; for example, topical negative pressure (e.g., vacuum-assisted wound closure) (Lone et al., 2014), electroporation technique (Rouabhia et al., 2013; Snyder et al., 2017) and pulsed electromagnetic therapy (Choi et al., 2018).

IMMUNOMODULATORY BIOMATERIALS FOR SKIN TISSUE ENGINEERING

The act of implanting biomaterials into the human body is subject to the body's immune response, and the complex nature of the immune system involves many different cell types and biological processes that will ultimately determine the success of a skin implant. Following implantation, the immune response can be categorized into three major phases in which the innate response acts on the order of days, the adaptive response acts on the order of weeks, and resolution occurs on the order of months (Chung et al., 2017). The underlying strategy in immunomodulation for regenerative medicine is to harness pro-regenerative cell types and biological functions that will not result in an inflammatory response and avoid foreign body giant cell formation. For current commercially available skin substitutes (e.g., Allografts, Dermagraft®, Apligraft®, and Transcyte®), immunosuppressive drugs are often paired with implantation to avoid rejection of the implant (Skardal et al., 2012). The use of immunomodulatory biomaterials in an implant localizes immunosuppression to the wound site by removing the need for immunosuppressive drugs while having the potential to further reduce poor cosmetic outcomes. Common strategies in immunomodulation for skin regeneration include macrophage polarization (Sun, 2017; Castellano et al., 2018), the use of glycosaminoglycans (GAGs) (Bhowmick et al., 2017; Pezeshki-Modaress et al., 2017), and the use of decellularized matrices (Kuna et al., 2017).

Macrophages, mature myeloid cells differentiated from circulating monocytes, display a range of phenotypes varying from the M1, pro-inflammatory type to the M2, pro-regenerative type (Rodero and Khosrotehrani, 2010). Their sensitivity to stimuli and ubiquity in immune processes makes them a prime target for strategic immunomodulation, with polarization to the M2 type being the goal. For example, dextran-isocyanatoethyl methacrylate-ethylamine (DexIEME) used as a hydrogel scaffold for cutaneous wound healing was shown to be effective in treating both pre-existing scars in mice and deep wounds in porcine animal models by promoting M2 macrophage polarization (Sun, 2017). DexIEME first led to differentiation of monocytes into

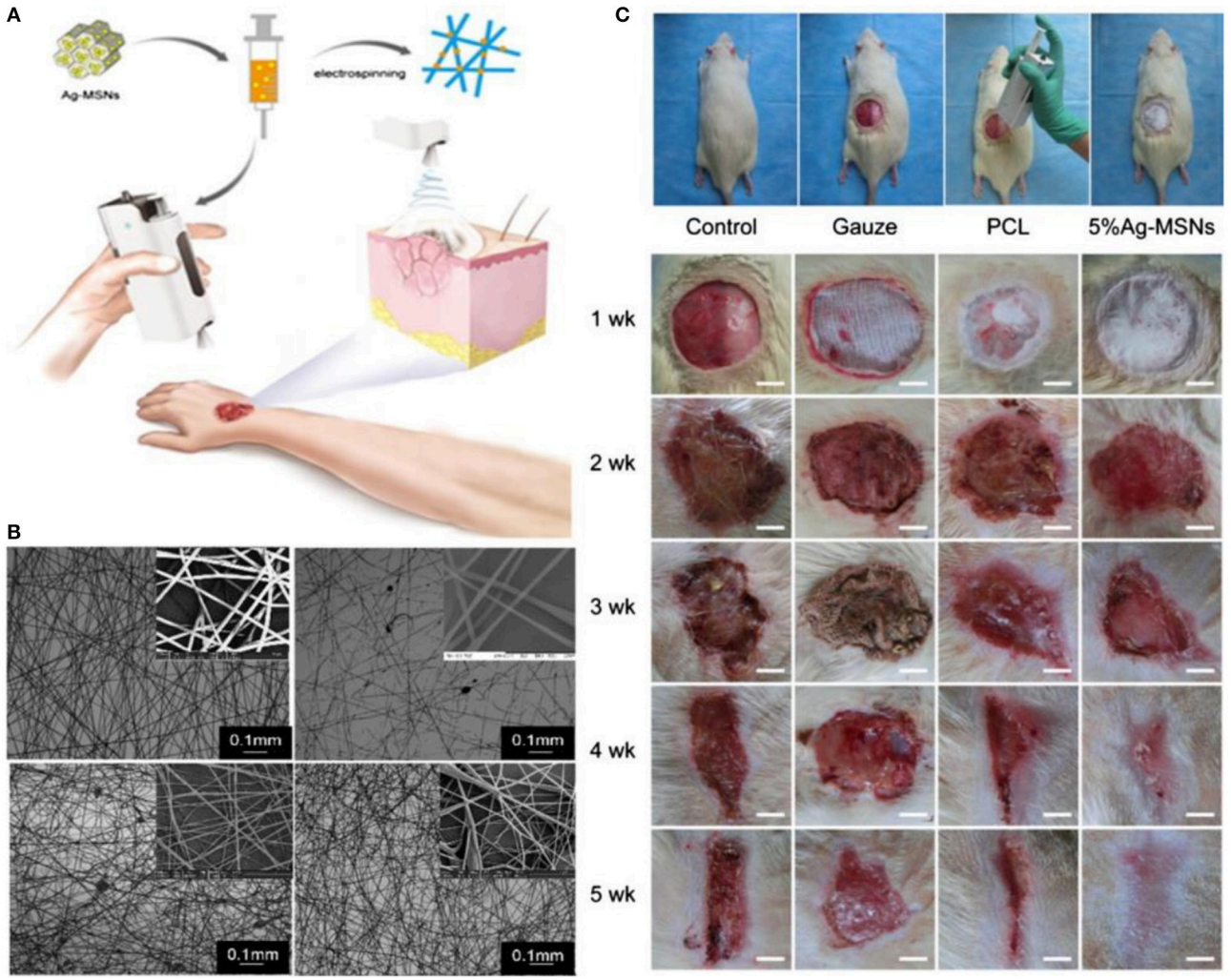

FIGURE 5 | The use of *in situ* electrospinning process for wound management. **(A)** Schematic of the process showing the handheld electrospinning system. **(B)** SEM image of electrospun mats made by the handheld system. **(C)** *In vivo* evaluation of in situ electrospun mats, polycaprolactone (PCL), Ag-MSNs -mesoporous silica nanoparticles. Reprinted with permission from Xu et al. (2015) and (Dong et al., 2016). Copyright 2015 and 2016, Royal Society of Chemistry.

macrophages followed by further polarization of differentiated macrophages to the M2 phenotype *in vitro*. This resulted in full skin regeneration *in vivo* after 5 weeks with ∼75% of skin containing hair follicles when treating mice with third degree burn scars (**Figures 6A,B**). When treating deep wounds in porcine models, the hydrogel treatment showed full regeneration of skin with a reduction in fibrosis and the regenerated skin retains a reticulated endothelial layer. In another study, Castellano et al. showed a significant reduction in the M1/M2 ratio of biopsied tissue of mice implanted with electrospun poly (hydroxybutarate) (PHB) scaffolds when compared to MatriDerm® and PCL implants (**Figure 6C**; Castellano et al., 2018). The implant developed in this study was a dermo-epidermal skin equivalent in which human fibroblasts or endothelial cells were seeded and grown in the scaffold before xenograft implantation onto mice.

Glycosaminoglycans (GAGs) are long, linear polysaccharides that populate the ECM of the dermis and are important in promoting tissue regeneration in the wound healing process because they modulate the attraction of skin precursor cells (Ansari et al., 2018). Incorporation of GAGs into biomaterials has been shown to improve wound healing and promote a pro-regenerative environment in the wound. For example, chondroitin sulfate (CS), a major GAG, blended with gelatin and electrospun into scaffolds with varying ratios of gelatin to CS was shown to increase human dermal fibroblast (HDF) proliferation with increasing ratios of CS in the scaffold (Pezeshki-Modaress et al., 2017). The acellular and HDF seeded scaffolds were then implanted in excised rat skin wounds and showed reduced inflammation, complete re-epithelialization, and acceleration of wound healing with a reduction in fibrosis seen from the acellular scaffold to the HDF seeded scaffold.

Further strategies in immunomodulatory biomaterials include the use of decellularized ECM to reduce inflammation and promote a pro-regenerative host response. The major benefit of using decellularized ECM as a tissue scaffold is that the ECM inherently has a set of biomolecules that are naturally involved in the wound healing process. For example, decellularized pig skin was prepared as a gel with hyaluronic acid (HA) (Kuna et al., 2017). The gel, which contained 66.6, 3.5, and 4.6 μg/mL of collagen, elastin, and GAGs, respectively, showed a marked improvement in wound healing in nude mice by promoting rapid infiltration of host cells and improved wound stabilization. The gel was later mixed with human peripheral blood mononuclear cells before treatment to further improve the gels ability to promote neovascularization, resulting in improved wound healing capability. With an understanding of how the regenerative wound healing process works and how biomaterials can be modified to promote an anti-inflammatory and pro-regenerative environment in the wound, there is great potential to significantly reduce fibrosis and improve the cosmetic features of implanted skin grafts.

BIOMATERIAL RISK ASSESSMENT FOR SKIN TISSUE ENGINEERING

Due to the expensive cost of toxicological studies and difficulty of clinical trials to assess safety and efficacy, it is often easier to repurpose previously approved biomaterials for new applications. Nevertheless, there is a need for new, smarter biomaterials to improve the regenerative ability of future treatments in wound healing. The development of biomaterials for skin tissue engineering must be conducted with a desired end application and clinical trials in mind. In other words, rigorous standardized testing to consider a materials biocompatibility, toxicity, and long-term effects before going into clinical trials must be conducted. This requires not only a significant characterization of a biomaterials benefits for its' desired application, but also intelligent experimental design to disprove any potential safety concerns of the biomaterial.

Chiapinni et al. developed biodegradable silicon nanoneedles that have the ability to induce neovascularization *in vivo* by delivering nucleic acids to skin (Chiappini et al., 2015). Before moving to *in vivo* studies, the cytotoxicity of their treatment was assessed *in vitro* with HeLa cells, showing that their treatment was not cytotoxic when compared to a control with an MTT proliferation assay. They paired this cytotoxicity assessment with an *in vitro* degradation test to exemplify that their biomaterial would not remain in the skin for long periods of time after treatment. They displayed the *in vivo* drug distribution by delivering fluorescent dyes with the nanoneedles and tracking the dyes over time to show local treatment with their system. In order to assess any potential acute inflammation from their treatment, real-time bioluminescent imaging was employed with administration of luminol, a compound which reacts with superoxides generated during acute inflammation to emit light (**Figure 7**; Gross et al., 2009). They further compared treated tissues with haematoxylin and eosin (H&E) histology to show intact tissue membranes after injection along with preserved epidermis, dermis, and sebaceous gland structure (Chiappini et al., 2015). They also observed no sign of leukocyte infiltration or capillary vessel disruption, and negligible hyperkeratosis and necrotic keratinocytes. A similar risk assessment was conducted for a urea based-bolaamphiphile injectable hydrogel with the potential use in skin tissue regeneration (Ramin et al., 2017). They noted the importance of their material to elicit a limited chronic inflammatory reaction, reduce fibrosis, and degrade on a optimal time scale for tissue regeneration. In order to exemplify limited chronic inflammation *in vivo*, they used lucigenin, a reagent which produces light when activated by reactive oxygen species produced by macrophages in chronic inflammation. Fibrosis was monitored via histological analysis with Masson's Trichrome staining, and *in vivo* degradation was analyzed by incorporating cyanin dye into their hydrogel and showing the decrease in fluorescence over a period of 21 days.

Presently, there is a move toward the use of more efficient and accurate evaluation systems for toxicity and inflammatory response. A more complete risk assessment can be conducted with the involvement of organ-on-a-chip systems and *in silico* studies. Organ-on-a-chip systems are a viable alternative to animal testing and can have strong predictive power on how human cells will react to biomaterials, which is a major limitation of animal models (O'Neill et al., 2008; Mohammadi et al., 2016). They also have the ability to be used for high-throughput screening of new biomaterials with a major cost-benefit. Modelling and simulations, or *in silico* studies, also provide valid arguments for new strategies in regenerative medicine, such as the argument made by Yannas et al. that the regeneration of injured skin is dependent upon the wound contraction process, rather than the scar formation process (Yannas et al., 2017). In this study, they suggest the use of a collagen scaffold in the wound healing process by determining the physical characteristics for optimized wound healing conditions and matching a biomaterial with those characteristics.

A combination of *in vitro, in vivo,* and *in silico* risk assessment will significantly strengthen the case for using new biomaterials in skin tissue regeneration. Extensive risk assessment in combination with strong consideration of the clinical hurdles to be encountered will facilitate the development of a new biomaterial, or an innovated old biomaterial, into stage I clinical trials.

In Vitro Models for Skin Substitute Testing

Substantial efforts have been made in recent years to model and create substitutes that mimic human skin, placing the skin amongst the most developed *in vitro* engineered constructs. Since it is the body's first barrier being exposed to many types of cosmetics and therapeutics, extensive funding has been allocated by different industries for *in vitro* skin modulation in an effort to end continuous legal and ethical issues regarding product testing on skin (Karimi et al., 2016; Geraili et al., 2017). The *in vitro* modeling of the human skin can be divided into two main streams in terms of research motivation (Mathes et al., 2014). One stream places focus on obtaining deeper insight into the physiology of skin, requiring more complex models of

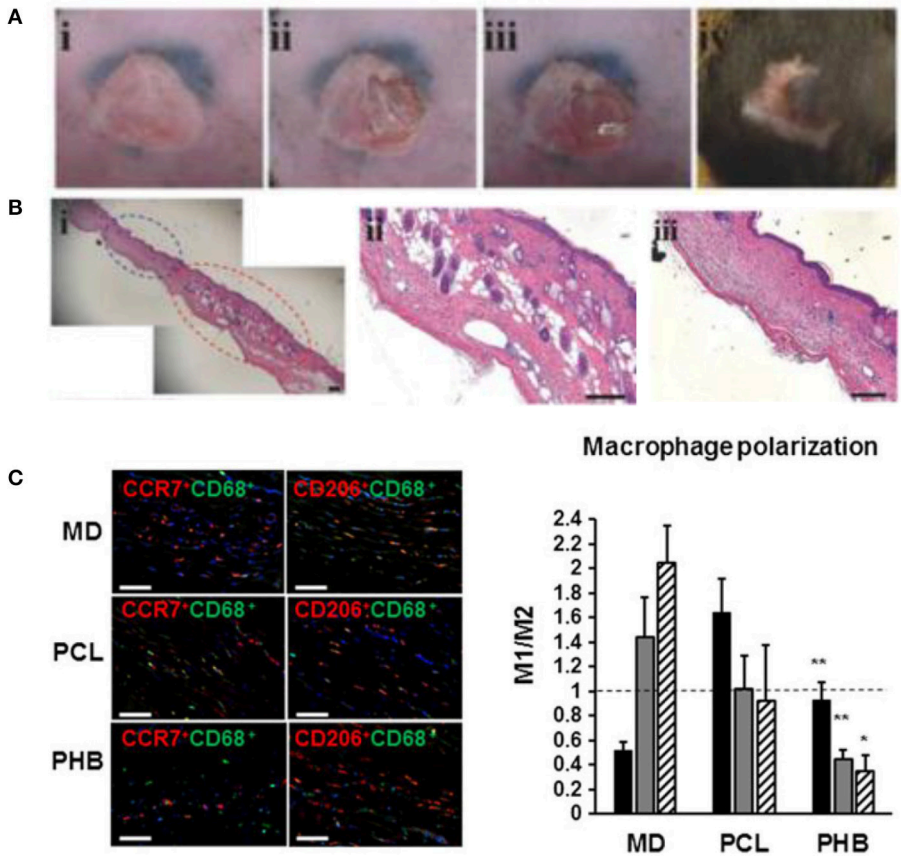

FIGURE 6 | Immunomodulating biomaterials are effective in wound healing applications. **(A)** Creation of scar and treatment with immunomodulating DexIEME hydrogel. (i) Scar created by third degree burn, (ii) partial excision of scarred skin, (iii) apply hydrogel, (iv) wound healed after 5 weeks. **(B)** (i) H&E Stained scarred and regenerated skin, (ii) regenerated skin shows development of hair follicles, (iii) scarred skin lacking normal skin structure. Scale bars = 200 μm. Reprinted with permission from Sun (2017). Copyright 2017, John Wiley & Sons. **(C)** Macrophage polarization employed by treatment with Matriderm® (MD), PCL scaffolds, and PHB electrospun scaffolds. Nuclei were stained with DAPI (blue). M1($CCR7^+CD68^+$)/M2($CD206^+CD68^+$) ratio of macrophages present in the scaffold surrounding region 14 days following implantation. Scale bars = 50 μm (*$p < 0.05$, **$p < 0.01$). Reprinted with permission from Castellano et al. (2018). Copyright 2018, John Wiley & Sons.

the skin to further understand skin homeostasis. This branch places emphasis on studying transdermal drug administration and development of skin diseases for therapeutic intervention. Considering how common transdermal drug therapy is, it is necessary to optimize the drug delivery mechanism though the skin in order to enhance the outcome of the therapy (Savoji et al., 2014b; Flaten et al., 2015). This of course requires complex and robust predictive models which can realistically mimic the skin's intrinsic properties. The other branch focuses on developing validated *in vitro* skin models for risk assessment and toxicological screening. Strict legal and ethical restrictions on animal and human skin use and testing have created the basis for advancements in this branch, which in turn have led to the creation of optimal skin models (Hewitt et al., 2013). As a whole, these efforts have led to sophisticated *in vitro* skin models which are widely used for clinical applications, advancements in wound healing and as a test system for pharmaceutical and cosmetic research (Xie et al., 2010).

In vitro skin substitutes use 3D arranged human cells to mimic cell-cell and cell-matrix interactions. Most developed models are intended toward modeling the healthy skin with intact barrier properties, with only a few models mimicking the compromised skin. *In vitro* models can be broadly categorized into lipid and non-lipid based model membranes. Non-lipid based models are mainly silicon model membranes, which are used in a wide variety of studies to evaluate different methods and mechanisms of drug transport across the skin (Watkinson et al., 2009; Oliveira et al., 2011, 2012). A diverse range of lipid based models have also been developed. Kansy et al. developed a poly(2-acrylamido-2-methyl-1-propanamide) (PAMPA) (Kansy et al., 1998) membrane containing a phosphatidylcholine coated hydrophobic filter as a membrane barrier, and Sinko and his group enhanced the model to create the skin-PAMPA (Sink et al., 2012) containing synthetic certramides as a replacement for naturally existing ceramides in SC. Tsinman and Sinko further modified skin-PAMPA to predict skin penetration and screen topical formulations (silicone-based gel, silicone and acrylic

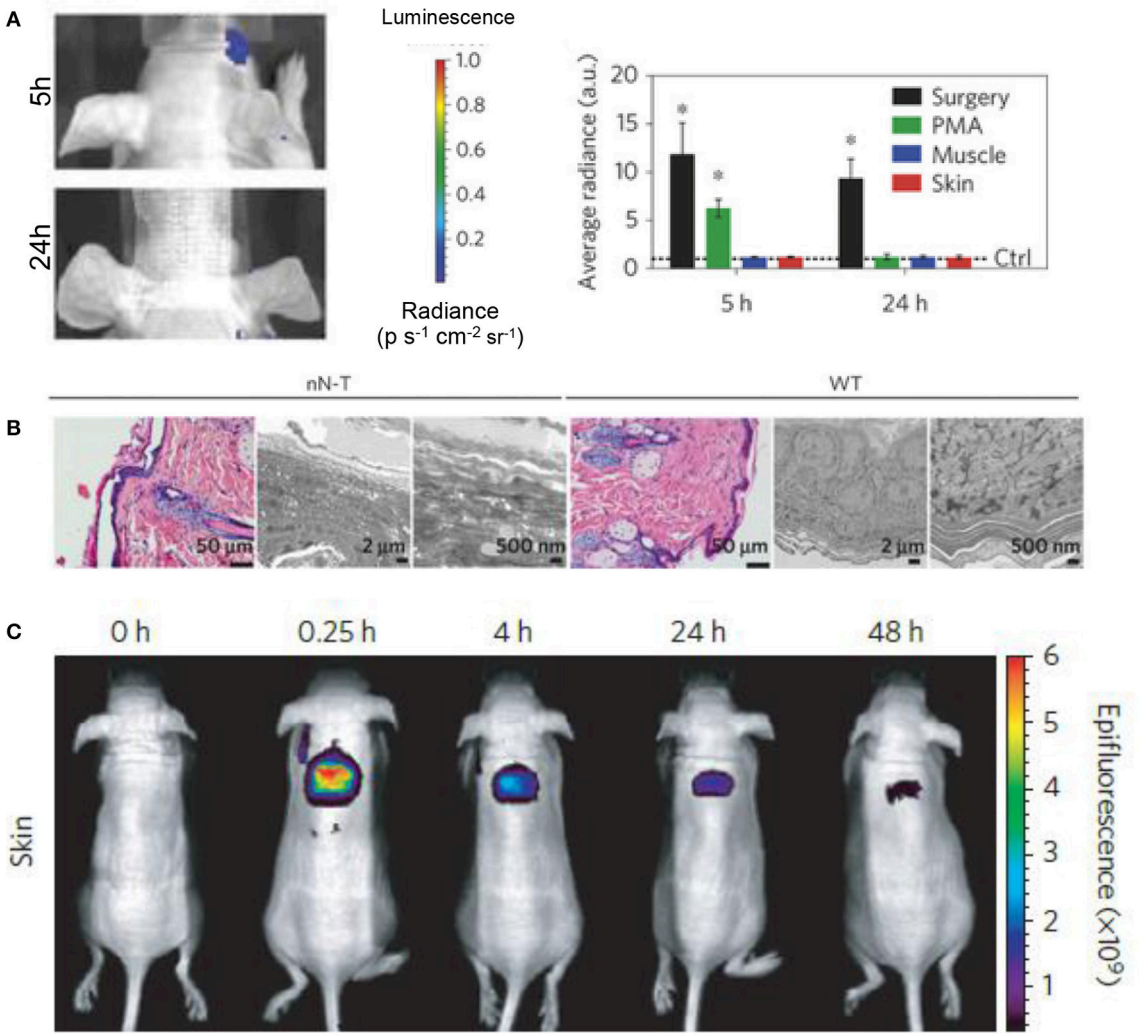

FIGURE 7 | Biomarkers and fluorescent dyes are beneficial in biomaterial risk assessment. **(A)** Imaging and quantification of the luminol luminescence in mice treated with silicon nanoneedles. Phorbol-12-myristate-13-acetate (PMA) treatment and surgical incisions were employed as positive controls for acute inflammation and the data was normalized to the control represented by the dashed line (*$p < 0.05$, $n = 3$). Silicon nanoneedle treatment showed no acute inflammatory response in muscle or skin at 5 and 24 h. **(B)** H&E and transmission electron microscopy (TEM) micrographs of nanoneedle treated (nN-T) and wild-type (WT), or control, tissues show complex structure regenerated by the nanoneedle treatment. **(C)** Localized drug distribution in skin over 48h was shown by delivering fluorescent dyes with silicon nanoneedles. Reprinted with permission from Chiappini et al. (2015). Copyright 2015, Nature publishing Groups.

copolymer) (Tsinman and Sinko, 2013). PVPA is another model designed to mimic the cells of biological barriers using a tight liposome layer on a filter (Flaten et al., 2006). PVPA was further improved by Engesland's work, which resulted in the production of a novel PVPA model which closely mimics the SC barrier of the skin (Engesland et al., 2013, 2015). This model was adopted by Palac et al. to study the effect of vesicle carrier on the skin penetration (Palac et al., 2014). In other efforts, Schurr and his team combined keratinocytes with degradable scaffolds to promote autologous healing (Schurr et al., 2012). Prior to this, Falanga et al. had attempted promoting autologous healing using allogeneic human fibroblasts (Falanga and Sabolinski, 1999).

The majority of skin substitute models are limited to an epidermal layer. These models can be significantly improved by integrating a dermal layer containing fibroblasts into the *in vitro* model. In the skin itself the interaction between fibroblasts and keratinocytes is fundamental to the wound healing process (Falanga et al., 2002). *In vitro* experiments demonstrated that the crosstalk between fibroblasts and keratinocytes promotes the keratinocytes growth by means of soluble growth factors (Groeber et al., 2011). Evidence from studies on skin substitutes have shown that fibroblasts also have a key role in the natural epidermal histogenesis and keratinocytes differentiation is greatly affected in the absence of fibroblasts (Boehnke et al., 2007; Groeber et al., 2011). Bell et al. were the first to describe such a complex model (Bell et al., 1981), which are referred to as full-thickness *in vitro* models. Many different techniques have since been used for the formation of such dermal layers (Parenteau

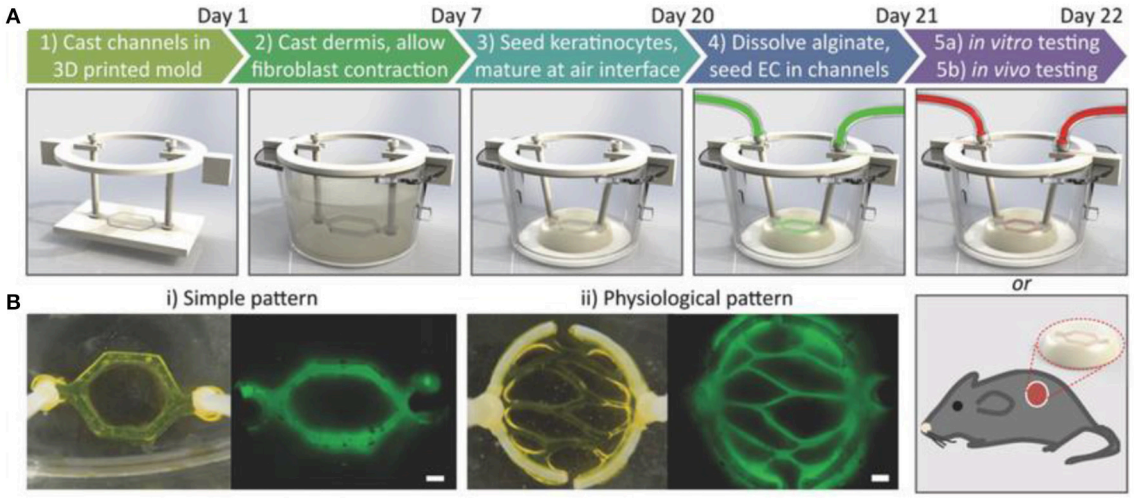

FIGURE 8 | Development of vascularized human skin equivalents. **(A)** Schematic description of the protocol to develop human skin equivalents. **(B)** Two different vasculature patterns were generated using fluorescently tagged alginate. Scale bar: 600 μm. Reprinted with permission from Abaci et al. (2016). Copyright 2016, John Wiley & Sons.

et al., 1992; Sahuc et al., 1996; Stark et al., 2006). The extensive studies carried through within recent years have led to the commercial availability of many *in vitro* skin models (Boyce and Lalley, 2018) such as Apligraf™, StrataGraft™, DermaGraft™ (Frykberg et al., 2015), EpiCel™ (Sood et al., 2010), ReCell™ (Gravante et al., 2007), and TESTSKIN™ (Laska et al., 1992).

Another emerging *in vitro* skin modeling approach is on-chip platforms which help to fabricate more physiologically relevant skin models for better understanding the underlying mechanism of skin diseases and discovery of new therapeutic agents. For example, a multi-organ-on-chip platform for skin and its appendages was fabricated using a multi-chamber microfluidics platform (Maschmeyer et al., 2015). The device was successfully tested for real-time immunohistological analysis and cell metabolic activity measurements. In another study, a simpler model containing bi-layer of keratinocytes-fibroblasts and endothelial cells-fibroblasts between three microfluidic channels was proposed to investigate penetration in skin (Wufuer et al., 2016). Furthermore, a simple full thickness skin-on-a-chip platform using a pumpless microfluidic device was developed to investigate pharmacokinetics of various substances (Abaci et al., 2015). To further mimic physiologically relevant skin model, a perfusable vascularized full-thickness model was also developed to mimic the dermis containing collagen seeded by induced pluripotent stem cells (iPSC) derived endothelial cells (**Figure 8**; Abaci et al., 2016). Overall, skin-on-chip models have shown great promise for substance testing, discovery and screening.

Despite fascinating advancements in the development of *in vitro* skin substitutes, there is still a long path laying ahead for full simulation of all functions and structures of the skin. Current major differences between skin substitutes and the skin itself include the absence of stable vascular and lymphatic networks, skin appendages (such as hair follicles, sweat glands and sebaceous) and hypopigmentation (Boyce and Lalley, 2018). The continuation of current developmental trends promises the correction of the remaining deficiencies in the near future, paving the path for complete replication of skin anatomy and physiology and further enhancement of skin disease and wound treatment.

In Vivo Models for Skin Substitute Testing

Wound healing in human skin is an extremely complex process involving inflammation, re-epithelialization, granulation tissue formation, and dermal remodeling (Martínez-Santamaría et al., 2013). Finding accurate *in vivo* models for this process can be a challenge due to the high cost of *in vivo* work and the differences between animal models and human skin. Common *in vivo* skin tissue models for skin substitute testing include the guinea pig, mouse, rat, and pig. **Table 1** summarizes these models and compares them based on their cost, thickness, hair follicle density, skin attachment, and the wound healing mechanism.

The guinea pig is an *in vivo* model in skin tissue engineering because, like human skin, guinea pig skin exhibits thick epidermal and dermal skin structure (Summerfield et al., 2015). Areas where the guinea pig is lacking in similarity to the human skin are skin-attachment, hair coat, and the healing mechanism. Guinea pigs have a contractile wound healing mechanism whereas humans heal wounds via re-epithelialization. Mice are another species that have been widely used for evaluating the performance and safety of skin substitutes, mainly due to their low cost. Similar to guinea pigs, mouse skin differs from human skin in that it is loosely attached, has a dense coat of hair, has a thin epidermis and dermis, and heals through contraction rather than re-epithelialization (Summerfield et al., 2015). Past research has gone into developing humanized mouse models, in which human keratinocytes and fibroblasts are grafted onto mouse skin to mimic human skin (Martínez-Santamaría et al., 2013). These types of humanized skin models have yet to be used for assessing the efficacy of other skin substitutes. In another study, the ability of a bioprinted skin substitute to differentiate was assessed in immunodeficient athymic mice with excised wounds

TABLE 1 | Comparative properties and cost of *in vivo* wound healing models (Godin and Touitou, 2007; Gainza et al., 2015; Summerfield et al., 2015).

Species	Thickness (mm)	Hair follicle density	Skin attachment	Wound healing mechanism	Cost
Human	2.97	Low	Tight	Re-epithelialization	N/A
Guinea Pig	1-2	High	Loose	Contraction	Medium
Mouse	0.70	High	Loose	Contraction	Low
Rat	2.09	High	Loose	Contraction	Low
Pig	2.5	Low	Tight	Re-epithelialization	High

(Cubo et al., 2016). It was found that the grafted area of skin closely resembled the structure and appearance of native human skin. This exemplifies the usefulness of mice as an *in vivo* model in developing a fully differentiated form of human skin.

Another commonly used *in vivo* model for skin substitute testing are rats. Similarly to mice, they have loosely attached skin, dense hair, and they heal through contraction (Summerfield et al., 2015). Rats offer an affordable *in vivo* model that are widely used for modeling wounds of various types. For example, Sprague-Dawley rats were used to model third degree burn wounds in developing a skin substitute made of collagen seeded with genetically modified immortal keratinocyte cells (Hu et al., 2012). However, there are large differences in the speed at which rats heal when compared to humans and that further investigation is required to verify the potential efficacy for the treatment of human wounds.

Pigs have the most similarities to human skin in that it is firmly attached, has sparse hair follicle distribution, has similar epidermal and dermal thickness, and heals through the process of re-epithelialization (Summerfield et al., 2015). On top of these structural and wound healing similarities, porcine skin also has a similar blood supply and immunological function. The limiting factor for the use of pigs as an *in vivo* model for most researchers is the high cost due to their difficulty in handling, longer gestation time, and large space requirements (Gainza et al., 2015). However, due to their large size, a single pig can act as a model for multiple wound sites. In a study by Shevchenko et al. pigs were chosen for their similarities with human skin and each pig modeled 6 separate wound sites to assess the efficacy of a gelatin scaffold as a dermal replacement (Shevchenko et al., 2014). However, their animal study did not go as planned and the pseudo-epidermal silicone layer on their models peeled off, exposing their gelatin dermal scaffolds. They did not repeat the experiment and speculated, based on their *in vitro* results that their treatment has the potential to accelerate wound healing in human skin. This exemplifies the importance of being completely prepared before conducting expensive *in vivo* testing.

ROADMAP FOR BIOMATERIAL SELECTION, RISK ASSESSMENT AND TESTING

Any medical device and therapeutic strategy should first pass some regulatory obligations to reach the market. Therefore, devices are categorized as Class I, II, or III based on the level of regulation required to guarantee their safety and efficacy (Morrison et al., 2015). Low-risk Class I devices only undergo general and simple regulatory controls, while high-risk Class III devices (e.g., most implants), are subjected to the most rigorous regulations. The latter are usually permitted an initial Investigational Device Exemption (IDE) to be employed in a FDA-regulated clinical trial to gather required safety and efficacy data prior to market application. These devices can obtain premarket approval (PMA) pathway for commercialization (Morrison et al., 2015).

Skin substitutes are regulated by the regulating agency in different regions of the world including the US Food and Drug Administration (FDA), Health Canada and regional and centralized regulatory bodies in the European Union (EU) (Van Norman, 2016). Full thickness skin grafts combine scaffolds, multiple cell types and sources. As each of these elements must be regulated, a lengthy and complicated regulatory process has been enforced for the commercialization process. For example, different regulatory centers are involved to evaluate, review and register a new skin graft in the USA including: The Center for Biologics Evaluation and Research (CBER), The Center for Devices and Radiologic Health (CDRH), and The Center for Drug Evaluation and Research (CDER).

Biomaterials that are used in fabrication of the skin grafts must be evaluated according to the FDA Quality System Regulation (QSR)/Medical Device Good Manufacturing Practices (GMP) for industry manufactured devices (Lincoln, 2010). Furthermore, the cells that undergo culture, expansion, and/or differentiation, or combined with biomaterial scaffold must meet the CBER premarket approval requirement (PMA). On the other hand, if a graft is fabricated by the emerging manufacturing technologies (e.g., 3D printing, electrospinning, microfluidics, etc.), a number of quality measures have to be taken into account to ensure repeatability of the process and reliability of the grafts. This data could facilitate the review process by the regulating bodies and expedite the PMA pathway.

The FDA has been proactively involved in communicating with different bodies in research and development settings in industries and academics to define a clear roadmap for commercialization of a medical device to the market. For example, tissue-engineered medical products (TEMPs) are being reviewed by a specific collaborative commission with the FDA through the American Society for Testing and Materials (ASTM).

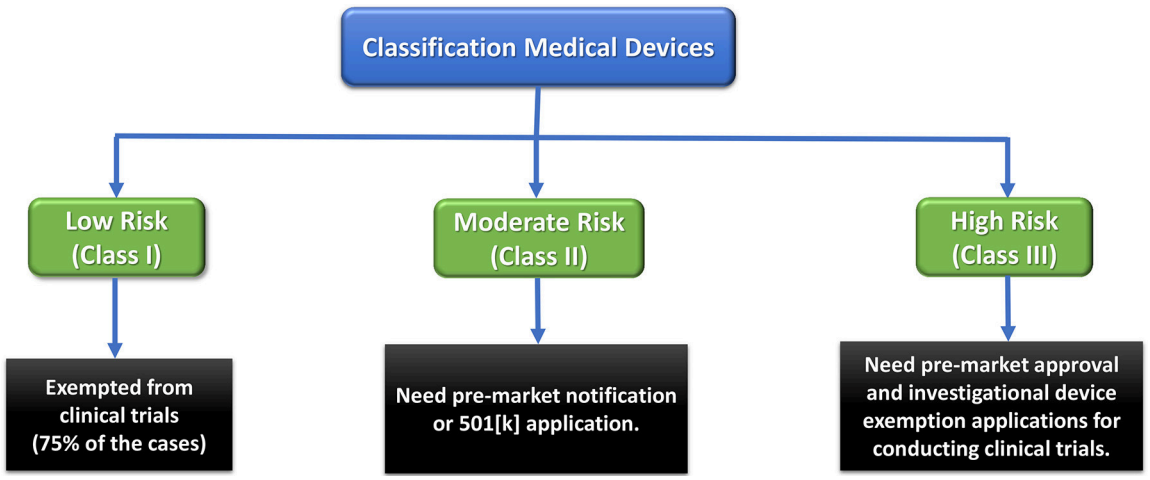

FIGURE 9 | Schematic of FDA medical device approval roadmap.

The mandate of this commission is to define new materials and provision of standard methods for calibration and testing of these materials including tissue engineered skin grafts according to the "Standard Guide for Classification of Therapeutic Skin Substitutes."

In addition, the Office of Combination Products review the new combination therapies and endorse their safety and efficacy in collaboration with different centers (e.g., Centers for Human Therapeutics) and regulating offices. This office assigns the premarket review and evaluation of a combination product based on determination of its primary mode of action (PMOA). For example, if the main PMOA of a combination product attributes to the biological product, the related agency responsible for the biological product will have primary role in regulating the combination product. However, if the PMOA of a combination product is diverse, the regulating agencies have to take the difficult and extensive decision (i.e., trade-off between rapid access to novel products for the patients in urgent need and appropriate promises on safety and efficacy) about which agency is responsible for reviewing and regulating this specific therapy.

Although extensive efforts have been made to clarify the medical devices regulatory pathway to the market, there has been an unmet need to expedite and facilitate this process in order to provide novel therapeutic strategies for patients with life-threatening diseases. To this end, the FDA has mandated some coherent and flexible designations to address the lengthy regulating process for the innovative medical devices including Fast Track development, Breakthrough Therapy designation, Accelerated Approval and Priority Review designation for drugs. In addition to the aforementioned, the most recent Regenerative Medicine Advanced Therapy (RMAT) designation based on the twenty-first Century Cures Act (Cures Act) has the mission to address the lengthy regulating process for innovative medical devices. **Figure 9** shows FDA medical device approval roadmap.

CONCLUSION AND FUTURE PERSPECTIVE

Tissue engineering of skin is a well-established but growing field in regenerative medicine. There have been tremendous efforts to employ emerging micro- and nano-fabrication strategies, biomaterials synthesis, functionalization techniques and patient specific cells' utilization to fabricate remarkable potential functional skin substitutes that could tackle the challenges facing currently available skin grafts. For example, there have been many reports on resembling of the ECM with combining nontoxic immunomodulatory biomaterials, growth factors, proteins and biomolecules along with the advanced processing strategies. Although many newly synthesized biomaterials have been investigated as the scaffolds in wound dressings, only natural biopolymers such as collagen, gelatin, and chitosan have been extensively used for the commercial skin grafts (Sheikholeslam et al., 2017). However, these materials suffer from low mechanical stiffness and fast degradation which limits their applications in clinics. On the other hand, synthetic biomaterials such as poly vinylpyrrolidone (PVP), PCL, poly ethylene glycol (PEG), poly lactic acid (PLA) possess promising mechanical properties including elasticity and contractibility, similar to those of native skin with less biocompatibility and *in vitro* and *in vivo* functionality and performance. Therefore, researchers have attempted to address these issues surrounding tuning mechanical and structural properties of wound dressings by synthesizing novel elastomeric biodegradable biomaterial and/or optimizing the properties of the existing biomaterials.

However, there are yet unresolved complications such as wound contraction, impaired vascularization, scaring, and high cost associated with these products that need to be carefully addressed (Ho et al., 2017).Vascularization is vital for the success of artificial skin grafts which leads to increased life span and better integration with host skin. *In vivo* vasculogenesis of the grafts can be promoted by incorporating cells such as

endothelial cells and mesenchymal and adipose-derived stem cells to the scaffolding materials (Jackson et al., 2012; Marino et al., 2014), using angiogenic biomolecules (Briquez et al., 2015) and tuning the structural properties of the scaffolds (Bonvallet et al., 2015). On the other hand, application of the cell-based skin substitutes has been limited in clinics due to the time consuming and labor-intensive process and short shelf-life of the products. Therefore, *in situ* regeneration could be a promising alternative in the near future. The advancement of innovative fabrication techniques such as in situ electrospinning and 3D printing and microfluidics along with the emergence of the new functional biomaterials could provide the on-demand fabrication of skin substitutes that are tailored to a patient's wounds. It is possible to recruit stem cells and progenitor cells from the wound site by using bioactive materials with suitable morphology *in situ*, to encourage migration/infiltration of the residing cells and differentiation of stem cells into favorite cell types and finally regenerate newly-formed functional skin.

Translation of such artificial skins to the clinics, manufactured with the novel technologies stated above, needs predictive test methods and appropriate standards and regulations to ensure the reproducibility and functional reliability of the grafts.

In general, optimal functional skin substitutes need to possess the improved adhesion of cultured keratinocytes to the wound bed, improved neovascularization and enhanced resistance to the wound contraction and fibrosis. Although these criteria have almost been addressed by the exhaustive efforts during the past decades, other complicated challenges such as reconstruction of skin appendages, thermoregulation, touch, excretion and the esthetic function remain to be solved.

AUTHOR CONTRIBUTIONS

MA is the corresponding author of this work. He developed the outline with HS edited the paper. HS prepared the outline, led the project and wrote the paper. BG and MH wrote the manuscripts.

ACKNOWLEDGMENTS

MA and BG would like to thank the Canadian Institutes of Health Researches (CIHR). MA would also like to thank the Canadian Foundation for Innovation for supporting this work. HS gratefully acknowledges the Canadian Institutes of Health Research (CIHR) and the Fonds de recherche du Québec - Nature et Technologies (FRQNT) Postdoctoral Fellowships.

REFERENCES

Abaci, H. E., Gledhill, K., Guo, Z., Christiano, A. M., and Shuler, M. L. (2015). Pumpless microfluidic platform for drug testing on human skin equivalents. *Lab Chip* 15, 882–888. doi: 10.1039/C4LC00999A

Abaci, H. E., Guo, Z., Coffman, A., Gillette, B., Lee, W. H., Sia, S. K., et al. (2016). Human Skin Constructs with Spatially Controlled Vasculature Using Primary and iPSC-Derived Endothelial Cells. *Adv. Healthc. Mater.* 5, 1800–1807. doi: 10.1002/adhm.201500936

Akbari, M., Tamayol, A., Bagherifard, S., Serex, L., Mostafalu, P., Faramarzi, N., et al. (2016). Textile technologies and tissue engineering: a path toward organ weaving. *Adv. Healthc. Mater.* 5, 751–766. doi: 10.1002/adhm.201500517

Albanna, M., and Holmes IV, J. H. (2016). *Skin Tissue Engineering and Regenerative Medicine*. New York, NY: Academic Press.

Ansari, M., Kordestani, S. S., Nazralizadeh, S., and Eslami, H. (2018). Biodegradable cell-seeded collagen based polymer scaffolds for wound healing and skin reconstruction. *J. Macromol. Sci. B.* 57, 100–109. doi: 10.1080/00222348.2018.1435617

Atiyeh, B. S., and Costagliola, M. (2007). Cultured epithelial autograft (CEA) in burn treatment: three decades later. *Burns* 33, 405–413. doi: 10.1016/j.burns.2006.11.002

Bell, E., Ehrlich, H. P., Buttle, D. J., and Nakatsuji, T. (1981). Living tissue formed in vitro and accepted as skin-equivalent tissue of full thickness. *Science* 211, 1052–1054. doi: 10.1126/science.7008197

Bello, Y. M., Falabella, A. F., and Eaglstein, W. H. (2001). Tissue-engineered skin: current status in wound healing. *Am. J. Clin. Dermatol.* 2, 305–313. doi: 10.2165/00128071-200102050-00005

Bhowmick, S., Rother, S., Zimmermann, H., Lee, P. S., Moeller, S., Schnabelrauch, M., et al. (2017). Biomimetic electrospun scaffolds from main extracellular matrix components for skin tissue engineering application–The role of chondroitin sulfate and sulfated hyaluronan. *Mater. Sci. Eng. C*, 79, 15–22. doi: 10.1016/j.msec.2017.05.005

Blanpain, C., Lowry, W. E., Geoghegan, A., Polak, L., and Fuchs, E. (2004). Self-renewal, multipotency, and the existence of two cell populations within an epithelial stem cell niche. *Cell* 118, 635–648. doi: 10.1016/j.cell.2004.08.012

Boehnke, K., Mirancea, N., Pavesio, A., Fusenig, N. E., Boukamp, P., and Stark, H. J. (2007). Effects of fibroblasts and microenvironment on epidermal regeneration and tissue function in long-term skin equivalents. *Eur. J. Cell Biol.* 86, 731–746. doi: 10.1016/j.ejcb.2006.12.005

Bonvallet, P. P., Schultz, M. J., Mitchell, E. H., Bain, J. L., Culpepper, B. K., Thomas, S. J., et al. (2015). Microporous dermal-mimetic electrospun scaffolds pre-seeded with fibroblasts promote tissue regeneration in full-thickness skin wounds. *PLoS ONE* 10:e0122359. doi: 10.1371/journal.pone.0122359

Bouwstra, J. A., and Ponec, M. (2006). The skin barrier in healthy and diseased state. *Biochim. Biophys.Acta* 1758, 2080–2095. doi: 10.1016/j.bbamem.2006.06.021

Bouwstra, J. A., Honeywell-Nguyen, P. L., Gooris, G. S., and Ponec, M. (2003). Structure of the skin barrier and its modulation by vesicular formulations. *Prog. Lipid Res.* 42, 1–36. doi: 10.1016/S0163-7827(02)00028-0

Boyce, S. T., and Lalley, A. L. (2018). Tissue engineering of skin and regenerative medicine for wound care. *Burns Trauma* 6:4. doi: 10.1186/s41038-017-0103-y

Briquez, P. S., Hubbell, J. A., and Martino, M. M. (2015). Extracellular matrix-inspired growth factor delivery systems for skin wound healing. *Adv. Wound Care* 4, 479–489. doi: 10.1089/wound.2014.0603

Burke, J. F., Yannas, I. V., Quinby, W. C., Bondoc, C. C., and Jung, W. K. (1981). Successful use of a physiologically acceptable artificial skin in the treatment of extensive burn injury. *Ann. Surg.* 194, 413–428. doi: 10.1097/00000658-198110000-00005

Castellano, D., Sanchis, A., Blanes, M. D., Pérez del Caz, M., Ruiz-Saurí, A., Piquer-Gil, M., et al. (2018). Electrospun poly (hydroxybutyrate) scaffolds promote engraftment of human skin equivalents via macrophage M2 polarization and angiogenesis. *J. Tissue Eng. Regen. Med.* 12, e983–e994. doi: 10.1002/term.2420

Chiappini, C., De Rosa, E., Martinez, J. O., Liu, X., Steele, J., Stevens, M., et al. (2015). Biodegradable silicon nanoneedles delivering nucleic acids intracellularly induce localized *in vivo* neovascularization. *Nat. Mater.* 14:532. doi: 10.1038/nmat4249

Choi, H. M. C., Cheing, A. K. k., Ng, G. Y., and Cheing, G. L y., (2018). Effects of pulsed electromagnetic field (PEMF) on the tensile biomechanical properties of diabetic wounds at different phases of healing. *PLoS ONE* 13:e0191074. doi: 10.1371/journal.pone.0191074

Chua, A. W. C., Khoo, Y. C., Tan, B. K., Tan, K. C., Foo, C. L., and Chong, S. J. (2016). Skin tissue engineering advances in severe burns: review and therapeutic applications. *Burns Trauma* 4:3. doi: 10.1186/s41038-016-0027-y

Chung, L., Maestas., D. R., Housseau, F., and Elisseeff, J. H. (2017). Key players in the immune response to biomaterial scaffolds for regenerative medicine. *Adv. Drug Deliv. Rev.* 114, 184–192. doi: 10.1016/j.addr.2017.07.006

Cubo, N., Garcia, M., Del Caizo, J. F., Velasco, D., and Jorcano, J. L. (2016). 3D bioprinting of functional human skin: production and *in vivo* analysis. *Biofabrication* 9:015006. doi: 10.1088/1758-5090/9/1/015006

Dong, R., Yu, G., Guan, Y., Wang, B., Huang, J., Deng, S., et al. (2016). Occurrence and discharge of pharmaceuticals and personal care products in dewatered sludge from WWTPs in Beijing and Shenzhen. *Emerging Contaminants* 2, 1–6. doi: 10.1016/j.emcon.2015.10.003

Dong, R. H., Jia, Y. X., Qin, C. C., Zhan, L., Yan, X., Cui, L., et al. (2016). *In situ* deposition of a personalized nanofibrous dressing via a handy electrospinning device for skin wound care. *Nanoscale*, 8, 3482–3488. doi: 10.1039/C5NR08367B

Engesland, A., Škalko-Basnet, N., and Flaten, G. E. (2015). PVPA and EpiSkin® in assessment of drug therapies destined for skin administration. *J. Pharm. Sci.* 104, 1119–1127. doi: 10.1002/jps.24315

Engesland, A., Skar, M., Hansen, T., Škalko-basnet, N., and Flaten, G. E. (2013). New applications of phospholipid vesicle-based permeation assay: permeation model mimicking skin barrier. *J. Pharm. Sci.* 102, 1588–1600. doi: 10.1002/jps.23509

Falanga, V., and Sabolinski, M. (1999). A bilayered living skin construct (APLIGRAF®) accelerates complete closure of hard-to-heal venous ulcers. *Wound Repair Regenerat.* 7, 201–207. doi: 10.1046/j.1524-475X.1999.00201.x

Falanga, V., Isaacs, C., Paquette, D., Downing, G., Kouttab, N., Butmarc, J., et al. (2002). Wounding of bioengineered skin: cellular and molecular aspects after injury. *J. Investig. Dermatol.* 119, 653–660. doi: 10.1046/j.1523-1747.2002.01865.x

Flaten, G. E., Bunjes, H., Luthman, K., and Brandl, M. (2006). Drug permeability across a phospholipid vesicle-based barrier: 2. Characterization of barrier structure, storage stability and stability towards pH changes. *Eur. J. Pharm. Sci.* 28, 336–343. doi: 10.1016/j.ejps.2006.03.008

Flaten, G. E., Palac, Z., Engesland, A., Filipović-Grcić, J., Vanić, Ž., and Škalko-Basnet, N. (2015). *In vitro* skin models as a tool in optimization of drug formulation. *Eur. J. Pharm. Sci.* 75, 10–24. doi: 10.1016/j.ejps.2015.02.018

Wysocki AB., (2002). Evaluating and managing open skin wounds: colonization versus infection. *AACN Clin. Iss.* 13, 382–397. doi: 10.1097/00044067-200208000-00005

Frykberg, R. G., Marston, W. A., and Cardinal, M. (2015). The incidence of lower-extremity amputation and bone resection in diabetic foot ulcer patients treated with a human fibroblast-derived dermal substitute. *Adv. Skin Wound Care* 28, 17–20. doi: 10.1097/01.ASW.0000456630.12766.e9

Gainza, G., Villullas, S., Pedraz, J. L., Hernandez, R. M., and Igartua, M. (2015). Advances in drug delivery systems (DDSs) to release growth factors for wound healing and skin regeneration. *Nanomedicine* 11, 1551–1573. doi: 10.1016/j.nano.2015.03.002

Gallico, G. G., O'Connor, N. E., Compton, C. C., Kehinde, O., and Green, H. (1984). Permanent coverage of large burn wounds with autologous cultured human epithelium. *N. Engl. J. Med.* 311, 448–451. doi: 10.1056/NEJM198408163110706

Gentzkow, G. D., Iwasaki, S. D., Hershon, K. S., Mengel, M., Prendergast, J. J., Ricotta, J. J., et al. (1996). Use of dermagraft, a cultured human dermis, to treat diabetic foot ulcers. *Diab. Care* 19, 350–354. doi: 10.2337/diacare.19.4.350

Geraili, A., Jafari, P., Hassani, M. S., Araghi, B. H., Mohammadi, M. H., Ghafari, A. M., et al. (2017). *Controlling Differentiation of Stem Cells for Developing Personalized Organ-on-Chip Platforms*. *Adv. Healthcare Mater.* 7:1700426. doi: 10.1002/adhm.201700426

Godin, B., and Touitou, E. (2007). Transdermal skin delivery: predictions for humans from *in vivo*, *ex vivo* and animal models. *Adv. Drug Deliv. Rev.* 59, 1152–1161. doi: 10.1016/j.addr.2007.07.004

Gravante, G., Di Fede, M. C., Araco, A., Grimaldi, M., De Angelis, B., Arpino, A., et al. (2007). A randomized trial comparing ReCell® system of epidermal cells delivery versus classic skin grafts for the treatment of deep partial thickness burns. *Burns* 33, 966–972. doi: 10.1016/j.burns.2007.04.011

Griffiths, M., Ojeh, N., Livingstone, R., Price, R., and Navsaria, H. (2004). Survival of Apligraf in acute human wounds. *Tissue Eng.* 10, 1180–1195. doi: 10.1089/ten.2004.10.1180

Groeber, F., Holeiter, M., Hampel, M., Hinderer, S., and Schenke-Layland, K. (2011). Skin tissue engineering—*in vivo* and *in vitro* applications. *Adv. Drug Deliv. Rev.* 63, 352–366. doi: 10.1016/j.addr.2011.01.005

Groen, D., Poole, D. S., Gooris, G. S., and Bouwstra, J. A. (2011). Investigating the barrier function of skin lipid models with varying compositions. *Eur. J. Pharm. Biopharm.* 79, 334–342. doi: 10.1016/j.ejpb.2011.05.007

Gross, S., Gammon, S. T., Moss, B. L., Rauch, D., Harding, J., Heinecke, J. W., et al. (2009). Bioluminescence imaging of myeloperoxidase activity *in vivo*. *Nat. Med.* 15:455. doi: 10.1038/nm.1886

Grover, N., and Tomar, L. K. (2016). Biotextiles for tissue engineering. *Front. Biomaterials* 2:124. doi: 10.2174/978168108195311602 0009

Hadjizadeh, A., Savoji, H., and Ajji, A. (2016). A facile approach for the mass production of submicro/micro poly (Lactic Acid) fibrous mats and their cytotoxicity test towards neural Stem Cells. *Biomed Res. Int.* 2016, 1–12. doi: 10.1155/2016/8921316

Hakimi, N., Cheng, R., Leng, L., Sotoudehfar, M., Ba, P. Q., Bakhtyar, N., et al., (2018). Handheld skin printer: *in-situ* formation of planar biomaterials and tissues. *Lab on a Chip*. 10, 1440–1451. doi: 10.1039/C7LC0 1236E

Hansbrough, J. F., Morgan, J. L., Greenleaf, G. E., and Bartel, R. (1993). Composite grafts of human keratinocytes grown on a polyglactin mesh-cultured fibroblast dermal substitute function as a bilayer skin replacement in full-thickness wounds on athymic mice. *J. Burn Care Rehabil.* 14, 485–494. doi: 10.1097/00004630-199309000-00001

Hatta, I., Ohta, N., Inoue, K., and Yagi, N. (2006). Coexistence of two domains in intercellular lipid matrix of stratum corneum. *Biochim. Biophys. Acta* 1758, 1830–1836. doi: 10.1016/j.bbamem.2006.08.014

Hernon, C. A., Harrison, C. A., Thornton, D. J., and MacNeil, S. (2007). Enhancement of keratinocyte performance in the production of tissue-engineered skin using a low-calcium medium. *Wound Repair Regen.* 15, 718–726. doi: 10.1111/j.1524-475X.2007.00275.x

Hewitt, N. J., Edwards, R. J., Fritsche, E., Goebel, C., Aeby, P., Scheel, J., et al. (2013). Use of human *in vitro* skin models for accurate and ethical risk assessment: metabolic considerations. *Toxicol. Sci.* 133, 209–217. doi: 10.1093/toxsci/kft080

Ho, J., Walsh, C., Yue, D., Dardik, A., and Cheema, U. (2017). Current advancements and strategies in tissue engineering for wound healing: a comprehensive review. *Adv. Wound Care* 6, 191–209. doi: 10.1089/wound.2016.0723

Hu, D. H., Zhang, Z. F. Zhang, Y. G., Zhang, W. F., Wang, H. T., Cai, W. X., et al. (2012). A potential skin substitute constructed with hEGF gene modified HaCaT cells for treatment of burn wounds in a rat model. *Burns* 38, 702–712. doi: 10.1016/j.burns.2011.12.014

Hu, M. S., Maan, Z. N., Wu, J.-C., Rennert, R. C., Hong, W. X., Lai, T. S., et al. (2014). Tissue engineering and regenerative repair in wound healing. *Ann. Biomed. Eng.* 42, 1494–1507. doi: 10.1007/s10439-014-1010-z

Huang, S., Yao, B., Xie, J., and Fu, X. (2016). 3D bioprinted extracellular matrix mimics facilitate directed differentiation of epithelial progenitors for sweat gland regeneration. *Acta Biomater.* 32, 170–177. doi: 10.1016/j.actbio.2015.12.039

Huang, Y., Zhang, X. F., Gao, G., Yonezawa, T., and Cui, X., (2017). 3D bioprinting and the current applications in tissue engineering. *Biotechnol. J.* 12:1600734. doi: 10.1002/biot.201600734

Jackson, W. M., Nesti, L. J., and Tuan, R. S. (2012). Mesenchymal stem cell therapy for attenuation of scar formation during wound healing. *Stem Cell Res. Ther.* 3:20. doi: 10.1186/scrt111

Kansy, M., Senner, F., and Gubernator, K. (1998). Physicochemical high throughput screening: parallel artificial membrane permeation assay in the description of passive absorption processes. *J. Med. Chem.* 41, 1007–1010. doi: 10.1021/jm970530e

Karimi, M., Bahrami, S., Mirshekari, H., Basri, S. M. M., Nik, A. B., Aref, A. R., et al. (2016). Microfluidic systems for stem cell-based neural tissue engineering. *Lab. Chip* 16, 2551–2571. doi: 10.1039/C6LC00489J

Korrapati, P. S., Karthikeyan, K., Satish, A., Krishnaswamy, V. R., Venugopal, J. R., and Ramakrishna, S. (2016). Recent advancements in nanotechnological strategies in selection, design and delivery of biomolecules for skin regeneration. *Materials Sci. Eng. C* 67, 747–765. doi: 10.1016/j.msec.2016.05.074

Kuna, V. K., Padma, A. M., Håkansson, J., Nygren, J., Sjöback, R., Petronis, S., et al. (2017). Significantly accelerated wound healing of full-thickness skin using a novel composite gel of porcine acellular dermal matrix and human peripheral blood cells. *Cell Transplant.* 26, 293–307. doi: 10.3727/096368916X692690

Laska, D., Poulsen, R., Horn, J., Meador, V., and Hoover, D. (1992). An evaluation of TESTSKIN: an alternative dermal irritation model. *In Vitro Toxicol.* 5, 177–189.

Limongi, T., Schipani, R., Di Vito, A., Giugni, A., Francardi, M., Torre, B., et al. (2015). Photolithography and micromolding techniques for the realization of 3D polycaprolactone scaffolds for tissue engineering applications. *Microelectron. Eng.* 141, 135–139. doi: 10.1016/j.mee.2015.02.030

Lin, P.-H., Sermersheim, M., Li, H., Lee, P. H. U., Steinberg, S.M., and Ma, J. (2018). Zinc in wound healing modulation. *Nutrients* 10:16. doi: 10.3390/nu10010016

Lincoln, J. E. (2010). The 510 (k): its purpose, compilation, and submission. *J. Valid. Technol.* 16:24.

Lone, A. M., Zaroo, M. I., Laway, B. A., Pala, N. A., Bashir, S. A., and Rasool, A. (2014). Vacuum-assisted closure versus conventional dressings in the management of diabetic foot ulcers: a prospective case–control study. *Diabet. Foot Ankle* 5:23345. doi: 10.3402/dfa.v5.23345

Lu, Z. H., Zhao, D. M., and Li, C. S. (2017). Preparation and characterization of silk fibroin based antibacterial biotextiles as wound dressing. *Mater. Sci. Forum.* 898, 2095–2100. doi: 10.4028/www.scientific.net/MSF.898.2095

Ma, L., Gao, C., Mao, Z., Zhou, J., Shen, J., Hu, X., et al. (2003). Collagen/chitosan porous scaffolds with improved biostability for skin tissue engineering. *Biomaterials* 24, 4833–4841. doi: 10.1016/S0142-9612(03)00374-0

MacNeil, S. (2007). Progress and opportunities for tissue-engineered skin. *Nature* 445, 874–880. doi: 10.1038/nature05664

Mahmoudi, N., Eslahi, N., Mehdipour, A., Mohammadi, M., Akbari, M., Samadikuchaksaraei, A., et al. (2017). Temporary skin grafts based on hybrid graphene oxide-natural biopolymer nanofibers as effective wound healing substitutes: pre-clinical and pathological studies in animal models. *J. Mater. Sci.* 28:73. doi: 10.1007/s10856-017-5874-y

Marino, D., Luginbühl, J., Scola, S., Meuli, M., and Reichmann, E. (2014). Bioengineering dermo-epidermal skin grafts with blood and lymphatic capillaries. *Sci. Trans. Med.* 6:221ra14–221ra14. doi: 10.1126/scitranslmed.3006894

Martínez-Santamaría, L., Conti, C. J., Llames, S., García, E., Retamosa, L., Holguín, A., et al. (2013). The regenerative potential of fibroblasts in a new diabetes-induced delayed humanised wound healing model. *Exp. Dermatol.* 22, 195–201. doi: 10.1111/exd.12097

Maschmeyer, I., Lorenz, A. K., Schimek, K., Hasenberg, T., Ramme, A. P., Hübner, J., et al. (2015). A four-organ-chip for interconnected long-term co-culture of human intestine, liver, skin and kidney equivalents. *Lab Chip* 15, 2688–2699. doi: 10.1039/C5LC00392J

Masukawa, Y., Narita, H., Shimizu, E., Kondo, N., Sugai, Y., Oba, T., et al. (2008). Characterization of overall ceramide species in human stratum corneum. *J. Lipid Res.* 49, 1466–1476. doi: 10.1194/jlr.M800014-JLR200

Mathes, S. H., Ruffner, H., and Graf-Hausner, U. (2014). The use of skin models in drug development. *Adv. Drug Deliv. Rev.* 69, 81–102. doi: 10.1016/j.addr.2013.12.006

Midwood, K. S., Williams, L. V., and Schwarzbauer, J. E. (2004). Tissue repair and the dynamics of the extracellular matrix. *Int. J. Biochem. Cell Biol.* 36, 1031–1037. doi: 10.1016/j.biocel.2003.12.003

Mirani, B., Pagan, E., Currie, B., Siddiqui, M. A., Hosseinzadeh, R., Mostafalu, P., et al. (2017). An advanced multifunctional hydrogel-based dressing for wound monitoring and drug delivery. *Adv. Healthc. Mater.* 6:1700718. doi: 10.1002/adhm.201700718

Mohammadi, M. H., Heidary Araghi, B. H., Beydaghi, V., Geraili, A., Moradi, F., Jafari, P., et al. (2016). Skin diseases modeling using combined tissue engineering and microfluidic technologies. *Adv. Healthc. Mater.* 5, 2459–2480. doi: 10.1002/adhm.201600439

Monteiro, I. P., Shukla, A., Marques, A. P., Reis, R. L., and Hammond, P. T. (2015). Spray-assisted layer-by-layer assembly on hyaluronic acid scaffolds for skin tissue engineering. *J. Biomed. Mater. Res. A* 103, 330–340. doi: 10.1002/jbm.a.35178

Morrison, R. J., Kashlan, K. N., Flanangan, C. L., Wright, J. K., Green, G. E., Hollister, S. J., et al. (2015). Regulatory considerations in the design and manufacturing of implantable 3D-Printed medical devices. *Clin. Transl. Sci.* 8, 594–600. doi: 10.1111/cts.12315

Moustafa, M., Bullock, A. J., Creagh, F. M., Heller, S., Jeffcoate, W., Game, F., et al. (2007). Randomized, controlled, single-blind study on use of autologous keratinocytes on a transfer dressing to treat nonhealing diabetic ulcers. *Regen. Med.* 2, 887–902. doi: 10.2217/17460751.2.6.887

Navarro, F. A., Stoner, M. L., Park, C. S., Huertas, J. C., Lee, H. B., Wood, F. M., et al. (2000). Sprayed keratinocyte suspensions accelerate epidermal coverage in a porcine microwound model. *J. Burn Care Rehabil.* 21, 513–518. doi: 10.1097/00004630-200021060-00007

Ng, W. L., Wang, S., Yeong, W. Y., and Naing, M. W. (2016). Skin bioprinting: impending reality or fantasy? *Trends Biotechnol.* 34, 689–699. doi: 10.1016/j.tibtech.2016.04.006

Oliveira, G., Beezer, A. E., Hadgraft, J., and Lane, M. E. (2011). Alcohol enhanced permeation in model membranes. Part II. Thermodynamic analysis of membrane partitioning. *Int. J. Pharm.* 420, 216–222. doi: 10.1016/j.ijpharm.2011.08.037

Oliveira, G., Hadgraft, J., and Lane, M. (2012). The role of vehicle interactions on permeation of an active through model membranes and human skin. *Int. J. Cosmet. Sci.* 34, 536–545. doi: 10.1111/j.1468-2494.2012.00753.x

O'Neill, A. T., Monteiro-Riviere, N. A., and Walker, G. M. (2008). Characterization of microfluidic human epidermal keratinocyte culture. *Cytotechnology* 56:197. doi: 10.1007/s10616-008-9149-9

Palac, Z., Engesland, A., Flaten, G. E., Škalko-Basnet, N., Filipović-Grčić, J., and Ž., Vanić (2014). Liposomes for (trans) dermal drug delivery: the skin-PVPA as a novel *in vitro* stratum corneum model in formulation development. *J. Liposome Res.* 24, 313–322. doi: 10.3109/08982104.2014.899368

Papini, R. (2004). ABC of burns: management of burn injuries of various depths. *Br. Med. J.* 329:158. doi: 10.1136/bmj.329.7458.158

Parenteau, N. L., Bilbo, P., Nolte, C. J., Mason, V. S., and Rosenberg, M. (1992). The organotypic culture of human skin keratinocytes and fibroblasts to achieve form and function. *Cytotechnology* 9, 163–171. doi: 10.1007/BF02521744

Pedde, R. D., Mirani, B., Navaei, A., Styan, T., Wong, S., Mehrali, M., et al. (2017). Emerging biofabrication strategies for engineering complex tissue constructs. *Adv. Mater.* 29:1606061. doi: 10.1002/adma.201606061

Pereira, R. F., Barrias, C. C., Granja, P. L., and Bartolo, P. J. (2013). Advanced biofabrication strategies for skin regeneration and repair. *Nanomedicine* 8, 603–621. doi: 10.2217/nnm.13.50

Pezeshki-Modaress, M., Mirzadeh, H., Zandi, M. S., Rajabi-Zeleti, Sodeifi, N., Aghdami, N., et al. (2017). Gelatin/chondroitin sulfate nanofibrous scaffolds for stimulation of wound healing: *in-vitro* and *in-vivo* study. *J. Biomed. Materials Research Part A* 105, 2020–2034. doi: 10.1002/jbm.a.35890

Pham, C., Greenwood, J., Cleland, H., Woodruff, P., and Maddern, G. (2007). Bioengineered skin substitutes for the management of burns: a systematic review. *Burns* 33, 946–957. doi: 10.1016/j.burns.2007.03.020

Poursamar, S. A., Hatami, J., Lehner, A. N., da Silva, C. L., Ferreira, F. C., and Antunes, A. P. M. (2015). Gelatin porous scaffolds fabricated using a modified gas foaming technique: characterisation and cytotoxicity assessment. *Mater. Sci. Eng. C* 48, 63–70. doi: 10.1016/j.msec.2014.10.074

Ramin, M. A., Latxague, L., Sindhu, K. R., Chassande, O., and Barthélémy, P. (2017). Low molecular weight hydrogels derived from urea based-bolaamphiphiles as new injectable biomaterials. *Biomaterials* 145, 72–80. doi: 10.1016/j.biomaterials.2017.08.034

Rimann, M., Bono, E., Annaheim, H., Bleisch, M., and Graf-Hausner, U. (2016). Standardized 3D bioprinting of soft tissue models with human primary cells. *J. Lab. Autom.* 21, 496–509. doi: 10.1177/2211068214567146

Rodero, M. P., and Khosrotehrani, K. (2010). Skin wound healing modulation by macrophages. *Int. J. Clin. Exp. Pathol.* 3:643.

Ronfard, V., Rives, J. M., Neveux, Y., Carsin, H., and Barrandon, Y. (2000). Long-term regeneration of human epidermis on third degree burns transplanted with autologous cultured epithelium grown on a fibrin matrix. *Transplantation* 70, 1588–1598. doi: 10.1097/00007890-200012150-00009

Rouabhia, M., Park, H., Meng, S., Derbali, H., and Zhang, Z. (2013). Electrical stimulation promotes wound healing by enhancing dermal fibroblast activity and promoting myofibroblast transdifferentiation. *PLoS ONE* 8:e71660. doi: 10.1371/journal.pone.0071660

Ryssel, H., Gazyakan, E., Germann, G., and Ohlbauer, M. (2008). The use of MatriDerm in early excision and simultaneous autologous skin grafting in burns–a pilot study. *Burns* 34, 93–97. doi: 10.1016/j.burns.2007.01.018

Sahuc, F., Nakazawa, K., Berthod, F., Collombel, C., and Damour, O. (1996). Mesenchymal-epithelial interactions regulate gene expression of type VII collagen and kalinin in keratinocytes and dermal-epidermal junction formation in a skin equivalent model. *Wound Repair Regen.* 4, 93–102. doi: 10.1046/j.1524-475X.1996.40116.x

Sampson, S. L., Saraiva, L., Gustafsson, K., Jayasinghe, S. N., and Robertson, B. D. (2014). Cell electrospinning: an *in vitro* and *in vivo* study. *Small* 10, 78–82. doi: 10.1002/smll.201300804

Savoji, H., Hadjizadeh, A., Maire, M., Ajji, A., Wertheimer, M. R., and Lerouge, S. (2014a). Electrospun nanofiber scaffolds and plasma polymerization: a promising combination towards complete, stable endothelial lining for vascular grafts. *Macromol. Biosci.* 14, 1084–1095. doi: 10.1002/mabi.201300545

Savoji, H., Mehdizadeh, A., and Saadat Abadi, A. R. (2014b). Transdermal nitroglycerin delivery using acrylic matrices: design, formulation, and *in vitro* characterization. *ISRN Pharmaceutics* 2014:493245. doi: 10.1155/2014/493245

Savoji, H., Maire, M., Lequoy, P., Liberelle, B., De Crescenzo, G., Ajji, A., et al. (2016). Combining electrospun fiber mats and bioactive coatings for vascular graft prostheses. *Biomacromolecules* 18, 303–310. doi: 10.1021/acs.biomac.6b01770

Schurr, M. J., Foster, K. N., Lokuta, M. A., Rasmussen, C. A., Thomas-Virnig, C. L., Faucher, L. D., et al. (2012). Clinical evaluation of NIKS-based bioengineered skin substitute tissue in complex skin defects: phase I/IIa clinical trial results. *Adv. Wound Care* 1, 95–103. doi: 10.1089/wound.2011.0343

Shakespeare, P. G. (2005). The role of skin substitutes in the treatment of burn injuries. *Clin. Dermatol.* 23, 413–418. doi: 10.1016/j.clindermatol.2004.07.015

Sheikholeslam, M., Wright, M. E., Jeschke, M. G., and S., Amini-Nik (2017). Biomaterials for skin substitutes. *Adv. Healthcare Mater.* 7:1700897. doi: 10.1002/adhm.201700897

Shevchenko, R. V., Eeman, M., Rowshanravan, B., Allan, I. U., Savina, I. N., Illsley, M., et al. (2014). The *in vitro* characterization of a gelatin scaffold, prepared by cryogelation and assessed *in vivo* as a dermal replacement in wound repair. *Acta Biomater.* 10, 3156–3166. doi: 10.1016/j.actbio.2014.03.027

Shevchenko, R. V., James, S. L., and James, S. E. (2010). A review of tissue-engineered skin bioconstructs available for skin reconstruction. *J. R. Soc. Interface* 7, 229–258. doi: 10.1098/rsif.2009.0403

Sink,ó, B., Garrigues, T. M., Balogh, G. T., Nagy, Z. K., Tsinman, O., Avdeef, A., et al. (2012). Skin–PAMPA: a new method for fast prediction of skin penetration. *Eur. J. Pharm. Sci.* 45, 698–707. doi: 10.1016/j.ejps.2012.01.011

Skardal, A., Mack, D., Kapetanovic, E., Atala, A., Jackson, J. D., Yoo, J., et al. (2012). Bioprinted amniotic fluid-derived stem cells accelerate healing of large skin wounds. *Stem Cells Transl. Med.* 1, 792–802. doi: 10.5966/sctm.2012-0088

Snyder, S., DeJulius, C., and Willits, R. K. (2017). Electrical stimulation increases random migration of human dermal fibroblasts. *Ann. Biomed. Eng.* 45, 2049–2060. doi: 10.1007/s10439-017-1849-x

Sood, R., Roggy, D., Zieger, M., Balledux, J., Chaudhari, S., Koumanis, D. J., et al. (2010). Cultured epithelial autografts for coverage of large burn wounds in eighty-eight patients: the Indiana University experience. *J. Burn Care Res.* 31, 559–568. doi: 10.1097/BCR.0b013e3181e4ca29

Stark, H.-J., Boehnke, K., Mirancea, N., Willhauck, M. J., Pavesio, A., Fusenig, N. E., et al. (2006). Epidermal homeostasis in long-term scaffold-enforced skin equivalents. *J. Investig. Dermatol. Symp. Proc.* 11, 93–105. doi: 10.1038/sj.jidsymp.5650015

Summerfield, A., Meurens, F., and Ricklin, M. E. (2015). The immunology of the porcine skin and its value as a model for human skin. *Mol. Immunol.* 66, 14–21. doi: 10.1016/j.molimm.2014.10.023

Sun, G. (2017). Pro-regenerative hydrogel restores scarless skin during cutaneous wound healing. *Adv. Healthc. Mater.* 6:1700659. doi: 10.1002/adhm.201700659

Tamayol, A., Akbari, M., Annabi, N., Paul, A., Khademhosseini, A., and Juncker, D. (2013). Fiber-based tissue engineering: progress, challenges, and opportunities. *Biotechnol. Adv.* 31, 669–687. doi: 10.1016/j.biotechadv.2012.11.007

Tausche, A. K., Skaria, M., Bohlen, L., Liebold, K., Hafner, J., Friedlein, H., et al. (2003). An autologous epidermal equivalent tissue-engineered from follicular outer root sheath keratinocytes is as effective as split-thickness skin autograft in recalcitrant vascular leg ulcers. *Wound Repair Regen.* 11, 248–252. doi: 10.1046/j.1524-475X.2003.11403.x

Thadavirul, N., Pavasant, P., and Supaphol, P. (2014). Development of polycaprolactone porous scaffolds by combining solvent casting, particulate leaching, and polymer leaching techniques for bone tissue engineering. *J. Biomed. Mater. Res. A* 102, 3379–3392. doi: 10.1002/jbm.a.35010

Townsend-Nicholson, A., and Jayasinghe, S. N. (2006). Cell electrospinning: a unique biotechnique for encapsulating living organisms for generating active biological microthreads/scaffolds. *Biomacromolecules* 7, 3364–3369. doi: 10.1021/bm060649h

Tsinman, K., and Sinko, B. (2013). A high throughput method to predict skin penetration and screen topical formulations. *Cosmet Toiletries*, 128, 192–199.

Tumbar, T. (2006). "Epithelial skin stem cells," in *Methods in Enzymology*, eds J. N. Abelson and M. I. Simon (Elsevier), 73–99.

Vacher, D. (2003). [Autologous epidermal sheets production for skin cellular therapy]. *Ann. Pharm. Fr.* 61, 203–206.

Van Norman, G. A. (2016). Drugs and Devices: Comparison of European and U. S. Approval Processes. *JACC* 1, 399–412. doi: 10.1016/j.jacbts.2016.06.003

Vignesh, R. G. (1981). Grafting of burns with cultured epithelium prepared from autologous epidermal cells. *Lancet* 1981, 75–78.

Watkinson, R., Herkenne, C., Guy, R. H., Hadgraft, J., Oliveira, G., and Lane, M. (2009). Influence of ethanol on the solubility, ionization and permeation characteristics of ibuprofen in silicone and human skin. *Skin Pharmacol. Physiol.* 22, 15–21. doi: 10.1159/000183922

Wood, F. M., Kolybaba, M. L., and Allen, P. (2006). The use of cultured epithelial autograft in the treatment of major burn injuries: a critical review of the literature. *Burns* 32, 395–401. doi: 10.1016/j.burns.2006.01.008

Wufuer, M., Lee, G., Hur, W., Jeon, B., Kim, B. J., Choi, T. H., et al. (2016). Skin-on-a-chip model simulating inflammation, edema and drug-based treatment. *Sci. Rep.* 6:37471. doi: 10.1038/srep37471

Xiao, Y., Ahadian, S., and Radisic, M. (2017). Biochemical and biophysical cues in matrix design for chronic and diabetic wound treatment. *Tiss. Eng. B Rev.* 23, 9–26. doi: 10.1089/ten.teb.2016.0200

Xie, Y., Rizzi, S. C., Dawson, R., Lynam, E., Richards, S., Leavesley, D. I., et al. (2010). Development of a three-dimensional human skin equivalent wound model for investigating novel wound healing therapies. *Tiss. Eng. C Methods* 16, 1111–1123. doi: 10.1089/ten.tec.2009.0725

Xu, S.-C., Qin, C.-C., Yu, M., Dong, R.-H., Yan, X., Zhao, H., et al. (2015). A battery-operated portable handheld electrospinning apparatus. *Nanoscale* 7, 12351–12355. doi: 10.1039/C5NR02922H

Yannas, I. V., Tzeranis, D. S., and So, P. T. (2017). Regeneration of injured skin and peripheral nerves requires control of wound contraction, not scar formation. *Wound Repair Regen.* 25, 177–191. doi: 10.1111/wrr.12516

Conflict of Interest Statement: The authors declare that the research was conducted in the absence of any commercial or financial relationships that could be construed as a potential conflict of interest.

The reviewer JB and handling Editor declared their shared affiliation.

frontiers in Bioengineering and Biotechnology

REVIEW
published: 17 May 2018
doi: 10.3389/fbioe.2018.00062

An Effective Translation: The Development of Hyaluronan-Based Medical Products From the Physicochemical, and Preclinical Aspects

Gloria Huerta-Ángeles[1], Kristina Nešporová[1], Gabriela Ambrožová[2,3], Lukas Kubala[2,3] and Vladimir Velebný[1]*

[1] Department of Research and Development, Contipro a.s., Dolní Dobrouč, Czechia, [2] Free Radical Pathophysiology, Institute of Biophysics of the Czech Academy of Sciences, Brno, Czechia, [3] International Clinical Research Center, St. Anne's University Hospital Brno, Brno, Czechia

OPEN ACCESS

Edited by:
Amir Ghaemmaghami, University of Nottingham, United Kingdom

Reviewed by:
Jennifer Patterson, KU-Leuven, Belgium
Pinar Yilgor Huri, Ankara University, Turkey

***Correspondence:**
Gloria Huerta-Ángeles
huerta-angeles@contipro.com;
huertang77@gmail.com

Specialty section:
This article was submitted to Biomaterials, a section of the journal Frontiers in Bioengineering and Biotechnology

Received: *23 February 2018*
Accepted: *27 April 2018*
Published: *17 May 2018*

Citation:
Huerta-Ángeles G, Nešporová K, Ambrožová G, Kubala L and Velebný V (2018) An Effective Translation: The Development of Hyaluronan-Based Medical Products From the Physicochemical, and Preclinical Aspects. Front. Bioeng. Biotechnol. 6:62. doi: 10.3389/fbioe.2018.00062

This review shows the steps toward material selection focalized on the design and development of medical devices based on hyaluronan (HA). The selection is based on chemical and mechanical properties, biocompatibility, sterilization, safety, and scale-up costs. These facts play a vital role in the industrialization process. Approved medical devices containing-HA are illustrated to identify key parameters. The first part of this work involves the steps toward a complete characterization of chemical and mechanical aspects, reproducibility of the processes and scale up. In a second stage, we aimed to describe the preclinical *in vitro* and *in vivo* assays and selected examples of clinical trials. Furthermore, it is important to keep in mind the regulatory affairs during the research and development (R&D) using standardization (ISO standards) to achieve the main goal, which is the functionality and safety of the final device. To keep reproducible experimental data to prepare an efficient master file for the device, based on quality and recorded manufacturing data, and a rigorous R&D process may help toward clinical translation. A strong debate is still going on because the denominated basic research in HA field does not pay attention to the purity and quality of the raw materials used during the development. So that, to achieve the next generation of devices is needed to overcome the limitations of state of art in terms of efficacy, biodegradability, and non-toxicity.

Keywords: hyaluronan, chemical modification, cross-linked, hydrogel, preclinical data, clinical data, FDA, risk management

INTRODUCTION

Hyaluronic acid (HA), also referred to as hyaluronan is a linear polysaccharide ubiquitously present in the human body, which is found in the highest concentrations in synovial fluid, in eyes and skin. HA consists of alternating units of N-acetyl-β-D-glucosamine and β-D-glucuronic acid (**Figure 1**).

Traditionally, HA used for industrial applications was extracted from animal tissues i.e., umbilical cords or rooster combs (Shiedlin et al., 2004). HA isolated from living tissues is

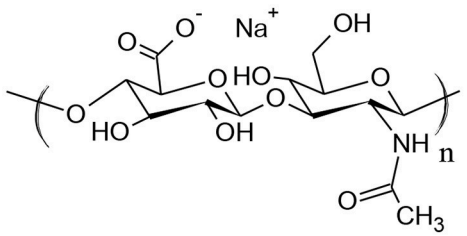

FIGURE 1 | Structure of hyaluronan (HA).

a mixture of several components, which does not satisfy the criteria of purity described by Pharmacopeia reference standard. Additionally, the purification and isolation procedures vary that it causes inconsistence between batches. Nowadays, bacterial fermentation is used for large-scale production. Besides, the production has been improved by metabolically-engineered recombinant bacteria strains that improved the yield (Kaur and Jayaraman, 2016).

The development of HA based-products is challenging because they are directly focused on human use. It is important to mention that the project manager based on an adequate risk assessment could mitigate many of the risks involved during the R&D (**Table 1**). HA-based products are covering a broad range of applications, which can be divided between cosmetic and therapeutic. The change of beauty standards led to increasing demand for cosmetics and asthetics procedures, including products made of HA. The dermal fillers containing-HA available in the market had to be approved by the Food and Drug Administration (FDA): Restylane®, Juvederm®, Bellotero®, Hylan B®, or Aliaxin®. In general, crosslinked HA is used as soft tissue fillers to eliminate wrinkles and shape the facial contour (Highley et al., 2016). However, the biological consequences of injecting these foreign materials into the dermis have not been studied to any great extent. Unfortunately, complications with these fillers can be difficult to address (Hwang, 2016).

Cosmetics products containing HA are increasing in the market and importance (Pavicic et al., 2011), as HA has been shown to be effective for the treatment of skin-aging (Papakonstantinou et al., 2012), skin, and wound repair (Tolg et al., 2014). For the above-mentioned reasons, HA is extensively used in many cosmetic preparations. As the market is relatively broad, many new preparations are currently under development; As an example, hydrophobized HA is able to encapsulate hydrophobic active compounds such as vitamins or antioxidants and acts as a carrier that helps the active compound to penetrate into dermis increasing its effect (Šmejkalová et al., 2017). Even though topical applications do not involve a very rigorous risk assessment, as they are externally used some regulations are followed. For controlling the use of prohibited substances on cosmetic products in Europe exists the regulation no. 1223/2009. Furthermore, as an effect of globalization, new markets in emerging countries are asking for strict quality controls to ensure the safety of cosmetic products. An urgent need for low cost, adequate, rapid methods is required, to allow the detection of forbidden compounds deliberately introduced in formulations. These methods should be able to identify of toxic components present as contaminants or impurities. Several proposals are emerging, and new regulations are expected.

In case of medical devices, the US and European regulatory agencies have established the classification to assure its safety and effectiveness. In Europe, there are four classes of devices ranging from low risk to high-risk (I, IIa, IIb, and III). Similarly, in the US there are three classes (I, II, III). The specific requirements and approval approaches for any medical device in EU and FDA were recently reviewed by (Van Norman, 2016). Most of the HA-based medical devices are classified as class III (in some cases as a class IIb in EU). For instance, HA is found in wound dressings, dermal fillers, anti-adhesive, osteoarthritis, ophthalmic, or vesicoureteral reflux devices. Between them, one of the most important medical applications is pain management (Migliore and Procopio, 2015) with eleven products receiving FDA approval for the treatment of knee osteoarthritis (OA) since 1997 (Doros et al., 2016). Intra-articular injections of HA, commonly referred to as viscosupplementation therapy have been classified in the US by the FDA as class III medical devices for more than 20 years. Two examples of these products are Monovisc®, a product currently in use in Europe (Laszlo et al., 2017) or Supartz®/Supartz FX™ for patients who failed to respond to non-pharmacologic therapy and simple analgesics in US market.

The first formulation approved by the FDA for use in the treatment of vesicoureteral reflux was stabilized HA/dextranomer (NASHA/Dx) (Geavlete et al., 2016). HA-based devices for the prevention of surgical post adhesion is also well-documented (Chen C.-H et al., 2017; Li et al., 2017); Seprafilm® is an anti-adhesion film to reduce abdominopelvic post-surgical adhesions, comprised of crosslinked HA with carboxymethylcellulose (CMC) (Diamond et al., 2012). This product was retired from the US-market due to allergic reactions in some patients.

HA is a natural lubricant and is well-suited for ophthalmic formulations (Battistini et al., 2017) and eye drops (Gross et al., 2017). Moreover, HA forms part of dietary formulations for the treatment of synovitis, knee pain, relief of synovial effusion or inflammation, and improvement of muscular knee strength (Oe et al., 2016).

This main goal of this review is to provide guidance to commonly used practices. Besides, this work intends to mention basic quality control parameters applied non-only to medical devices, but also to evaluate active ingredient based on ethics, and regulatory assessment and from a scientific and technological rationale. **Table 2** enlists the three main norms applied for ensuring, both quality and safety of medical devices as discussed in this manuscript (Ibrahim and Chassapis, 2014; Bedi et al., 2017). However, the classification of medical devices and regulatory pathways are complex and vary from country to country (Vasconcelos et al., 2016).

TABLE 1 | Risk assessment and evaluation toward designing a master file for a medical device product.

Characteristics	Hazard (potential cause of failure)	Harm (potential event of failure)	Reduction measures
PREMARKET LIST			
Raw materials do not meet desired specification	Unreproducible synthesis, purification, or isolation.	Unable to release/accept raw materials for processing into final device. Raised costs to manufacturer.	Implant an effective quality system. Control and monitoring of personnel and equipment.
Raw materials do not meet desired specification	Presence of impurities in the starting materials	Toxicity in the final product.	To characterize the raw materials.
The viscosity of the solution is low	Wrong choice of polymer	Incorrect function of the product.	To characterize the material following Pharmacopeia
The processing of the material is not reproducible	The polymer is not following specification.	Delays to production	To characterize the materials using highly sensitive methods.
Product is not possible to be sterilized.	Massive contamination during production or product handling. Degradation during sterilization.	Aseptic processing might not be feasible-product cannot be marketed	To study the effect of agents used for sterilization To change the way of sterilization.
PRODUCT DESIGN			
Mechanical properties of the product are not adequate for the application.	The material degraded during storage.	Incorrect function of the product.	Definition of mechanical properties according to state of art.
The material is not adequately stored.	Material decomposed	Incorrect function of the product	Characterization of the product before its use
The device is not stable.	Fast degradation.	Avoid of regeneration or efficacy.	To perform degradation studies *in vitro*.
***IN VITRO* USE**			
The material is cytotoxic.	Presence of impurities in the product.	Unable to be used *in vivo*.	To purify the product extensively. To develop validated and standardized *in vitro* assays of toxicity
The personnel do not correctly evaluate the material.	The cell model is not representative for the application	False biocompatibility.	Extensive *in vitro* characterization.
ANIMAL MODEL			
Macrophages are observed at the site of implantation.	Foreign body response is observed.	Limited biocompatibility.	Wrong choice of materials.
The material produces inflammatory responses in animals	Adverse reactions *in vivo*	Product cannot be translated	To develop an integrated strategy for toxicity testing *in vitro*.

TABLE 2 | Evaluation of products requirements toward medical device with respective norms.

Entry	Tasks in medical device development	Norms
1	Chemical characterization of materials, degradation products, toxico-kinetics, sample preparation, sterilization, and residues. Preclinical studies (*in vitro* and *in vivo* testing)	ISO 10993
2	Risk assessment (identification of hazards, design and production, and clinical usage risks)	ISO 14971
3	Clinical safety, performance, and evidence	SG5/N2R8

PHYSICO-CHEMICAL CHARACTERIZATION OF NATIVE HA

Design of HA Specification Under GMP Practice

In the case of polymeric materials (such as HA) several parameters of characterization are requested. The procedures are described in Pharmacopeia and should follow the American Society for Testing Materials standards (ASTM standards) or ISO norms. Consequently, each product should be accompanied with a list of tests (specification) along with the analytical (validated) procedures used for the determination and appropriated acceptance criteria. The specification establishes the criteria to which a substance should conform to be considerable acceptable for its intended use. Apart from analytical tests and acceptance specifications, new chemical entities require the data from at least three independent batches to demonstrate the reproducibility of the manufacturing process.

For instance, a full characterization is carried following international standards. Norm ISO 14971 is a key standard for a manufacturer and identify the hazards associated with medical devices. This norm is used as a guide for evaluation of manufacturing processes, including up-scaling. All manufacturing processes should be performed under good manufacturing practice (GMP) and characterized by validated analytical methods. Norm ISO 14971 dictates that all the components of the device should be included in the analysis,

including its source and purity. In the case of HA the presence of contaminants are reported to cause inflammatory responses even in extremely low concentrations (Šafránková et al., 2018). The analysis of raw materials and ingredients, as well as the quality of final products should be enunciated in the master file.

The required data for HA should be (i) description i.e. appearance, shape, color; (ii) identification/confirmation of structure (iii) assay describing the stability (iv) impurities describing the presence of organic volatile impurities and particulate matter, water content, residual chemicals, or solvents, degradation products. To address this, the final formulated sterilized product (medical device) is extracted (in both polar and non-polar solvents), and analyzed. The contaminants should be quantified by gas chromatography (GC-MS) as recommended by Pharmacopeia. Also, the specification includes physico-chemical properties, such as pH, viscosity, and particle size. Finally, microbial limits, endotoxins and pyrogens are enlisted. These contaminants (especially endotoxins and proteins) are not eliminated during sterilization and may be present in the finalized product (Baeva et al., 2017).

Native HA is used in medical devices as gel or solution. The absolute value of intrinsic viscosity identifies the material: i.e., HA with a value higher than 2.5 m^3/kg, is recommended for parenteral administration and intra-ocular use, while a value of 0.3–0.6 m^3/kg is recommended for cutaneous use; as an example, GenVisc 850® is a product containing highly pure HA (Doros et al., 2016), which is commonly used for the treatment of osteoarthritis knee pain. Unfortunately, the products found currently on the market differ drastically in rheological properties, and the relationship between viscosity and efficacy are still unclear (Wehling et al., 2017). Recently, more relevant techniques (tribological measurements) have been developed to elucidate the lubricating ability of HA formulations (Bonnevie et al., 2015). The tribology data effectively correlate the reduction of friction coefficient in cartilage with the viscosity and lubricant ability of a given formulation. Gigis et al. found that the efficacy might be related to the rheological properties and its origin (Gigis et al., 2016), but the existing data are still not possible to be correlated.

Nuclear magnetic resonance (NMR) is helpful for the chemical characterization of substances and mixtures in pharmaceutical formulations, medical devices, and drugs. Particularly, NMR identifies the structure of HA and impurities present in the samples. Therefore, this technique is applied to evaluate the downstream processes during the extraction and purification of HA and evaluates consistency between batches. A second technique is infrared spectroscopy (IR), a rapid procedure that provides a robust analysis and can supply functional-group information of samples.

Structural Elucidation of HA After Chemical Modification

Recently, chemically modified HA is the focus of active research for applications in biomedical device coatings, drug delivery systems, and scaffolds or cell-laden hydrogels for tissue engineering. Chemically modified HA is preferred due to the poor stability of native HA. It is important to mention that mild conditions for chemical modification are preferred due to possible degradation of HA during this process. Additionally, it is important to evaluate the cytotoxicity of the new formed chemical entities and its degradation products (Huerta-Angeles et al., 2016a). Additionally, reactive intermediates may change the native structure of HA or cause undesired cross-linking. So that, the new structure of HA is identified by a combination of analytic methods such as NMR, IR, and Mass Spectrometry (Picotti et al., 2013; Wende et al., 2016). However, chemically modified HA is not natural anymore, therefore, its biocompatibility cannot be assumed, even if the new chemical identity is based on natural components (Huerta-Angeles et al., 2017).

Chemical modification of HA can be roughly divided into two types based on the chemical or physical nature of the junctions: cross-linking and hydrophobization (Khunmanee et al., 2017). During the last decade, there are many works describing the covalently joint of several molecules and polymers to the HA-backbone. The most important parameter to evaluate after chemical modification of HA is the degree of substitution (DS) and the degree of cross-linking (DC). The DS of HA is commonly evaluated using ^{1}H NMR or chromatographic techniques. DS is usually defined as an average number of side groups attached to 100 HA dimers. Therefore, the DS is expressed in % when DS equal to 10 % indicates that 10 out of 100 HA dimers are modified. DS can be determined by ^{1}H NMR signals of HA anomeric H-atoms (from 4.3 to 4.6 ppm) or the methyl group located at 2.01 ppm corresponding to the -N-CO*CH3* in HA compared to the signals of the corresponding attached groups.

Dermal fillers are usually composed of cross-linked or stabilized HA, in a variety of chemistries and functionalities i.e., Hylaform® cross-linked with divinyl sulfone, or Aliaxin® with 1,4-butanediol diglycidyl ether (BDDE) (La Gatta et al., 2016). Particularly, a stabilized form of hyaluronic acid is necessary for aesthetic applications in order to increase the stability (Matarasso et al., 2006; Tran et al., 2014). In order to the determine DC in dermal fillers NMR is used (Guarise et al., 2012), carried out after enzymatic degradation (Wende et al., 2017).

In the case of hydrophobized HA, the use of ^{1}H NMR is not always satisfactory for the determination of DS of high MW HA or for insoluble (or partially soluble) derivatives. In the last case, ^{1}H NMR might overestimate the value due to more intense resonances of better soluble functional groups. Furthermore, the determination of the DS in hydrophobized HA can be performed after alkaline hydrolysis of the attached moieties, followed by its quantification by gas chromatography (GC), or Raman Spectroscopy (Chmelar et al., 2017). Similarly, Infrared spectroscopy (IR) reveals changes on the primary structure of HA after chemical modification. In the last case, a high degree of substitution is required due to the low sensitivity of the method (Choi et al., 2010; Huerta-Angeles et al., 2011).

Both DS or DC help to identify the process performance or product quality that is within the acceptable range, defined previously by customer standards. Also, it identifies defects in the process or the product itself.

Molecular Weight and Polydispersity of HA

HA biological effects are unique among other biologically active molecules and are dependable on HA fragment size (Cyphert et al., 2015). Mw in specification is reported as average weight molecular weight (Mw) i.e., 7×10^5 Da consists of polymer fragments of size from 3.4×10^5 Da up to 1.4×10^6 Da, while 16.9 kDa HA consists of oligosaccharides in the range of 2.2×10^3–4.5×10^4 Da. Therefore, it is important to include the value of polydispersity. Mw is a significant concern in the development of intra-articular injections of HA for the treatment of knee osteoarthritis (OA) due to striking differences in the product efficacy (Altman et al., 2016). Hylan G-F 20 (marketed as Synvisc®) is made of relatively high Mw (Mw of 6×10^6 Da) (Migliore et al., 2010). High molecular weight HA is preferred for the last mentioned application (Bannuru et al., 2011; Zhao et al., 2016). Mw also determines the effectivity of systemic distribution and clearance of targeted organs; low molecular weight HA showed more rapid systemic distribution, while 6.7×10^4 and 2.2×10^5 Da showed longer persistence in the lungs (Kuehl et al., 2016). Mw changes the swelling degree and viscoelasticity of dermal fillers (Chun et al., 2016), while in cosmetic formulations is satisfactory the use of low molecular weight HA (2.0×10^4–3.0×10^5 Da) because it passes through the stratum corneum. In contrast, the impermeability of high molecular weight HA (1–1.4 $\times 10^6$ Da) through stratum corneum was reported (Essendoubi et al., 2016).

For all the above-mentioned reasons, it is important to identify the Mw of the polysaccharide (Braithwaite et al., 2016). A good method for the determination of the average molecular weight of native and modified HA is size exclusion chromatography combined with multiangle light scattering (SEC-MALLS) (Cožíková et al., 2017). Hydrodynamic characterization of HA and commercial products were characterized using SEC-TDA (Size Exclusion Chromatography-Triple Detector Array) (Salzillo et al., 2016).

Sterilization of HA-Based Products

HA produces viscous solutions—particularly high molecular weight HA. The viscosity drastically decreased when the solutions are exposed to high temperatures (+100°C). Therefore, it can alter the properties of the medical device. However, HA-based products must be sterilized for their use.

Common sterilization methods include exposing HA-based materials to (i) ethylene oxide gas, (ii) dry or wet heat, (iii) electron beam, or (iv) γ-radiation. For liquids the preferred method of sterilization is filtration. The challenge is to sterilize the material with the minimal degradation (Liu et al., 2012). While all sterilization methods induce a decrease in the weight-average molecular weight (Drímalová et al., 2005), the irradiation methods, particularly γ rays, induced the highest decrease in Mw. Therefore, a post-sterilization validation (Mw determination) is essential to evaluate possible depolymerization of HA. UV absorbance measurement is also useful for the evaluation of possible degradation by an increase of absorbance due to the formation of double bonds due to oxidant conditions (Choi et al., 2010). In addition, rheology is used to evaluate the effect of sterilization heat cycles on the degradation of HA. Contaminants (especially endotoxins and proteins) are not eliminated during sterilization. In case of endotoxins, their concentration can even increase after the bacterial cell destruction during sterilization. The sterilization of medical devices is described under norm ISO 10993/7.

Stability

The stability determination of HA-based products is crucial during a development (Olejnik et al., 2015). The stability studies should be carried out for new chemical entities as well as for finished products. The purpose of stability is to provide evidence on how the quality of any product varies as a function of time under several environmental factors i.e., temperature, humidity, and light. At selected time points, the characteristics of the materials are evaluated: structure, Mw, mechanical and thermal properties. A practical example, during the development of sodium linolenyl HA as a cosmetic ingredient (Huerta-Angeles et al., 2016b). A list of parameters was enlisted and evaluated for 12 months (**Table 3**) to ensure the product preserved its activity. Using stability data, a recommendation about storage conditions and shelf life are given. A second crucial point for a successful product outcome is the stability toward hyaluronidases action. (La Gatta et al., 2016). This parameter allows to predict the relative *in vivo* duration of the aesthetic effect of dermal fillers.

Handling, Packing, and Storage

ISO 780 and ISO9001 norms are the standards to follow for handling and storage of HA-based products. A list of recommended actions is enlisted by the producer in the specification. Particularly, HA-based products are hygroscopic. Thus, the product should be stored in its original package in a clean and dry place, away from any sources of heat at low temperatures or room temperature (25°C). For HA-containing sensitive molecules, it is recommended that the product is stored at low temperature (4–8°C). Likewise, the products can be light sensitive, thereafter they are stored in dark or sealed package, or used immediately after opening. Unfortunately, it is not possible to describe a general rule as the stability varies between products, but it not expected to vary between batches. Finally, if the product is sterilized it should be used after opening and re-sterilization is not possible.

BIOLOGICAL TESTING AND SAFETY ASSESSMENT

HA-based products used as implants or with direct contact with damaged skin i.e., in wound healing, are classified as medical devices (Longinotti, 2014). To obtain FDA agency approval, the preclinical study submitted to the authority have to demonstrate that the intended product is safe. Preclinical information demonstrated that the product is not pyrogenic, mutagenic, toxigenic, hemolytic, or immunogenic. The guidance is included in norm ISO 10993. That norm also provides a framework for the biocompatibility evaluation based on three medical devices categories:

TABLE 3 | Sodium linolenyl hyaluronate and its specification; the table provides the identity of each batch, acceptance criteria, and analytical methods used for the test (Huerta-Angeles et al., 2016b).

Test	Specification limit value	Value	Method[a]
Appearance	Visual	White or yellow granules	EP
Appearance of the solution (A_{600})	Clear	–	EP 2.2.2.5
Average molecular weight Mw_1	10–30	kDa	EP method
Identification of sample (name, batch, structure)	Name and Number of batch	Pass	USP
Degree of substitution	7–13	%	NMR
Intrinsic viscosity	≥0.65 m^3/Kg	Absolute value	EP 5.1472
Dry matter	>85	%	USP/EP
Loss of drying	<10	%	USP/EP
IPA	<0.5	%	Residual solvents, EP, pass
TEA	<0.03	%	Residual solvents, EP, pass
DMAP	<0.03	%	Residual solvents, EP, pass
Free linolenic acid (FLA)	<0.5	%	Residual chemicals, EP pass
Bacterial endotoxins	<100	CFU/g	EP 2.6.14
Heavy metals	<20	ppm	EP 2.4.8
pH of solution (0.5% in water)	5.0–8.5	–	EP 2.2.3

[a] *EP stands for European pharmacopeia and the number described the method of limits and analytical determination, USP stands for United states pharmacopeia.*

i) Type of device (surface device, external communication device or implant)
ii) The duration of device/tissue contact (≤ 24 h, >24 h to 30 days, > 30 days)
iii) Type of tissue which is in contact with the device (e.g., intact skin, bone/tissue, blood etc.).

Cytotoxicity, sensitization, and irritation/intracutaneous reactivity assessment are recommended for all types of medical devices (Kim et al., 2014b).

HA is considered safe, but it possesses various biological functions depending on its molecular weight i.e., low Mw HA (oligosaccharides) are recognized by the immune system as damage-associated molecules patterns (DAMPs) and elicit inflammatory, angiogenic, and proliferative responses in various tissues. Mainly pro-inflammatory responses lead to foreign-body response (FBR) (Christo et al., 2015).

HA-Based Materials *in Vitro* Cytotoxicity

The norm ISO 10993/5 governs the determination of cytotoxicity of medical devices, primarily the assessment of acute toxicity *in vitro*. Still, it leaves rather large freedom in choosing proper cell type and method of cell viability measurement. Many commercially available cell lines have been used: cultured fibroblasts from human skin, buccal mucosa, periodontal membrane or embryonic lung; the epithelial cancer cells (HeLa) as well as murine cells cultured from liver and spleen; T-lymphocytes from lymph nodes and macrophages (Wiegand and Hipler, 2009).

In the case of HA, the use of human keratinocytes (La Gatta et al., 2016), HaCaT (Sacco et al., 2016; Sun et al., 2017); murine cell lines [NIH-3T3 (Sigen et al., 2018), or L929 (Zamboni et al., 2017)] have been reported. It is advisable to employ cell type homologous with the tissue/organ concerns for the specific application, i.e., endothelial cells for testing stents (Choi et al., 2016; Hauser et al., 2017), human dermal fibroblasts and epidermal keratinocytes for wound healing (D'Agostino et al., 2015), adipose-derived stem cells for dermal fillers or gels (Guo et al., 2017; Stellavato et al., 2017) and chondrocytes for cartilage knee repair (Brittberg, 2014).

Based on the nature of tested medical device three types of cytotoxicity testing are proposed in ISO 10993/5: extract-dilution method, test by direct contact or indirect contact.

For most of the soluble (e.g., injectables) and some of the non-soluble medical devices, the extract-dilution test is the most common. In case of soluble compounds, the cells are cultured in media containing a range of concentrations of tested product. The semi-soluble and non-soluble devices (such as wound dressings containing HA) can be extracted into cultivation media and cells are then cultured with these extracts. Usually, the extraction is performed in full media (serum supplemented) for 24 h at 37°C. The presence of serum accelerates the extraction of leachables, solubilizes the substances and increases degradation, therefore, it affects the cytotoxicity of tested materials.

The extraction can be also performed without serum if it is more relevant for the intended application. It is important to mention that the extraction conditions should simulate as possible the conditions under which the device will be used. The extract-dilution method is more commonly adapted for the *in vitro* cytotoxicity evaluation of materials and devices directly used in the body. In addition, it is applied to a wide variety of raw materials and finished products that may release contaminants or toxic degradation products after continuous exposition.

The most often used read-out method to test cell growth rate and toxicity of the culture includes (i) metabolic assay such as neutral red uptake (NRU), MTT (methyl thiazolyl tetrazolium) T, XTT, resazurin assay, or ATP concentration measurement (ii) metabolism-independent method, i.e., crystal violet staining or DNA content measurement by PicoGreen. There are no reported interactions of HA with these methods. All these methods produce very similar results mainly in the determination of acute toxicity (≤24 h). According to the norm, these tests are performed only in a finished product. However, changes in the composition of the material can also influence the cytotoxicity tests. For instance, it is advisable to test the individual components in the composition during development. As an example, the presence of inorganic particles (e.g., in HA-based bone cement) can affect the spectroscopic assays. It is recommended to utilize methods with fluorescent or luminescent

read-out (Kong et al., 2011) to evaluate effects of the individual components.

For water-insoluble HA-based products, the direct contact cytotoxicity test (or contact inhibition test) is used. The whole HA-based device or a piece is placed directly onto a cell monolayer and the subsequent changes of cell morphology and viability are assessed by microscopy, cell-staining, and viability measurement. This method is very sensitive but limited to specific devices i.e., very light or highly hydrophobic compounds will float and their attachment to cell monolayer is problematic. It is also necessary to determine if the HA-based device placement did not cause mechanical damage to the cell monolayer. This method enables even weak cytotoxicity to be detected because of its high sensitivity.

The indirect contact method includes molecular filtration and agar overlay test useful for the assay of leachables (Li et al., 2015).

A problem arises with slowly biodegradable devices such as cross-linked HA in fillers or anti-adhesives (Bhojani-Lynch, 2017). Some fillers are biodegradable in 12–18 months, or in 2–5 years (for slowly biodegradable fillers) as they are designed to last after implantation. Later, they are subsequently degraded and should be eliminated from the body without any cytotoxic reaction to both the intact material and its degradation products. Recent reports enunciated late inflammatory responses in patients (Wu et al., 2017). Prior to *in vitro* cytotoxicity testing, the biodegradable devices can be degraded in plasma or other suitable biological fluids with or without the addition of specific degrading enzymes, in particular, hyaluronidases for HA-based products (Li et al., 2015). Still, the translation from *in vitro* to *in vivo* conditions has limitations as the degradation rate depends on several factors such as the degree of modification of HA, impurities, manufacturing process, sterilization, device size, and the local tissue environment (hyaluronidase activity, inflammation) and the circulation rate (dilution of the degradation products). Similar difficulties were observed correlating *in vitro* and *in vivo* toxicity tests with other types of material, e.g., magnesium based implants, therefore, a modification of ISO 10993/5 cytotoxicity tests was proposed (Wang et al., 2015).

Nevertheless, a continuous progress is expected in the development of methods for cytotoxicity determination yielding more robust data with better correlation with *in vivo*. As an example, new methods include real-time measurement of cell attachment, and the real-time microscopic analysis including fluorescent viability assessment (calcein-AM assay, caspase activation assay etc.). However, these methods can only be used in standardized tests after proper optimization and validation. Finally, cytotoxicity tests are recommended for all medical devices as they allow a rapid evaluation, employ standard protocols, produce quantitative and comparable data, and due to their sensitivity, allow all the toxic materials to be withdrawn prior to animal testing.

Other *in Vitro* Tests of HA-Based Materials

Apart from cytotoxicity, only sensitization and irritation tests are required for all types of medical devices. Nowadays, different models are currently validated to assess skin irritation *in vitro* i.e., the reconstructed human skin model (EpiDerm®, MatTek Corp.) (Hayden et al., 2015; Pedrosa et al., 2017).

The measurement of viability, histological analysis or molecular biology methods are determined in order to evaluate the complex response to medical devices (Casas et al., 2013; Coleman et al., 2015). Other *in vitro* tests include hemocompatibility (ISO 10993/4) and genotoxicity (ISO 10993/3). Hemocompatibility is recommended for devices that get in direct contact with blood. For example: cardiovascular devices (Turner et al., 2004), or acute wound dressings such as Hylan® (Longinotti, 2014), while genotoxicity assessment is recommended or required for implanted devices which are in contact with tissues for more than 24 h or more than 30 days, respectively: as an example, dermal fillers (De Boulle et al., 2013). Devices utilizing native HA are, in general, safe with no hemocompatibility (Simon-Walker et al., 2017), or genotoxic issues (Strand et al., 2012).

IN VIVO TESTS OF HA-BASED MATERIALS

The HA-based materials are recognized as being non-toxic in *in vitro* tests described above are subjected to *in vivo* tests. The norm ISO-10993/10 governs the biocompatibility testing of medical devices using guinea pigs, mice, and other small animals. The selection of particular *in vivo* test is dependent on the intended application of the product and vary significantly for materials intended for topical or internal applications. HA based-products intended to be used for internal application or application into open wounds (e.g., surgical or chronic wounds) are considered a medical device (Longinotti, 2014). These assays are governed by a broad range of national and international regulations and standards (e.g., CE mark or FDA 510(k) or PMA approval), but the regulatory requirements for medical devices are complex and vary between regions. In Europe, the regulations for active implantable medical devices (AIMD) is the EU Directive 90/385/EEC. The objective of the *in vivo* tests is to characterize the evolution of the tissue response after implantation of a medical device including its integration and the absorption/degradation.

The intended material for implantation should be manufactured, processed, cleaned of contaminants, and sterilized by the method intended for the final product. Subsequently, the samples to be implanted are aseptically handled to avoid contamination prior or during implantation. Surgery is performed under appropriate general anesthesia, carried out under aseptic conditions, and minimizing trauma. It is important to remove the hair from the surgical area and disinfecting the exposed area of skin. A small opening in the peritoneum is performed for the implantation and follows a well-established method for assessing the biological response and safety of any implant (Wortman et al., 1983). For example, this model was used for testing the effectivity of Seprafilm® (Morse et al., 2005).

An alternative method for assessing the biological response and safety of an implanted material is an implantation in the

dorsal subcutaneous tissue of mice, rats, guinea-pigs, or rabbits (Pi et al., 2017). For example, the implantation of films made of HA tested by subcutaneous implantation into the backs of Wistar rats (Liu et al., 2005). An incision is made in the skin and one or more subcutaneous pockets are prepared by blunt dissection. In the last case, two or more pieces of material can be implanted but the gears should not touch each other.

The local effects of a new HA based-product are evaluated by comparison of the tissue response caused by the surgical procedure (sham controls). Furthermore, the effects of novel HA-based product are evaluated by direct pair comparison of two products. The first one, a reference (specimen) should refer to a product whose clinical acceptability and biocompatibility characteristics has already been established (Norm ISO 10993/6).

The tested-sample should be implanted into the tissues most relevant to the intended clinical use and evaluated in terms of mechanical and functional loading and safety. Normal rat and rabbit knee joints were used as a model to determine the tissue reaction to a material (Ishikawa et al., 2014); the inflamed or damage knee joint in rat or rabbit models was helpful for the evaluation of inflammation, joint lubrication, chondroprotective effects and antinociceptive effects (Gomis et al., 2009; Oliveira et al., 2014); air pouches established in BALB/c mice for the evaluation of inflammatory response of Hylan G-F 20 (Synvisc®) (Markel et al., 2014) and bilateral meniscectomies in sheep for assessment of the therapeutic potential of HYADD® (Smith et al., 2008).

Furthermore, it is important to consider the physical characteristics of tested sample (such as form, size, geometry, density, hardness, surface chemistry, swelling degree) because they influence the tissue response to the foreign material (Rayahin and Gemeinhart, 2017). In general, HA based-materials are degradable and absorbable with the consistence of a liquid or soft hydrogel (Khunmanee et al., 2017; Larrañeta et al., 2018). In this case, the swelling degree should be assessed as a considerable increased size of the implant is expected because HA binds a large amount of biological fluids. The determination of swelling helps to mitigate the risk of a potentially harmful situation of overdosing or mechanical damage.

The process of HA based-materials degradation and integration are key factors. Degradation studies *in vitro* should help to establish the proper time points for *in vivo* evaluation. Therefore, before starting preclinical studies with degradable materials, relevant information providing the degradation rate should be considered (Zhang et al., 2016), as tissue reaction on degradable materials is very different to non-degradable materials. The clinical exposure time to the device determines the test period. The preclinical study should span the degradation period for the device: (i) early period (when minimal degradation occurs) (ii) mid-period (when degradation is taking place) (iii) late period (when the implant is essentially absorbed). During the material degradation process, chronic inflammation can be also observed (Morais et al., 2010). Shortly after implantation, the reaction due to the surgical procedure itself is difficult to distinguish from the reaction caused by the implant. Finally, a homeostatic state of the tissue is expected after complete absorption of the material.

Evaluation of *in Vivo* Testing

The health of the animals is observed and recorded minimally once per 24 h. After the animal has been humanely euthanized, the implant site is excised together with sufficient unaffected surrounding tissue to enable evaluation of the local macroscopic and histopathological responses (D'Este et al., 2016). The sample for histopathological analysis should include the tissue debris. The organs sensitive to systemic or local damage should be also collected (lymph nodes, liver, kidneys, spleen) for evaluation of subchronic systemic toxicity (Kim et al., 2014a).

Parameters of biological response to the tested material which should be assessed and recorded according to ISO-10993:

i. Inflammatory and fibrotic response to the tested material;
ii. Degenerative changes in the tissue morphology;
iii. Number and distribution of the inflammatory cells (polymorphonuclear cells, lymphocytes, plasma cells, eosinophils, macrophages, and multinucleated cells) as a function of distance from the material/tissue interface;
iv. Signs of necrosis;
v. other types of changes in tissues (e.g., vascularization, adipocytes infiltration, granuloma formation);
vi. Material characteristics (presence of fragments and/or debris, form, and location of debris);
vii. Tissue ingrowth to the material;
viii. Protocol (laboratory and personnel responsible for test, details of operations, description of test and control materials, description of animals, implantation and retrieval techniques and histological procedures, evaluation and observations of the above-mentioned parameters, statistical analysis) and final evaluation.

Foreign Body Response to HA-Based Materials

Inflammatory reactions due to limited biocompatibility induces foreign body response (FBR). All materials implanted into living tissue initiate some host response as the first step of tissue repair (Franz et al., 2011). This process arises in consequence of the host reactions after implantation of the (bio)material and involves blood/plasma proteins adherence to the implant (acute inflammation). Moreover, monocytes/macrophages occurrence is observed at the site of implantation, together with foreign body cells formation, and extracellular matrix overexpression (chronic inflammation) (Anderson et al., 2008). Bruising, swelling, edema, infections, lumps and bumps, skin discoloration, and biofilm formation are common complications due to FBR (Urdiales-Gálvez et al., 2018). Even though, the risk associated to the use of HA is low, the use of cross-linkers may induce FBR. As an example, 0.6% of patients injected with Restylane® documented an incidence of hypersensitivity, divided equally between immediate and delayed reactions (Bitterman-Deutsch et al., 2015; Pérez-Pérez et al., 2017). There are reported cases with different characteristics i.e., a case of cellulitis-like FBR after HA-dermal filler injection (Shin et al., 2018). For the above mentioned reasons, FBR and the fate of scaffolds implanted should be cautiously evaluated in the animal model (Dondossola et al., 2016). Also, it is necessary to describe the method that

will be used to extrapolate from the animal data to an effective regimen in humans. Safety studies obtained after preclinical findings allows the translation of a medical device into the clinics (Phillips and Wang, 2017).

CLINICAL INFORMATION

Extensive and complete documentation must be submitted to by the competent authority in the European Union, Japan, or the United States to obtain a marketing-authorization of a new HA-based therapeutic product. One of the most critical documents to be submitted is the clinical study report (CSR), which represents the integrated full report of efficacy and safety data. The only document available from a regulatory authority is the guideline issued by the FDA in 1999, which recommends the required information to be included (Alfaro et al., 2007).

In the case of dermal fillers, Hylaform® (Gold, 2007), Juvéderm® (Romagnoli and Belmontesi, 2008), Belotero Balance®, and Restylane® were approved by the FDA. All of them have demonstrated to be safe after being injected intradermally into the iliac crest region in 15 subjects (Tran et al., 2014). The clinical use of Seprafilm® was supported by preclinical and animal studies relating to surgical and obstetrical/gynecological applications (Diamond et al., 2012). HA was used also as a targeted transport vehicle of irinotecan in the treatment of metastatic colorectal cancer and underwent randomized Phase II clinical trial in 2005 (Gibbs et al., 2008). HA-based scaffolds (Hyalograft C) in the treatment of knee cartilage defects also reported preliminary clinical findings (Pavesio et al., 2003). The efficacy of Viscoderm® was demonstrated in patients undergoing facial rejuvenation procedures (Iannitti et al., 2016).

Randomized clinical studies have shown efficacy within 3 weekly intra-articular injections of Hylan G-F 20® (Boutefnouchet et al., 2017). Similarly, Hymovis® also underwent clinical studies and demonstrated effectivity and safety (Priano, 2017).

HA PRODUCTS DEVELOPMENT TOWARD NEW MEDICAL APPLICATIONS

In this section, we would like to address potential medical devices and medical device-related technologies that are likely to generate significant innovation over a ten-year period, based on reported cases (Kim et al., 2017). HA-based hydrogel was able to restore brain function following ischemic stroke (Nih et al., 2016). Using self-assembled HA to deliver agents to a cancer tumor has attracted increasing attention in the recent decade (Smejkalová et al., 2014; Chen M. et al., 2017; Quinones et al., 2018). The targeting properties and biodistribution of HA-based nanoparticles is very promising for atherosclerosis treatment (Beldman et al., 2017). Using HA hydrogels as tissue analog for stem cells-based therapies are merging as a promising strategy (Loebel et al., 2017; Wong et al., 2017). Oral administration of HA for the prevention of dry skin was established (Kawada et al., 2015; Kimura et al., 2016). The use of fragments of HA (35 kDa) was proposed as an additive in infant milk formula promoting intestinal defense (Kessler et al., 2018).

Still, the translation of these innovative approaches to clinics has been hindered by the poor correlation between *in vitro* and *in vivo* models. The same could be predicted for animal and human *in vivo* response.

OVERVIEW OF GAPS, CHALLENGES, AND POTENTIAL OPPORTUNITIES IN HA-BASED MEDICAL DEVICES

More than 80 years after HA discovery we still lack the fundamental understanding of HA biological role. While biologists continue to unravel the complex biological functions of HA, the problem is complex, therefore, it some cases is not clear for the developer, whether a device works because HA is biologically active or because of its physical properties. HA cannot be considered a "filler," because HA presents many biological functions and regulates immune responses. Therefore, a deeper understanding of the mechanisms underlying the roles of HA in various physiological processes can provide new insights and tools for the engineering of new medical devices.

Up to now, the role of HA in wound healing, chronic inflammation and cancer is not well-understood. Even now, new HA-binding proteins or HA-degrading enzymes are being described (Yamamoto et al., 2017) adding to HA's complexity. Moreover, the presence and biological effect of HA in healthy and diseased biological fluids and tissues is poorly understood (Cowman, 2017). The incidence of long-term adverse reactions secondary to the injection of a foreign material is still ignored. Thus, clinicians should be aware of the fate to these injectable agents. Improving the understanding of required steps toward the registration of a new a product is helpful for researchers. Increasing the knowledge of the therapeutic (and non-therapeutic) uses of HA through the understanding of clinical effects, safety, and efficacy is required.

Potential opportunities of the use of HA based materials and devices such as dry eye syndrome devices due to the aging of the population can be envisaged on the market. Additionally, the commercialization of oral HA-based formulations is expected. The global HA market was valued at USD 7.2 billion in 2016 and is growing over the forecast period.

CONCLUSIONS

The natural origin of HA is both its benefit and its shortcoming in development of HA-based medical devices. In its native state, HA is highly biocompatible and biodegradable. HA is recognized by several cellular receptors and is degraded by enzymes which substrate specificity, expression profile and involvement in different pathophysiological processes vary. Moreover, it is still not clear how are various biological responses to HA directed by its structure and molecular weight. HA is a paradoxical molecule—is not the simple linear polymer because it forms

part of very biological processes not well-understood. The chemical derivatization and processing into different forms and materials just add another level of complexity. Moreover, chemical modification broadens the spectrum of HA therapeutic applications.

Finally, it is impossible to separate biocompatibility and safety from performance and efficacy. Thus, the high-quality assessment of chemical, physical, and biological properties of HA-based products is mandatory. Collecting enough information of a well-characterized-product and an adequate risk assessment will provide an effective translation from the lab bench to the clinic.

AUTHOR CONTRIBUTIONS

GH-Á revised the state of art of current devices based on HA and wrote the manuscript. KN evaluated all the necessary steps for *in vitro* characterization. GA and LK evaluated the data corresponding to animal model and *in vivo* testing. VV revised the manuscript.

FUNDING

GA and LK received support from MEYS-CR [project no. LQ1605].

REFERENCES

Alfaro, V., Cullell-Young, M., and Tanovic, A. (2007). Abbreviated clinical study reports with investigational medicinal products for human use: current guidelines and recommendations. *Croat. Med. J.* 48, 871–877. doi: 10.3325/cmj.2007.6.871

Altman, R. D., Bedi, A., Karlsson, J., Sancheti, P., and Schemitsch, E. (2016). Product differences in intra-articular hyaluronic acids for osteoarthritis of the knee. *Am. J. Sports Med.* 44, 2158–2165. doi: 10.1177/0363546515609599

Anderson, J. M., Rodriguez, A., and Chang, D. T. (2008). Foreign body reaction to biomaterials. *Semin. Immunol.* 20, 86–100. doi: 10.1016/j.smim.2007.11.004

Baeva, L. F., Das, S. S., and Hitchins, V. M. (2017). Bacterial endotoxin detection in hyaluronic acid-based medical devices. *J. Biomed. Mater. Res. Part B Appl. Biomater.* 105, 1210–1215. doi: 10.1002/jbm.b.33659

Bannuru, R. R., Natov, N. S., Dasi, U. R., Schmid, C. H., and McAlindon, T. E. (2011). Therapeutic trajectory following intra-articular hyaluronic acid injection in knee osteoarthritis–meta-analysis. *Osteoarthr. Cartil.* 19, 611–619. doi: 10.1016/j.joca.2010.09.014

Battistini, F. D., Tártara, L. I., Boiero, C., Guzmán, M. L., Luciani-Giaccobbe, L. C., Palma, S. D., et al. (2017). The role of hyaluronan as a drug carrier to enhance the bioavailability of extended release ophthalmic formulations. Hyaluronan-timolol ionic complexes as a model case. *Eur. J. Pharm. Sci.* 105, 188–194. doi: 10.1016/j.ejps.2017.05.020

Bedi, O., Krishan, P., and Singh, G. (2017). Regulatory requirements for medical devices: an insight. *Appl. Clin. Res. Clin. Trials Regul. Affairs* 4, 16–25. doi: 10.2174/2213476X03666160804153513

Beldman, T. J., Senders, M. L., Alaarg, A., Pérez-Medina, C., Tang, J., Zhao, Y., et al. (2017). Hyaluronan nanoparticles selectively target plaque-associated macrophages and improve plaque stability in atherosclerosis. *ACS Nano* 11, 5785–5799. doi: 10.1021/acsnano.7b01385

Bhojani-Lynch, T. (2017). Late-onset inflammatory response to hyaluronic acid dermal fillers. *Plastic Reconstr. Surg. Global Open* 5:e1532. doi: 10.1097/GOX.0000000000001532

Bitterman-Deutsch, O., Kogan, L., and Nasser, F. (2015). Delayed immune mediated adverse effects to hyaluronic acid fillers: report of five cases and review of the literature. *Dermatol Rep.* 7:5851. doi: 10.4081/dr.2015.5851

Bonnevie, E. D., Galesso, D., Secchieri, C., Cohen, I., and Bonassar, L. J. (2015). Elastoviscous transitions of articular cartilage reveal a mechanism of synergy between lubricin and hyaluronic acid. *PLoS ONE* 10:e0143415. doi: 10.1371/journal.pone.0143415

Boutefnouchet, T., Puranik, G., Holmes, E., and Bell, K. M. (2017). Hylan GF-20 viscosupplementation in the treatment of symptomatic osteoarthritis of the knee: clinical effect survivorship at 5 years. *Knee Surg. Relat. Res.* 29, 129–136. doi: 10.5792/ksrr.16.061

Braithwaite, G. J., Daley, M. J., and Toledo-Velasquez, D. (2016). Rheological and molecular weight comparisons of approved hyaluronic acid products—preliminary standards for establishing class III medical device equivalence. *J. Biomat. Sci. Polym. Ed.* 27, 235–246. doi: 10.1080/09205063.2015.1119035

Brittberg, M. (2014). "Knee cartilage repair with hyalograft® (Hyaff-11 scaffold with seeded autologous chondrocytes)," in *Techniques in Cartilage Repair Surgery,* eds A. A. Shetty, S. J. Kim, N. Nakamura, and M. Brittberg (Berlin; Heidelberg: Springer Berlin Heidelberg), 227–235.

Casas, J. W., Lewerenz, G. M., Rankin, E. A., Willoughby, J. A. Sr., Blakeman, L. C., McKim, J. M. Jr., et al. (2013). *In vitro* human skin irritation test for evaluation of medical device extracts. *Toxicol. In Vitro* 27, 2175–2183. doi: 10.1016/j.tiv.2013.08.006

Chen, C.-H., Chen, S.-H., Mao, S.-H., Tsai, M.-J., Chou, P.-Y., Liao, C.-H., et al. (2017). Injectable thermosensitive hydrogel containing hyaluronic acid and chitosan as a barrier for prevention of postoperative peritoneal adhesion. *Carbohydr. Polym.* 173, 721–731. doi: 10.1016/j.carbpol.2017.06.019

Chen, M., Zhang, W., Yuan, K., Bo, M., Chen, B., Li, L., et al. (2017). Preclinical evaluation and monitoring of the therapeutic response of a dual targeted hyaluronic acid nanodrug. *Contrast Media Mol. Imaging* 2017:4972701. doi: 10.1155/2017/4972701

Chmelar, J., Kotzianova, A., Hermannova, M., Sulakova, R., Smejkalova, D., Kulhanek, J., et al. (2017). Evaluating the degree of substitution of water-insoluble acyl derivatives of hyaluronan using Raman spectroscopy: method development and comparison with gas chromatography and 1H NMR. *Anal. Methods* 9, 232–239. doi: 10.1039/C6AY03067J

Choi, D. H., Kang, S. N., Kim, S. M., Gobaa, S., Park, B. J., Kim, I. H.,.,et al. (2016). Growth factors-loaded stents modified with hyaluronic acid and heparin for induction of rapid and tight re-endothelialization. *Colloids Surf. B Biointerfaces* 141, 602–610. doi: 10.1016/j.colsurfb.2016.01.028

Choi, J., Kim, J.-K., Kim, J.-H., Kweon, D.-K., and Lee, J.-W. (2010). Degradation of hyaluronic acid powder by electron beam irradiation, gamma ray irradiation, microwave irradiation and thermal treatment: a comparative study. *Carbohydr. Polym.* 79, 1080–1085. doi: 10.1016/j.carbpol.2009.10.041

Christo, S. N., Diener, K. R., Bachhuka, A., Vasilev, K., and Hayball, J. D. (2015). Innate immunity and biomaterials at the nexus: friends or foes. *Biomed. Res. Int.* 2015:342304. doi: 10.1155/2015/342304

Chun, C., Lee, D. Y., Kim, J. T., Kwon, M. K., Kim, Y. Z., and Kim, S. S. (2016). Effect of molecular weight of hyaluronic acid (HA) on viscoelasticity and particle texturing feel of HA dermal biphasic fillers. *Biomater Res.* 20:24. doi: 10.1186/s40824-016-0073-3

Coleman, K. P., McNamara, L. R., Grailer, T. P., Willoughby, J. A., Keller, D. J., Patel, P., et al. (2015). Evaluation of an *in vitro* human dermal sensitization test for use with medical device extracts. *Appl. In Vitro Toxicol.* 1, 118–130. doi: 10.1089/aivt.2015.0007

Cowman, M. K. (2017). Hyaluronan and hyaluronan fragments. *Adv. Carbohydr. Chem. Biochem.* 74, 1–59. doi: 10.1016/bs.accb.2017.10.001

Cožíková, D., Šílová, T., Moravcová, V., Šmejkalová, D., Pepeliaev, S., Velebný, V., and Hermannová, M. (2017). Preparation and extensive characterization of hyaluronan with narrow molecular weight distribution. *Carbohydr. Polym.* 160, 134–142. doi: 10.1016/j.carbpol.2016.12.045

Cyphert, J. M., Trempus, C. S., and Garantziotis, S. (2015). Size matters: molecular weight specificity of hyaluronan effects in cell biology. *Int. J. Cell Biol.* 2015:563818. doi: 10.1155/2015/563818

De Boulle, K., Glogau, R., Kono, T., Nathan, M., Tezel, A., Roca-Martinez, J.-X., et al. (2013). A review of the metabolism of 1,4-butanediol diglycidyl ether–crosslinked hyaluronic acid dermal fillers. *Dermatol. Surg.* 39, 1758–1766. doi: 10.1111/dsu.12301

D'Agostino, A., Stellavato, A., Busico, T., Papa, A., Tirino, V., Papaccio, G., et al. (2015). *In vitro* analysis of the effects on wound healing of high- and low-molecular weight chains of hyaluronan and their hybrid H-HA/L-HA complexes. *BMC Cell Biol.* 16:19. doi: 10.1186/s12860-015-0064-6

D'Este, M., Sprecher, C. M., Milz, S., Nehrbass, D., Dresing, I., Zeiter, S., et al. (2016). Evaluation of an injectable thermoresponsive hyaluronan hydrogel in a rabbit osteochondral defect model. *J. Biomed. Mater. Res. A.* 104, 1469–1478. doi: 10.1002/jbm.a.35673

Diamond, M. P., Burns, E. L., Accomando, B., Mian, S., and Holmdahl, L. (2012). Seprafilm® adhesion barrier: a review of preclinical, animal, and human investigational studies. *Gynecol. Surg.* 9, 237–245. doi: 10.1007/s10397-012-0741-9

Dondossola, E., Holzapfel, B. M., Alexander, S., Filippini, S., Hutmacher, D. W., and Friedl, P. (2016). Examination of the foreign body response to biomaterials by nonlinear intravital microscopy. *Nat. Biomed. Eng.* 1:0007. doi: 10.1038/s41551-016-0007

Doros, G., Lavin, P. T., Daley, M., and Miller, L. E. (2016). A method for establishing class III medical device equivalence: sodium hyaluronate (GenVisc 850) for the treatment of knee osteoarthritis. *Med. Devices* 9, 205–211. doi: 10.2147/MDER.S104327

Drímalová, E., Velebný, V., Sasinková, V., Hromádková, Z., and Ebringerová, A. (2005). Degradation of hyaluronan by ultrasonication in comparison to microwave and conventional heating. *Carbohydr. Polym.* 61, 420–426. doi: 10.1016/j.carbpol.2005.05.035

Essendoubi, M., Gobinet, C., Reynaud, R., Angiboust, J. F., Manfait, M., and Piot, O. (2016). Human skin penetration of hyaluronic acid of different molecular weights as probed by Raman spectroscopy. *Skin Res. Technol.* 22, 55–62. doi: 10.1111/srt.12228

Franz, S., Rammelt, S., Scharnweber, D., and Simon, J. C. (2011). Immune responses to implants - a review of the implications for the design of immunomodulatory biomaterials. *Biomaterials* 32, 6692–6709. doi: 10.1016/j.biomaterials.2011.05.078

Geavlete, P. A., Georgescu, D., Multescu, R., and Geavlete, B. (2016). "Chapter 9: Endoscopic approach to intramural ureter pathology," in *Endoscopic Diagnosis and Treatment in Urinary Bladder Pathology*, ed P. A. Geavlete (San Diego, CA: Academic Press), 293–348.

Gibbs, P., Brown, T. J., Ng, R., Jennens, R., Cinc, E., Pho, M., et al. (2008). A pilot human evaluation of a formulation of irinotecan and hyaluronic acid in 5-fluorouracil-refractory metastatic colorectal cancer patients. *Chemotherapy* 55, 49–59. doi: 10.1159/000180339

Gigis, I., Fotiadis, E., Nenopoulos, A., Tsitas, K., and Hatzokos, I. (2016). Comparison of two different molecular weight intra-articular injections of hyaluronic acid for the treatment of knee osteoarthritis. *Hippokratia* 20, 26–31.

Gold, M. H. (2007). Use of hyaluronic acid fillers for the treatment of the aging face. *Clin. Interv. Aging* 2, 369–376. doi: 10.2147/CIA.S1244

Gomis, A., Miralles, A., Schmidt, R. F., and Belmonte, C. (2009). Intra-articular injections of hyaluronan solutions of different elastoviscosity reduce nociceptive nerve activity in a model of osteoarthritic knee joint of the guinea pig. *Osteoarthr. Cartil.* 17, 798–804. doi: 10.1016/j.joca.2008.11.013

Gross, D., Childs, M., and Piaton, J. M. (2017). Comparison of 0.2% and 0.18% hyaluronate eye drops in patients with moderate to severe dry eye with keratitis or keratoconjunctivitis. *Clin. Ophthalmol.* 11, 631–638. doi: 10.2147/OPTH.S131384

Guarise, C., Pavan, M., Pirrone, L., and Renier, D. (2012). SEC determination of cross-link efficiency in hyaluronan fillers. *Carbohydr. Polym.* 88, 428–434. doi: 10.1016/j.carbpol.2011.12.004

Guo, J., Guo, S., Wang, Y., and Yu, Y. (2017). Adipose derived stem cells and hyaluronic acid based gel compatibility, studied *in vitro*. *Mol. Med. Rep.* 16, 4095–4100. doi: 10.3892/mmr.2017.7055

Hauser, S., Jung, F., and Pietzsch, J. (2017). Human endothelial cell models in biomaterial research. *Trends Biotechnol.* 35, 265–277. doi: 10.1016/j.tibtech.2016.09.007

Hayden, P. J., Michael, B., Seyoum, A., Silvia, L., Yulia, K., Mitchell, K., et al. (2015). Application of mattek *in vitro* reconstructed human skin models for safety, efficacy screening, and basic preclinical research. *Appl. In Vitro Toxicol.* 1, 226–233. doi: 10.1089/aivt.2015.0012

Highley, C. B., Prestwich, G. D., and Burdick, J. A. (2016). Recent advances in hyaluronic acid hydrogels for biomedical applications. *Curr. Opin. Biotechnol.* 40, 35–40. doi: 10.1016/j.copbio.2016.02.008

Huerta-Angeles, G., Brandejsová, M., Knotková, K., Hermannová, M., Moravcová, M., Šmejkalová, D., and Velebný, V. (2016a). Synthesis of photo-crosslinkable hyaluronan with tailored degree of substitution suitable for production of water resistant nanofibers. *Carbohydr. Polym.* 137, 255–263. doi: 10.1016/j.carbpol.2015.10.077

Huerta-Angeles, G., Brandejsová, M., Kulhánek, J., Pavlík, V., Šmejkalová, D., Vágnerová, H., and Velebný, V. (2016b). Linolenic acid grafted hyaluronan: process development, structural characterization, biological assessing, and stability studies. *Carbohydr. Polym.* 152, 815–824. doi: 10.1016/j.carbpol.2016.07.030

Huerta-Angeles, G., Brandejsová, M., Nigmatullin, R., Kopecká, K., and Vágnerová, H., Šmejkalová, D. et al. (2017). Synthesis of graft copolymers based on hyaluronan and poly(3-hydroxyalkanoates). *Carbohydr. Polym.* 171, 220–228. doi: 10.1016/j.carbpol.2017.05.011

Huerta-Angeles, G., Šmejkalová, D., Chládková, D., Ehlová, T., Radovan, B., and Velebný, V. (2011). Synthesis of highly substituted amide hyaluronan derivatives with tailored degree of substitution and their crosslinking via click chemistry. *Carbohydr. Polym.* 84, 1293–1300. doi: 10.1016/j.carbpol.2011.01.021

Hwang, C. J. (2016). Periorbital injectables: understanding and avoiding complications. *J. Cutan. Aesthet. Surg.* 9, 73–79. doi: 10.4103/0974-2077.184049

Iannitti, T., Morales-Medina, J. C., Coacci, A., and Palmieri, B. (2016). Experimental and clinical efficacy of two hyaluronic acid-based compounds of different cross-linkage and composition in the rejuvenation of the skin. *Pharm. Res.* 33, 2879–2890. doi: 10.1007/s11095-014-1354-y

Ibrahim, I. H., and Chassapis, C. (2014). Recent patents on risk management during medical device lifecycle: managing the transition from bench to market. *Recent Patents Eng.* 8, 133–142. doi: 10.2174/1872212108666140829011303

Ishikawa, M., Yoshioka, K., Urano, K., Tanaka, Y., Hatanaka, T., and Nii, A. (2014). Biocompatibility of cross-linked hyaluronate (Gel-200) for the treatment of knee osteoarthritis. *Osteoarthr. Cartil.* 22, 1902–1909. doi: 10.1016/j.joca.2014.08.002

Kaur, M., and Jayaraman, G. (2016). Hyaluronan production and molecular weight is enhanced in pathway-engineered strains of lactate dehydrogenase-deficient Lactococcus lactis. *Metab. Eng. Commun.* 3, 15–23. doi: 10.1016/j.meteno.2016.01.003

Kawada, C., Kimura, M., Masuda, Y., and Nomura, Y. (2015). Oral administration of hyaluronan prevents skin dryness and epidermal thickening in ultraviolet irradiated hairless mice. *J. Photochem. Photobiol. B.* 153, 215–221. doi: 10.1016/j.jphotobiol.2015.09.020

Kessler, S. P., Obery, D. R., Nickerson, K. P., Petrey, A. C., McDonald, C., and de la Motte, C. A. (2018). Multifunctional role of 35 kilodalton hyaluronan in promoting defense of the intestinal epithelium. *J. Histochem. Cytochem.* 66, 273–287. doi: 10.1369/0022155417746775

Khunmanee, S., Jeong, Y., and Park, H. (2017). Crosslinking method of hyaluronic-based hydrogel for biomedical applications. *J. Tissue Eng.* 8. doi: 10.1177/2041731417726464

Kim, H., Jeong, H., Han, S., Beack, S., Hwang, B. W., Shin, M., et al.. (2017). Hyaluronate and its derivatives for customized biomedical applications. *Biomaterials* 123, 155–171. doi: 10.1016/j.biomaterials.2017.01.029

Kim, J.-T., Lee, D. Y., Kim, E.-J., Jang, J.-W., and Cho, N.-I. (2014a). Tissue response to implants of hyaluronic acid hydrogel prepared by microbeads. *Tissue Eng. Regener. Med.* 11, 32–38. doi: 10.1007/s13770-013-1106-9

Kim, J.-T., Lee, D. Y., Kim, T.-H., Song, Y.-S., and Cho, N.-I. (2014b). Biocompatibility of hyaluronic acid hydrogels prepared by porous hyaluronic acid microbeads. *Metals Mater. Internat.* 20, 555–563. doi: 10.1007/s12540-014-3022-5

Kimura, M., Maeshima, T., Kubota, T., Kurihara, H., Masuda, Y., Nomura, Y. (2016). Absorption of orally administered hyaluronan. *J. Med. Food* 19, 1172–1179. doi: 10.1089/jmf.2016.3725

Kong, B., Seog, J. H., Graham, L. M., and Lee, S. B. (2011). Experimental considerations on the cytotoxicity of nanoparticles. *Nanomedicine* 6, 929–941. doi: 10.2217/nnm.11.77

Kuehl, C., Zhang, T., Kaminskas, L. M., Porter, C. J. H., Davies, N. M., Forrest, L., et al. (2016). Hyaluronic acid molecular weight determines lung clearance and biodistribution after instillation. *Mol. Pharm.* 13, 1904–1914. doi: 10.1021/acs.molpharmaceut.6b00069

La Gatta, A., De Rosa, M., Frezza, M. A., Catalano, C., Meloni, M., and Schiraldi, C. (2016). Biophysical and biological characterization of a new line of hyaluronan-based dermal fillers: a scientific rationale to specific clinical indications. *Mater. Sci. Eng. C* 68, 565–572. doi: 10.1016/j.msec.2016.06.008

Larrañeta, E., Henry, M., Irwin, N. J., Trotter, J., Perminova, A. A., and Donnelly, R. F. (2018). Synthesis and characterization of hyaluronic acid hydrogels crosslinked using a solvent-free process for potential biomedical applications. *Carbohydr. Polym.* 181, 1194–1205. doi: 10.1016/j.carbpol.2017.12.015

Laszlo, H., Robert, S., Piotr, L., Wojciech, Z., Endre, L., Eva, D., et al. (2017). Intraarticular injection of a cross-linked sodium hyaluronate combined with triamcinolone hexacetonide (Cingal) to provide symptomatic relief of osteoarthritis of the knee: a randomized, double-blind, placebo-controlled multicenter clinical trial. *Cartilage* 1:1947603517703732. doi: 10.1177/1947603517703732

Li, J., Feng, X., Liu, B., Yu, Y., Sun, L., Liu, T., et al. (2017). Polymer materials for prevention of postoperative adhesion. *Acta Biomater.* 61, 21–40. doi: 10.1016/j.actbio.2017.08.002

Li, W., Zhou, J., and Xu, Y. (2015). Study of the *in vitro* cytotoxicity testing of medical devices. *Biomed. Rep* 3, 617–620. doi: 10.3892/br.2015.481

Liu, X. M., Heiler, D. J., Menzel, T., Brongo, A., Burke, S. E., and Cummins, K. (2012). *Sterile Hyaluronic Acid Solutions*. US 8283463 B2.

Liu, Y., Zheng Shu, X., and Prestwich, G. D. (2005). Biocompatibility and stability of disulfide-crosslinked hyaluronan films. *Biomaterials* 26, 4737–4746. doi: 10.1016/j.biomaterials.2005.01.003

Loebel, C., Szczesny, S. E., Cosgrove, B. D., Alini, M., Zenobi-Wong, M., Mauck, R. L., et al. (2017). Cross-linking chemistry of tyramine-modified hyaluronan hydrogels alters mesenchymal stem cell early attachment and behavior. *Biomacromolecules* 18, 855–864. doi: 10.1021/acs.biomac.6b01740

Longinotti, C. (2014). The use of hyaluronic acid based dressings to treat burns: a review. *Burns Trauma* 2, 162–168. doi: 10.4103/2321-3868.142398

Markel, D. C., Jackson, N. M., Esquivel, A. O., Ren, W., and Flynn, J. C. (2014). Immunological response to bolus versus multiple injections of hylan G-F 20 (Synvisc®) in a murine biocompatibility model. *J. Biomed. Mat. Res. B Appl. Biomat.* 102, 1375–1380. doi: 10.1002/jbm.b.33116

Matarasso, S. L., Carruthers, J. D., and Jewell, M. L. (2006). Consensus recommendations for soft-tissue augmentation with nonanimal stabilized hyaluronic acid (Restylane). *Plast Reconstr. Surg.* 117(3 Suppl.), 3S—34S; discussion 35S—43S. doi: 10.1097/01.prs.0000204759.76865.39

Migliore, A., and Procopio, S., (2015). Effectiveness and utility of hyaluronic acid in osteoarthritis. *Clin. Cases Min. Bone Metab.* 12, 31–33. doi: 10.11138/ccmbm/2015.12.1.031

Migliore, A., Giovannangeli, F., Granata, M., and Laganà, B. (2010). Hylan G-F 20: review of its safety and efficacy in the management of joint pain in osteoarthritis. *Clin. Med. Insights Arthr. Musculoskelet. Disord.* 3, 55–68. doi: 10.1177/117954411000300001

Morais, J. M., Papadimitrakopoulos, F., and Burgess, D. J. (2010). Biomaterials/tissue interactions: possible solutions to overcome foreign body response. *AAPS J.* 12, 188–196. doi: 10.1208/s12248-010-9175-3

Morse, A. N., Hammer, R. A., Cornella, J. L., and Loftus, J. C. (2005). Validation of a mouse adhesion reduction model using seprafilm®. *J. Gynecol. Surg.* 21, 147–153. doi: 10.1089/gyn.2005.21.147

Nih, L. R., Carmichael, S. T., and Segura, T. (2016). Hydrogels for brain repair after stroke: an emerging treatment option. *Curr. Opin. Biotechnol.* 40, 155–163. doi: 10.1016/j.copbio.2016.04.021

Oe, M., Tashiro, T., Yoshida, H., Nishiyama, H., Masuda, Y., Maruyama, K., et al. (2016). Oral hyaluronan relieves knee pain: a review. *Nutr. J.* 15:11. doi: 10.1186/s12937-016-0128-2

Olejnik, A., Goscianska, J., Zielinska, A., and Nowak, I. (2015). Stability determination of the formulations containing hyaluronic acid. *Int. J. Cosmet. Sci.* 37, 401–407. doi: 10.1111/ics.12210

Oliveira, M. Z., Albano, M. B., Namba, M. M., da Cunha, L. A. M., de Lima Gonçalves, R. R., Trindade, E. S., et al. (2014). Effect of hyaluronic acids as chondroprotective in experimental model of osteoarthrosis. *Rev. Bras. Ortop.* 49, 62–68. doi: 10.1016/j.rbo.2013.04.006

Papakonstantinou, E., Roth, M., and Karakiulakis, G. (2012). Hyaluronic acid: a key molecule in skin aging. *Dermatoendocrinol* 4, 253–258. doi: 10.4161/derm.21923

Pavesio, A., Abatangelo, G., Borrione, A., Brocchetta, D., Hollander, A. P., Kon, E., et al. (2003). Hyaluronan-based scaffolds (Hyalograft C) in the treatment of knee cartilage defects: preliminary clinical findings. *Novartis Found Symp.* 249, 203–217; discussion 229–233, 234–208, 239–241. doi: 10.1002/0470867973.ch15

Pavicic, T., Gauglitz, G. G., Lersch, P., Schwach-Abdellaoui, K., Malle, B., Korting, H. C., et al. (2011). Efficacy of cream-based novel formulations of hyaluronic acid of different molecular weights in anti-wrinkle treatment. *J. Drugs Dermatol.*10, 990–1000.

Pedrosa, T. D. N., Catarino, C. M., Pennacchi, P. C., Assis, S. R., Gimenes, F., Consolaro, M. E. L., et al. (2017). A new reconstructed human epidermis for *in vitro* skin irritation testing. *Toxicol. In Vitro* 42, 31–37. doi: 10.1016/j.tiv.2017.03.010

Pérez-Pérez, L., García-Gavín, J., Wortsman, X., and Santos-Briz, Á. (2017). Delayed adverse subcutaneous reaction to a new family of hyaluronic acid dermal fillers with clinical, ultrasound, and histologic correlation. *Dermatol. Surg.* 43, 605–608. doi: 10.1097/DSS.0000000000000945

Phillips, K. S., and Wang, Y. (2017). U.S. Food and drug administration authors publish articles on dermal filler materials, injections, methods, and skin preparation. *Plast Reconstr. Surg.* 140, 632e—633e. doi: 10.1097/PRS.0000000000003723

Pi, S., Choi, Y. J., Hwang, S., Lee, D. W., Yook, J. I., Kim, K. H., et al. (2017). Local injection of hyaluronic acid filler improves open gingival embrasure: validation through a rat model. *J. Periodontol.* 88, 1221–1230. doi: 10.1902/jop.2017.170101

Picotti, F., Fabbian, M., Gianni, R., Sechi, A., Stucchi, L., and Bosco, M. (2013). Hyaluronic acid lipoate: synthesis and physicochemical properties. *Carbohydr. Polym.* 93, 273–278. doi: 10.1016/j.carbpol.2012.04.009

Priano, F. (2017). Early efficacy of intra-articular HYADD® 4 (Hymovis®) injections for symptomatic knee osteoarthritis. *Joints* 5, 79–84. doi: 10.1055/s-0037-1603677

Quinones, J. P., Jokinen, J., Keinänen, S., Covas, C. P., Brüggemann, O., and Ossipov, D. (2018). Self-assembled hyaluronic acid-testosterone nanocarriers for delivery of anticancer drugs. *Eur. Polym. J.* 99, 384–393. doi: 10.1016/j.eurpolymj.2017.12.043

Rayahin, J. E., and Gemeinhart, R. A. (2017). "Activation of Macrophages in response to biomaterials," in *Macrophages: Origin, Functions and Biointervention,* ed M. Kloc (Cham: Springer International Publishing), 317–351.

Romagnoli, M., and Belmontesi, M. (2008). Hyaluronic acid-based fillers: theory and practice. *Clin. Dermatol.* 26, 123–159. doi: 10.1016/j.clindermatol.2007.09.001

Sacco, P., Sechi, A., Trevisan, A., Picotti, F., Gianni, R., Stucchi, L., et al. (2016). A silver complex of hyaluronan–lipoate (SHLS12): synthesis, characterization and biological properties. *Carbohydr. Polym.* 136, 418–426. doi: 10.1016/j.carbpol.2015.09.057

Šafránková, B., Hermannová, M., Nešporová, K., Velebný, V., and Kubala, L. (2018). Absence of differences among low, middle, and high molecular weight hyaluronan in activating murine immune cells *in vitro*. *Int. J. Biol. Macromol.* 107, 1–8. doi: 10.1016/j.ijbiomac.2017.08.131

Salzillo, R., Schiraldi, C., Corsuto, L., D'Agostino, A., Filosa, R., De Rosa, M., et al. (2016). Optimization of hyaluronan-based eye drop formulations. *Carbohydr. Polym.*153, 275–283. doi: 10.1016/j.carbpol.2016.07.106

Shiedlin, A., Bigelow, R., Christopher, W., Arbabi, S., Yang, L., Maier, R. V., et al. (2004). Evaluation of hyaluronan from different sources: *Streptococcus zooepidemicus*, rooster comb, bovine vitreous, and human umbilical cord. *Biomacromolecules* 5, 2122–2127. doi: 10.1021/bm0498427

Shin, Y. S., Kwon, W. J., Cho, E. B., Park, E. J., Kim, K. H., and Kim, K. J. (2018). A case of cellulitis-like foreign body reaction after hyaluronic acid dermal filler injection. *Dermatol. Sin.* 36, 46–49. doi: 10.1016/j.dsi.2017.06.004

Sigen, A., Xu, Q., McMichael, P., Gao, Y., Li, X., Wang, X., et al. (2018). A facile one-pot synthesis of acrylated hyaluronic acid. *Chem. Commun.* 54, 1081–1084. doi: 10.1039/C7CC08648B

Simon-Walker, R., Cavicchia, J., Prawel, D. A., Dasi, L. P., James, S. P., and Popat, K. C. (2017). Hemocompatibility of hyaluronan enhanced linear low density polyethylene for blood contacting applications. *J. Biomed. Mater. Res. B Appl. Biomater.* doi: 10.1002/jbm.b.34010. [Epub ahead of print].

Šmejkalová, D., Muthný, T., Nešporová, K., Hermannová, M., Achbergerová, E., Huerta-Angeles, G. et al. (2017). Hyaluronan polymeric micelles for topical drug delivery. *Carbohydr. Polym.* 156, 86–96. doi: 10.1016/j.carbpol.2016.09.013

Smejkalová, D., Nešporová, K., Hermannová, M., Huerta-Angeles, G., Cožiková, D., Víštejnova, L. et al. (2014). Paclitaxel isomerisation in polymeric micelles based on hydrophobized hyaluronic acid. *Int. J. Pharm.* 466, 147–155. doi: 10.1016/j.ijpharm.2014.03.024

Smith, M. M., Cake, M. A., Ghosh, P., Schiavinato, A., Read, R. A., and Little, C. B. (2008). Significant synovial pathology in a meniscectomy model of osteoarthritis: modification by intra-articular hyaluronan therapy. *Rheumatology* 47, 1172–1178. doi: 10.1093/rheumatology/ken219

Stellavato, A., La Noce, M., Corsuto, L., Pirozzi, A. V. A., De Rosa, M., Papaccio, G., et al. (2017). Hybrid complexes of high and low molecular weight hyaluronans highly enhance HASCs differentiation: implication for facial bioremodelling. *Cell. Physiol. Biochem.* 44, 1078–1092. doi: 10.1159/000485414

Strand, V., Baraf, H. S. B., Lavin, P. T., Lim, S., and Hosokawa, H. (2012). A multicenter, randomized controlled trial comparing a single intra-articular injection of Gel-200, a new cross-linked formulation of hyaluronic acid, to phosphate buffered saline for treatment of osteoarthritis of the knee. *Osteoarthr. Cartil.* 20, 350–356. doi: 10.1016/j.joca.2012.01.013

Sun, F., Niu, H., Wang, D., Wu, Y., Mu, H., Ma, L., et al. (2017). Novel moisture-preserving derivatives of hyaluronan resistant to hyaluronidase and protective to UV light. *Carbohydr. Polym.* 157, 1198–1204. doi: 10.1016/j.carbpol.2016.10.086

Tolg, C., Telmer, P., and Turley, E. (2014). Specific sizes of hyaluronan oligosaccharides stimulate fibroblast migration and excisional wound repair. *PLoS ONE* 9:e88479. doi: 10.1371/journal.pone.0088479

Tran, C., Carraux, P., Micheels, P., Kaya, G., and Salomon, D. (2014). *In vivo* bio-integration of three hyaluronic acid fillers in human skin: a histological study. *Dermatology* 228, 47–54. doi: 10.1159/000354384

Turner, N. J., Kielty, C. M., Walker, M. G., and Canfield, A. E. (2004). A novel hyaluronan-based biomaterial (Hyaff-11) as a scaffold for endothelial cells in tissue engineered vascular grafts. *Biomaterials* 25, 5955–5964. doi: 10.1016/j.biomaterials.2004.02.002

Urdiales-Gálvez, F., Delgado, N. E., Figueiredo, V., Lajo-Plaza, J. V., Mira, M., Moreno, A., et al. (2018). Treatment of soft tissue filler complications: expert consensus recommendations. *Aesthetic Plast. Surg.* 42, 498–510. doi: 10.1007/s00266-017-1063-0

Van Norman, G. A. (2016). Drugs and devices: comparison of European and U.S. approval processes. *JACC* 1, 399–412. doi: 10.1016/j.jacbts.2016.06.003

Vasconcelos, D. M., Cortez, J., and Lamghari, M. (2016). *Technical Standards and Legislation for Implants and Implantable Medical Devices Reference Module in Materials Science and Materials Engineering*. Amsterdam: Elsevier.

Wang, J., Witte, F., Xi, T., Zheng, Y., Yang, K., Yang, Y., et al. (2015). Recommendation for modifying current cytotoxicity testing standards for biodegradable magnesium-based materials. *Acta Biomater.* 21, 237–249. doi: 10.1016/j.actbio.2015.04.011

Wehling, P., Evans, C., Wehling, J., and Maixner, W. (2017). Effectiveness of intra-articular therapies in osteoarthritis: a literature review. *Ther. Adv. Musculoskelet. Dis.* 9, 183–196. doi: 10.1177/1759720X17712695

Wende, F. J., Gohil, S., Mojarradi, H., Gerfaud, T., Nord, L. I., and Karlsson, A., et al (2016). Determination of substitution positions in hyaluronic acid hydrogels using NMR and MS based methods. *Carbohydr. Polym.* 136, 1348–1357. doi: 10.1016/j.carbpol.2015.09.112

Wende, F. J., Gohil, S., Nord, L. I., Helander Kenne, A., and Sandström, C. (2017). 1D NMR methods for determination of degree of cross-linking and BDDE substitution positions in HA hydrogels. *Carbohydr. Polym.*157, 1525–1530. doi: 10.1016/j.carbpol.2016.11.029

Wiegand, C., and Hipler, U. C. (2009). Evaluation of biocompatibility and cytotoxicity using keratinocyte and fibroblast cultures. *Skin Pharmacol. Physiol.* 22, 74–82. doi: 10.1159/000178866

Wong, T. Y., Chang, C.-H., Yu, C.-H., and Huang, L. L. H. (2017). Hyaluronan keeps mesenchymal stem cells quiescent and maintains the differentiation potential over time. *Aging Cell* 16, 451–460. doi: 10.1111/acel.12567

Wortman, R. S., Merritt, K., and Brown, S. A. (1983). The use of the mouse peritoneal cavity for screening for biocompatibility of polymers. *Biomater. Med. Devices Artif. Organs* 11, 103–114. doi: 10.3109/10731198309118799

Wu, L., Liu, X., Jian, X., Wu, X., Xu, N., Dou, X., et al. (2017). Delayed allergic hypersensitivity to hyaluronidase during the treatment of granulomatous hyaluronic acid reactions. *J. Cosmet. Dermatol.* doi: 10.1111/jocd.12461. [Epub ahead of print].

Yamamoto, H., Tobisawa, Y., Inubushi, T., Irie, F., Ohyama, C., and Yamaguchi, Y. (2017). A mammalian homolog of the zebrafish transmembrane protein 2 (TMEM2) is the long-sought-after cell-surface hyaluronidase. *J. Biol. Chem.* 292, 7304–7313. doi: 10.1074/jbc.M116.770149

Zamboni, F., Keays, M., Hayes, S., Albadarin, A. B., Walker, G. M., Kiely, P. A., et al. (2017). Enhanced cell viability in hyaluronic acid coated poly(lactic-co-glycolic acid) porous scaffolds within microfluidic channels. *Int. J. Pharm.* 532, 595–602. doi: 10.1016/j.ijpharm.2017.09.053

Zhang, Y., Rossi, F., Papa, S., Violatto, M. B., Bigini, P., Sorbona, M.,., et al. (2016). Non-invasive *in vitro* and *in vivo* monitoring of degradation of fluorescently labeled hyaluronan hydrogels for tissue engineering applications. *Acta Biomater.* 30, 188–198. doi: 10.1016/j.actbio.2015.11.053

Zhao, H., Liu, H., Liang, X., Li, Y., Wang, J., and Liu, C. (2016). Hylan G-F 20 versus low molecular weight hyaluronic acids for knee osteoarthritis: a meta-analysis. *BioDrugs* 30, 387–396. doi: 10.1007/s40259-016-0186-1

Conflict of Interest Statement: GH-Á and KN are currently employed by the company CONTIPRO a.s. VV is CONTIPRO's CEO.

The other authors declare that the research was conducted in the absence of any commercial or financial relationships that could be construed as a potential conflict of interest.

frontiers in Bioengineering and Biotechnology

ORIGINAL RESEARCH
published: 28 June 2018
doi: 10.3389/fbioe.2018.00087

Designed Surface Topographies Control ICAM-1 Expression in Tonsil-Derived Human Stromal Cells

*Aliaksei S. Vasilevich[1], Frédéric Mourcin[2], Anouk Mentink[1], Frits Hulshof[3], Nick Beijer[1], Yiping Zhao[4], Marloes Levers[4], Bernke Papenburg[4], Shantanu Singh[5], Anne E. Carpenter[5], Dimitrios Stamatialis[3], Clemens van Blitterswijk[6], Karin Tarte[2] and Jan de Boer[1]**

[1] Laboratory for Cell Biology-Inspired Tissue Engineering, MERLN Institute for Technology-Inspired Regenerative Medicine, Maastricht University, Maastricht, Netherlands, [2] Institut National de la Santé et de la Recherche Médicale, U917, Equipe Labelisée Ligue Contre le Cancer, Université Rennes, l'Etablissement Français du Sang Bretagne, Rennes, France, [3] Department of Biomaterials Science and Technology, MIRA Institute for Biomedical Technology and Technical Medicine, University of Twente, Enschede, Netherlands, [4] Materiomics BV, Maastricht, Netherlands, [5] Imaging Platform, Broad Institute of MIT and Harvard, Cambridge, MA, United States, [6] Department of Complex Tissue Regeneration, MERLN Institute for Technology-Inspired Regenerative Medicine, Maastricht University, Maastricht, Netherlands

OPEN ACCESS

Edited by:
Nihal Engin Vrana, Protip Medical, France

Reviewed by:
Tim Woodfield, University of Otago, New Zealand
Mark William Tibbitt, ETH Zürich, Switzerland

***Correspondence:**
Jan de Boer
jan.deboer@maastrichtuniversity.nl

Specialty section:
This article was submitted to Biomaterials, a section of the journal Frontiers in Bioengineering and Biotechnology

Received: *18 February 2018*
Accepted: *11 June 2018*
Published: *28 June 2018*

Citation:
Vasilevich AS, Mourcin F, Mentink A, Hulshof F, Beijer N, Zhao Y, Levers M, Papenburg B, Singh S, Carpenter AE, Stamatialis D, van Blitterswijk C, Tarte K and de Boer J (2018) Designed Surface Topographies Control ICAM-1 Expression in Tonsil-Derived Human Stromal Cells. Front. Bioeng. Biotechnol. 6:87. doi: 10.3389/fbioe.2018.00087

Fibroblastic reticular cells (FRCs), the T-cell zone stromal cell subtype in the lymph nodes, create a scaffold for adhesion and migration of immune cells, thus allowing them to communicate. Although known to be important for the initiation of immune responses, studies about FRCs and their interactions have been impeded because FRCs are limited in availability and lose their function upon culture expansion. To circumvent these limitations, stromal cell precursors can be mechanotranduced to form mature FRCs. Here, we used a library of designed surface topographies to trigger FRC differentiation from tonsil-derived stromal cells (TSCs). Undifferentiated TSCs were seeded on a TopoChip containing 2176 different topographies in culture medium without differentiation factors, then monitored cell morphology and the levels of ICAM-1, a marker of FRC differentiation. We identified 112 and 72 surfaces that upregulated and downregulated, respectively, ICAM-1 expression. By monitoring cell morphology, and expression of the FRC differentiation marker ICAM-1 via image analysis and machine learning, we discovered correlations between ICAM-1 expression, cell shape and design of surface topographies and confirmed our findings by using flow cytometry. Our findings confirmed that TSCs are mechano-responsive cells and identified particular topographies that can be used to improve FRC differentiation protocols.

Keywords: mechanobiology, surface topography, fibroblastic reticular cells, lymph node, ICAM-1

INTRODUCTION

Successful engineering of an artificial lymph node would enable *in vitro* investigation of the immune system, allow toxicological tests on a system closely mimicking the *in vivo* situation, and, ultimately, clinical transplantation (Cupedo et al., 2012). The lymph nodes are secondary lymphoid organs that control the immune system: they maintain hematopoietic cell functioning by serving as a tissue scaffold and provide pro-survival signals. They also facilitate the formation of

antigen-presenting sites, which promotes the immune response to antigens. Lymph nodes consist of hematopoietic and non-hematopoietic cells that are closely interconnected. Moreover, they harbor unique microenvironments, where either T cells or B cells are located and become activated (Crivellato et al., 2004; Cupedo et al., 2012). Stromal cells of lymph nodes are difficult to purify and culture due to their scarcity (<1% in secondary lymphoid organs (SLOs), strong interaction with extracellular matrix compounds (Fletcher et al., 2011), and rapid loss of functionality when removed from their native environment (Zeng et al., 2011). The culture of primary lymph node stromal cells has been successfully accomplished by only few groups (Katakai et al., 2004; Fletcher et al., 2011; Onder et al., 2012). The most abundant stromal cell type in lymph nodes is the fibroblastic reticular cell (FRC), which builds a three-dimensional network. (Katakai et al., 2004; Link et al., 2007). One of their key roles is to secrete cytokines such as CCL19/21 that specifically attract naïve T, naïve B, and mature dendritic cells, and they further act as a scaffold for anchoring and navigating cells, allowing them to interact and initiate an immune response (Turley et al., 2010; Malhotra et al., 2013).

An alternative to studying primary FRCs is to induce FRC differentiation from mesenchymal progenitor cells, derived from tonsil. We and others have shown that human SLOs contain bona-fide mesenchymal stromal cells (MSCs) that can be robustly differentiated to FRC in response to a combination of tumor necrosis factor-α (TNF-α) and lymphotoxin-α1β2 (LT-α1β2), the two main factors involved in differentiation and maintenance of SLO (Ame-Thomas et al., 2007; Fletcher et al., 2015; Bar-Ephraim et al., 2016). We reported that exposure of tonsil-derived stromal cells (TSCs, a polyclonal cell type that can be cultured from fresh tonsil tissue) to Tumor Necrosis Factor-α (TNF-α) and Lymphotoxin-α1β2 (LT-α1β2) leads to expression of FRC specific markers *in vitro*. These markers include adhesion molecules

CXCL12 chemokines (Ame-Thomas et al., 2007). Moreover, it was shown that ICAM-1 together with VCAM-1 expression reflects the differentiation process from stromal progenitors to FRC (Bénézech et al., 2012). Human tonsils can be obtained after a routine tonsillectomy. Tonsil stromal cells can be isolated by digestion of tonsils in collagenase and DNAse, centrifugation on a discontinuous Percoll gradient and collection of plastic- adherent cells. During expansion, cells lose their phenotype and thus it is not possible to track back their anatomical location and function in the tonsil, however, it was shown that these cells express mesenchymal markers CD90, CD73, CD105 and CXCL12 and exhibit a spindle-shaped fibroblastic morphology (Ame-Thomas et al., 2007). Moreover, the bone marrow and the adipose tissue can be considerate as alternative sources of stromal cells. BM-MSCs (Bone Marrow Mesenchymal Stromal Cells) and ASCs (Adipose Stromal Cells) are mostly used for regenerative medicine (Gentile et al., 2012) or for their immunosuppressive properties (Uccelli et al., 2008). While MSCs derived from bone marrow (BM-MSCs) can also be used for FRC differentiation, these cells are more sensitive to replicative senescence (Tarte et al., 2010) that reduces their immunological properties (Loisel et al., 2017). Adipose precursors from adipose tissue can differentiate into a variety of lymph node stromal cells (Bénézech et al., 2012). We demonstrated that adipose stromal cells (ASCs), like BM-MSCs, were able to acquire a FRC-like phenotype after TNF-α/LT-α1β2 stimulation (Pandey et al., 2017).

All three stromal cell sources—TSCs, ASCs and BM-MSCs—can be routinely obtained and used for achieving the FRC-like phenotype. However, it is known that the anatomical source of stromal cells can predefine their differentiation capabilities: for example, BM-MSCs overall yield better osteogenesis compared to ASCs (Liao and Chen, 2014), which in turn have better adipogenic differentiation ability compared to BM-MSCs *in vitro* (Tsuji et al., 2014). Taking this into account, we have chosen TSCs as the source for FRC differentiation for these studies. Cytokine-induced FRC differentiation can be complemented with biomaterials manipulation. And potentially allows simultaneous co-culturing of multiple cell types which all required their own differentiation factors and may not be compatible with each other. It has been widely recognized that material properties such as chemistry, stiffness, and surface topography affect the biological processes of cells that grow on them (Guvendiren and Burdick, 2013; Luong-Van et al., 2013; Janson and Putnam, 2015). Interestingly, recent studies show that interstitial flow causes mechano-induced FRC differentiation of cancer-associated fibroblasts and subsequent modulation of T cell differentiation (Swartz and Lund, 2012). This finding suggests that mechanotransduction can be used as a tool to induce FRC differentiation.

One of the approaches to induce mechanical loading on cells is to introduce microtopography on the surface on which the cells are growing. Topographical cues have been repeatedly shown to dramatically influence cell behavior and phenotype (Unadkat et al., 2011; Kolind et al., 2012; Wong et al., 2014). For instance, we discovered surfaces with topographical structures were able to maintain Oct4 expression, support proliferation and cell-cell adhesion of human-induced pluripotent stem cells without added growth factors (Reimer et al., 2016). Furthermore, we have demonstrated that surface topographies exert a mitogenic effect on BM-MSCs (Unadkat et al., 2011) and have profound effects on cell shapes (Hulsman et al., 2015). Recently, we have shown that some topographies increase mineralization in BM-MSCs and improve bone bonding *in vivo* (Hulshof et al., 2017). The advantages of this approach are that topographies can be designed *in silico* and produced on virtually any surface, from culture plates to medical devices, using micro-fabrication technologies (Zhao et al., 2013; Ryan et al., 2015; Sackmann et al., 2015).

To study systematically the effect of topography on TSCs differentiation, we employed the TopoChip, a microtopography screening platform developed in our laboratory (Unadkat et al., 2011). The TopoChip enables the assessment of cell response to 2176 unique topographies in a single high-throughput slide. Topographical features were randomly selected from the *in silico* library of more than 150 million topographies, which

were designed using an algorithm that generates patterns based on three simple geometric elements – circles, triangles, and rectangles (**Supplementary Figure 1**).

We cultured human TSCs on the TopoChip platform, and evaluated, by high-content imaging, cellular response, cell morphology and the expression of the phenotypic marker ICAM-1. We identify topographical patterns that modulate ICAM-1 expression in TSCs, complementing differentiation into FRC by chemical inducers of differentiation.

MATERIALS AND METHODS

Cell Culture

Stromal cells were obtained from human tonsils collected from children undergoing routine tonsillectomy, after informed consent as described previously (Ame-Thomas et al., 2007). Cells were cultured in αMEM media supplemented with 10% FBS at 37°C in a humid atmosphere with 5% CO^2 unless stated differently. For induction of FRC phenotype, cells were treated with TNF-α (10 ng/mL) and LT-α1β2 (100 ng/mL; R&D Systems, Abingdon, United Kingdom). On TopoChips, cells were seeded at a density of 10,000 cells/cm^2, using a seeding device (Unadkat et al., 2013) and cultured for 48 h (**Supplementary Figure 2**).

Adipogenesis

To induce adipogenesis, cells were cultured for 3 weeks in adipogenic media (DMEM (Gibco, 41-965-062), 100 U/ml penicillin +100 mg/ml streptomycin (Gibco, 15140-122), 10% fetal bovine serum, 0.2 mM Indomethacin (Sigma, 57413), 0.5 mM IBMX (Sigma, I5879), 10^{-6} M dexamethasone (Sigma, D8893), 10 ug/ml insulin (human, Sigma, I9278). Cells were seeded at a density of 15,000 cells/cm^2; media was refreshed twice per week. To visualize lipid formation, cells were stained with Oil Red O as described before (De Boer et al., 2004). Briefly, cells were fixed with 10% formalin for 30 min at room temperature, rinsed with a water and washed with 60 % isopropanol. The sample was stained for 5 min in freshly filtered Oil Red O solution (stock: 500 mg Oil Red O (Sigma, O0625), 99 ml isopropanol, 1 ml water; stain: 15 ml stock + 10 ml water).

Oil Red O staining was quantified by extraction with 1 ml of 4% Igepal (Sigma, 56741) in isopropanol for 15 min by shaking at room temperature. Absorbance was measured at 540 nm.

Mineralization

To induce mineralization, cells were cultured for 4 weeks in mineralization media (α-MEM (Gibco, 22-571-038), 10% fetal bovine serum (Sigma), 2 mM L-glutamine (Gibco, 25030), 0.2 mM ascorbic acid (Sigma, A8960), 100 U/ml

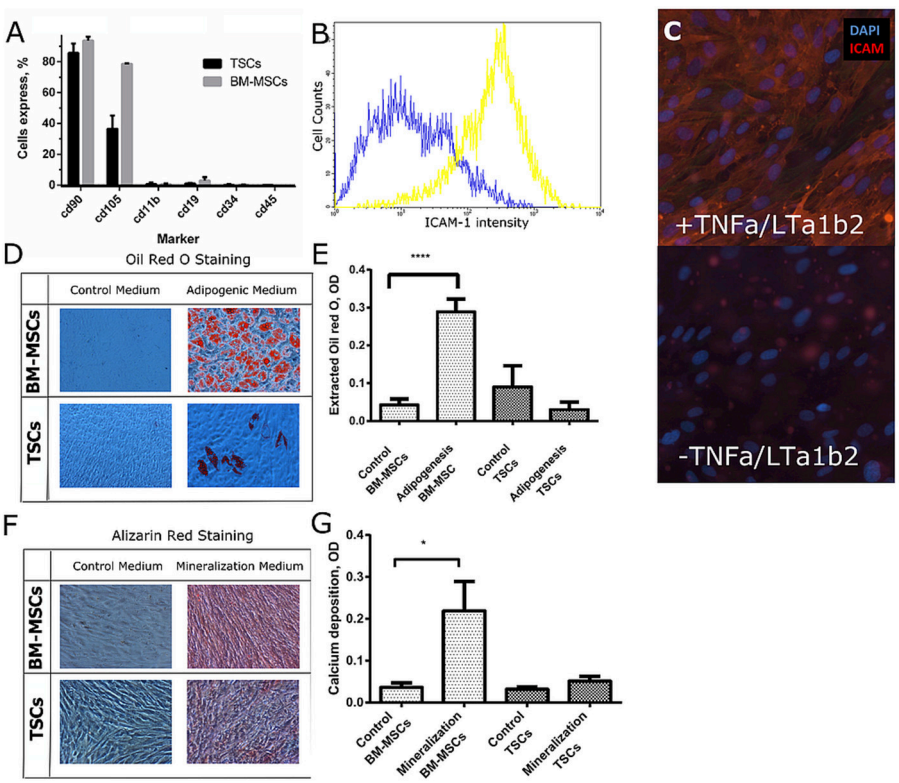

FIGURE 1 | Characterization of TSCs in comparison with BM-MSCs. **(A)** BM-MSCs and TSCs were screened on a panel of mesenchymal markers. **(B,C)** TSCs were cultured with and without TNF-α and LT-α1β2 for 48 h. ICAM-1 expression was assessed by FACS analysis **(B)**, and by immunofluorescent staining **(C)**. **(D)** BM-MSCs and TSCs were cultured in adipogenic medium for 3 weeks; lipids were stained with oil red O. **(E)** Lipid quantification was performed by lysis of stained lipids with Oil red O in a mixture of isopropanol and Igepal. **(F)** BM-MSCs and TSCs were cultured in osteogenic medium for 4 weeks; deposited calcium was stained with Alizarin red. **(G)** Calcium deposition was quantified using a calcium assay kit. *Indicates significant difference with a $p < 0.05$. ****Indicates significant difference with a $p < 0.0001$.

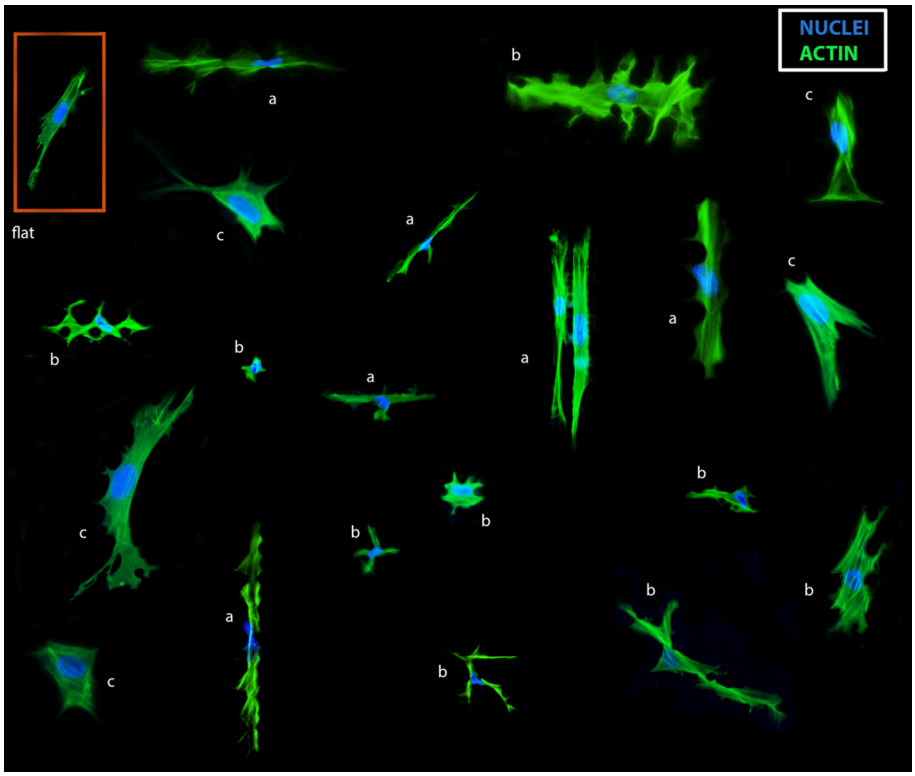

FIGURE 2 | Collage of TSC shapes on the TopoChip. TSCs were cultured for 48 h on a TopoChip in basic media and images of cells on different surfaces are displayed. Actin (green) was stained with phalloidin, DNA (blue) was stained with DAPI: cells in-between pillars: **(a)** extremely elongated cells, **(b)** cells with multiple lobes. Cells on top of pillars: **(c)** large cells.

penicillin + 100 mg/ml streptomycin (Gibco, 15140-122), 10^{-8} M dexamethasone (Sigma, D8893) plus 0.01 M β-glycerol phosphate (Sigma, 50020). Media was changed twice per week. To visualize mineral formation, samples were stained with Alizarin Red. Cells were fixed with neutral buffered formalin (10%) for 30 min, rinsed with water, and Alizarin Red was added for 45 min. Calcium deposition was quantified using a Calcium Assay Kit (Gibco, 10010-056) as described in the manual.

Staining and Imaging

Cells were fixed with 4% paraformaldehyde for 10 min; afterwards, samples were permeabilized with 0.5% Tween-20 for 20 min with following blocking step in 5% bovine serum albumin (BSA; Sigma) at room temperature for 30 min. Samples were incubated with primary antibodies against ICAM-1 (Abcam, ab53013) overnight at 4°C. Labeling with secondary antibodies conjugated to fluorochrome Alexa 594 and phalloidin conjugated to fluorochrome Alexa 488 was performed for 1 h at room temperature, followed by 10-min incubation with DAPI. Imaging was acquired on a Hamamatsu Nanozoomer Slide Scanner II.

Image and Data Analysis

Open source software Cell Profiler (CP) was used for the image analysis (Carpenter et al., 2006). In order to perform automated image analysis in CP, a robust pipeline able to recognize different cell features was built. Data analysis was performed using R, a programming language and software environment for statistical computing and graphics. Potential miss segmentation of cells was detected based on cell area and perimeter. Cells with cell perimeter and area that exceeded 1.5 quantiles from the median among all replicas for a particular surface were excluded from further analysis.

ICAM-1–positive or –negative cells were identified based on a threshold value. The threshold value was determined as the intersection of ICAM-1 cells median intensities distributions of positive and negative controls (**Figure 4B**) and corresponded to the 93rd percentile of all ICAM-1 median cell intensities in the negative control (**Figure 4B**). The threshold value was determined for each TopoChip replica separately and equalled the 93rd percentile of all ICAM-1 median intensities per replica. This adaptive threshold strategy allowed us to take a variation of median intensities between TopoChip replicas into account (**Supplementary Figure 5**).

To evaluate the correlation between ICAM-1 expression and surface design parameters, we trained a machine-learning model with 10-fold cross-validation with 75% of the data by employing a random forest classification algorithm. We analyzed design parameters of 72 low-scoring units and 112 high-scoring units that had a significant difference in frequency of ICAM-1–positive cells. The accuracy of the obtained model was assessed on a

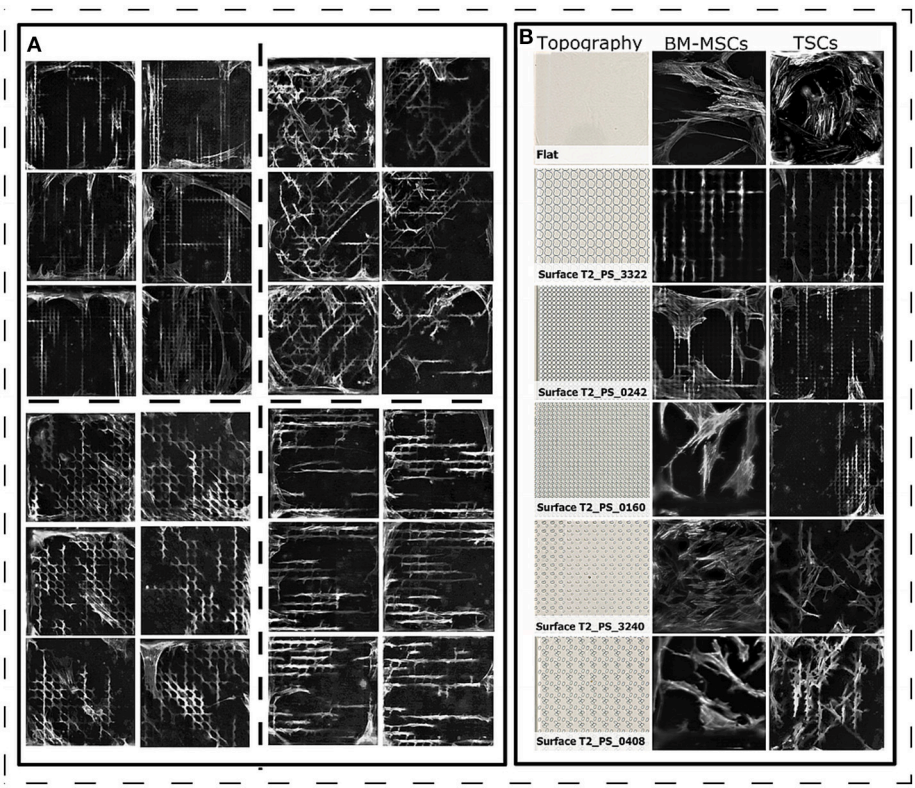

FIGURE 3 | Cell morphology of TSCs on polystyrene surfaces. **(A)** Diverse cell shapes on the TopoChip, that are highly reproducible within replicas (close located images). Actin staining is in gray. TSCs cells were cultured for 2 days in basic media. **(B)** Comparison of BM-MSC and TSC shapes on topographies with a different design. Actin staining is in gray. BM-MSCs were cultured in basic media for 5 days on titanium-coated topographies. TSCs cells were cultured for 2 days in basic media on polystyrene topographies.

held-out data set that was not used for model training (25% of the data). To ensure that the model was robust, we performed model training 100 times with random splitting of the data in training and testing sets. Models were trained with 10-fold cross-validation in the "caret" package (Kuhn, 2008).

Flow Cytometry

BM-MSCs and TSCs were characterized by flow cytometry as described previously (Mentink et al., 2013). Briefly, after trypsinization, cells were incubated for 30 min in blocking buffer (5% BSA (Sigma) in PBS), followed by incubation for 30 min with primary antibodies (1:50 dilution) or with an isotype control antibody. Cells were washed 3 times and incubated with secondary antibodies (1:100 dilution) for 30 min, followed by 2 times washing. To characterize surface markers, we used the following antibodies CD105, CD90, CD11b, CD19, CD45 (R&D Systems), and CD34 (Abcam). Expression levels were analyzed on a FACS Calibur (Becton Dickinson Immunocytometry Systems, Mountain View, CA).

For the validation on enlarged surfaces, cells were stained using the following monoclonal antibodies (mAbs): CD54 PE (Clone 84H10, Beckman Coulter) and Podoplanin/gp38 PerCP-efluor710 (clone NZ-1.3, Affymetrix). Appropriate isotype-matched mAbs were used as negative controls. Cells were analyzed using a Gallios (Beckman Coulter) flow cytometer and Kaluza 1.2 software (Beckman Coulter).

Quantitative RT-PCR

RNA was extracted using the Nucleospin RNA XS kit (Macherey-Nagel) and cDNA was generated using Superscript II reverse transcriptase and random hexamers (Life Technologies). For quantitative RT-PCR, assay-on-demand primers and probes, and TaqMan Universal Master Mix from Applied Biosystems (Life Technologies) were used. Gene expression was measured using StepOnePlus (Life Technologies) based on the ΔC_t calculation method. PUM1 was used as an internal standard gene. For each sample, the C_t value for the gene of interest was determined, normalized to its respective value for PUM1, and compared to the value obtained with a flat surface.

TopoChip and Fabrication of Enlarged Surfaces

The TopoChip was designed by selecting 2176 algorithm-generated topographies from an *in-silico* library and fabricated with the unique topographies in a 66×66 array of $300 \times 300\,\mu m$ wells, each known as a TopoUnit. Each 2×2 cm TopoChip includes duplicates of all 2176 unique topographies as well as 4 unpatterned TopoUnits (Unadkat et al., 2011).

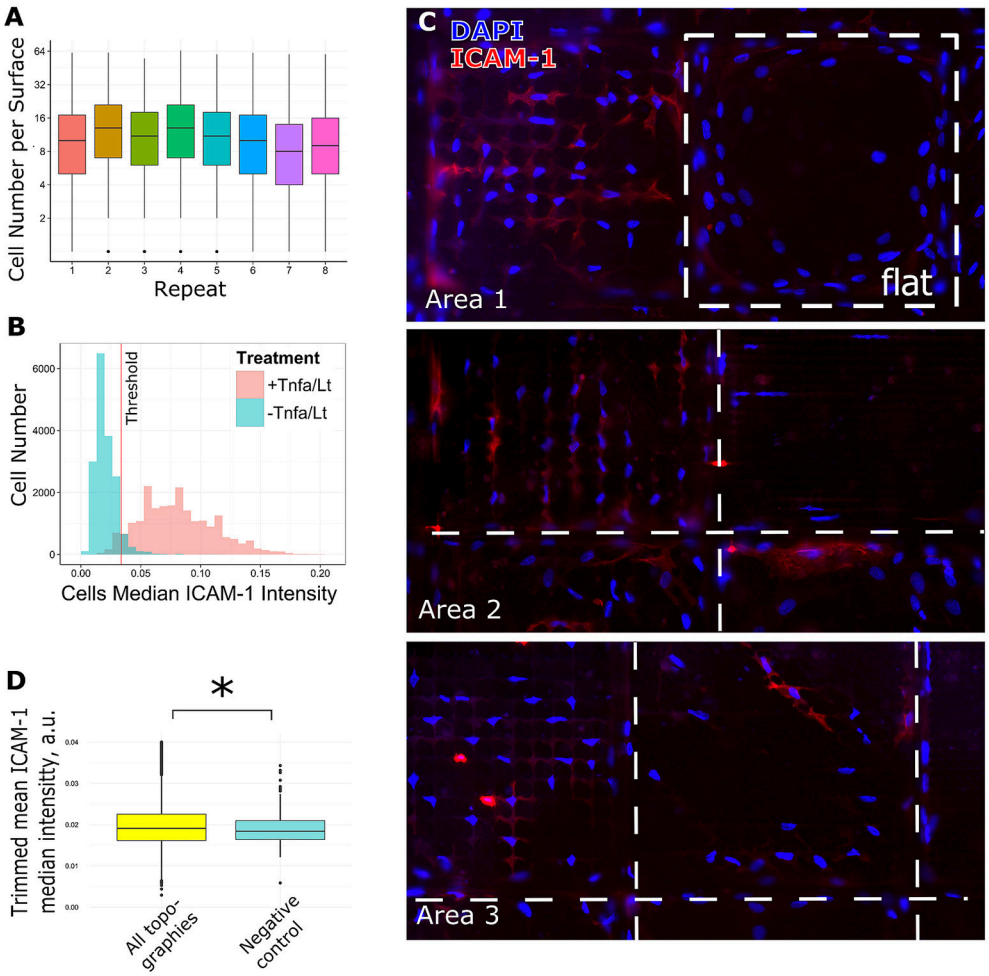

FIGURE 4 | Analysis of screening data and selection of hits. TSCs cells were cultured on 8 Topochips in basic media for 48 h. **(A)** Distribution of cell number per TopoUnit among all replicas. Cell numbers were counted by DAPI staining. **(B)** TSCs cells were cultured with or without TNF-α and LT-α1β2 on flat polystyrene for 48 h. The difference in ICAM-1 expression in samples treated and untreated with TNF-α and LT-α1β2., positive and negative control correspondingly. The threshold for identification of ICAM-1 positive vs. negative cells is shown as a red line. **(C)** The difference in ICAM-1 expression in cells, shown on random areas of the Topochip. DNA (blue) was stained with DAPI, ICAM-1 (red) was stained using an antibody against ICAM-1. Dashed white line shows borders between different topographies. **(D)** Median expression of ICAM-1 in cells on topographies was higher than in negative control and significantly different with a *p*-value less than 0.01 using a Wilcoxon rank sum test. *indicates significant difference with a *p*-value < 0.01.

Both the TopoChips and enlarged surface areas of hit topographies were prepared by hot embossing of (poly)styrene (PS) films (Goodfellow) (Zhao et al., 2013). Briefly, standard photolithography and deep reactive etching were used to produce the inverse structures of the topographies on a silicon wafer. The silicon master mold was then used to make a positive mold in poly(dimethylsiloxane) (PDMS). Subsequently, a second negative mold in OrmoStamp hybrid polymer (micro resist technology Gmbh) was obtained from the PDMS mold. This mold serves as the template for hot embossing (10 bar at 140°C for 5 min) the TopoChips and enlarged topographically enhanced surface areas in 190-μm-thick PS films. Prior to cell culture, the topographically enhanced PS films were O_2-plasma treated to increase protein attachment to the substrate surface in order to increase cell attachment.

Statistical Analyses Ad Data Visualization

Statistical analysis was performed in R ver. 3.2.5, graphs were generated in R package ggplot2 (Wickham, 2009) or in Graph Pad version 6.0. Unless stated differently, statistical analysis was performed with Student *t*-test, with a significance threshold of $p < 0.05$.

RESULTS

Characterization of TSCs

We isolated TSCs from a human tonsil and characterized surface marker expression and their response to a panel of differentiation media. BM-MSCs were used as a reference cell type (**Figure 1A**). Flow cytometry indicated that 37% of TSCs, compared to 79% of BM-MSCs, expressed the

CD105 mesenchymal marker (Ame-Thomas et al., 2007), and the mesenchymal marker CD90 was highly expressed in both TSCs and BM-MSCs. Neither TSCs nor BM-MSCs expressed markers indicative of macrophages (CD11b), B-cells (CD19), hematopoietic stem cells (CD34), or leukocytes (CD45).

To assess if TSCs cells can differentiate into FRCs, we cultured them for 48 h in media containing TNF-α and LT-α1β2. We used ICAM-1 as a phenotypic marker associated with FRC differentiation, which was previously shown to correlate with induction of FRC-like phenotype in TSCs (Ame-Thomas et al., 2007). We observed upregulation of ICAM-1 by flow cytometry (**Figure 1B**). Moreover, we were able to capture the difference in ICAM-1 expression clearly by immunofluorescence imaging (**Figure 1C**), which is essential for image-based screening assays (Bray and Carpenter, 2004).

To investigate multipotency of TSCs, we exposed them to adipogenic media and mineralization media. Following exposure to adipogenic media for 3 weeks, we observed most BM-MSCs with abundant lipid droplet formation (**Figure 1D**) but only few TSCs with lipids (**Figures 1D,E**). Upon exposure to mineralization medium for 4 weeks, mineralization was clearly observed in BM-MSCs but only occasionally detected minerals in TSCs (**Figure 1F**). As expected, the amount of deposited calcium in BM-MSCs treated with mineralization media was higher than in the untreated condition, while calcium was not significantly increased in TSCs (**Figure 1G**). These results demonstrate that the osteogenic and adipogenic differentiation capacity of TSCs was low compared to that of BM-MSCs.

TSCs Respond to Surface Topography

To evaluate the response of TSCs to surface topography, we seeded cells on polystyrene TopoChips, and cultured them for 48 h in basic medium and stained them with phalloidin and DAPI to visualize the cytoskeleton and nuclei, respectively. On flat control surfaces, TSCs displayed a typical spindle shape and oval nuclei (**Figure 2**), but showed very diverse cell shapes on the different topographies (**Figure 2**). For example, some topographies induced an extremely elongated morphology, cells with multiple lobes bulging out of the main body, or cells with extremely deformed nuclei. Within units and between replicas of the same topographies, cell shape was highly reproducible (**Figure 3A**). We noticed that cell shape was affected by the spacing between topography pillars. Previously, we were able to construct a computational model that was able to predict cell morphology based on surface design (Hulsman et al., 2015).

Next, we compared cell morphologies of TSCs and BM-MSCs grown on the same topographies. Images of BM-MSCs were taken from a previous experiment, where cells were cultured on titanium-coated surfaces (Hulshof et al., 2017). Here, we noted that the morphology of TSCs and BM-MSCs were similar on some topographies (for example, surface T2_PS_3322, **Figure 3B**) but different for others. For instance, on surface T2_PS_0242, TSCs grew in the valleys between the topographical pillars, whereas many BM-MSCs grew on top of the pillars. This may be due to the difference in cell size or cytoskeletal organizations (**Figure 3B**). In addition, observed changes can be due to the different protein absorption on the two materials (Stevens and George, 2005). However, we have compared MSC morphologies on titanium and polystyrene flat surfaces (**Supplementary Figure 6**) and found out that cells morphology is on flat surfaces is comparable, regardless of the chemistry. In order to draw strong conclusions, a pairwise comparison of BM-MSC and TSC morphologies on the TopoChip is required though, which is beyond the aim of the current paper.

Surface Topographies Induce Differences in ICAM-1 Expression

To assess the effect of surface topography on ICAM-1 expression, we cultured TSCs on eight TopoChips for 48 h in basic medium without TNF-α and LT-α1β2. Each TopoChip contains 2176 unique topographies, in duplicate, resulting in 16 replicas per unique topography. As positive and negative controls, respectively, we cultured TSCs on flat polystyrene ofapproximately equal area to the TopoChip with or without TNF-α and LT-α1β2. Cells were stained with DAPI to identify nuclei and phalloidin to visualize the cytoskeleton. The median cell number per unique topography varied between TopoChip replicas, with a range of 8–13 cells that corresponds to ∼160 cells per surface (**Figure 4A**). Next, we visually observed ICAM-1 staining as a marker of FRC differentiation using a robust image analysis pipeline using the open-source software, CellProfiler (Kamentsky et al., 2011). We found an increase in ICAM-1 staining in TSCs cultured on the TopoChips (**Figure 4B**), with the striking differences in ICAM-1 expression between topographies (**Figure 4C**). ICAM-1 expression was higher on the majority of topographies compared to the unpatterned surfaces in the TopoChips (**Figure 4C**). Quantitative analysis of the images showed that the median ICAM-1 expression on all topographies was significantly higher than that found from the negative control, which is TSCs cultured on flat polystyrene in basic media (**Figure 4D**).

To determine how different topographies affect the expression of ICAM-1, we ranked surfaces based on the ratio of ICAM-1–positive cells in all replicas per unique surface. Cells were classified as either ICAM-1–positive or –negative based on a threshold value of fluorescence intensity (**Figure 4B**). Among the ICAM-1–positive hits, we identified ICAM-1^{High} and ICAM-1^{Low} surfaces by employing a chi-square test: we identified 112 surfaces that had a significantly higher number of ICAM-1–positive cells compared to the negative control (ICAM-1^{High} surfaces) and 72 with a lower number of ICAM-1–positive cells (ICAM-1^{Low}) (**Figure 5A**). The morphology of TSCs from ICAM-1^{High} and ICAM-1^{Low} surfaces were different (**Figure 5B**). Among the hits, we noticed that ICAM-1^{High} and ICAM-1^{Low} surfaces not only have a drastically different level of ICAM-1 expression but also unique cell shapes (**Figure 5B**), which will be discussed below. From the hits, we selected four topographies that belong to either ICAM-1^{High} or ICAM-1^{Low} (**Figure 5C**, **Supplementary Figure 3**) and have different cell

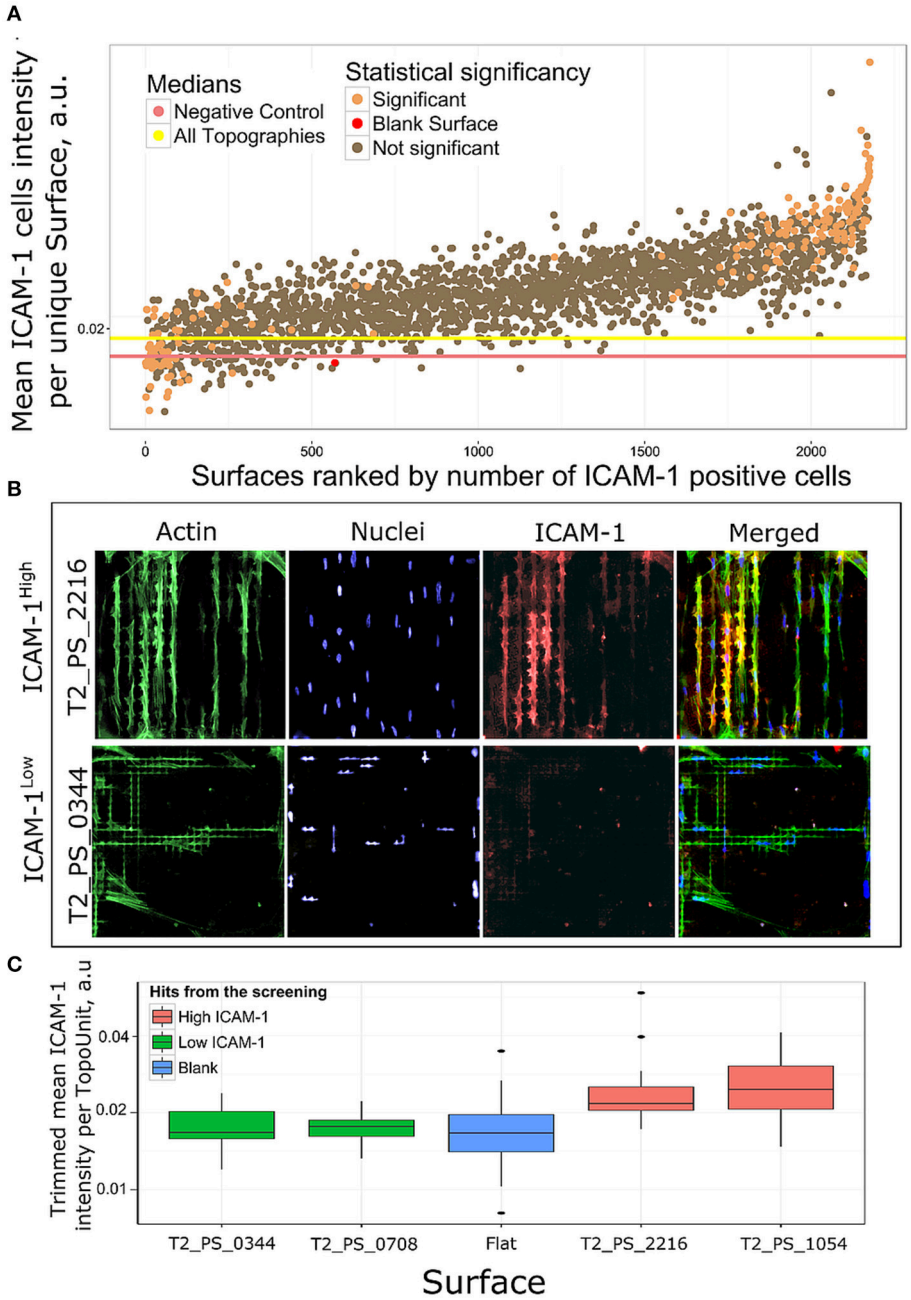

FIGURE 5 | Rank of surfaces based on ICAM-1 intensity. **(A)** Mean ICAM-1 expression in all replicas was ranked by a number of ICAM-1 positive cells. Using chi-square test we identified 184 surfaces with significantly different number of ICAM-1 positive cells in comparison with flat polystyrene, orange dots. **(B)** Immunofluorescent images of cell morphologies represented by actin (green), nuclei (blue) and FRC differentiation marker ICAM-1 (red) staining on a high scoring surface T2_PS_2216 and low scoring T2_PS_0344. Actin was stained with phalloidin, nuclei were stained with DAPI. **(C)** Distribution of ICAM-1 expression in surfaces selected for further validation.

shapes (**Supplementary Figure 4**). These topographies were used for further validation studies. We discovered that topographies have a diverse effect on ICAM-1 expression in TSCs. TSCs on flat topographies are among the lowest ICAM-1 expression from all the tested surfaces. We were able to rank topographies based on ICAM-1 presence and selected topographies for validation studies taking into account cells shapes. Selected surfaces had a very clear contrasting expression of ICAM-1 which was visible on immunofluorescent images and was validated by the analysis (**Figure 5B**, **Supplementary Figure 3**).

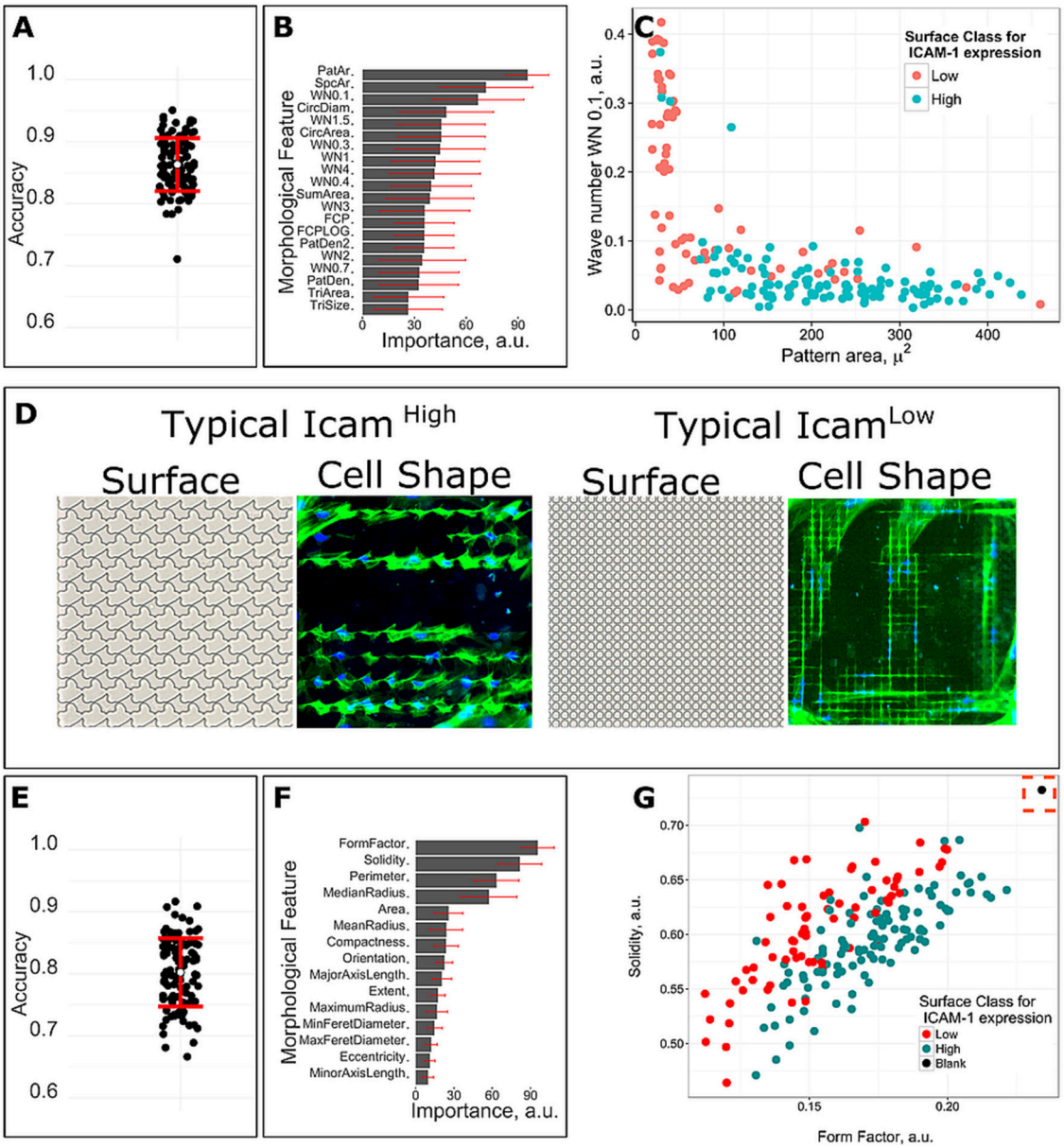

FIGURE 6 | Correlations between surface design, cell shape and ICAM-1 expression. A machine learning model was trained with 10 fold cross-validation by employing random forest classification algorithm. Seventy-two low scoring units and one hundred twelve high-scoring units with significantly different frequency of ICAM-1 positive cells were used for the analysis. **(A)** The accuracy of 100 predicted models based on surface design parameters. **(B)** Feature mean and standard deviation of importance for predicting surface class for ICAM-1 level based on surface design parameters. **(C)** Surfaces with different level of ICAM-1 can be distinguished based on surfaces design parameters that were predicted as the most important by the model. **(D)** Typical cell morphologies and topography structure of ICAM-1^{Low} and ICAM-1^{High} surfaces. Green corresponds to actin and blue for nuclei. **(E)** The accuracy of 100 predicted models based on cell shape parameters. **(F)** Feature mean and standard deviation of cell shape parameters importance for predicting surface class for ICAM-1 level. **(G)** Surfaces with the different level of ICAM-1 can be distinguished based on cell shape parameters that were predicted as the most important by the model. Black dot is a control, cells on flat surfaces.

ICAM-1 Expression Correlates to Surface Design Parameters and Cell Shape

To evaluate the correlation between ICAM-1 expression and surface design parameters, we trained a machine learning model with 10-fold cross-validation by employing random forest (RF) classification, a pattern-recognition, computational algorithm that is able to unravel non-linear relationships in data. We used RF and binary classification to identify the surface design parameters that are unique to the 112 ICAM-1^{High} and 72 ICAM-1^{Low} surfaces. This was done by binary classification, which means that we had 2 different classes with ICAM-1^{High} or ICAM-1^{Low} surfaces and found similar design properties

within those groups. We analyzed design parameters of seventy-two low scoring units and one hundred twelve high-scoring units that had a significant difference in frequency of ICAM-1 positive cells. The accuracy of the obtained model was assessed on a held-out data set, which was randomly selected from 1/3 of the original data, and not used for model training. To ensure robustness of the model, we performed model training 100 times with random splitting of the data into training and testing data sets. The average accuracy of the 100 simulations validated on the held-out data set was 86%, which means that from 100 surfaces, the algorithm was able to accurately predict expression of ICAM-1 on 86 of them (**Figure 6A**). In addition, we also quantified the importance of surface design parameters for separation of defined classes according to pattern recognition algorithm. The parameters that correlate to ICAM-1 expression based on average importance across all simulations (**Figure 6B**) include pattern area, space area, and the WN0.1 (Wave Number 0.1, which describes both density of structures and their size) (**Figure 6C**). A typical ICAM-1^{High} surface has pillars with the area in the range between 100 and 400 μm^2 with moderate spacing between them (**Figure 6D**), while the typical ICAM-1^{Low} surface has densely located patterns with the area typically lower than 100 μm^2 (**Figure 6D**).

Having observed that ICAM-1^{High} and I-CAM-1^{Low} surfaces resulted in different cell morphologies, we wished to obtain a model describing the relationship between cell shape and ICAM-1 expression, using the same machine-learning approach. The average accuracy of 100 simulations was 80% (**Figure 6E**). We found that the cell shape parameters Solidity, Form Factor, Perimeter, and Median Radius were the most important to separate the 2 classes in 100 simulations (**Figure 6F**), with Form Factor as the most important feature. Cells on flat surfaces were large and spread and thus had a large Form Factor value which is shown as a black dot in **Figure 6G**. At the same time, both positive and negative ICAM-1 cells were stretched elongated cells, but a typical ICAM-1 negative cell was thinner than ICAM-1 positive cells which also means more eccentric (**Figure 6D**).

Validation of the Screening Results on Enlarged Surfaces

To validate results of our screening, we selected four topographies that belong to either ICAM-1^{High} or ICAM-1^{Low} (**Figure 5C**, **Supplementary Figure 3**) and have different cell shapes (**Supplementary Figure 4**), then fabricated enlarged surfaces (12 mm in diameter each). We cultured TSCs on one TopoChip for 48 h in basic medium without stimulation with TNF-α and LT-α1β2. TSCs were also cultured on these larger surfaces for 48 h without TNF-α and LT-α1β2. Cells were stained with DAPI to identify nuclei and antibodies to display ICAM-1 level. Similar to the screening data, the ICAM-1 expression levels on the larger surfaces were also different on ICAM-1^{High} and ICAM-1^{Low} topographies (**Figure 7A**). Using flow cytometry, we found a significant difference in ICAM-1 levels between TSCs on the flat control surface and the two ICAM-1^{High} surfaces (pooled medians) (**Figure 7B**).

To investigate whether upregulated ICAM-1 expression in TSCs on selected topographies correlates to co-expression of other FRC markers, we evaluated the expression of some FRC-specific genes using qPCR analysis. On ICAM-1^{High} surface and ICAM-1^{Low} surface ICAM-1 expression was significantly different with more than 2 – fold change in comparison with cells on the flat surface (**Figure 7C**). Interestingly, ICAM-1 gene expression level on the $ICAM^{High}$ surface was the lowest of the three surfaces despite having the highest ICAM-1 expression at the protein level. None of the other markers of the FRC phenotype that we evaluated, such as VCAM-1, IL7, or CCL5, were differentially expressed in cells cultured on ICAM-1^{High} or ICAM-1^{Low} surfaces (data not shown).

However, we did observe an increase of LTBR gene expression on all four surfaces containing topography. The possibility of modulation of LTBR by the topography by our knowledge was not reported before, and certainly needed further investigation (**Figure 8A**). Moreover, expression of ICAM-1 and LTBR highly correlated on selected topographies with R^2 equal to 0.73 (**Figure 8B**).

We were able to validate results of the screening by immunofluorescent imaging, however, we did not observe consistent upregulation of FRC specific phenotypical markers.

DISCUSSION AND CONCLUSION

The objective of this study was to investigate whether TSCs are mechanoresponsive, and topography alone is sufficient to induce an FRC phenotype. We used ICAM-1 as readout because it is strongly upregulated during differentiation from stromal progenitors to FRC, making it a sensitive marker (Bénézech et al., 2012). ICAM-1 expression strongly increases in response to TNF-α and LT-α1β2, and ICAM-1 is an adhesion molecule known to be involved in mechanotransduction (Lessey-Morillon et al., 1950; Marjoram et al., 2014). Although ICAM-1 is an intercellular adhesion molecule (Rothlein et al., 1986), it has been reported as responsible for cell-cell interaction between lymphocytes and endothelial cells (Luscinskas et al., 1991). Moreover, it is known to be transcriptionally activated by the mechano-sensitive transcription factor egr-1 (Zhang et al., 2013). However, before our study, there has been no evidence that intercellular adhesion molecules can be manipulated by topography. Our investigation shows that ICAM-1 expression can be manipulated by topographical cues.

Differences in the number of ICAM-1–positive cells per unit may be explained by differential adhesion of ICAM-1–positive cells or by the proliferative advantage of ICAM-1–positive cells on selected topographies. Subpopulations of TSCs have an intrinsic expression of ICAM-1 (Ame-Thomas et al., 2007). Importantly, we did not observe surfaces where all cells were ICAM-1–positive in all replicas. However, the difference between the median cell numbers on ICAM-1^{Low} topographies and ICAM-1^{High} topographies is negligible (16 vs. 17 cells, respectively), which makes differential growth or adhesion advantages unlikely (**Figure 8C**). Similarly, topographies do strongly influence migratory behavior of cells, as has been reported for other cell types (Park et al., 2016). However, our TopoChip contains walls between units that make it unlikely that subpopulations of ICAM-1–positive cells migrated to hit topographies. Furthermore, we could predict accurately

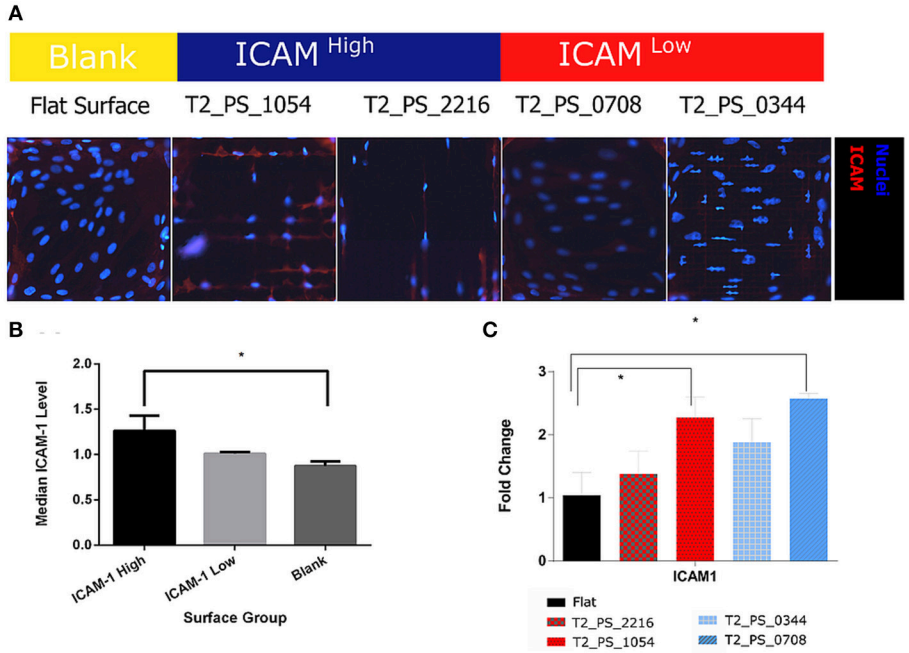

FIGURE 7 | Validation of ICAM-1 staining. TSCs cells were grown on polystyrene topographical surfaces in basic media for 48 h. **(A)** Fluorescent images of ICAM-1 staining in TSCs, ICAM-1 is red, and nuclei are blue. **(B)** Median ICAM-1 level, quantified by FACS, results from hits topographies are pooled. **(C)** Expression of ICAM-1 on hits topographies measured by qPCR. *Indicates significant difference with a $p < 0.05$.

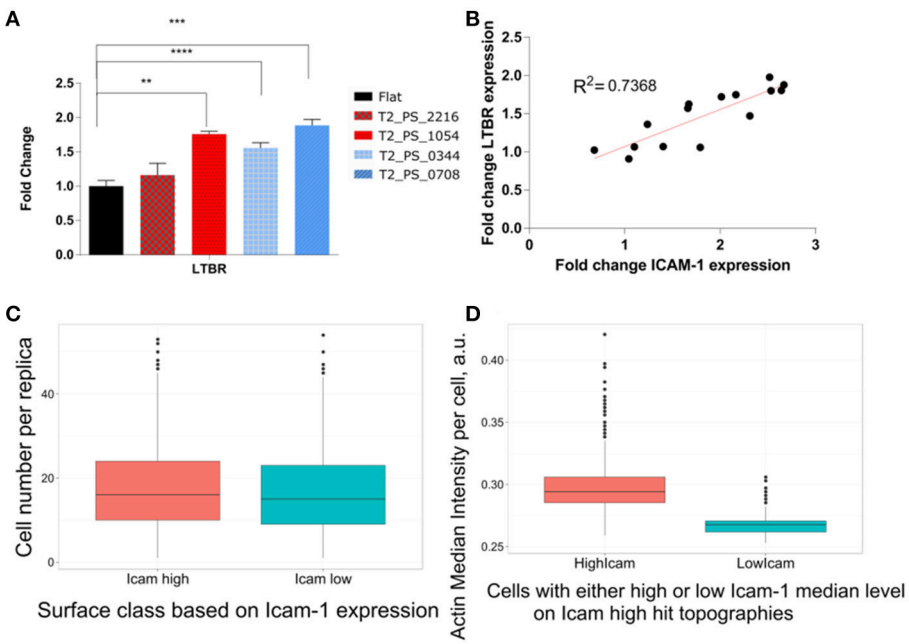

FIGURE 8 | Expression of FRC phenotypical markers. TSCs cells were cultured on polystyrene topographical surfaces in basic media for 48 h. **(A)** Expression of LTBR on selected topographies measured by qPCR. **(B)** Correlation between fold change in LTBR and ICAM-1. **(C)** Differences in Cell number on ICAM-1^{High} and ICAM-1^{Low} topographies. TSCs cells were cultured on 8 Topochips in basic media for 48 h. A number of cells were quantified based on nuclei staining. **(D)** Actin intensity comparison between cells with high and low median ICAM-1 level on ICAM-1^{High} topographies. TSCs cells were cultured on 8 Topochips in basic media for 48 h. Actin Intensity was measured in images of cells stained with fluorescently labeled phalloidin. *Indicates significant difference with a $p < 0.05$. **Indicates significant difference with a $p < 0.01$. ***Indicates significant difference with a $p < 0.001$. ****Indicates significant difference with a $p < 0.0001$.

the class of surfaces (ICAM-1^{High} or ICAM-1^{Low}) from the screening based on surface design and cell shape data. Moreover, the differences between selected hits were clearly visible on immunostained images (**Supplementary Figure 4**), indicating that topography induced ICAM-1 expression in TSCs.

The different levels of ICAM-1 in TSCs on ICAM-1^{High} surfaces might be related to cell cycle, as expression heterogeneity is well known for primary cell lines (Sivasubramaniyan et al., 2012; Gothard et al., 2014). Whether this applies for TSCs here requires further investigation. Interestingly, ICAM-1 intensity directly correlated to actin intensity (**Figure 8D**). Actin is the main transducer of mechanical signals to the cell (Gaspar and Tapon, 2014); if the actin network is less filamentous, it also provides less signal for ICAM-1 upregulation. It is known that actin directly binds to adhesion molecules such as ICAM-1 via ezrin, radixin, and moesin complexes (Lévesque and Simmons, 1999; Neisch and Fehon, 2011). Therefore, it is very likely that the expression of ICAM-1 is regulated through a mechanotransduction pathway involving actin. The effect of mechanical loading on the level of ICAM-1 has been described: an increase in interstitial flow can upregulate ICAM-1 in lymphatic endothelial cells (Swartz and Lund, 2012). This finding suggests that upregulation of ICAM-1 is a part of the global cell response to mechanical cues. For future work, it will be interesting to use cytoskeleton-disrupting agents to see how they affect ICAM-1 expression on the topographies.

In our validation studies with FACS, we saw small differences between selected topographies and flat surfaces which can be explained by first upregulation of ICAM-1 is not very high in comparison with TNF-α and LT-α1β2 and that this is bulk measurement. For such studies with heterogeneous cell population method that allows single-cell analysis, such as single cell qPCR, should be preferred.

Our findings of elongated cell shape correlating with I-CAM1^{High} surfaces are consistent with TSCs *in vivo*. Stromal cells in tonsils experience mechanical stress during the acute phase of inflammation when many lymphocytes enter the tonsil and subsequently expand the organ. For lymph nodes, it was shown that the total number of stromal cells does not increase, rather individual stromal cells stretch (Fletcher et al., 2015) during the early stages of organ expansion. Our elongated, ICAM-1–positive TSCs phenotypically resemble stretched cells.

Although a clear correlation was found between ICAM-1 expression, cell shape, and surface design, the cells did not adopt a mature FRC phenotype. We hypothesize that mechanotransduction can support but not fully trigger FRC differentiation.

TSCs respond very strongly to our library of topographies. We noted that TSCs are able to penetrate between dense pillars, and seem to do this more efficiently than BM-MSCs (**Figure 3B**). Different cell types behave differently on micropatterned topography, for example, Lecric et al. showed that when cultured together, fibroblasts tend to grow on ridges, while epithelial cells grow inside the grooves (Leclerc et al., 2013). Additionally, F. Badique et al. reported experiments on nuclear deformation on topographies with 3 osteosarcoma cell lines and demonstrated that cytoskeletal organization plays a major role in the cells' response to the microtopographies (Badique et al., 2013). It appears that TSCs more tightly adhere on topographical surfaces, and this may mimic their behavior in tonsils, where they have to create a very compact cellular structure and adhere to many cell types simultaneously. The findings reported here open up many avenues for further investigations. For example, it will be interesting to examine how topography affects meshwork formation in lymph node stromal cells.

In conclusion, we demonstrate that TSCs respond to surface topography and ICAM-1 expression correlates to both cell shape and surface design. Our ICAM-1–inducing surfaces are a valuable starting point to investigate the role of mechanobiology in FRC functions and in ICAM-1 mechanoregulation.

AUTHOR CONTRIBUTIONS

AV and SS performed screening and analyzed the data. FM, AM, ML, and AV performed differentiation studies, flow cytometry analysis and qRT-PCR. FH, NB, and YZ fabricated TopoChip and enlarged surfaces. BP, AC, DS, CvB, KT, and JdB provided reagents and critically reviewed the manuscript before the submission.

FUNDING

Funding for AC and SS was provided by the National Institute of General Medical Sciences of the National Institutes of Health under MIRA award number R35 GM122547 (to AC).

ACKNOWLEDGMENTS

We thank Céline Monvoisin and Marion Guirriec (University of Rennes, Rennes, France) and Natalie Fekete (Materiomics) for technical support. FM and KT received funding from the Ligue Nationale Contre le Cancer (Equipe labellisée). This research is supported by funding from the European Union's Seventh Framework Programme (FP7/2007-2013) under grant agreement no 289720. AV, NB, and JdB acknowledge the financial contribution of the Province of Limburg.

SUPPLEMENTARY MATERIAL

The Supplementary Material for this article can be found online at: https://www.frontiersin.org/articles/10.3389/fbioe.2018.00087/full#supplementary-material

Supplementary Figure 1 | TopoChip. A micro topography screening platform contains 2176 unique topographies. The topographical features were randomly selected from an *in silico* library of more than 150 million of topographies, which were designed from an algorithm that synthesized patterns based on simple geometric elements – circles, triangles, and rectangles.

Supplementary Figure 2 | Cells isolation schematic representation. Stromal cells were obtained from human tonsils collected from children undergoing routine tonsillectomy, after informed consent was obtained. Tonsils were cut into pieces and flushed using syringe and needle. Cell suspension was treated with DNAse I and collagenase IV followed by centrifugation on a discontinuous Percoll gradient. Cells were initially allowed to adhere for 48 h followed by elimination of nonadherent cells and culture in RPMI 1640 supplemented with 10% selected fetal calf serum, and penicillin/streptomycin.

Supplementary Figure 3 | ICAM-1 expression on replicas from the screening. TSC cells were cultured on 8 Topochips in basic media for 48 h. DNA (blue) was stained with DAPI, ICAM-1 (Red) was stained using a combination of primary against ICAM-1 and specific secondary antibodies.

Supplementary Figure 4 | Cell shapes of selected topographies. TSC cells were cultured on 8 Topochips in Basic media for 48 h. Actin (green) was stained with phalloidin, DNA (blue) was stained with DAPI.

Supplementary Figure 5 | Distribution of ICAM-1 expression among replicas. Every dot is a median ICAM-1 expression in a single cell, in yellow corresponding box plot is showing. The adaptive threshold value for ICAM-1 positive cells is shown as a red line.

Supplementary Figure 6 | Comparison of BM-MSC and TSC shapes on flat polystyrene and titanium coated surfaces. BM-MSCs were cultured in basic media for 5 days on titanium-coated flat surfaces and 24 h on polystyrene flat surfaces. TSCs cells were cultured for 48 h in basic media on polystyrene topographies.

REFERENCES

Amé-Thomas, P., Maby-El Hajjami, H., Monvoisin, C., Jean, R., Monnier, D., Caulet-Maugendre, S., et al. (2007). Human mesenchymal stem cells isolated from bone marrow and lymphoid organs support tumor B-cell growth: role of stromal cells in follicular lymphoma pathogenesis. *Blood* 109, 693–702. doi: 10.1182/blood-2006-05-020800

Badique, F., Stamov, D. R., Davidson, P. M., Veuillet, M., Reiter, G., Freund, J. N., et al. (2013). Directing nuclear deformation on micropillared surfaces by substrate geometry and cytoskeleton organization. *Biomaterials* 34, 2991–3001. doi: 10.1016/j.biomaterials.2013.01.018

Bar-Ephraim, Y. E., Konijn, T., Gönültas, M., Mebius, R. E., and Reijmers, R. M. (2016). A reproducible method for isolation and *in vitro* culture of functional human lymphoid stromal cells from tonsils. *PLoS ONE* 11:e0167555. doi: 10.1371/journal.pone.0167555

Bénézech, C., Mader, E., Desanti, G., Khan, M., Nakamura, K., White, A., et al. (2012). Lymphotoxin-β receptor signaling through NF-κB2-RelB pathway reprograms adipocyte precursors as lymph node stromal cells. *Immunity* 37, 721–734. doi: 10.1016/j.immuni.2012.06.010

Bray, M. A., and Carpenter, A. (2004). "Imaging platform, Broad Institute of MIT and Harvard. Advanced assay development guidelines for image-based high content screening and analysis," in *Assay Guidance Manual [Internet]*, eds G. S. Sittampalam, N. P. Coussens, K. Brimacombe, A. Grossman, M. Arkin, D. Auld et al. (Bethesda, MD: Eli Lilly & Company and the National Center for Advancing Translational Sciences).

Carpenter, A. E., Jones, T. R., Lamprecht, M. R., Clarke, C., Kang, I. H., Friman, O., et al. (2006). CellProfiler: image analysis software for identifying and quantifying cell phenotypes. *Genome Biol.* 7:R100. doi: 10.1186/gb-2006-7-10-r100

Crivellato, E., Vacca, A., and Ribatti, D. (2004). Setting the stage: an anatomist's view of the immune system. *Trends immunol.* 25, 210–217. doi: 10.1016/j.it.2004.02.008

Cupedo, T., Stroock, A., and Coles, M. (2012). Application of tissue engineering to the immune system: development of artificial lymph nodes. *Front. Immunol.* 3:343. doi: 10.3389/fimmu.2012.00343

De Boer, J., Wang, H. J., and Van Blitterswijk, C. (2004). Effects of Wnt signaling on proliferation and differentiation of human mesenchymal stem cells. *Tissue Eng.* 10, 393–401. doi: 10.1089/107632704323061753

Fletcher, A. L., Acton, S. E., and Knoblich, K. (2015). Lymph node fibroblastic reticular cells in health and disease. *Nat. Rev. Immunol.* 15, 350–561. doi: 10.1038/nri3846

Fletcher, A. L., Malhotra, D., Acton, S. E., Lukacs-Kornek, V., Bellemare-Pelletier, A., Curry, M., et al. (2011). Reproducible isolation of lymph node stromal cells reveals site-dependent differences in fibroblastic reticular cells. *Front. Immunol.* 2:35. doi: 10.3389/fimmu.2011.00035

Gaspar, P., and Tapon, N. (2014). Sensing the local environment: actin architecture and Hippo signalling. *Curr. Opin. Cell Biol.* 31:74–83. doi: 10.1016/j.ceb.2014.09.003

Gentile, P., Orlandi, A., Scioli, M. G., Di Pasquali, C., Bocchini, I., and Cervelli, V. (2012). Concise review: adipose-derived stromal vascular fraction cells and platelet-rich plasma: basic and clinical implications for tissue engineering therapies in regenerative surgery. *Stem Cells Transl. Med.* 1:230–236. doi: 10.5966/sctm.2011-0054

Gothard, D., Greenhough, J., Ralph, E., and Oreffo, R. O. (2014). Prospective isolation of human bone marrow stromal cell subsets: a comparative study between Stro-1-, CD146- and CD105-enriched populations. *J. Tissue Eng.* 5:2041731414551763. doi: 10.1177/2041731414551763

Guvendiren, M., and Burdick, J. A. (2013). Stem cell response to spatially and temporally displayed and reversible surface topography. *Adv. Healthc. Mater.* 2, 155–164. doi: 10.1002/adhm.201200105

Hulshof, F. F. B., Papenburg, B., Vasilevich, A., Hulsman, M., Zhao, Y., Levers, M., et al. (2017). Mining for osteogenic surface topographies: *in silico* design to *in vivo* osseo-integration. *Biomaterials* 137, 49–60. doi: 10.1016/j.biomaterials.2017.05.020

Hulsman, M., Hulshof, F., Unadkat, H., Papenburg, B. J., Stamatialis, D. F., Truckenmuller, R., et al. (2015). Analysis of high-throughput screening reveals the effect of surface topographies on cellular morphology. *Acta biomater.* 15, 29–38. doi: 10.1016/j.actbio.2014.12.019.

Janson, I. A., and Putnam, A. J. (2015). Extracellular matrix elasticity and topography: Material-based cues that affect cell function via conserved mechanisms. *J. Biomed. Mater. Res. A* 103, 1246–1258. doi: 10.1002/jbm.a.35254

Kamentsky, L., Jones, T. R., Fraser, A., Bray, M. A., Logan, D. J., Madden, K. L., et al. (2011). Improved structure, function and compatibility for CellProfiler: modular high-throughput image analysis software. *Bioinformatics* 27, 1179–1180. doi: 10.1093/bioinformatics/btr095

Katakai, T., Hara, T., Sugai, M., Gonda, H., and Shimizu, A. (2004). Lymph node fibroblastic reticular cells construct the stromal reticulum via contact with lymphocytes. *J. Exp. Med.* 200, 783–795. doi: 10.1084/jem.20040254

Kolind, K., Leong, K. W., Besenbacher, F., and Foss, M. (2012). Guidance of stem cell fate on 2D patterned surfaces. *Biomaterials* 33, 6626–6633. doi: 10.1016/j.biomaterials.2012.05.070

Kuhn, M. (2008). Building predictive models in r using the caret package. *J. Stat. Softw.* 28:26. doi: 10.18637/jss.v028.i05

Leclerc, A., Tremblay, D., Hadjiantoniou, S., Bukoreshtliev, N. V., Rogowski, J. L., Godin, M., et al. (2013). Three dimensional spatial separation of cells in response to microtopography. *Biomaterials* 34, 8097–8104. doi: 10.1016/j.biomaterials.2013.07.047

Lessey-Morillon, E. C., Osborne, L. D., Monaghan-Benson, E., Guilluy, C., O'Brien, E. T., Superfine, R., et al. (1950). The RhoA GEF, LARG, mediates ICAM-1-dependent mechanotransduction in endothelial cells to stimulate transendothelial migration. *J. immunol.* 192, 3390–3398. doi: 10.4049/jimmunol.1302525

Lévesque, J. P., and Simmons, P. J. (1999). Cytoskeleton and integrin-mediated adhesion signaling in human CD34+ hemopoietic progenitor cells. *Exp. Hematol.* 27, 579–586.

Liao, H.-T., and Chen, C. T. (2014). Osteogenic potential: Comparison between bone marrow and adipose-derived mesenchymal stem cells. *World J. Stem Cells* 6, 288–295. doi: 10.4252/wjsc.v6.i3.288

Link, A., Vogt, T. K., Favre, S., Britschgi, M. R., Acha-Orbea, H., Hinz, B., et al. (2007). Fibroblastic reticular cells in lymph nodes regulate the homeostasis of naive T cells. *Nat. immunol.* 8, 1255–1265. doi: 10.1038/ni1513

Loisel, S., Dulong, J., Ménard, C., Renoud, M. L., Meziere, N., Isabelle, B., et al. (2017). Brief report: proteasomal indoleamine 2, 3-dioxygenase degradation reduces the immunosuppressive potential of clinical grade-mesenchymal stromal cells undergoing replicative senescence. *Stem Cells* 35, 1431–1436. doi: 10.1002/stem.2580

Luong-Van, E., Rodriguez, I., Low, H. Y., Elmouelhi, N., Lowenhaupt, B., Natarajan, S., et al. (2013). Review: Micro- and nanostructured surface engineering for biomedical applications. *J. Mater. Res.* 28, 165–174. doi: 10.1557/jmr.2012.398

Luscinskas, F. W., Cybulsky, M. I., Kiely, J. M., Peckins, C. S., Davis, V. M., and Gimbrone, M. A. (1991). Cytokine-activated human endothelial monolayers support enhanced neutrophil transmigration via a mechanism involving both endothelial-leukocyte adhesion molecule-1 and intercellular adhesion molecule-1. *J. Immunol.* 146, 1617–1625.

Malhotra, D., Fletcher, A. L., and Turley, S. J. (2013). Stromal and hematopoietic cells in secondary lymphoid organs: partners in immunity. *Immunol. Rev.* 251, 160–176. doi: 10.1111/imr.12023

Marjoram, R. J., Lessey, E. C., and Burridge, K. (2014). Regulation of RhoA Activity by Adhesion Molecules and Mechanotransduction. *Curr. Mol. Med.* 14, 199–208. doi: 10.2174/1566524014666140128104541

Mentink, A., Hulsman, M., Groen, N., Licht, R., Dechering, K. J., van der Stok, J., et al. (2013). Predicting the therapeutic efficacy of MSC in bone tissue engineering using the molecular marker CADM1. *Biomaterials* 34, 4592–4601. doi: 10.1016/j.biomaterials.2013.03.001

Neisch, A. L., and Fehon, R. G. (2011). Ezrin, Radixin and Moesin: key regulators of membrane-cortex interactions and signaling. *Curr. opin. Cell Biol.* 23, 377–382. doi: 10.1016/j.ceb.2011.04.011.

Onder, L., Narang, P., Scandella, E., Chai, Q., Iolyeva, M., Hoorweg, K., et al. (2012). IL-7–producing stromal cells are critical for lymph node remodeling. *Blood.* 120, 4675–4683. doi: 10.1182/blood-2012-03-416859.

Pandey, S., Mourcin, F., Marchand, T., Nayar, S., Guirriec, M., Pangault, C., et al. (2017). IL-4/CXCL12 loop is a key regulator of lymphoid stroma function in follicular lymphoma. *Blood 129*, 2507–2518. doi: 10.1182/blood-2016-08-737239

Park, J., Kim, D. H., Kim, H. N., Wang, C. J., Kwak, M. K., Hur, E., et al. (2016). Directed migration of cancer cells guided by the graded texture of the underlying matrix. *Nat Mater.* 15, 792–801. doi: 10.1038/nmat4586

Reimer, A., Vasilevich, A., Hulshof, F., Viswanathan, P., van Blitterswijk, C. A., de Boer, J., et al. (2016). Scalable topographies to support proliferation and Oct4 expression by human induced pluripotent stem cells. *Sci. Rep.* 6:18948. doi: 10.1038/srep18948

Rothlein, R., Dustin, M. L., Marlin, S. D., and Springer, T. A. (1986). A human intercellular adhesion molecule (ICAM-1) distinct from LFA-1. *J. Immunol.* 137, 1270–1274.

Ryan, C. N., Fuller, K. P., Larrañaga, A., Biggs, M., Bayon, Y., Sarasua, J. R., et al. (2015). An academic, clinical and industrial update on electrospun, additive manufactured and imprinted medical devices. *Expert Rev. Med. Dev.* 12, 601–612. doi: 10.1586/17434440.2015.1062364

Sackmann, J., Burlage, K., Gerhardy, C., Memering, B., Liao, S., and Schomburg, W. K. (2015). Review on ultrasonic fabrication of polymer micro devices. *Ultrasonics* 56, 189–200. doi: 10.1016/j.ultras.2014.08.007

Sivasubramaniyan, K., Lehnen, D., Ghazanfari, R., Sobiesiak, M., Harichandan, A., Mortha, E., et al. (2012). Phenotypic and functional heterogeneity of human bone marrow– and amnion-derived MSC subsets. *Ann. N Y Acad. Sci.* 1266, 94–106. doi: 10.1111/j.1749-6632.2012.06551.x

Stevens, M. M., and George, J. H. (2005). Exploring and engineering the cell surface interface. *Science.*310, 1135–1138. doi: 10.1126/science.1106587

Swartz, M. A., and Lund, A. W. (2012). Lymphatic and interstitial flow in the tumour microenvironment: linking mechanobiology with immunity. *Nat. Rev. Cancer* 12, 210–219. doi: 10.1038/nrc3186

Tarte, K., Gaillard, J., Lataillade, J. J., Fouillard, L., Becker, M., Mossafa, H., et al. (2010). Clinical-grade production of human mesenchymal stromal cells: occurrence of aneuploidy without transformation. *Blood* 115, 1549–1553. doi: 10.1182/blood-2009-05-219907

Tsuji, W., Rubin, J. P., and Marra, K. G. (2014). Adipose-derived stem cells: Implications in tissue regeneration. *World J. Stem Cells* 6, 312–321. doi: 10.4252/wjsc.v6.i3.312

Turley, S. J., Fletcher, A. L., and Elpek, K. G. (2010). The stromal and haematopoietic antigen-presenting cells that reside in secondary lymphoid organs. *Nat. Rev. Immunol.* 10, 813–825. doi: 10.1038/nri2886

Uccelli, A., Moretta, L., and Pistoia, V. (2008). Mesenchymal stem cells in health and disease. *Nat. Rev. Immunol.* 8, 726–736. doi: 10.1038/nri2395

Unadkat, H. V., Hulsman, M., Cornelissen, K., Papenburg, B. J., Truckenmüller, R. K., Carpenter, A. E., et al. (2011). An algorithm-based topographical biomaterials library to instruct cell fate. *Proc. Nat. Acad. Sci. U.S.A.* 108, 16565–16570. doi: 10.1073/pnas.1109861108

Unadkat, H. V., Rewagad, R. R., Hulsman, M., Hulshof, G. F., Truckenmüller, R. K., Stamatialis, D. F., et al. (2013). A modular versatile chip carrier for high-throughput screening of cell-biomaterial interactions. *J. R. Soc. Interf. R. Soc.* 10:20120753. doi: 10.1098/rsif.2012.0753

Wickham, H. (2009). *ggplot2: Elegant Graphics for Data Analysis*. New York, NY: Springer Science & Business Media.

Wong, S. T., Teo, S. K., Park, S., Chiam, K. H., and Yim, E. K. (2014). Anisotropic rigidity sensing on grating topography directs human mesenchymal stem cell elongation. *Biomech. Model. Mechanobiol.* 13, 27–39. doi: 10.1007/s10237-013-0483-2

Zeng, M., Smith, A. J., Wietgrefe, S. W., Southern, P. J., Schacker, T. W., Reilly, C. S., et al. (2011). Cumulative mechanisms of lymphoid tissue fibrosis and T cell depletion in HIV-1 and SIV infections. *J. Clin. Invest.* 121, 998–1008. doi: 10.1172/JCI45157

Zhang, K., Cao, J., Dong, R., and Du, J. (2013). Early growth response protein 1 promotes restenosis by upregulating intercellular adhesion molecule-1 in vein graft. *Oxidat. Med. Cell. Long.* 2013:432409. doi: 10.1155/2013/432409

Zhao, Y., Truckenmuller, R., Levers, M., Hua, W. S., de Boer, J., and Papenburg, B. (2013). High-definition micropatterning method for hard, stiff and brittle polymers. *Mater. Sci. Eng. C Mater. Biol. Appl.* 71, 558–564. doi: 10.1016/j.msec.2016.11.004

Conflict of Interest Statement: CvB and JdB are co-founders of and have a financial interest in Materiomics b.v.

The remaining authors declare that the research was conducted in the absence of any commercial or financial relationships that could be construed as a potential conflict of interest.

frontiers in Bioengineering and Biotechnology

ORIGINAL RESEARCH
published: 19 September 2018
doi: 10.3389/fbioe.2018.00116

Photocrosslinkable Gelatin Hydrogels Modulate the Production of the Major Pro-inflammatory Cytokine, TNF-α, by Human Mononuclear Cells

*Amy R. Donaldson[1], Constantin Edi Tanase[1], Dennis Awuah[1], Pranav Vasanthi Bathrinarayanan[1], Laurence Hall[1], Mehdi Nikkhah[2], Ali Khademhosseini[3], Felicity Rose[4], Cameron Alexander[5] and Amir M. Ghaemmaghami[1]**

[1] Immunology and Tissue Modelling Group, School of Life Sciences, University of Nottingham, Nottingham, United Kingdom, [2] School of Biological and Health Systems Engineering, Arizona State University, Tempe, AZ, United States, [3] Center for Minimally Invasive Therapeutics (C-MIT), California NanoSystems Institute (CNSI), University of California, Los Angeles, Los Angeles, CA, United States, [4] Division of Regenerative Medicine and Cellular Therapies, School of Pharmacy, University of Nottingham, Nottingham, United Kingdom, [5] Division of Molecular Therapeutics and Formulation, School of Pharmacy, University of Nottingham, Nottingham, United Kingdom

OPEN ACCESS

Edited by:
Jian Yang,
Pennsylvania State University,
United States

Reviewed by:
Lin Wang,
Union Hospital, Tongji Medical College, Huazhong University of Science and Technology, China
Jennifer Patterson,
KU Leuven, Belgium

***Correspondence:**
Amir M. Ghaemmaghami
amir.ghaemmaghami@nottingham.ac.uk

Specialty section:
This article was submitted to Biomaterials, a section of the journal Frontiers in Bioengineering and Biotechnology

Received: 14 March 2018
Accepted: 27 July 2018
Published: 19 September 2018

Citation:
Donaldson AR, Tanase CE, Awuah D, Vasanthi Bathrinarayanan P, Hall L, Nikkhah M, Khademhosseini A, Rose F, Alexander C and Ghaemmaghami AM (2018) Photocrosslinkable Gelatin Hydrogels Modulate the Production of the Major Pro-inflammatory Cytokine, TNF-α, by Human Mononuclear Cells. Front. Bioeng. Biotechnol. 6:116. doi: 10.3389/fbioe.2018.00116

Hydrogels are an attractive class of biomaterials in tissue engineering due to their inherently compatible properties for cell culture. Gelatin methacryloyl (GelMA) has shown significant promise in the fields of tissue engineering and drug delivery, as its physical properties can be precisely tuned depending on the specific application. There is a growing appreciation for the interaction between biomaterials and cells of the immune system with the increasing usage of biomaterials for *in vivo* applications. Here, we addressed the current lack of information regarding the immune-modulatory properties of photocrosslinked GelMA. We investigated the ability of human mononuclear cells to mount inflammatory responses in the context of a GelMA hydrogel platform. Using lipopolysaccharide to stimulate a pro-inflammatory immune response, we found tumor necrosis factor-α (TNF-α) expression was suppressed in GelMA culture conditions. Our findings have important implications on the future use of GelMA, and potentially similar hydrogels, and highlight the significance of investigating the potential immune-modulatory properties of biomaterials.

Keywords: tissue engineering, biomaterials, immunology, Gelatin methacryloyl, TNF-α

INTRODUCTION

Hydrogels are widely used in the field of tissue engineering and regenerative medicine (El-Sherbiny and Yacoub, 2013). They are an attractive class of biomaterials since their highly hydrated structure closely resembles the natural extracellular matrix (ECM) of soft tissues (Slaughter et al., 2009). A diverse range of hydrogels, formulated from natural and synthetic polymers, has been developed for tissue engineering applications (Annabi et al., 2014).

Gelatin methacryloyl (GelMA) is a hydrogel which has shown promise in various areas of tissue engineering including cardiac (Shin et al., 2013; Saini et al., 2015), bone (Ovsianikov et al., 2011; Dolatshahi-Pirouz et al., 2014), and vascularization (Chen et al., 2012; Bertassoni et al., 2014) as well as development of tumor microenvironment models (Peela et al., 2016). Derived from collagen, a naturally abundant ECM protein, GelMA has inherently biocompatible properties (Hutson et al., 2011). This includes the preservation of cell adhesion motifs, these specific sequences of amino acids are recognized by various cell-surface ECM receptors, such as integrins (Knight et al., 2000), which mediate cell attachment, motility, survival, and differentiation (Rosso et al., 2004).

Crosslinked GelMA has been used successfully in a variety of tissue engineering applications. For instance, Nikkhah et al. demonstrated the application of micropatterned GelMA in an investigation into the impact of geometry on endothelial cells in the context of vasculature organization and development (Nikkhah et al., 2012). Also, due to its mechanical stability, GelMA is an attractive material for incorporation into microfluidic systems. This has been successfully implemented by Chen et al. in the development of a microfluidic device which models the heart valve microenvironment (Chen et al., 2013). Furthermore, the *in vitro cell-compatibility* of GelMA has been established with a range of cell types including NIH 3T3 fibroblasts (Aubin et al., 2010), immortalized human umbilical vein endothelial cells (Nichol et al., 2010), monocytic cell line THP-1 (Cha et al., 2017), mesenchymal stem cells (Chen et al., 2012), and myoblasts (Ramón-Azcón et al., 2012).

The synthesis of GelMA involves chemical modification of gelatin by methacryloyl derivatives resulting in the formation of polymerisable methacrylamide or methacrylate side groups. These side-chains enable tuning of the physical properties of GelMA derivatives in a way not possible over its unmodified counterparts, collagen and gelatin. Thus, the mechanical strength and degradability of GelMA hydrogels may be controlled depending on the desired application (Van Den Bulcke et al., 2000). Although methacryloyl-functionalised gelatin retains properties similar to unmodified gelatin, polymerisation gives rise to a highly crosslinked, stiffer hydrogel (Van Den Bulcke et al., 2000). For example, with the addition of a photoinitiator, GelMA is photo-polymerisable upon exposure to an ultra violet (UV) light source. Thus, soft lithography micropatterning techniques can be used to achieve a high level of control over the architectural features of GelMA hydrogels (Nichol et al., 2010).

GelMA is evidently compatible with a range of cell types, however, there is a current lack of information regarding its interactions with immune cells. The requirement of understanding how materials of this type interact with the immune system is largely being driven by the increasing usage of synthetic materials *in vivo*, as vehicles for cell, protein and DNA delivery.

Immune cells have a natural propensity to mount responses against foreign bodies, which extends to biomaterials. Briefly, upon recognition of a foreign material, cells of the immune system (e.g., antigen presenting cells such as monocytes and macrophages), become activated in order to attempt to eradicate it by phagocytosis (Anderson et al., 2008; Ekdahl et al., 2011). Production of cytokines including tumor necrosis factor (TNF)-α, interleukin (IL)-1β, IL-6, and IL-8 (Gretzer et al., 2003), by activated cells are characteristic of this response and mediate inflammation and wound healing *in vivo* (Chang et al., 2008).

Recently, certain biomaterials, such as poly(lactic-co-glycolic acid) based particles, have been shown to have profound effects in terms of modulating the immune system (Yoshida and Babensee, 2004; Silva et al., 2015). These properties can be harnessed in areas such as vaccine delivery, autoimmune disease and cancer therapeutics to direct appropriate immune responses *in vivo*. In the development of vaccines, for example, biomaterial adjuvanticity enhances the induction of adaptive immune responses, thereby potentially increasing the level of protection offered by the vaccine (Lewis et al., 2014).

To the best of our knowledge, despite its wide usage in the field of tissue engineering, the immunological properties of GelMA have not yet been characterized. We addressed this by assessing the interaction between GelMA hydrogels and human primary peripheral blood mononuclear cells (PBMCs) with a focus on GelMA's ability to induce and/or modulate immune responses. To do this, we measured the elicitation of an immune reaction to GelMA based on the production of pro-inflammatory cytokines. In addition, to investigate whether GelMA affects the ability of immune cells to mount appropriate immune responses, we used lipopolysaccharide (LPS) to elicit an inflammatory reaction (Donaldson, 2017). We anticipate the findings from this study will have important implications on the future applications of GelMA and potentially similar hydrogels in tissue engineering.

MATERIALS AND METHODS

PBMC Preparation and Monocyte Isolation

Heparinized blood from healthy donors was obtained with consent and ethical committee approval. PBMCs were separated on a Histopaque-1077 (Sigma-Aldrich) density gradient as described before (García-Nieto et al., 2010). In some experiments we used $CD14^+$ monocytes that were isolated using magnetic assisted cell sorting (MACS) and CD14 conjugated magnetic beads (Miltenyi Biotec, UK) as we have previously described (Al-Ghouleh et al., 2012; Salazar et al., 2017).

Methacryloyl Gelatin (GelMA) Hydrogel Preparation

The GelMA foam was synthesized as described previously (Van Den Bulcke et al., 2000) and kindly provided by the Khademhosseini Lab. The photoinitiator, 2-Hydroxy-4′-(2-hydroxyethoxy)-2-methylpropiophenone (Irgacure 2959) (Sigma-Aldrich, UK) was dissolved in PBS to make a 0.25% (w/v) solution. A 5% (w/v) GelMA pre-polymer was prepared by dissolving GelMA into the 0.25% photoinitiator solution at 60°C. One hundred microliter of pre-polymer solution was added per well of a 48-well tissue culture plate and photo-cross linked by UV exposure (40 s, 800 mW, 8 cm). Hydrogels were washed in PBS and sterilized by submersion in a 20% antibiotic\antimycotic solution overnight. A final wash was done in PBS before cell seeding.

Cell Culture on Hydrogels

PBMCs or purified monocytes (5×10^5) were seeded per gel in 500 μL RPMI-1640 supplemented with 100 U/mL penicillin, 100 mg/mL streptomycin, 2 mM L-glutamine, and 10% fetal calf serum (FCS) (all purchased from Sigma Aldrich). For the simulated conditions, 0.1 μg/mL *E. coli* LPS (0111:B4) was added to the appropriate wells. Plates were transferred to a humidified incubator (37°C, 5% CO_2). Cultures were maintained for up to 5 days to assess cell viability. Supernatant sampled after 4 and 24 h for cytokine analysis.

$CD14^+$ monocytes were stimulated with LPS for 1hr in polypropylene tubes prior to culture on TC, GelMA or gelatin coated well plates for 4 and 24h ($n = 6$). Since the $CD14^+$ monocytes are stimulated with LPS prior to transfer to different substrates the level of LPS stimulation is considered to be similar for all conditions (GelMA, Gelatin, and TC). One way ANOVA-Tukey's multiple comparisons test was used to assess statistical significance ($^{****}P \leq 0.0001$).

Cell Viability Assay

To assess the viability of cells on day 5 of culture on hydrogel substrates the Annexin V-FITC cell viability kit (purchased from Beckman Coulter) was used. This assay is based on the principle that in early apoptosis cells lose the asymmetry of the plasma membrane. Thus, phosphotidylserine (PS), normally located on the inside of the cell membrane, appears on the outer surface. Annexin V has a high affinity for PS, therefore when conjugated with a fluorochrome (e.g., FITC), can be used to label cells in early apoptosis. During late apoptosis, the integrity of the cell membrane is lost allowing penetration of propidium iodide (PI), which intercalates DNA. Upon DNA binding, PI fluoresces allowing detection of non-viable cells. Cells were harvested from the gels by gentle washing with ice cold PBS and immediately placed on ice. After washing, cells were re-suspended in 1X binding buffer and the staining method was carried out according to manufacturer's instructions. Samples were analyzed on the Beckman Coulter FC500.

Live/Dead Assay

Cells grown on GelMA and tissue culture plastic were subjected to a LIVE/DEAD assay (L3224) according to manufacturer's guidelines (Thermo Fisher). Cells were imaged using a ZOE Fluorescent Cell Imager microscope (Bio-Rad, UK).

TNF-α Depletion Experiments

Recombinant human TNF-α (purchased from Invitrogen) was added to complete RPMI-1640 media at either 5 or 2.5 ng/mL. GelMA hydrogels were made as described above in the GelMA hydrogel preparation section. Five hundred microliter of media with or without the addition of TNF-α was incubated with the gels for 4 h in a humidified incubator (37°C, 5% CO_2). Supernatant was collected and stored at −80°C for cytokine analysis.

TABLE 1 | Primers for real-time PCR.

Genes	Primer	Sequence (5′- 3′)
GAPDH	Forward	GAGTCAACGGATTTGGTCGT
	Reverse	GACAAGCTTCCCGTTCTCAG
TNF-α	Forward	CAGAGGGAAGAGTTCCCCAG
	Reverse	CCTTGGTCTGGTAGGAGACG

Cytokine Analysis

Interleukin 1β, interleukin 6, interleukin 8 and tumor necrosis factor-α were measured using a multiplex bead-based analyte detection system according to manufacturer's instructions (Procartaplex) (purchased from eBioscience) as we have described before (Sharquie et al., 2013). Supernatants from cell-free TNF-α depletion experiments were analyzed for TNF-α by ELISA following manufacturer's instructions (Human TNF-α DuoSet) (purchased from R&D systems).

Preparation of Thin Hydrogel Layers for Immuno-Fluorescent Staining

GelMA was photo-polymerised on surface-treated glass chips cut to 1 cm^2. Glass slides were coated with 3-(Trimethoxysilyl) propyl methacrylate (TMSPMA) in order to functionalise the surface to enhance hydrogel attachment. Briefly, glass microscope slides were submerged in a 10% (w/v) sodium hydroxide solution overnight. Slides were thoroughly rinsed and soaked overnight in diH_2O. They were washed 3 times in 100% ethanol and air-dried. Slides were then stacked in a beaker and wetted with TMSPMA. The beaker was covered with aluminum foil and the slides were baked at 80°C overnight. Finally, slides were washed in 100% ethanol 3 times, wrapped in aluminum foil and baked for a further 2 h at 80°C. A 5% (w/v) pre-polymer GelMA solution was prepared as described previously. Five microliter gel solution was dispensed onto a glass chip, a spacer with a depth of 100 μm was placed on top to form an even layer and then the gel was crosslinked for 8.5 s (Nikkhah et al., 2012). The glass chips were transferred to a 24 well plate and washed with PBS. Then gels were submerged in control media or media containing recombinant human TNF-α and incubated for 4 h in a humidified incubator (37°C, 5% CO_2).

Immuno-Fluorescent Staining of GelMA-Bound TNF-α

Following a 4 h incubation with or without TNF-α-containing media, the supernatant was removed and the gels were washed in PBS. The samples were blocked for 30 min with 5% (w/v) FCS in PBS. A 1:200 dilution [in 5% (w/v) FCS in PBS] was made for the mouse anti-human TNF-α monoclonal antibody (purchased from abcam) and incubated with samples overnight at 4°C. Samples were washed 3 times in PBS and then incubated for 1 h with a Rhodamine red-conjugated goat anti-mouse secondary antibody (purchased from Life Technologies) diluted 1:250 with 5% (w/v) FCS in PBS. Finally, samples were washed in PBS and mounted for imaging using a 20x objective on a Zeiss LSM710 confocal microscope.

mRNA Isolation and cDNA Synthesis

Cells were harvested from hydrogel substrates by washing with cold PBS and immediately transferred to a Falcon tube on ice.

Cells were washed twice in PBS, then 1 mL of MACS lysis/ re suspension buffer was added to 10^7 cells and mixed until lysate was clear. mRNA purification and cDNA synthesis were carried out using the μMACS one-step cDNA kit (Miltenyi Biotech, UK) following the manufacturer's instructions. The purity and quantity of the cDNA was assessed with a NanoDrop 1000 Spectrophotometer (Thermo Scientific).

Conventional PCR

Conventional PCR was carried out in a TC-312 PCR Thermocycler (Bibby Scientific Ltd., UK) using the Phusion Flash High-Fidelity PCR Master Mix (Thermo Fisher Scientific) and 20 ng of μMACS cDNA per reaction. Primers were obtained from Eurofin, UK (**Table 1**): PCR was carried out with an initial denaturation at 98°C for 10 s, followed by 32 cycles of denaturation (98°C, 0–1 s), annealing (62°C, 30 s), extension (72°C, 30 s), final extension was performed at 72°C for 60 s. Then, the PCR products were analyzed in an E-gel pre-cast 2% agarose electrophoresis system (Thermo Fisher Scientific) and the molecular weight of the bands were calculated with a standard 100 bp Directload DNA ladder (Sigma-Aldrich).

Quantitative Real-Time PCR Analysis

Real time PCR was performed in a Strategene MxPro 3005P qPCR System with the Brilliant III Ultra-Fast SYBR Green qPCR Master Mix (Agilent Technologies, USA). Primers were obtained from Eurofin, details for GAPDH and TNF-α as above. Cycling was initiated at 95°C for 3 min, followed by 45 cycles of 95°C for 20 s and 62°C for 30 s, a melting curve was done at the end. Samples were run in triplicates and relative expression

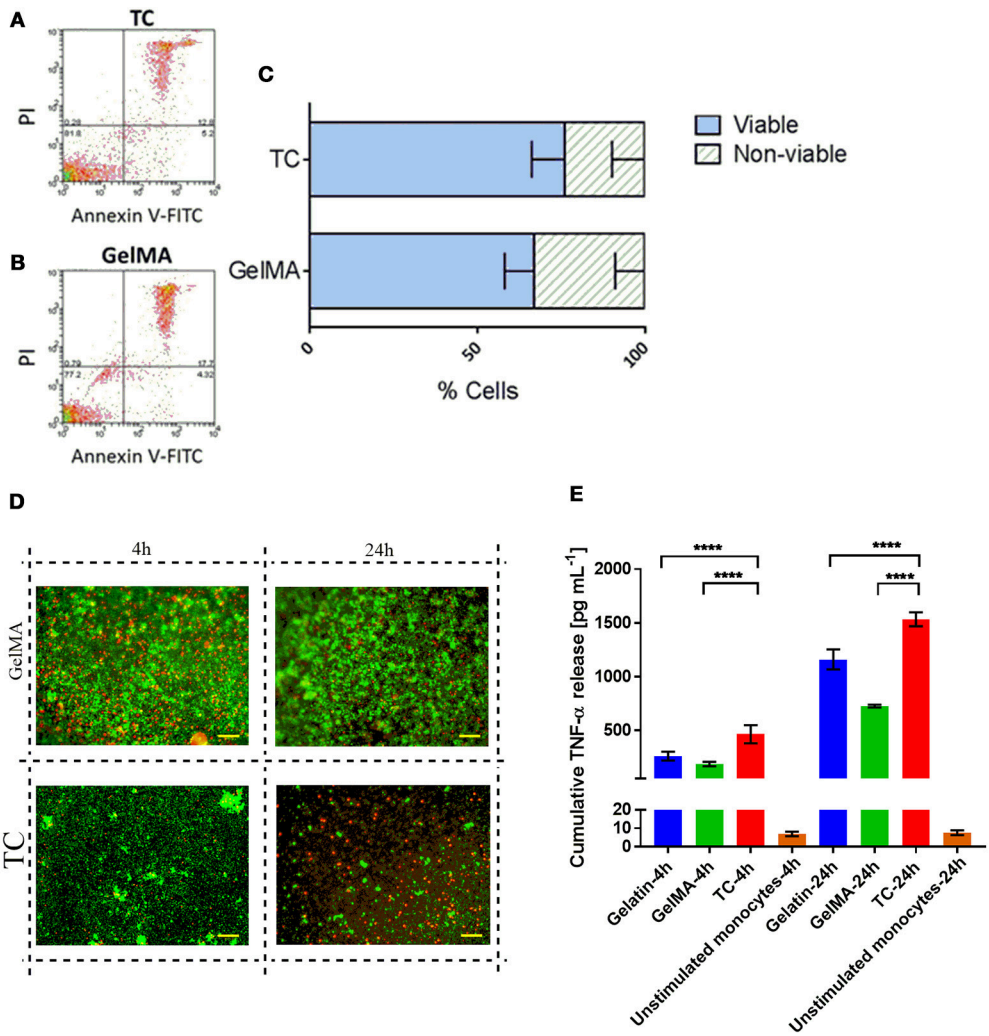

FIGURE 1 | PBMC viability is not impaired by culture with GelMA hydrogels. **(A,B)** Annexin V-FITC/PI staining profiles of cells harvested from TC and GelMA cultures respectively. **(C)** Percentage of viable (dark gray bars) and non-viable (light gray bars) cells collected from GelMA and TC. Two-tailed *t*-tests determined that there were no significant differences ($P > 0.05$) in the proportion of viable cells, or dead cells harvested from GelMA cultures compared to TC. Error bars represent standard deviation ($n = 3$). **(D)** Live/Dead staining of PBMC on GelMA and TC for 4 and 24 h (scale bar 100 μm) where green fluorescent highlights live and red highlights dead cells respectively. **(E)** Measurement of TNF-α production by LPS stimulated $CD14^+$ monocytes seeded on different substrates. ****$p < 0.0001$.

calculated using comparative threshold cycle method normalized to GAPDH (Breloer and Fleischer, 2008; Benton et al., 2009). For all the experiments, three independent donors were used.

Statistical Analysis

Analysis was carried out using GraphPad Prism version 6.00 for Windows, GraphPad Software, La Jolla California USA (www.graphpad.com). Results are expressed as mean values ± standard deviation (SD) from three or more independent experiments. Statistical differences were determined using the student *t* test or one-way ANOVA with Tukey *post-hoc* testing. A *p*-value <0.05 was considered statistically significant. Data shown is indicative of three independent experiments with three donors, unless stated otherwise.

RESULTS

GelMA Hydrogels Do Not Have a Detrimental Impact on Immune Cell Viability

PBMCs, isolated from the blood of healthy donors, were used as a source of primary human immune cells in our experiments since it comprises the cell types of interest for this work. The cellular composition of PBMCs is 70–90% lymphocytes [T cells, B cells, and natural killer (NK) cells], 3–10% monocytes, 1–2% dendritic cells, and small numbers of basophils. **Figure 1** shows the results from the cytotoxicity and viability assays on PBMCs [cultured on tissue culture plastic (TC) or GelMA] using Annexin V-FITC/PI staining (**Figures 1A–C**) and LIVE/DEAD staining respectively (**Figure 1D**). Data from both assays indicate comparable levels of viability in cells cultured on TC or GelMA. Data with $CD14^+$ monocytes shows that detectable soluble TNF-α for cells transferred to GelMA is significantly lower than cells transferred to TC ($p < 0.0001$) for both time points. This suggests that GelMA potentially "mops up" the TNF-α released in the medium by $CD14^+$ monocytes. Interestingly enzymatically cross-linked gelatin hydrogels seem to have a similar effect on soluble TNF-α (Paguirigan and Beebe, 2007).

Characterizing the Immune-Modulatory Properties of GelMA

To characterize the immune-modulatory properties of GelMA, we investigated the responsiveness of PBMCs to immunological manipulation in the presence of GelMA (**Figure 2**). This was done by assessing the response of PBMCs to lipopolysaccharide (LPS), an immunogenic agent derived from the outer membrane of Gram-negative bacteria. PBMCs were cultured on TC or GelMA hydrogels, with or without LPS for 4 h. Secretion of a panel of inflammatory cytokines (IL-1β, IL-6, IL-8, and TNF-α)

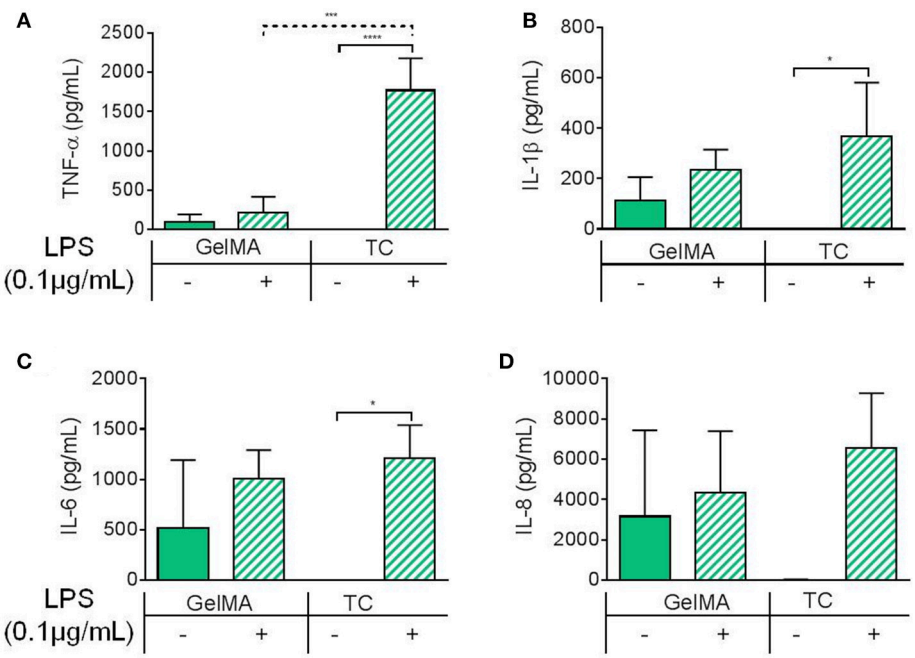

FIGURE 2 | Inflammatory cytokine production by PBMCs cultured on GelMA hydrogels. Soluble cytokine production after 4 h by PBMCs cultured on GelMA hydrogels or TC, with (+) or without (–) LPS stimulation. **(A)** TNF-α was not significantly increased following LPS stimulation in GelMA cultures. Secretion of TNF-α, into the cell culture medium, was found to increase significantly in the LPS-stimulated TC control (****$P \leq 0.0001$). A significant difference in the level of LPS-induced TNF-α production was found between GelMA and TC conditions (***$P \leq 0.001$). **(B)** Production of IL-1β was not significantly increased with LPS stimulation in the presence of GelMA, whereas in TC it was (*≤0.05). **(C)** IL-6 secretion was not significantly increased in GelMA cultures following LPS stimulation, this was found to be significant in TC (*$P \leq 0.05$). **(D)** No significant rise in IL-8 production with LPS stimulation GelMA or TC cultures ($P \geq 0.05$). One-way ANOVA performed to determine statistically significant differences in cytokine production ($n = 3$ independent experiments). Error bars represent standard deviation. **$p < 0.01$.

was used to assess the immune response (**Figures 2A–D**). In cells cultured on TC, levels of all cytokines increased significantly in response to LPS stimulation. In the presence of GelMA hydrogels, background levels of all inflammatory cytokines were raised. Production of IL1-β, IL-6, and IL-8 increased to some extent with LPS stimulation, although the differences were not statistically significant. Crucially, there was no change in the level of TNF-α detected following stimulation by LPS.

To assess whether the main responders to LPS stimulation in these experiments are monocytes and to rule out low LPS availability as the reason for low TNF-α levels in cells stimulated on GelMA, we repeated these experiments using purified monocytes that were stimulated with LPS prior to transfer to TC plates or GelMA coated wells. These data showed the same pattern of TNF-α production with significantly lower levels of soluble TNF-a detected in the supernatant of cells transferred to GelMA coated plates compared to TC (**Figure 1E**).

GelMA Suppresses LPS-Induced TNF-α Gene Expression in PBMCs

Given the observation that GelMA has potentially suppressive effects on levels of LPS-induced TNF-α, further investigation at the level of gene expression was carried out. In these experiments, PBMCs were cultured on photo-polymerised GelMA hydrogel layers, with and without LPS. The cells were then harvested for analysis of TNF-α gene expression after 30 min and 4 h of culture. TNF-α gene expression by PBMCs in culture with GelMA hydrogels was then measured by both conventional gel-based and reverse transcription PCR (**Figure 3**). As shown, TNF-α expression is substantially induced at 30 min following LPS stimulation in both TC and GelMA; however, after 4 h TNF-α mRNA expression in cells cultured on GelMA is reduced to the levels observed in un-stimulated cells (**Figure 3B**).

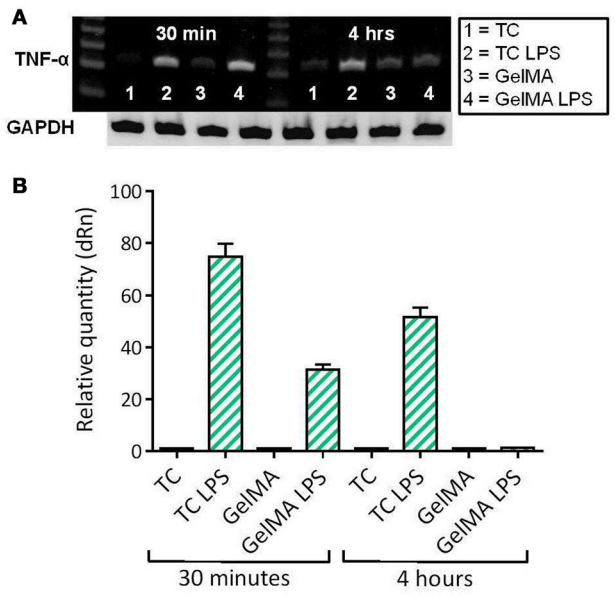

FIGURE 3 | LPS-induced TNF-α gene expression is down-regulated in PBMCs cultured on GelMA. **(A)** Measurement of TNF-α gene expression by conventional ethidium bromide gel-based RT PCR. After 30 min in culture, the band intensity indicates TNF-α gene expression has increased as a result of LPS stimulation in both GelMA and TC cultures. At 4 h, expression of TNF-α was maintained in the TC control, however, it was down-regulated in the GelMA condition. **(B)** Analysis of TNF-α gene expression by real time quantitative PCR. Thirty minute after LPS stimulation the relative quantity of TNF-α expression increased in GelMA and TC cultures. After 4 h, up-regulation of TNF-α gene expression was maintained in TC cultures, however, LPS-induced TNF-α gene expression was attenuated in the presence of GelMA. ΔΔ Ct Analysis normalized against GAPDH. Data shown is representative of 3 independent donors.

GelMA Hydrogels "Mop Up" TNF-α

We used a cell-free system to determine whether soluble TNF-α protein is depleted by GelMA. In these experiments, recombinant human TNF-α was added to the tissue culture media and incubated with GelMA hydrogels. After 4 h, the supernatants were collected for cytokine analysis by ELISA.

As shown in **Figure 4**, there was a large reduction in soluble TNF-α detected in supernatants collected from GelMA coated wells compared to TC. This was shown over a titration of concentrations of TNF-α in **Figure 4A**. By calculating the residual TNF-α in the media collected from GelMA (30%), relative to TC (100%), a significant reduction of TNF-α recovered from GelMA was determined ($^{**}P = 0.0006$) as shown in **Figure 4B**. To confirm the fate of the TNF-α protein, GelMA was incubated with the TNF-α-containing media for 4 h. Immunofluorescent staining was performed for TNF-α in order to determine whether it was bound within the gel. As shown in **Figure 4C**, GelMA hydrogels which had been incubated with TNF-α were positively and specifically stained for human TNF-α, indicating the presence of TNF-α bound within the hydrogel.

DISCUSSION

A number of factors can determine the cytotoxicity of biomaterials, for example, by-products of degradation. Therefore, cytotoxicity is a critical parameter when assessing the suitability of a biomaterial for *in vivo* and *in vitro* applications (Williams, 2008). In our experiments, quantification of apoptotic and necrotic cells, using Annexin V/PI staining, showed a comparable percentage of dead cells on GelMA and TC plastic after 5 days of culture (**Figures 1A–C**) indicating that GelMA hydrogels did not have a detrimental impact on the health of immune cells compared to conventional TC. This was further confirmed by direct visualization of live and dead cells *in situ* using a LIVE/DEAD assay, which also showed similar levels of cell viability on GelMA and TC (**Figure 1D**).

Having established the comparable viability of immune cells in TC and GelMA we assessed their pro-inflammatory cytokine profile after stimulation with LPS. In the TC condition, levels of all cytokines increased significantly in response to LPS. In the presence of GelMA hydrogels however background levels of all inflammatory cytokines were raised. This could be explained by either the immunogenicity of xenogeneic proteins in porcine gelatin (Chan and Leong, 2008), which is used as raw material for synthesizing GelMA, or the presence of low-level endotoxin

in GelMA preparations. Nevertheless, cells on GelMA still responded to LPS stimulation with an increase in IL-1β, IL-6, and IL-8 production which was on a par with the concentration of these cytokines from cells cultured on TC. However, levels of TNF-α in the supernatant of cells cultured on GelMA did not change in response to LPS stimulation and was significantly lower than cells cultured on TC (**Figure 2**). Within the PBMC population, monocytes are the main responders to LPS (Tazi et al., 2006) and are largely accountable for the production of pro-inflammatory cytokines particularly TNF-α. Therefore, we also examined the level of TNF-α production in response to LPS on TC and GelMA using purified monocytes. To rule out the possibility of LPS being adsorbed on GelMA, hence lower levels of TNF production in these experiments, monocytes were first stimulated with LPS (for 1 h) before being transferred to either TC plates or GelMA. Data from these experiments also showed significantly lower levels of TNF-α detected in the supernatant of monocytes cultured on GelMA compared to TC plates. Interestingly, the same pattern was also observed when monocytes were seeded on an enzymatically cross-linked gelatin hydrogel (**Figure 1E**).

Given the comparable viability of cells cultured on TC and GelMA but significant reduction in soluble TNF-α in GelMA condition, it was reasonable to assume that GelMA could actually mop up TNF. Indeed data presented in **Figure 4** clearly show that GelMA seems to act as a sink for TNF-α (**Figure 4C**) which leads to a significant reduction in soluble TNF-α in the media (**Figures 4A,B**) decreasing the bio-availability of soluble TNF for interaction with immune cells in suspension. Collagen has previously been demonstrated to have similar modulatory properties over certain pro-inflammatory cytokines with clinically relevant effects (Wiegand et al., 2010). Since GelMA is gelatin based, it seems feasible for GelMA to possess similar cytokine-binding properties. Gelatin has a repeating

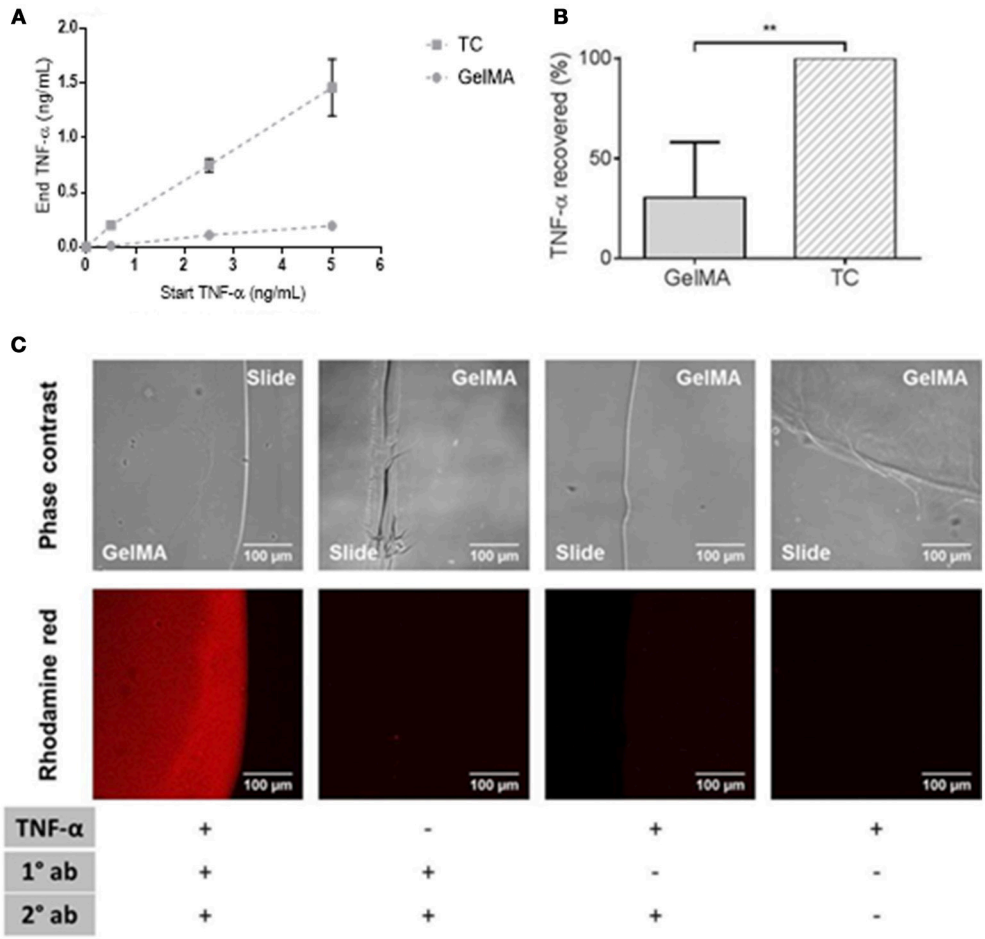

FIGURE 4 | Depletion of soluble TNF-α by GelMA hydrogels. **(A)** Residual TNF-α detected after incubation of GelMA hydrogels in media containing 0.5, 2.5, and 5 ng/mL recombinant TNF-α. Error bars represent standard error of the mean. **(B)** TNF-α recovered from TC (100%) and GelMA (30%), a significant reduction in residual TNF-α recovered from GelMA was found relative to TC (**$P = 0.0006$). A two-tailed t-test was performed to determine statistical significance ($n = 3$ independent experiments). Error bars represent standard deviation. **(C)** TNF-α-treated GelMA, labeled with mouse anti-human TNF-α (primary) and rhodamine red goat anti-mouse (secondary) antibodies. Untreated GelMA, stained with primary and secondary antibodies. GelMA, secondary antibody control. GelMA, unlabelled. Images acquired on an LSM710 META Zeiss confocal system, using a 20X objective. Scale bars represent 100 µm.

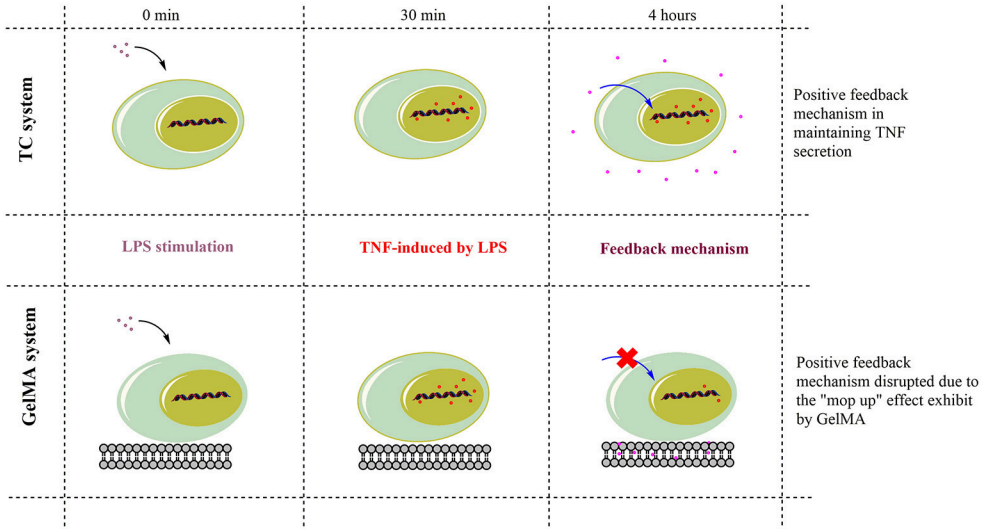

FIGURE 5 | Schematic action mechanism for GelMA in the modulation of TNF-α. TNF-α gene expression increased within 30 min of LPS stimulation in both TC and GelMA conditions. After 4 h, LPS-induced TNF-α expression is maintained through a positive feedback mechanism and levels of secreted TNF-α peak in TC. Whereas the GelMA hydrogel sequesters secreted TNF-α protein, thereby effectively removing it from solution. This disrupts the relay of positive feedback signals to the cell for the maintenance of TNF-α expression. Thus, by 4 h, in cells cultured on GelMA TNF-α mRNA levels are suppressed to the levels of un-stimulated cells and there is also no detectable increase in soluble TNF-α in the supernatant.

amino acid sequence of Gly-Pro-X and contains many chemical side groups (Van Den Bulcke et al., 2000). The functional groups are likely to interact non-covalently with a variety of small molecules and form macromolecular complexes with the proteins to which it binds by means of hydrogen links, providing a potential mop up mechanism (Taravel and Domard, 1993; Nezu and Winnik, 2000; Vaidyanathan et al., 2003; Frasca et al., 2012). In addition, the three dimensional (3D), porous nature of the GelMA hydrogel could also assist in the wicking away of cytokines (Benton et al., 2009). However, more detailed studies may be required to elucidate the exact nature of TNF-α interaction with GelMA.

To better understand observed changes in TNF-α production in immune cell cultured on GelMA we also investigated TNF-α mRNA expression using conventional and real-time PCR. Data from these experiments showed an increase in TNF-α mRNA expression within 30 min of LPS stimulation in both TC and GelMA cultures, indicating that TNF-α gene expression was up-regulated. However, interestingly at 4-h time point, the levels of TNF-α mRNA in cells cultured on GelMA hydrogels was reduced to the levels observed in unstimulated cells, suggesting TNF-α gene expression had been suppressed in these cells. In contrast, LPS-stimulated cells cultured in the TC condition maintained high expression of TNF-α (**Figure 3**), albeit at lower levels compared to 30 min. It is important to highlight that TNF mRNA expression in response to LPS stimulation, and in the absence of other stimulatory signals (e.g., IFNs), peaks at 2 h post-stimulation (Kohn et al., 1992) which explains the observed decrease in mRNA expression in LPS stimulated cells on TC at 4hr time point.

Collectively these data indicate that while GelMA hydrogels induce an inflammatory cytokine profile under resting conditions, they seem to reduce the availability of soluble TNF-α following stimulation with LPS, showing that GelMA has the potential to modulate the production of a key regulator of the immune system under pro-inflammatory conditions. TNF-α has diverse roles in the function and regulation of the immune system, dependent on tissue type, immunological context and timing (Wajant et al., 2003). It predominantly has pro-inflammatory effects in affected tissues and can exacerbate, or lead to the progression of disease, for example, rheumatoid arthritis and chronic wounds (Albillos et al., 2004).

Therefore, TNF-α is under strict regulatory mechanisms which control its expression. For instance, the signaling pathways involved in TNF-α production include MAP kinases (ERK1/2, p38 and JNK) and NF-kappaB (Tazi et al., 2006). Soluble TNF-α signals through the receptor TNF-R1, which in turn activates a variety of signal transduction pathways, including MAP kinases and NF-kappaB. These in turn regulate transcription factors involved in the production of inflammatory cytokines, such as TNF-α (MacEwan, 2002; Ronkina et al., 2010). Indeed, different studies have shown that soluble TNF-α provides positive feedback to cells via paracrine or autocrine signaling in order to maintain expression during acute inflammation (Wu et al., 1993; Coward et al., 2002; Guergnon et al., 2003; Yarilina et al., 2008; Gane et al., 2016). Thus, while understanding the full mechanism of TNF-α suppression on GelMA may need further investigations, we propose that TNF-α sequestration in GelMA reduces the availability of soluble TNF-α hence switching off such a feedback mechanism resulting in the suppression of

TNF-α gene expression and potential dampening of TNF-α production (**Figure 5**). Cross-linked gelatin is more resistant to degradation by proteolytic enzymes such as gelatinase and collagenases. For example enzymatic degradation of GelMA hydrogels with collagenase II showed ∼30% mass loss during 14 days incubation period (Kang et al., 2014). Therefore, due to its low degradation rate, GelMA can sequester TNF-α before potential release of TNF-α due to GelMA degradation. This together with the short bioavailability and TNF-α half-life (5–10 min; Kamada et al., 2000; Harrison et al., 2004) means it is unlikely that sequestered TNF-α will be released back to the culture media and/or have any biological activity. However, the potential activity of the sequestered TNF-α in GelMA remains unknown and further studies are needed to fully understand this process.

This potentially anti-inflammatory property of GelMA could be harnessed. For example, in situations where excess TNF-α has a role in disease, such as severe tissue damage, the ability of GelMA to both mop up TNF-α and subsequently suppress expression in a localized environment could be beneficial. Previous work have shown that biomaterials can have profound influences on immune cell behavior, such effects must be taken into consideration when choosing biomaterials for applications where the immunological output is key to the functionality of the construct (Singh and Peppas, 2014). We anticipate research in this area will have significant implications, particularly since *in vivo* applications are becoming closer to reality with the development of increasingly complex biologically engineered constructs. This study contributes to a recent trend in the characterization of biomaterials for culture with immune cells. Although work in this area is still in the early stages, studies such as this highlight the importance of fully understanding the immunogenic properties of biomaterials to ensure the scaffold is appropriate for the required application.

ETHICS STATEMENT

This study was carried out in accordance with the recommendations of Faculty of Medicine and Health Services Research Ethics Committee. The protocol was approved by the Faculty of Medicine and Health Services Research Ethics Committee, University of Nottingham. All subjects gave written informed consent in accordance with the Declaration of Helsinki.

AUTHOR CONTRIBUTIONS

ARD, PVB, CET, DA, and LH performed experiments and analyzed data. MN and AK provided reagents and contributed to data analyses. AMG, FR, and CA designed the study and contributed to data analyses. ARD, CET, and AMG wrote the manuscript. All authors read and approved the manuscript.

ACKNOWLEDGMENTS

Some of the data presented in this manuscript is part of ARD's Ph.D. thesis. This work was supported by the National Centre for the Replacement, Refinement & Reduction of Animals in Research [grant number NC/K500318/1].

REFERENCES

Albillos, A., Hera Ad Ade, L., Reyes, E., Monserrat, J., Muñoz, L., Nieto, M., et al. (2004). Tumour necrosis factor-alpha expression by activated monocytes and altered T-cell homeostasis in ascitic alcoholic cirrhosis: amelioration with norfloxacin. *J. Hepatol.* 40, 624–631. doi: 10.1016/j.jhep.2003.12.010

Al-Ghouleh, A., Johal, R., Sharquie, I. K., Emara, M., Harrington, H., Shakib, F., et al. (2012). The glycosylation pattern of common allergens: the recognition and uptake of Der p 1 by epithelial and dendritic cells is carbohydrate dependent. *PLoS ONE* 7:e33929. doi: 10.1371/journal.pone.0033929

Anderson, J. M., Rodriguez, A., and Chang, D. T. (2008). Foreign body reaction to biomaterials. *Semin. Immunol.* 20, 86–100. doi: 10.1016/j.smim.2007.11.004

Annabi, N., Tamayol, A., Uquillas, J. A., Akbari, M., Bertassoni, L. E., Cha, C., et al. (2014). 25th anniversary article: Rational design and applications of hydrogels in regenerative medicine. *Adv. Mater.* 26, 85–123. doi: 10.1002/adma.201303233

Aubin, H., Nichol, J. W., Hutson, C. B., Bae, H., Sieminski, A. L., Cropek, D. M., et al. (2010). Directed 3D cell alignment and elongation in microengineered hydrogels. *Biomaterials* 31, 6941–6951. doi: 10.1016/j.biomaterials.2010.05.056

Benton, J. A., DeForest, C. A., Vivekanandan, V., and Anseth, K. S. (2009). Photocrosslinking of gelatin macromers to synthesize porous hydrogels that promote valvular interstitial cell function. *Tissue Eng. Part A* 15, 3221–3230. doi: 10.1089/ten.tea.2008.0545

Bertassoni, L. E., Cecconi, M., Manoharan, V., Nikkhah, M., Hjortnaes, J., Cristino, A. L., et al. (2014). Hydrogel bioprinted microchannel networks for vascularization of tissue engineering constructs. *Lab Chip* 14, 2202–2211. doi: 10.1039/C4LC00030G

Breloer, M., and Fleischer, B. (2008). CD83 regulates lymphocyte maturation, activation and homeostasis. *Trends Immunol.* 29, 186–194. doi: 10.1016/j.it.2008.01.009

Cha, B. H., Shin, S. R., Leijten, J., Li, Y. C., Singh, S., Liu, J. C., et al. (2017). Integrin-mediated interactions control macrophage polarization in 3D hydrogels. *Adv. Healthc. Mater.* 6:1700289. doi: 10.1002/adhm.201700289

Chan, B. P., and Leong, K. W. (2008). Scaffolding in tissue engineering: general approaches and tissue-specific considerations. *European . Spine J.* 17 (Suppl. 4), 467–479. doi: 10.1007/s00586-008-0745-3

Chang, D. T., Jones, J. A., Meyerson, H., Colton, E., Kwon, I. K., Matsuda, T., et al. (2008). Lymphocyte/macrophage interactions: biomaterial surface-dependent cytokine, chemokine, and matrix protein production. *J. Biomed. Mater. Res. A* 87, 676–687. doi: 10.1002/jbm.a.31630

Chen, M. B., Srigunapalan, S., Wheeler, A. R., and Simmons, C. A. (2013). A 3D microfluidic platform incorporating methacrylated gelatin hydrogels to study physiological cardiovascular cell-cell interactions. *Lab Chip* 13, 2591–2598. doi: 10.1039/c3lc00051f

Chen, Y.-C., Lin, R.-Z., Qi, H., Yang, Y., Bae, H., Melero-Martin, J. M., et al. (2012). Functional human vascular network generated in photocrosslinkable gelatin methacrylate hydrogels. *Adv. Funct. Mater.* 22, 2027–2039. doi: 10.1002/adfm.201101662

Coward, W. R., Okayama, Y., Sagara, H., Wilson, S. J., Holgate, S. T., and Church, M. K. (2002). NF-kappa B and TNF-alpha: a positive autocrine loop in human lung mast cells? *J. Immunol.* 169, 5287–5293. doi: 10.4049/jimmunol.169.9.5287

Dolatshahi-Pirouz, A., Nikkhah, M., Gaharwar, A. K., Hashmi, B., Guermani, E., Aliabadi, H., et al. (2014). A combinatorial cell-laden gel microarray for inducing osteogenic differentiation of human mesenchymal stem cells. *Sci. Rep.* 4:3896. doi: 10.1038/srep03896

Donaldson, A. R. (2017). *Development of Biomimetic Platforms to Investigate the Influence of Extra-Cellulra Environment on Immunological Responses,* Ph. D. thesis, Nottingham: University of Nottingham.

Ekdahl, K. N., Lambris, J. D., Elwing, H., Ricklin, D., Nilsson, P. H., Teramura, Y., et al. (2011). Innate immunity activation on biomaterial surfaces: a mechanistic model and coping strategies. *Adv. Drug Deliv. Rev.* 63, 1042–1050. doi: 10.1016/j.addr.2011.06.012

El-Sherbiny, I. M., and Yacoub, M. H. (2013). Hydrogel scaffolds for tissue engineering: progress and challenges. *Global Cardiol. Sci. Pract.* 2013, 316–342. doi: 10.5339/gcsp.2013.38

Frasca, G., Cardile, V., Puglia, C., Bonina, C., and Bonina, F. (2012). Gelatin tannate reduces the proinflammatory effects of lipopolysaccharide in human intestinal epithelial cells. *Clin. Exp. Gastroenterol.* 5, 61–67. doi: 10.2147/CEG.S28792

Gane, J. M., Stockley, R. A., and Sapey, E. (2016). TNF-α autocrine feedback loops in human monocytes: the pro- and anti-inflammatory roles of the TNF-α receptors support the concept of selective TNFR1 blockade *in vivo*. *J. Immunol. Res.* 2016:1079851. doi: 10.1155/2016/1079851

García-Nieto, S., Johal, R. K., Shakesheff, K. M., Emara, M., Royer, P. J., Chau, D. Y., et al. (2010). Laminin and fibronectin treatment leads to generation of dendritic cells with superior endocytic capacity. *PLoS ONE* 5:e10123. doi: 10.1371/journal.pone.0010123

Gretzer, C., Gisselfält, K., Liljensten, E., Rydén, L., and Thomsen, P. (2003). Adhesion, apoptosis and cytokine release of human mononuclear cells cultured on degradable poly(urethane urea). polystyrene and titanium *in vitro*. *Biomaterials* 24, 2843–2852. doi: 10.1016/S0142-9612(03)00097-8

Guergnon, J., Chaussepied, M., Sopp, P., Lizundia, R., Moreau, M. F., Blumen, B., et al. (2003). A tumour necrosis factor alpha autocrine loop contributes to proliferation and nuclear factor-kappa B activation of Theileria parva-transformed B cells. *Cell. Microbiol.* 5, 709–716. doi: 10.1046/j.1462-5822.2003.00314.x

Harrison, L. M., van Haaften, W. C., and Tesh, V. L. (2004). Regulation of proinflammatory cytokine expression by Shiga toxin 1 and/or lipopolysaccharides in the human monocytic cell line THP-1. *Infect. Immun.* 72, 2618–2627. doi: 10.1128/IAI.72.5.2618-2627.2004

Hutson, C. B., Nichol, J. W., Aubin, H., Bae, H., Yamanlar, S., Al-Haque, S., et al. (2011). Synthesis and characterization of tunable poly(ethylene glycol): gelatin methacrylate composite hydrogels. *Tissue Eng. Part A* 17, 1713–1723. doi: 10.1089/ten.tea.2010.0666

Kamada, H., Tsutsumi, Y., Yamamoto, Y., Kihira, T., Kaneda, Y., Mu, Y., et al. (2000). Antitumor activity of tumor necrosis factor-alpha conjugated with polyvinylpyrrolidone on solid tumors in mice. *Cancer Res.* 60 , 6416–6420.

Kang, H., Shih, Y. V., Hwang, Y., Wen, C., Rao, V., Seo, T., et al. (2014). Mineralized gelatin methacrylate-based matrices induce osteogenic differentiation of human induced pluripotent stem cells. *Acta Biomater.* 10, 4961–4970. doi: 10.1016/j.actbio.2014.08.010

Knight, C. G., Morton, L. F., Peachey, A. R., Tuckwell, D. S., Farndale, R. W., and Barnes, M. J. (2000). The collagen-binding A-domains of integrins alpha(1)beta(1) and alpha(2)beta(1) recognize the same specific amino acid sequence, GFOGER, in native (triple-helical) collagens. *J. Biol. Chem.* 275, 35–40. doi: 10.1074/jbc.275.1.35

Kohn, F. R., Phillips, G. L., and Klingemann, H. G. (1992). Regulation of tumor necrosis factor-alpha production and gene expression in monocytes. *Bone Marrow Transplant.* 9, 369–376.

Lewis, J. S., Roy, K., Keselowsky, B. G. (2014). Materials that harness and modulate the immune system. *MRS Bull.* 39, 25–34. doi: 10.1557/mrs.2013.310

MacEwan, D. J. (2002). TNF receptor subtype signalling: differences and cellular consequences. *Cell. Signal.* 14, 477–492. doi: 10.1016/S0898-6568(01)00262-5

Nezu, T., and Winnik, F. M. (2000). Interaction of water-soluble collagen with poly(acrylic acid). *Biomaterials* 21, 415–419. doi: 10.1016/S0142-9612(99)00204-5

Nichol, J. W., Koshy, S. T., Bae, H., Hwang, C. M., Yamanlar, S., and Khademhosseini, A. (2010). Cell-laden microengineered gelatin methacrylate hydrogels. *Biomaterials* 31, 5536–5544. doi: 10.1016/j.biomaterials.2010.03.064

Nikkhah, M., Eshak, N., Zorlutuna, P., Annabi, N., Castello, M., Kim, K., et al. (2012). Directed endothelial cell morphogenesis in micropatterned gelatin methacrylate hydrogels. *Biomaterials* 33, 9009–9018. doi: 10.1016/j.biomaterials.2012.08.068

Ovsianikov, A., Deiwick, A., Van Vlierberghe, S., Dubruel, P., Möller, L., Dräger, G., et al. (2011). Laser fabrication of three-dimensional CAD scaffolds from photosensitive gelatin for applications in tissue engineering. *Biomacromolecules* 12, 851–858. doi: 10.1021/bm1015305

Paguirigan, A. L., and Beebe, D. J. (2007). Protocol for the fabrication of enzymatically crosslinked gelatin microchannels for microfluidic cell culture. *Nat. Protoc.* 2, 1782–1788. doi: 10.1038/nprot.2007.256

Peela, N., Sam, F. S., Christenson, W., Truong, D., Watson, A. W., Mouneimne, G., et al. (2016). A three dimensional micropatterned tumor model for breast cancer cell migration studies. *Biomaterials* 81, 72–83. doi: 10.1016/j.biomaterials.2015.11.039

Ramón-Azcón, J., Ahadian, S., Obregón, R., Camci-Unal, G., Ostrovidov, S., Hosseini, V., et al. (2012). Gelatin methacrylate as a promising hydrogel for 3D microscale organization and proliferation of dielectrophoretically patterned cells. *Lab Chip* 12, 2959–2969. doi: 10.1039/c2lc40213k

Ronkina, N., Menon, M. B., Schwermann, J., Tiedje, C., Hitti, E., Kotlyarov, A., et al. (2010). MAPKAP kinases MK2 and MK3 in inflammation: complex regulation of TNF biosynthesis via expression and phosphorylation of tristetraprolin. *Biochem. Pharmacol.* 80, 1915–1920. doi: 10.1016/j.bcp.2010.06.021

Rosso, F., Giordano, A., Barbarisi, M., and Barbarisi, A. (2004). From Cell–ECM interactions to tissue engineering. *J. Cell. Physiol.* 199, 174–180. doi: 10.1002/jcp.10471

Saini, H., Navaei, A., Van Putten, A., and Nikkhah, M. (2015). 3D cardiac microtissues encapsulated with the co-culture of cardiomyocytes and cardiac fibroblasts. *Adv. Healthc. Mater.* 4, 1961–1971. doi: 10.1002/adhm.201500331

Salazar, F., Awuah, D., Negm, O. H., Shakib, F., and Ghaemmaghami, A. M. (2017). The role of indoleamine 2,3-dioxygenase-aryl hydrocarbon receptor pathway in the TLR4-induced tolerogenic phenotype in human DCs. *Sci. Rep.* 7:43337. doi: 10.1038/srep43337

Sharquie, I. K., Al-Ghouleh, A., Fitton, P., Clark, M. R., Armour, K. L., Sewell, H. F., et al. (2013). An investigation into IgE-facilitated allergen recognition and presentation by human dendritic cells. *BMC Immunol.* 14, 54–54. doi: 10.1186/1471-2172-14-54

Shin, S. R. Jung, S. M., Zalabany, M., Kim, K., Zorlutuna, P., Kim, S. B., et al. (2013). Carbon-nanotube-embedded hydrogel sheets for engineering cardiac constructs and bioactuators. *ACS Nano* 7, 2369–2380. doi: 10.1021/nn305559j

Silva, A. L., Rosalia, R. A., Varypataki, E., Sibuea, S., Ossendorp, F., and Jiskoot, W. (2015). Poly-(lactic-co-glycolic-acid)-based particulate vaccines: particle uptake by dendritic cells is a key parameter for immune activation. *Vaccine* 33, 847–854. doi: 10.1016/j.vaccine.2014.12.059

Singh, A., and Peppas, N. A. (2014). Hydrogels and scaffolds for immunomodulation. *Adv. Mater.* 26, 6530–6541. doi: 10.1002/adma.201402105

Slaughter, B. V., Khurshid, S. S., Fisher, O. Z., Khademhosseini, A., and Peppas, N. A. (2009). Hydrogels in regenerative medicine. *Adv. Mater.* 21, 3307–3329. doi: 10.1002/adma.200802106

Taravel, M. N., and Domard, A. (1993). Relation between the physicochemical characteristics of collagen and its interactions with chitosan: I. *Biomaterials* 14, 930–938. doi: 10.1016/0142-9612(93)90135-O

Tazi, K. A., Quioc, J.-J., Saada, V., Bezeaud, A., Lebrec, D., and Moreau, R. (2006). Upregulation of TNF-alpha production signaling pathways in monocytes from patients with advanced cirrhosis: possible role of Akt and IRAK-M. *J. Hepatol.* 45, 280–289. doi: 10.1016/j.jhep.2006.02.013

Vaidyanathan, J., Chinnaswamy, K., and Vaidyanathan, T. K. (2003). Biomimetic recognition and immunochemical assay of ligand binding to collagen. *J. Adhes. Dent.* 5, 7–17. doi: 10.3290/j.jad.a8208

Van Den Bulcke, A. I., Bogdanov, B., De Rooze, N., Schacht, E. H., Cornelissen, M., and Berghmans, H. (2000). Structural and rheological properties of methacrylamide modified gelatin hydrogels. *Biomacromolecules* 1, 31–38. doi: 10.1021/bm990017d

Wajant, H., Pfizenmaier, K., and Scheurich, P. (2003). Tumor necrosis factor signaling. *Cell Death Differ.* 10, 45–65. doi: 10.1038/sj.cdd.4401189

Wiegand, C., Schönfelder, U., Abel, M., Ruth, P., Kaatz, M., and Hipler, U. C. (2010). Protease and pro-inflammatory cytokine concentrations are elevated in chronic compared to acute wounds and can be modulated by collagen type I *in vitro*. *Arch. Dermatol. Res.* 302, 419–428. doi: 10.1007/s00403-009-1011-1

Williams, D. F. (2008). On the mechanisms of biocompatibility. *Biomaterials* 29, 2941–2953. doi: 10.1016/j.biomaterials.2008.04.023

Wu, S., Boyer, C. M., Whitaker, R. S., Berchuck, A., Wiener, J. R., Weinberg, J. B., et al. (1993). Tumor-necrosis-factor-alpha as an autocrine and paracrine growth-factor for ovarian-cancer - monokine induction of tumor-cell proliferation and tumor-necrosis-factor-alpha expression. *Cancer Res.* 53, 1939–1944.

Yarilina, A., Park-Min, K. H., Antoniv, T., Hu, X., and Ivashkiv, L. B. (2008). TNF activates an IRF1-dependent autocrine loop leading to sustained expression of chemokines and STAT1-dependent type I interferon-response genes. *Nat. Immunol.* 9, 378–387. doi: 10.1038/ni1576

Yoshida, M., and Babensee, J. E. (2004). Poly(lactic-co-glycolic acid) enhances maturation of human monocyte-derived dendritic cells. *J. Biomed. Mater. Res. Part A* 71A, 45–54. doi: 10.1002/jbm.a.30131

Conflict of Interest Statement: The authors declare that the research was conducted in the absence of any commercial or financial relationships that could be construed as a potential conflict of interest.

frontiers in Bioengineering and Biotechnology

ORIGINAL RESEARCH
published: 14 August 2018
doi: 10.3389/fbioe.2018.00104

In vivo Implantation of a Bovine-Derived Collagen Membrane Leads to Changes in the Physiological Cellular Pattern of Wound Healing by the Induction of Multinucleated Giant Cells: An Adverse Reaction?

*Sarah Al-Maawi[1], Chakorn Vorakulpipat[1], Anna Orlowska[1], Tomislav A. Zrnc[2], Robert A. Sader[1], C James Kirkpatrick[1] and Shahram Ghanaati[1]**

[1] Department for Oral, Cranio-Maxillofacial and Facial Plastic Surgery, Frankfurt Orofacial Regenerative Medicine Lab, University Hospital Frankfurt Goethe University, Frankfurt am Main, Germany, [2] Department of Oral and Maxillofacial Surgery, Medical University of Graz, Graz, Austria

OPEN ACCESS

Edited by:
Amir Ghaemmaghami, University of Nottingham, United Kingdom

Reviewed by:
Martin (Marco) Harmsen, University Medical Center Groningen, Netherlands
Saeid Kargozar, Tehran University of Medical Sciences, Iran
Xin Zhao, Hong Kong Polytechnic University, Hong Kong

***Correspondence:**
Shahram Ghanaati
shahram.ghanaati@kgu.de

Specialty section:
This article was submitted to Biomaterials, a section of the journal Frontiers in Bioengineering and Biotechnology

Received: 04 March 2018
Accepted: 05 July 2018
Published: 14 August 2018

Citation:
Al-Maawi S, Vorakulpipat C, Orlowska A, Zrnc TA, Sader RA, Kirkpatrick CJ and Ghanaati S (2018) *In vivo* Implantation of a Bovine-Derived Collagen Membrane Leads to Changes in the Physiological Cellular Pattern of Wound Healing by the Induction of Multinucleated Giant Cells: An Adverse Reaction? Front. Bioeng. Biotechnol. 6:104. doi: 10.3389/fbioe.2018.00104

The present study evaluated the tissue response toward a resorbable collagen membrane derived from bovine achilles tendon (test group) in comparison to physiological wound healing (control group). After subcutaneous implantation in Wistar rats over 30 days, histochemical and immunohistochemical methods elucidated the cellular inflammatory response, vascularization pattern, membrane protein and cell absorbance capacity. After 30 days, the test-group induced two different inflammatory patterns. On the membrane surface, multinucleated giant cells (MNGCs) were formed after the accumulation of CD-68-positive cells (macrophages), whereas only mononuclear cells (MNCs) were found within the membrane central region. Peri-implant vascularization was significantly enhanced after the formation of MNGCs. No vessels were found within the central region of the membrane. Physiological wound healing revealed no MNGCs at any time point. These dynamic changes in the cellular reaction and vascularization within the test-group are related typical indications of a foreign body reaction. Due to the membrane-specific porosity, mononuclear cells migrated into the central region, and the membrane maintained its integrity over 30 days by showing no breakdown or disintegration. The *ex vivo* investigation analyzed the interaction between the membrane and a blood concentrate system, liquid platelet-rich fibrin (liquid PRF), derived from human peripheral blood and consisting of platelets, leukocytes and fibrin. PRF penetrated the membrane after just 15 min. The data question the role of biomaterial-induced MNGCs as a pathological reaction and whether this is acceptable to trigger vascularization or should be considered as an adverse reaction. Therefore, further pre-clinical and clinical studies are needed to identify the types of MNGCs that are induced by clinically approved biomaterials.

Keywords: multinucleated giant cells, adverse reaction, collagen-based biomaterial, memebrane, regeneration, wound healing, integration, disintegration

INTRODUCTION

The biomaterial physicochemical properties play a major role in induced cellular reactions (Ghanaati et al., 2012). Synthetic biomaterials are precisely synthetized under controlled conditions to produce a specific biomaterial porosity, thickness and surface topography (Moore et al., 2001). In contrast, natural biomaterials e.g., allogeneic and xenogeneic biomaterials are mostly derived from a particular region of the donor body without *de novo* synthesis (Ghanaati et al., 2011). Thereby, these materials undergo strict processing using different chemical and physical methods to reach an adequate state of purification and deactivation of potential pathogens and donor-cells, which may also affect the native structure (Ghanaati et al., 2014). In this sense, the resultant structure and surface characteristics of natural biomaterials depend on the donor tissues and the processing techniques used for their purification (Al-Maawi et al., 2017).

The type of the triggered cellular reaction in response to a biomaterial is imperative for the success of tissue engineering strategies (Dollinger et al., 2018). After biomaterial application, interaction with the surrounding host tissues and cells leads to the induction of a specific cellular inflammatory reaction that may characterize the biomaterial regeneration capacity (Ghanaati, 2012). In a complex process, the cellular reaction toward the implanted biomaterial occurs in concert with wound healing. Initially, the biomaterial surface capacity to absorb specific proteins such as fibrin is a trend-setting property for the subsequent cellular reactions and was described to be involved in the foreign body reaction (Anderson et al., 2008). The formation of a provisional matrix on the interface between the implanted biomaterial and the host tissue is the initial nexus for the host cells to interact with the biomaterial (Anderson et al., 2008). Different *in vitro* and *in vivo* models are utilized to understand the patterns of inflammatory responses to biomaterials and assess their biocompatibility and potential adverse reactions.

In the last decade, our group has presented a systematic series of *in vivo* investigations to analyze the cellular reactions toward different biomaterials using a subcutaneous implantation model (Al-Maawi et al., 2017). Basically, two types of cellular reactions were observed. A physiological reaction that includes the induction of solely mononuclear cells was observed in the case of a non-cross-linked bilayer collagen membrane leading to its integration within the host tissue (Ghanaati, 2012; Al-Maawi et al., 2017). In this *in vivo* study, the porcine-derived biomaterial maintained its structure over 60 days and showed the capacity to serve as a functional barrier without undergoing a premature breakdown or degradation. Moreover, transmembraneous vascularization was not necessary for the integration of this collagen membrane (Ghanaati, 2012). A similar reaction was detected within the implantation bed of a non-cross-linked collagen matrix made from porcine skin and peritoneum (Ghanaati et al., 2011). This biomaterial evoked only mononuclear cells over 60 days and maintained its native structure, which led to its integration within the implantation region. In addition, these findings were successfully translated to the clinic, showing the same mononuclear cell-based reaction (Ghanaati et al., 2011).

The second type of tissue response included the formation of multinucleated giant cells (MNGCs) as a pathological cellular reaction toward the biomaterials (Al-Maawi et al., 2017). The presence of MNGCs within the subcutaneous implantation bed of two non-cross-linked, collagen-based biomaterials of different thicknesses led to their disintegration in terms of premature loss of their native structure as well as an influx of the host connective tissue into the membrane after 30 days, leading to biomaterial disintegration. Thus, the cellular reaction toward biomaterials depends on their physicochemical properties (Barbeck et al., 2015a,b; Al-Maawi et al., 2017). The role of biomaterial induced MNGCs within the regeneration process is not yet fully understood. Different aspects are discussed in the literature to whether these cells may have any contribution to the regeneration process by expressing possible anti-inflammatory mediators (Miron and Bosshardt, 2018). On the other hand aliterature review has shown that biomaterial induced MNGCs actually express similar proinflammatory pattern as pathological MNGCs known from inflammatory diseases such as tubercolusis (Al-Maawi et al., 2017).

In addition to the manufacturing techniques, further methods are used to enhance the stability of collagen-based biomaterials including different types of cross-linking. However, cross linking techniques, especially chemical cross linking was shown to induce a high foreign body reaction (Rothamel et al., 2005). To avoid this, clinical techniques were introduced to provide the membrane higher biomechanical stability without cross linking. In this sense, the collagen double layer technique was introduced for enhanced membrane stability during guided bone regeneration (Abou Fadel et al., 2018). However, degradable biomaterials cannot be considered as a physically occlusive barrier as it is the case for non-resorbable biomaterials (Ghanaati, 2012). Recent studies have shown that resorbable biomaterials serve rather as a functional barrier for a defined time period and get then integrated into the implantation region (Ghanaati et al., 2011; Ghanaati, 2012).

Further developments have focused on harvesting collagen from different animal groups and compartments. Thereby, a novel collagen biomaterial with a specific structural architecture was derived from bovine achilles tendon. The aim of the present study was to analyze the *in vivo* cellular response toward this biomaterial. A subcutaneous implantation model in Wistar rats was used to analyze the cellular reaction in comparison to physiological wound healing without a biomaterial over 30 days. Special focus was placed on the inflammatory pattern, vascularization and regenerative capacity. A liquid platelet-rich fibrin (liquid PRF), which is a blood concentrate system derived from centrifuged human peripheral blood components including fibrin, leukocytes and platelets, was used to examine the protein absorption capacity and interaction with human cells as a novel *ex vivo* assessment system.

MATERIALS AND METHODS

SYMBIOS® Collagen Membrane SR

SYMBIOS® Collagen Membrane SR (SB, Dentsply Implants, Germany) is a slowly resorbing membrane matrix engineered from highly purified type I collagen fibers derived from bovine achilles tendon. According to the manufacturer, the harvested collagen underwent a purification and processing procedure including the use of sodium hydroxide for the inactivation of pathogens such as those associated with bovine spongiform encephalopathy (BSE). The processing and purification methods met the European and international standards for animal tissue sourcing.

Ex vivo Study

The *ex vivo* part of the study focused on the histological analysis of the initial biomaterial-cell interaction to assess the membrane capacity to absorb human proteins and interact with mononuclear cells from the peripheral blood.

Liquid Platelet-Rich Fibrin (Liquid PRF) Preparation

PRF is a blood concentrate system derived from centrifuged human peripheral blood. This concentrate contains a high number of platelets and leukocytes in addition to fibrinogen and plasma proteins. Liquid PRF was chosen to mimic the initial interaction between the biomaterial and the host tissue after biomaterial application.

Three healthy volunteers between 20 and 60 years old donated blood for this study. All volunteers gave written informed consent beforehand. The liquid PRF preparation was performed as previously published (Chia-Lai et al., 2017; Wend et al., 2017). Peripheral blood was collected using 10-ml plastic tubes (orange tubes, PROCESS for PRF, France) and clinically approved butterflies. Two 10-ml tubes per donor were collected and immediately placed in a preprogramed centrifuge (DUO™, PROCESS for PRF, France). Centrifugation was performed for 8 min at 600 rpm, 44 g. The resultant upper layer (liquid PRF) was collected using a syringe with a needle (BD Microlance™ 3, Germany). Nine biomaterial samples (3 per donor) 10×10 mm^2 in size were placed in a 24-well plate. One milliliter of liquid PRF was added to each biomaterial sample and incubated for 15 min. Thereafter, the samples were fixed in 4% buffered formalin for 24 h for further histological analysis.

In vivo Experimental Design: Animal Surgery

The present *in vivo* protocol was approved by the committee on the Use of Live Animals in Teaching and Research (State, Darmstadt, Hessen Germany). A total number of 32 female 8-week-old Wistar rats were purchased from Charles River Laboratories (Germany) and housed for a week before use at the Animal Welfare Office and Central Facility (Goethe University, Frankfurt, Germany). The animals were randomly distributed into 2 groups ($n = 16$ animals per group). The surgical procedure followed standardized methods as previously described (Ghanaati, 2012). In brief, after intraperitoneal anesthesia (10 ml of ketamine (50 mg /ml) with 1.6 ml of 2% xylazine), the first group ($n = 4$ per time point) of animals was placed under anesthesia, and a sterile collagen membrane (SYMBIOS® Collagen Membrane SR, Dentsply Implants, Germany) was implanted under strict sterile conditions into a subcutaneous pocket within the rostral subscapular region. The second group was sham operated ($n = 4$ per time point) to analyze the cellular reaction under physiological wound healing. The animals were sacrificed by means of an overdose (ketamine and xylazine 4 times the anesthetic dose). After the evaluation time points at 3, 10, 15, and 30 days post-operation, the biomaterial including the peri-implantation region in the first group as well as the sham operated region in the second group were explanted and fixed in 4% buffered formalin for 24 h for further histological preparation.

Tissue Preparation for Histology and Immunohistochemistry

The histological processing and staining procedures were performed as previously described (Ghanaati, 2012; Barbeck et al., 2016). Briefly, the explants were cut into three identical segments, which included the margins and the center of the implantation area. Subsequently, the *ex vivo* and *in vivo* samples were processed using a series of graded alcohol and xylene followed by paraffin embedding. For the histological and immunohistochemical staining, four consecutive 3–4-μm slices from the central segment were cut using a rotation microtome (Rotationsmicrotom RM2255, Leica, Germany). After deparaffinization and rehydration, histochemical staining of the *in vivo* and *ex vivo* samples included Mayer's hematoxylin and eosin (H and E), Azan stain and Masson-Goldner stain. To identify tartrate-resistant acid phosphatase (TRAP) activity of the cells, specific staining was performed for TRAP as previously described (Ghanaati et al., 2013). A Sample from previous (Ghanaati et al., 2010a) study showing TRAP-positive cells in Wistar rats served as a positive control for TRAP-staining (data not shown). Two more slices of the *in vivo* samples were used for further immunohistochemical staining to determine blood vessel density and identify macrophages. Immunohistochemical staining was performed using a Lab Vision™ Autostainer 360-2D instrument (ThermoFisher Scientific, Germany) as previously described (Barbeck et al., 2016). Next, endogenous peroxidase activity was blocked using 4% H_2O_2 in methanol, and endogenous avidin- and biotin-binding proteins were blocked by avidin and biotin blocking solutions (Avidin/Biotin Blocking Kit, Vector Laboratories, USA). The first antibody anti CD-68 (MCA341GA; 1:400; 30 min) for macrophages and Anti-Actin, α-Smooth Muscle (SMA) A5228; 1:1,000; 2 h) for vascular endothelial cells. *Ex vivo* samples were stained using anti CD-61 (Dako; 1:50; 1 h) to stain platelets. Thereafter, the secondary antibody goat anti-rabbit IgG-B (sc-2040; 1:200, Santa Cruz Biotechnology, USA) was applied. Subsequently, the avidin-biotin-peroxidase complex (ABC, ThermoFisher Scientific, Germany) for CD-68 and the Histostain-Plus IHC

Kit including AEC (ThermoFisher Scientific, Germany) for SMA were applied for 30 min and 20 min, respectively. As negative controls, immunological staining in the absence of the primary antibody was performed on 2 control sections. For visualization by light microscopy, the sections used for immunohistochemistry were counterstained with Mayer's hematoxylin.

Qualitative Histological Analysis

Qualitative histopathological evaluation was performed using a Nikon ECLIPSE 80i light microscope (Nikon, Japan). The analysis focused on characterizing of the cellular reactions, inflammatory responses and vascularization. A further aim of the histological analysis was to examine the interaction of the biomaterial with liquid PRF *ex vivo*. Photomicrographs were captured using a camera DS-Fi1 (Nikon, Japan).

Quantitative Histomorphometric Analysis

Quantitative histomorphometric analysis of the stained slides was performed with a light microscope (ECLIPSE 80i; Nikon, Japan) including a motorized scanning stage (ProScan III, Prior, USA) connected to a PC running NIS Elements software (Nikon, Japan). As previously described (Ghanaati, 2012; Barbeck et al., 2015a), images of the total implantation beds (total scans), large images of the sample including the collagen membrane and the peri-implant tissue, were reconstructed automatically by merging 100-130 individual micrographs. To evaluate the mean membrane thickness at each time point, the total scans of the H and E-stained slides were used. Fifteen distinct points along the length of the biomaterial per animal were measured manually using the "annotations and measurements" function of the NIS Elements software (Nikon, Tokyo, Japan). The mean of these measurements per slide was calculated as the absolute membrane thickness in µm. The values obtained from later time points were calculated as a percent, while the membrane thickness at day 3 was defined as 100% to avoid artifacts due to histological preparation. The number of MNGCs as well as CD-68-positive macrophages was counted manually using the "count" tool in NIS Elements on the total scans of the TRAP staining and CD-68 staining, respectively, in each animal. The total number of each cell type was calculated with respect to the total implant area on the slides (cell number/mm²) at each time point. The SMA-stained slides were used for evaluation the vascularization pattern. The number and the area (in mm²) of vessels within the implantation beds were determined by manually marking the vessels within the digitized scans. Thus, the total number of vessels was calculated in relation to the total area (in vessels/mm²) and as a percentage of the vessel area (as a fraction of the total implant area in %).

Statistical Analysis

The results from the calculated histomorphometrical analysis were evaluated for significant differences at different time points using one-way and two-way analyses of variance (ANOVA). Statistical significance was defined via p-values (*/•$p < 0.05$; **/••$p < 0.01$; ***/•••$p < 0.001$ and ****/••••$p < 0.0001$) using GraphPad Prism 7 Software (La Jolla, USA). The results are presented as the mean ± standard deviation, and GraphPad Prism 7 was used to produce charts and complete the statistical analysis.

RESULTS

Ex vivo Histological Analysis

The interaction between the liquid PRF and the collagen membrane SB was analyzed histologically. The membrane showed a specific structure with differently oriented collagen fibers (**Figure 1A**). The membrane absorbed PRF, showing a fibrin clot within its porous structure (**Figures 1B,C**). In addition, leukocytes and platelets were detected within the central region of the membrane (**Figures 1D,E**).

In vivo Histological and Histomorphometrical Analyses

All animals survived the implantation period. The wound healing was appropriate in the test group as well as in the sham operated animals. No signs of infection or atypical feeding or sleeping behaviors were observed during the evaluation period.

Qualitative Analysis of the Cellular Reaction Over Time

For the test group, the biomaterial was detected within the implantation region at all-time points. Three days after implantation, the membrane maintained its native structure and integrity and induced mononuclear cells, which were found on the membrane surface (**Figures 2A–D**). The biomaterial central region was mostly free of cells (**Figure 2A**).

After 10 days, the biomaterial showed a stable structure. More mononuclear cells were accumulated on both sides of the membrane. Moreover, mononuclear cells started invading the membrane and were found within the pores of the membrane (**Figure 2B**). CD-68-positive macrophages were accumulated on the biomaterial surface (**Figure 4A**). At this time point, single MNGCs were sporadically found within the biomaterial implantation bed and on the biomaterial surface. Most of the MNGCs showed no TRAP activity (data not shown). Additionally, micro-vessels were detected in proximity to the biomaterial. However, no vessels were detected within the membrane central region.

Fifteen days following implantation, the membrane maintained its integrity and showed stable structure. No signs of breakdown were observed. The membrane was embedded in a cell- and vessel-rich connective tissue. At this time point, more mononuclear cells invaded the membrane and reached its central region. The membrane interfibrillar area contained connective tissue (**Figures 3A,B**). The number of MNGCs increased remarkably, while fewer CD-68-positive macrophages were found in proximity to the biomaterial (**Figure 4B**). However, in general, the MNGCs showed no TRAP expression. The implantation bed showed higher vascularization at 15 days than at the previous time point. However, no vessels

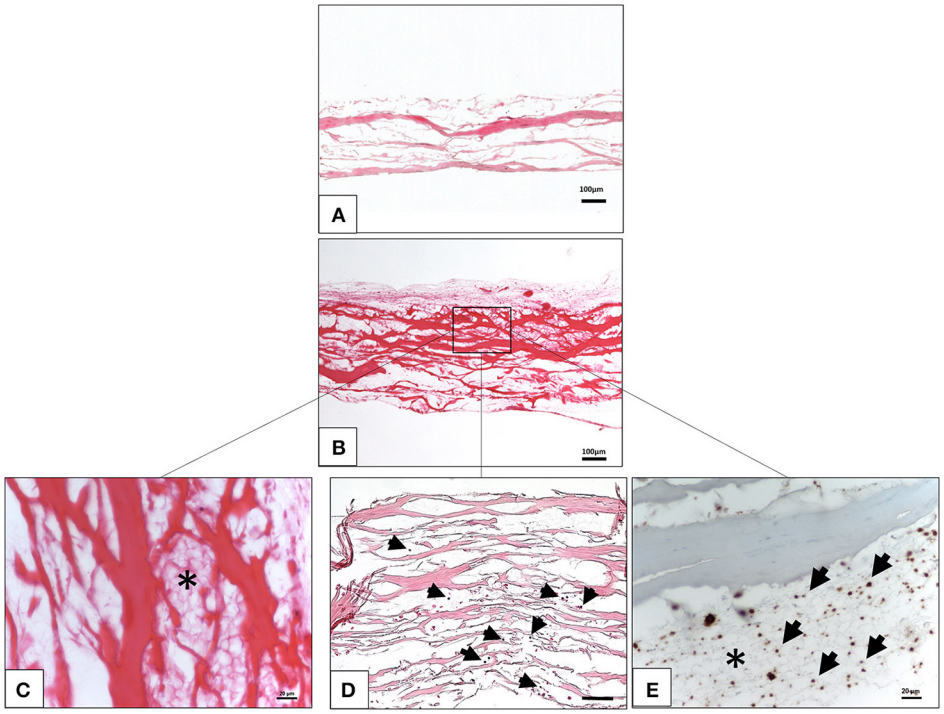

FIGURE 1 | *Ex vivo* interaction between liquid platelet-rich fibrin and the collagen membrane SB. **(A)** A control of the SB illustrating the membrane-specific porous structure (H and E staining; x10 magnification; scale bar = 100 µm). **(B)** Total penetration of leukocytes and platelets from liquid PRF into the SB central region (H and E staining; x100 magnification; scale bar = 100 µm). **(C)** High magnification micrograph showing the fibrin network (*) within the SB collagen fibers (H and E staining; x400 magnification; scale bar = 20 µm). **(D)** High magnification micrograph showing the leukocytes (black arrows) within the SB collagen fibers (H and E staining; x200 magnification; scale bar = 100 µm). **(E)** High magnification micrograph showing the platelets (black arrows) and fibrin network (*) within the SB collagen fibers (anti CD-61 staining; x400 magnification; scale bar = 20 µm).

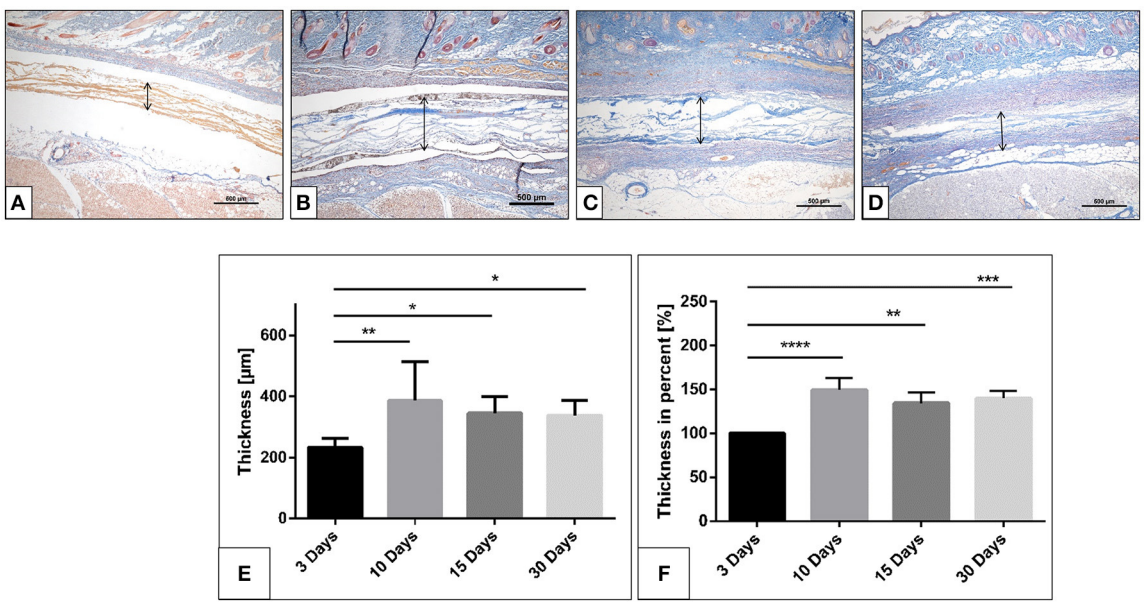

FIGURE 2 | The collagen membrane SB within the implantation bed over the investigates time points. **(A)** after 3 days; **(B)** after 10 days; **(C)** after 15 days; **(D)** after 30 days. (Azan staining; x40 magnification; scale bars = 500 µm). **(E,F)** Histomorphometrical image of the membrane thickness and percentage thickness over 30 days (*$p < 0.05$; **$p < 0.01$; ***$p < 0.001$; and ****$p < 0.0001$).

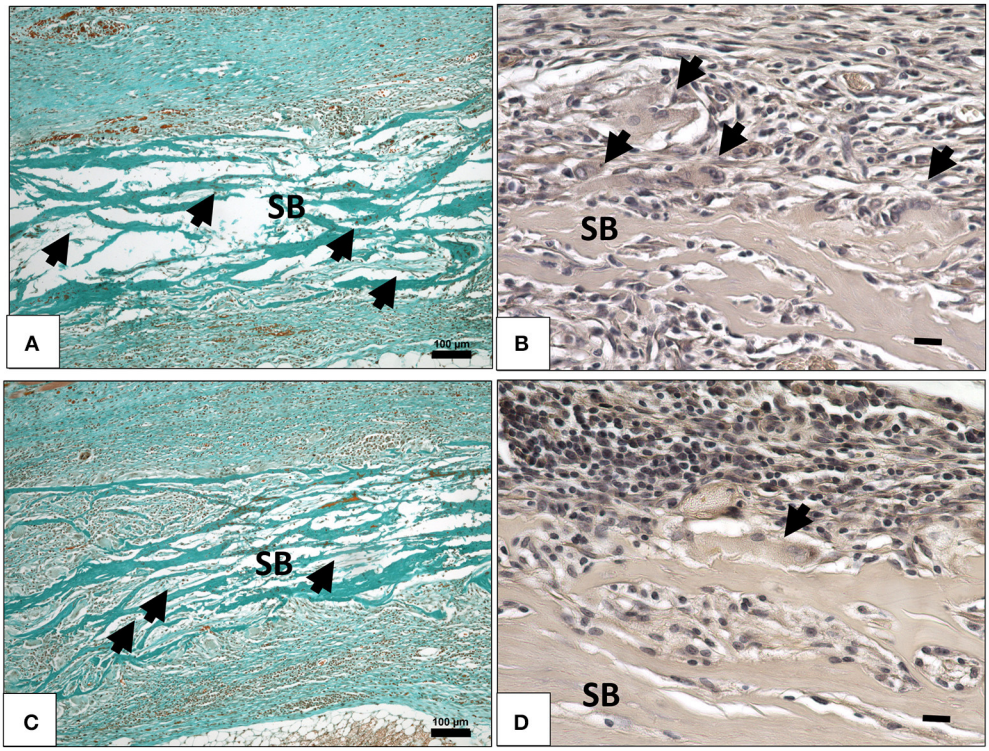

FIGURE 3 | (A) Cellular and connective tissue infiltration (black arrows) of the collagen membrane (SB) on day 15, (Masson Goldner staining; x100 magnification; scale bar= 100 µm). **(B)** TRAP- negative MNGCs (black arrows) on the membrane surface (SB) on day 15, (TRAP staining; x400 magnification; scale bar = 20 µm). **(C)** Cellular and connective tissue infiltration (black arrows) of the collagen membrane (SB) on day 30, (Masson Goldner staining; x100 magnification; scale bar = 100 µm). **(D)** TRAP-negative MNGCs (black arrows) on the membrane surface (SB) on day 30, (TRAP staining; x400 magnification; scale bar = 20 µm).

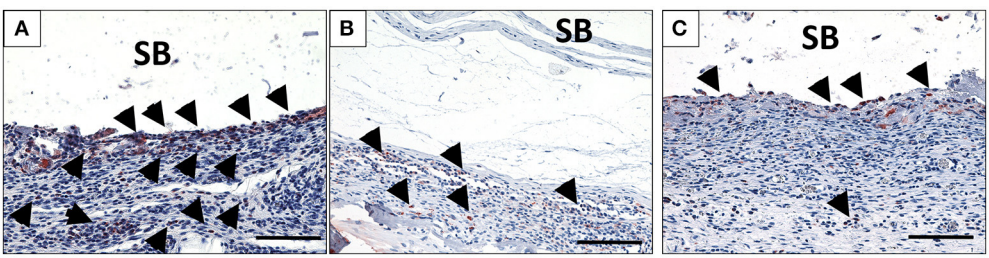

FIGURE 4 | The behavior of macrophage (black arrows) accumulation on days 10 **(A)**, 15 **(B)**, and 30 **(C)** on the surface of the biomaterial (CD-68 immunohistochemical staining; x200 magnification; scale bar =100 µm).

were found within the membrane central region (**Figures 2D**, **3A,B**).

At 30 days after implantation, the membrane was detectable within the implantation bed, showing a stable volume and sustained integrity. No signs of breakdown or disintegration were revealed. The membrane was embedded in a cell- and vessel-rich host connective tissue and allowed the infiltration of mononuclear cells and connective tissue into its central region without losing its native structure (**Figure 3D**). Similar to the observations at day 10, some CD-68-positive macrophages were observed close to the biomaterial surface (**Figure 4C**). However, the MNGCs persisted but were not increased in number and were located on the membrane surface. Thus, no infiltration of MNGCs within the central region was observed. At this time point, most of the MNGCs showed no TRAP activity (**Figure 3D**). The implantation area showed new, well-vascularized connective tissue, while the biomaterial retained its native structure and included the newly formed connective tissue (**Figures 2E**, **3C,D**).

In the control group, the physiological wound healing was uneventful during the observation period. The cellular reaction included only mononuclear cells. No MNGCs were observed at any time point. At day 3, a high number of macrophages

(CD-68-positive) was observed within the evaluation area. The number of macrophages decreased progressively toward day 30. A mild vascularization pattern was detected in the healing area with an increasing tendency from day 3 to day 30.

Quantitative Histomorphometrical Analysis

Evaluation of the Membrane Thickness Over Time

The membrane maintained its stable structure over the observation time period. The histomorphometrical analysis showed that on day 3 the membrane exhibited a mean thickness of 233.5 ± 29.4 μm. The mean thickness increased toward day 10 (366.4 ± 104.8 μm). The membrane thickness at day 15 (345.3 ± 54.2 μm) was comparable to that at day 10. Thus, no statistically significant difference was detected between day 15 and day 10. Finally, a similar value was measured on day 30 (325.7 ± 51.3 μm). The statistical analysis showed a significant difference in the membrane thickness on day 3 and those measured on days 10 ($^{**}p < 0.01$), 15 ($^{*}p < 0.05$) and 30 ($^{*}p < 0.05$). However, no statistically significant differences were found among the thicknesses measured on days 10, 15, and 30 (**Figure 2C**).

The analysis of the percent thickness in relation to day 3 showed a similar pattern. Thereby, the mean percent thickness increased after 10 days (149.2 ± 13.5%). The membrane maintained the percent thickness on days 15 (134.5 ± 12.1%) and 30 (139.9 ± 8.2%). Statistically significant differences were detected between the measured percent thickness on day 3 and those measured on days 10 ($^{****}p < 0.0001$), 15 ($^{**}p < 0.01$), and 30 ($^{***}p < 0.001$). Whereas no statistically significant differences were found comparing the thickness measured on days 10, 15, and 30 (**Figure 2F**).

Evaluation of the Number of CD-68-Positive Cells (Macrophages) Over Time

The number of CD-68-positive macrophages was calculated histomorphometrically per square millimeter. Three days after implantation, some CD-68-positive cells were found within the implantation bed in the test group (33.7 ± 12.5 cells/mm²), whereas a significantly higher number was found within the implantation bed in the control group (105.9 ± 16.3 cells/mm²; $\bullet\bullet\bullet\bullet p < 0.0001$). The number of these cells increased by day 10 (185.9 ± 8.5 cells/mm²) in the test group. On the contrary, there was a rapid decrease in the number of CD-68-positive cells in the control group (19.6 ± 3.7 cells/mm²). At this time point, the highest number of macrophages was measured in the test group throughout the study period and was significantly higher than in the control group ($\bullet\bullet\bullet\bullet p < 0.0001$). By day 15, the number of macrophages was decreased in the test group (118.9 ± 8.5 cells/mm²) and in the control group (12.5 ± 4.2 cells/mm²). At this time point, the difference was still highly significant ($p < 0.0001$). Similar numbers of macrophages observed on day 15 were observed on day 30 in the respective test (109.8 ± 14.4 cells/mm²) and control groups (8.9 ± 2.9 cells/mm²). At this timepoint, significantly higher number of CD-68 positive cells was detected within the test group compared to the control group ($\bullet\bullet\bullet\bullet p < 0.0001$).

Within-group analyses in the test group showed that the increase in the number of macrophages from day 3 to 10 was highly significant ($^{****}p < 0.0001$). Moreover, the decrease from day 10 to 15 showed a statistically significant difference ($^{***}p < 0.001$). Additionally, the difference in macrophage number between day 10 and 30 was statistically highly significant ($^{****}p < 0.0001$). Despite the decrease from day 10 onward, the numbers of macrophages on days 15 and 30 were higher. The difference was statistically highly significant when comparing the numbers between day 3 and day 15 ($^{****}p < 0.0001$) and between day 3 and day 30 ($^{****}p < 0.0001$). However, no statistically significant difference was observed in the macrophage numbers between days 15 and 30 (**Figure 5A**).

Evaluation of the Number of Multinucleated Giant Cells Over Time

No MNGCs were observed in the control group at any time point; therefore, it was not considered for the statistical analysis.

The number of the MNGCs was determined histomorphometrically per square millimeter. Three days after implantation, no MNGCs were found within the implantation bed of the biomaterial. After 10 days, a moderate number of MNGCs were present within the biomaterial implantation bed (4.6 ± 1.3 MNGCs/mm²). The number of the MNGCs increased significantly toward day 15 (9.3 ± 2.1 MNGCs/mm²). However, after 30 days, a slight decrease in the MNGC number was detected (7.2 ± 2.7 MNGCs/mm²) compared to the number of MNGCs at day 15.

Statistical analysis showed a significant difference in the MNGC number between days 3 and 10 ($^{*}p < 0.05$). The number of MNGCs was significantly higher on day 15 than on day 3 ($^{****}p < 0.0001$) and on day 10 ($^{*}p < 0.05$). The slight decrease from day 15 to 30 showed no statistically significant difference. Moreover, no statistically significant difference was observed in the MNGC numbers between days 30 and 10. However, the number of MNGCs was significantly higher on day 30 than on day 3 ($^{***}p < 0.001$). Generally, the MNGCs showed no TRAP expression. Therefore, no histomorphometrical analysis of the TRAP expression was performed (**Figure 5C**).

Evaluation of the Vascularization Pattern Over Time

The vascularization pattern was evaluated histomorphometrically in the biomaterial implantation bed as well as the sham operation group.

The vessel density on day 3 within the SB implantation bed (6.4 ± 2.8 vessels/mm²) and the control group (5.3 ± 2.7 vessels/mm²) showed comparable results. Thus, no statistically significant difference was revealed at this time point. Ten days after implantation, the SB implantation bed (33.7 ± 8.4 vessels/mm²) showed a higher vascularization rate than that on day 3. The difference was statistically significant ($^{**}p < 0.01$). The vessel density within the control group increased only slightly on day (5.9 ± 2.2 vessels/mm²). Therefore, the vessel density within the SB group showed a significantly higher rate than that in the control group ($\bullet\bullet\bullet\bullet p < 0.0001$). After 15 days, the vessel density within the SB implantation bed was increased slightly (35.4 ± 13.4 vessels/mm²). No statistically significant difference

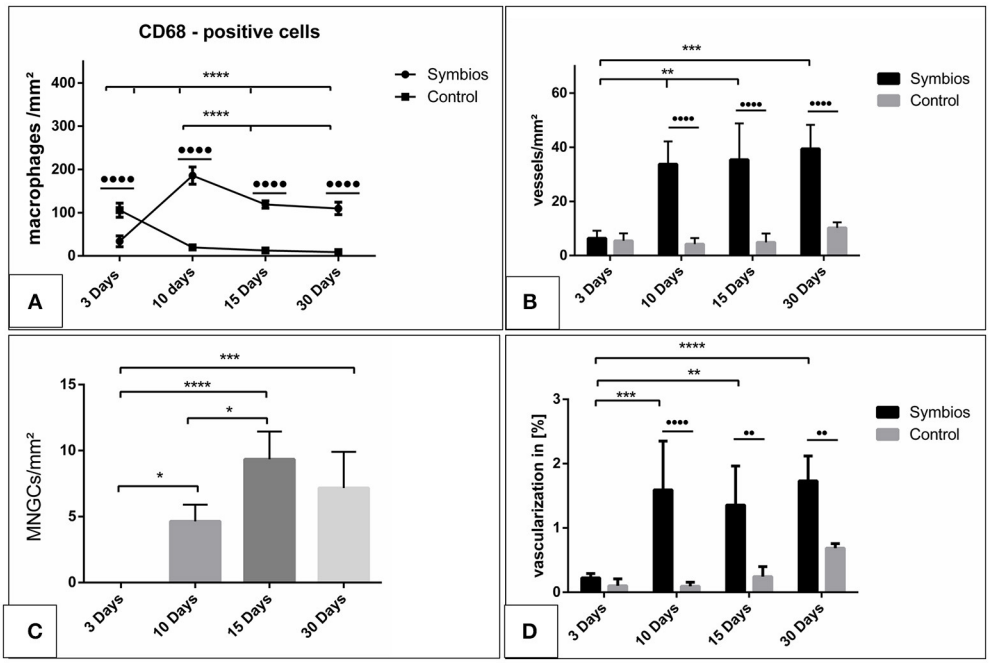

FIGURE 5 | Histomorphometrical analysis. **(A)** The numbers of CD-68-positive cells (macrophages) per square millimeter over the time. **(B)** The vascularization pattern over the time in vessels per square millimeter in comparison to the control group. **(C)** The numbers of multinucleated giant cells (MNGCs) per square millimeter over the time. **(D)** The percent vascularization of the implantation bed over the time in comparison to the control group. ($^{*}/^{\bullet}p < 0.05$; $^{**}/^{\bullet\bullet}p < 0.01$; $^{***}/^{\bullet\bullet\bullet}p < 0.001$; and $^{****}/^{\bullet\bullet\bullet\bullet}p < 0.0001$).

was detected compared to day 10. However, the vessel density was significantly higher than that on day 3 ($^{**}p < 0.01$). In addition, a minor increase in the vessel number was observed in the control group (6.3 ± 3.8 vessels/mm²). The SB group showed a significantly higher vessel number than the control group at this time point ($\bullet\bullet\bullet\bullet p < 0.0001$). On day 30, an increase in the vessel density within the SB group was observed (39.4 ± 8.8 vessels/mm²). However, no statistically significant difference was revealed between days 10 and 15. The number of vessels was significantly higher than the vessel density on day 3 ($^{***}p < 0.001$). The vascularization of the control group showed an increase in the vessel density (10.2 ± 2.1 vessels/mm²). However, the SB group showed a significantly higher vessel density compared to the control group at this time point ($\bullet\bullet\bullet\bullet p < 0.0001$; **Figure 5B**).

The vascularization was quantified with respect to the implantation area in both the SB group and the control group. The percent vascularization increased over 30 days in both groups. On day 3, both groups showed comparable values (SB: 0.2 ± 0.07%; control: 0.15 ± 0.08%), and there was no statistically significant difference. The percent vascularization increased in the SB group significantly by day 10 (1.6 ± 0.06%). At this time point, the percent vascularization within the SB implantation bed was significantly higher than that in the control group (0.12 ± 0.06%; $\bullet\bullet\bullet\bullet p < 0.001$). Subsequently, on day 15, the percent vascularization rate within the SB group (1.3 ± 0.6%) showed a slight decrease compared to the previous time point. However, the vascularization was significantly higher than that on day 3 ($^{**}p < 0.01$), whereas no statistically significant difference was detected compared to the vascularization on day 10. The difference between the vascularization in the SB group and in the control group (0.2 ± 0.1%) showed a significantly higher vascularization in the SB group at this time point ($\bullet\bullet p < 0.001$). Finally, after 30 days, the percent vascularization increased in the SB group (1.7 ± 0.3%). This value was significantly higher than the percent vascularization on day 3 ($^{****}p < 0.0001$). In contrast, no statistically significant differences were evident compared to the percent vascularization on days 15 or 10. The percent vascularization within the control group (0.7 ± 0.07%) increased compared to the previous time point. Nevertheless, the percent vascularization was significantly higher in the SB group than in the control group at this time point ($\bullet\bullet p < 0.01$; **Figure 5D**).

Additionally, similar kinetics were detected in the vascularization and induction of MNGCs. The vascularization pattern increased corresponding to the increasing number of the induced MNGCs over time (**Figures 6A–C**).

DISCUSSION

Numerous collagen-based membranes are available as naturally derived xenogeneic membranes that should meet the defined requirements to serve as a scaffold and maintain integrity for a suitable time period. However, the naturally derived xenogeneic collagen-based biomaterials must undergo different purification

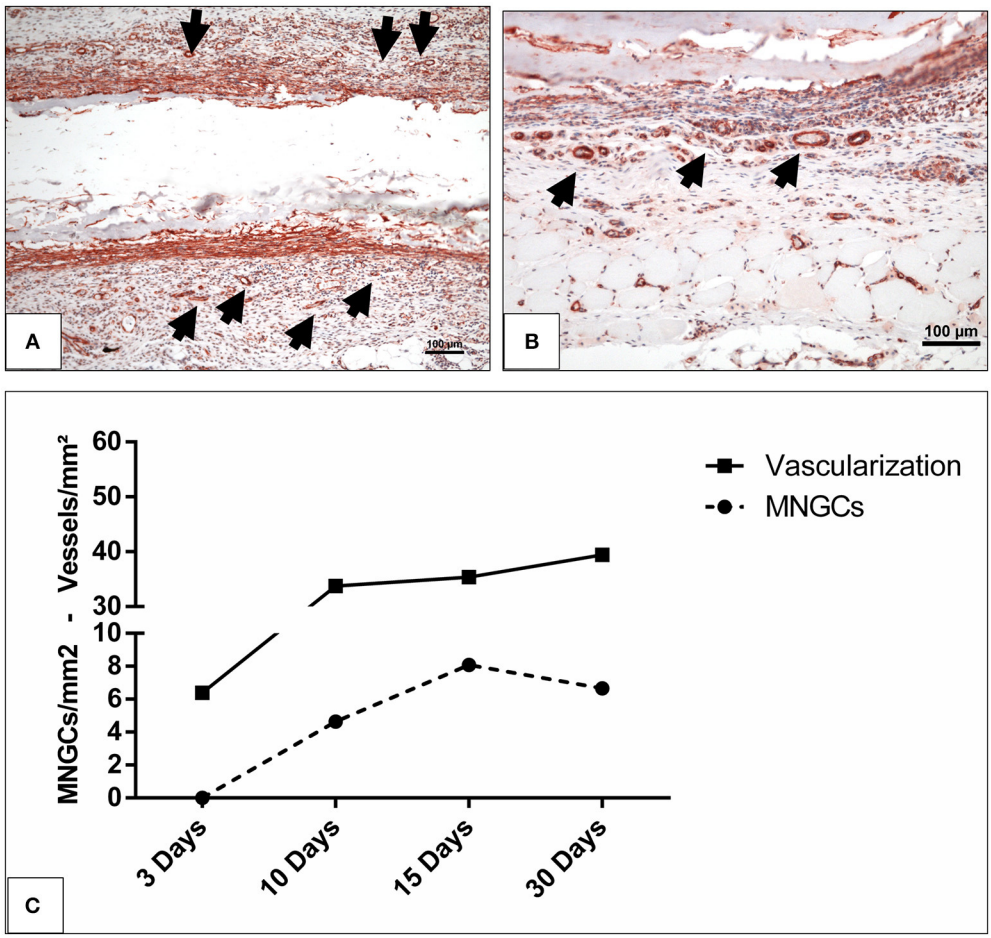

FIGURE 6 | The vascularization pattern **(A)** on day 10 and **(B)** on day 15 highlighted with immunohistochemical staining of SMA in x200 magnification. Black arrow heads, vessels; scale bar, 100 µm. **(C)** The correlation between the induced MNGCs and the vascularization in the test group.

and processing procedures that influence their native structure. In this context, the cellular reaction toward different membranes is primarily related to the membrane-specific physicochemical properties (Dadsetan et al., 2004; Ghanaati et al., 2012).

The *in vivo* tissue response toward a novel collagen-based biomaterial SB that is derived from bovine achilles tendon showed that SB initially induced a mononuclear cell-based reaction on day 3. At this time point, single mononuclear cells had already infiltrated the membrane. Immunohistochemical staining showed that some of the mononuclear cells were CD-68-positive, representing the presence of macrophages on the SB surface. The mid-term cellular reaction on day 10 was characterized by a high number of macrophages (CD-68-positive) on the membrane surface, reflecting a significant increase in their number compared the number of macrophages observed on day 3. Additionally, some MNGCs were found on the biomaterial surface at this time point. The induction of MNGCs was accompanied by significantly increased vascularization. However, the localization of the mononuclear cells was rather triggered within the central region, whereas MNGCs were only located on the membrane surface (**Figure 3**).

MNGCs the potential to express vascular endothelial growth factor, which may explain the enhanced vascularization within the implantation bed after their formation (Moens et al., 2014). This phenomenon was previously observed within the implantation bed of different biomaterials including synthetic and xenogeneic bone substitute materials and collagen based-membranes (Ghanaati et al., 2010a; Barbeck et al., 2015b,c). By day 15, a course change was detected in the number of the macrophages and MNGCs (**Figure 4**). The macrophage number decreased significantly in comparison to that observed on day 10. Simultaneously, the number of the MNGCs increased significantly compared to that observed on day 10. Macrophages are precursors cells of MNGCs (Anderson et al., 2008; Chen et al., 2010). Their interaction with the biomaterial surface and the inflammatory microenvironment around the implanted biomaterial is essential for the fusion and formation of MNGCs, which possess an enhanced oxidative capacity (Enelow et al., 1992; McNally and Anderson, 2002; Chang et al., 2009). This

process was previously described as frustrated phagocytosis. Thus, after the frustrated attempts of macrophages to degrade the biomaterial, they fuse to form MNGCs (Xia and Triffitt, 2006; MacLauchlan et al., 2009). Accordingly, the dynamic changes observed here in the numbers of macrophages and MNGCs might be due to their fusion and the process of MNGC formation. At the last observation time point, neither the macrophages nor the MNGCs showed a significant change in the number of cells. These findings were similar to the rate of vascularization, which showed a stable level from day 10 onwards. All the parameters presented here, including the formation of MNGCs and enhanced vascularization, are circumstantial evidence of a foreign body reaction (Mcnally and Anderson, 2015). In this sense, it is questionable whether an exuberant vascularization is required for the regeneration process. It was previously shown that a mild vascularization that is derived by mononuclear, similar to the physiological vascularization pattern is sufficient for membrane integration *in vivo* (Ghanaati, 2012).

The present results showed that the occurrence of MNGCs is induced by the implanted biomaterial, thus no MNGCs were observed within the control group, which simulated physiological wound healing. Previous assumptions questioned whether the formation of MNGCs is a physiological reaction related to biomaterial resorption or might be associated with collagen-based biomaterials harvested from a specific compartment (Barbeck et al., 2015b). However, MNGCs were observed within the implantation bed of different biomaterials including collagen-based biomaterial (Barbeck et al., 2015b) and silk-based polymers (Ghanaati et al., 2010c), as well as different synthetic and xenogeneic bone substitute materials (Ghanaati et al., 2010b). The biomaterial-induced MNGCs show common characteristics with pathological MNGCs (Langerhans' giant cells) that exist in sarcoidosis and tuberculosis (Al-Maawi et al., 2017). These are not only morphological characteristics in terms of the number of nuclei but also in the expressed surface proteins such as CD-68, Integrin ß 1/2 and HLA-DR (Al-Maawi et al., 2017). In this sense, the question arises as to whether the presence of MNGCs within the implantation bed of clinically applicable biomaterials is an acceptable reaction or rather an adverse reaction after chronic inflammation.

It is noteworthy that collagen-based biomaterials, such as non-cross-linked bilayer collagen matrix from porcine skin and peritoneum, induced solely mononuclear cells and maintained their native structure over a period of 60 days. This collagen matrix allowed slow penetration into the biomaterial superficial layer but served as a functional barrier within its central region and was integrated within the host tissue (Ghanaati et al., 2011).

Additionally, in the present study MNGCs were only localized on the surface of the biomaterial and did not enter the biomaterial body, while the mononuclear cells migrated into the membrane body and were integrated after 30 days. Therefore, the vascularization was enhanced at the peri-implantation region, but no vessels were observed within the membrane central region in terms of transmembraneous vascularization. The occurrence of inflammatory responses with two different outcomes, i.e., mononuclear cells vs. MNGCs, is noteworthy. This specific inflammatory pattern may be beneficial to recruit vessels to the implantation region without manipulating the membrane structure. This may be related to the specific architecture of the biomaterial that includes pores within the membrane body, which allowed the mononuclear cells to migrate into the center region and integrate within the biomaterial so that the macrophages were not over-accumulated at the surface, resulting in a high number of MNGCs. In addition, despite the presence of MNGCs, the SB maintained its integrity over 30 days and allowed only mononuclear cells to enter its central region while resisting the MNGCs (**Figure 3**). Thereby, no signs of breakdown or disintegration in terms of loss of the initial structure, were detected during the evaluation period. Additionally, within the observation period of this study, the biomaterial did not show typical signs of encapsulation as it was previously found in non-resorbable biomaterials (Ghanaati, 2012) Furthermore, it is interesting to further elucidate whether the presence of MNGCs will lead to a classical foreign body reaction and encapsulation of the biomaterial or whether these cells could be involved within the resorption process of the biomaterial.

In contrast, other non-cross-linked, collagen-based biomaterials that induced MNGCs underwent disintegration after a clear backdown leading to their disintegration (Barbeck et al., 2015b). In that case, the loss of integrity allowed premature ingrowth of the peri-implantation connective tissue into the membrane body including MNGC- and vessel-rich granulation tissue (Barbeck et al., 2015b). This phenomenon was not observed in this study during the evaluation period. Within the limitations of this study, it is presumable that the membrane may experience disintegration after 60 days or more.

Another naturally derived biomaterial of silk fibroin underwent disintegration after the induction of MNGCs. The silk fibroin showed transmembraneous vascularization and a loss of integrity after 60 days (Ghanaati, 2012). However, most of the induced MNGCs in silk fibroin expressed TRAP, which might be a sign for their pro-inflammatory activity (Ghanaati, 2012). On the other hand, the present results showed mostly no TRAP-positive MNGCs, which might represent a different MNGC type that did not contribute to the disintegration of the biomaterial. Another parameter may be the harvesting compartment of the SB, i.e., bovine achilles tendon. This may include a different collagen quality that does not evoke a severe pro-inflammatory reaction.

Furthermore, different processing and purification methods have an impact on changing the surface characteristics of the native collagen, which leads to different tissue responses (Jones et al., 2004). This may influence the cellular activation and thus the macrophage polarization and expression pattern, which possibly influence their fusion to MNGCs (Jones et al., 2004; Kajahn et al., 2012). However, further studies are needed to determine the interaction between differently activated macrophages and the formation of MNGCs for a better understanding of the mononuclear cells and multinucleated giant cell activation and polarization.

The *ex vivo* results of the interaction between SB and the liquid PRF showed that the membrane was infiltrated by liquid PRF including leukocytes and platelets. Therefore, the membrane absorbed the liquid PRF and allowed cellular invasion during the

early time period (**Figure 1**). However, *in vivo* results after 3 days showed some cellular infiltration intro the superficial layer of the membrane, whereas the central region was still free of murine cells of the peri-implantation region. This occurs because of the difference between the qualities of subcutaneous tissue and the liquid PRF. Thereby, *in vivo* cellular infiltration require longer time period until cells migrate from the extracellular matrix of the peri-implantation region into the membrane compartment. Nevertheless, cellular infiltration was then reached after an initial time period of 10–15 days *in vivo*.

Accordingly, the *in vivo* thickness measurements showed that the SB thickness increased significantly from day 3 to day 10 and then maintained the thickness level over 30 days. This occurred because the SB allowed cells and connective tissue to enter the membrane body. The specific structure and interfibrillar compartments allowed the membrane to include the host cells and connective tissue and thus increase in thickness without undergoing a breakdown or disintegration (**Figure 3**). Recently, the application of this method for the evaluation of a sugar cross linked porcine derived collagen membrane showed that the membrane was occlusive to the fibrin and cells of PRF (Chia-Lai et al., 2017). These results were in correlation to the *in vivo* evaluation using subcutaneous implantation. This frequent agreement in the *ex vivo* and *in vivo* results make liquid PRF a potential tool to investigate the membrane absorbance capacity and provide information about the *in vivo* cellular reaction while avoiding animal experiments. Recent studies used blood serum and plasma proteins to investigate the biomaterial surface absorption capacity (Nguyen et al., 2016). In the present study, a more complex system was used i.e., liquid PRF, which includes not only plasma proteins but also cells (Platelets and leukocytes). Thereby, the focus of the present study was placed on the cellular infiltration of the collagen-based membrane by the cells and the formation of the fibrin network within the membrane pores. Additionally, to further elucidate the mechanisms of protein absorbance and the interaction between collagen and PRF, further methods are required such as atomic force microscopy. These aspects are further topics of our research group and are presently under investigation to elucidate the capacity of different collagen based biomaterials to incorporate PRF with special focus on different plasma proteins respecting the competitive protein exchange and the vroman effect (Hirsh et al., 2013).

In addition, the specific porous structure and the ability to include the host connective tissue might be a reason for the maintained integrity after inducing a foreign body reaction by MNGCs. It might be that including the host cells within the membrane is favorable for the regeneration process to serve as a scaffold to promote guided tissue regeneration. In an animal study using a tooth dehiscence model for periodontological regeneration, a collagen biomaterial of bovine achilles origin showed comparable results to a non-cross-linked, porcine-derived collagen membrane, which led to successful tissue regeneration (Behfarnia et al., 2012). Furthermore, a clinical study showed that bovine-derived collagen membranes are suitable for successful root coverage (Schlee et al., 2012).

In summary, the present findings raise the need for further research to characterize the types of biomaterial-related MNGCs and whether they should be accepted as a biomaterial-related cellular reaction or considered as an adverse reaction following chronic inflammation. These findings are clinically highly interesting to evaluate the clinical suitability of different biomaterials and define suitable indications with respect to the biomaterial physicochemical properties.

CONCLUSION

The present study evaluated the cellular reaction toward a novel collagen membrane derived from bovine achilles tendon. The tissue response showed an initial reaction of mononuclear cells followed by the formation of MNGCs from day 10 onwards, whereas no MNGCs were detected within the control group that mimicked physiological wound healing. The presence of these cells was accompanied by a reduction in the CD-68-positive cell number (macrophages), indicating their fusion to form MNGCs, which were only localized on the membrane surface. Along with the enhanced MNGC number, the vascularization of the peri-implantation area increased significantly. No transmembraneous vascularization was found within the membrane body, and only mononuclear cells were able to migrate. These characteristics refer to a foreign body reaction toward the biomaterial surface. Thereby, the role of the MNGCs induced by this biomaterial requires further investigation.

Ex vivo and *in vivo* experiments showed that the biomaterial allows protein absorbance and mononuclear cells to migrate into its central region. These findings were observed along with the *in vivo* increase in thickness reflecting the membrane capacity to incorporate the host cells and connective tissue and form a scaffold without undergoing any signs of breakdown or disintegration. These findings raise the question of whether the formation of MNGCs should be accepted as a biomaterial-related reaction or considered as an adverse reaction.

AUTHOR CONTRIBUTIONS

SA-M: Immunohistochemical analysis, data acquisition, statistical analysis, manuscript preparation, manuscript editing, literature research; CV: Histological preparation, Data acquisition, histomorphometric analysis, statistical analysis, literature research, *Ex vivo* study part; AO: Animal surgery, data acquisition, histology; TZ: *Ex vivo* study part, literature research, data analysis; RS: Definition of intellectual content, manuscript review; CK: Definition of intellectual content, manuscript review; SG: Study concept, study design, definition of intellectual content, manuscript review, manuscript editing.

FUNDING

This work was partially funded by Marie Curie Actions under EU FP7 Initial Training Network SNAL 608184.

ACKNOWLEDGMENTS

The authors would like to thank the excellent technical support of Mrs. Verena Hoffmann and Mrs. Yunxin Zhang.

REFERENCES

Abou Fadel, R., Samarani, R., and Chakar, C. (2018). Guided bone regeneration in calvarial critical size bony defect using a double-layer resorbable collagen membrane covering a xenograft: a histological and histomorphometric study in rats. *Oral Maxillofac. Surg.* 22, 203–213. doi: 10.1007/s10006-018-0694-x

Al-Maawi, S., Orlowska, A., Sader, R., James Kirkpatrick, C., and Ghanaati, S. (2017). *In vivo* cellular reactions to different biomaterials—Physiological and pathological aspects and their consequences. *Semin. Immunol.* 29, 49–61. doi: 10.1016/j.smim.2017.06.001

Anderson, J. M., Rodriguez, A., and Chang, D. T. (2008). Foreign body reaction to biomaterials. *Semin. Immunol.* 20, 86–100. doi: 10.1016/j.smim.2007.11.004

Barbeck, M., Lorenz, J., Holthaus, M. G., Raetscho, N., Kubesch, A., Booms, P., et al. (2015a). Porcine dermis and pericardium-based, non-cross-linked materials induce multinucleated giant cells after their *in vivo* implantation: a physiological reaction? *J. Oral Implantol.* 41, e267–e281. doi: 10.1563/aaid-joi-D-14-00155

Barbeck, M., Lorenz, J., Kubesch, A., Böhm, N., Booms, P., Choukroun, J., et al. (2015b). Porcine dermis-derived collagen membranes induce implantation bed vascularization via multinucleated giant cells: a physiological reaction? *J. Oral Implantol.* 41, e238–e251. doi: 10.1563/aaid-joi-D-14-00274

Barbeck, M., Motta, A., Migliaresi, C., Sader, R., Kirkpatrick, C. J., and Ghanaati, S. (2016). Heterogeneity of biomaterial-induced multinucleated giant cells: possible importance for the regeneration process? *J. Biomed. Mater. Res. Part A* 104, 413–418. doi: 10.1002/jbm.a.35579

Barbeck, M., Udeabor, S., Lorenz, J., Schlee, M., Holthaus, M. G., Raetscho, N., et al. (2015c). High-temperature sintering of xenogeneic bone substitutes leads to increased multinucleated giant cell formation: *in vivo* and preliminary clinical results. *J. Oral Implantol.* 41, e212–e222. doi: 10.1563/aaid-joi-D-14-00168

Behfarnia, P., Khorasani, M. M., Birang, R., and Abbas, F. M. (2012). Histological and histomorphometric analysis of animal experimental dehiscence defect treated with three bio absorbable GTR collagen membrane. *Dent. Res. J. (Isfahan).* 9, 574–581. doi: 10.4103/1735-3327.104876

Chang, D. T., Colton, E., Matsuda, T., and Anderson, J. M. (2009). Lymphocyte adhesion and interactions with biomaterial adherent macrophages and foreign body giant cells. *J. Biomed. Mater. Res. A* 91, 1210–1220. doi: 10.1002/jbm.a.32218

Chen, S., Jones, J. A., Xu, Y., Low, H.-Y., Anderson, J. M., and Leong, K. W. (2010). Characterization of topographical effects on macrophage behavior in a foreign body response model. *Biomaterials* 31, 3479–3491. doi: 10.1016/j.biomaterials.2010.01.074

Chia-Lai, P.-J., Orlowska, A., Al-Maawi, S., Dias, A., Zhang, Y., Wang, X., et al. (2017). Sugar-based collagen membrane cross-linking increases barrier capacity of membranes. *Clin. Oral. Investig.* 22, 1851–1863. doi: 10.1007/s00784-017-2281-1

Dadsetan, M., Jones, J. A., Hiltner, A., and Anderson, J. M. (2004). Surface chemistry mediates adhesive structure, cytoskeletal organization, and fusion of macrophages. *J. Biomed. Mater. Res. A* 71, 439–448. doi: 10.1002/jbm.a.30165

Dollinger, C., Ciftci, S., Knopf-Marques, H., Guner, R., Ghaemmaghami, A. M., Debry, C., et al. (2018). Incorporation of resident macrophages in engineered tissues: multiple cell type response to microenvironment controlled macrophage-laden gelatine hydrogels. *J. Tiss. Eng. Regen. Med.* 12, 330–340. doi: 10.1002/term.2458

Enelow, R. I., Sullivan, G. W., Carper, H. T., and Mandell, G. L. (1992). Cytokine-induced human multinucleated giant cells have enhanced candidacidal activity and oxidative capacity compared with macrophages. *J. Infect. Dis.* 166, 664–668. doi: 10.1093/infdis/166.3.664

Ghanaati, S. (2012). Non-cross-linked porcine-based collagen I-III membranes do not require high vascularization rates for their integration within the implantation bed: a paradigm shift. *Acta Biomater.* 8, 3061–3072. doi: 10.1016/j.actbio.2012.04.041

Ghanaati, S., Barbeck, M., Booms, P., Lorenz, J., Kirkpatrick, C. J., and Sader, R. A. (2014). Potential lack of "standardized" processing techniques for production of allogeneic and xenogeneic bone blocks for application in humans. *Acta Biomater.* 10, 3557–3562. doi: 10.1016/j.actbio.2014.04.017

Ghanaati, S., Barbeck, M., Detsch, R., Deisinger, U., Hilbig, U., Rausch, V., et al. (2012). The chemical composition of synthetic bone substitutes influences tissue reactions *in vivo*: histological and histomorphometrical analysis of the cellular inflammatory response to hydroxyapatite, beta-tricalcium phosphate and biphasic calcium phosphate ceramics. *Biomed. Mater.* 7:015005. doi: 10.1088/1748-6041/7/1/015005

Ghanaati, S., Barbeck, M., Orth, C., Willershausen, I., Thimm, B. W., Hoffmann, C., et al. (2010a). Influence of β-tricalcium phosphate granule size and morphology on tissue reaction *in vivo*. *Acta Biomater.* 6, 4476–4487. doi: 10.1016/j.actbio.2010.07.006

Ghanaati, S., Orth, C., Barbeck, M., Willershausen, I., Thimm, B. W., Booms, P., et al. (2010b). Histological and histomorphometrical analysis of a silica matrix embedded nanocrystalline hydroxyapatite bone substitute using the subcutaneous implantation model in wistar rats. *Biomed. Mater.* 5:035005. doi: 10.1088/1748-6041/5/3/035005

Ghanaati, S., Orth, C., Unger, R. E., Barbeck, M., Webber, M. J., Motta, A., et al. (2010c). Fine-tuning scaffolds for tissue regeneration: effects of formic acid processing on tissue reaction to silk fibroin. *J. Tissue Eng. Regen. Med.* 4, 464–472. doi: 10.1002/term.257

Ghanaati, S., Schlee, M., Webber, M. J., Willershausen, I., Barbeck, M., Balic, E., et al. (2011). Evaluation of the tissue reaction to a new bilayered collagen matrix *in vivo* and its translation to the clinic. *Biomed. Mater.* 6:015010. doi: 10.1088/1748-6041/6/1/015010

Ghanaati, S., Udeabor, S. E., Barbeck, M., Willershausen, I., Kuenzel, O., Sader, R. A., et al. (2013). Implantation of silicon dioxide-based nanocrystalline hydroxyapatite and pure phase beta-tricalciumphosphate bone substitute granules in caprine muscle tissue does not induce new bone formation. *Head Face Med.* 9:1. doi: 10.1186/1746-160X-9-1

Hirsh, S. L., McKenzie, D. R., Nosworthy, N. J., Denman, J. A., Sezerman, O. U., and Bilek, M. M. M. (2013). The Vroman effect: competitive protein exchange with dynamic multilayer protein aggregates. *Colloids Surfaces B Biointerfaces* 103, 395–404. doi: 10.1016/j.colsurfb.2012.10.039

Jones, J. A., Dadsetan, M., Collier, T. O., Ebert, M., Stokes, K. S., Ward, R. S., et al. (2004). Macrophage behavior on surface-modified polyurethanes. *J. Biomater. Sci. Polym. Ed.* 15, 567–84. doi: 10.1163/156856204323046843

Kajahn, J., Franz, S., Rueckert, E., Forstreuter, I., Hintze, V., Moeller, S., et al. (2012). Artificial extracellular matrices composed of collagen I and high sulfated hyaluronan modulate monocyte to macrophage differentiation under conditions of sterile inflammation. *Biomatter* 2, 226–236. doi: 10.4161/biom.22855

MacLauchlan, S., Skokos, E. A., Meznarich, N., Zhu, D. H., Raoof, S., Shipley, J. M., et al. (2009). Macrophage fusion, giant cell formation, and the foreign body response require matrix metalloproteinase 9. *J. Leukoc. Biol.* 85, 617–626. doi: 10.1189/jlb.1008588

McNally, A. K., and Anderson, J. M. (2002). β1 and β2 integrins mediate adhesion during macrophage fusion and multinucleated foreign body giant cell formation. *Am. J. Pathol.* 160, 621–630. doi: 10.1016/S0002-9440(10)64882-1

Mcnally, A. K., and Anderson, J. M. (2015). Phenotypic expression in human monocyte-derived interleukin-4-induced foreign body giant cells and macrophages *in vitro*: dependence on material surface properties. *J. Biomed. Mater. Res. A.* 103, 1380–1390. doi: 10.1002/jbm.a.35280

Miron, R. J., and Bosshardt, D. D. (2018). Multinucleated giant cells: good guys or bad guys? *Tiss. Eng. B Rev.* 24, 53–65. doi: 10.1089/ten.teb.2017.0242

Moens, S., Goveia, J., Stapor, P. C., Cantelmo, A. R., and Carmeliet, P. (2014). The multifaceted activity of VEGF in angiogenesis – Implications for therapy responses. *Cytokine Growth Factor Rev.* 25, 473–482. doi: 10.1016/j.cytogfr.2014.07.009

Moore, W. R., Graves, S. E., and Bain, G. I. (2001). Synthetic bone graft substitutes. *ANZ J. Surg.* 71, 354–361. doi: 10.1046/j.1440-1622.2001.2128.x

Nguyen, D. H. K., Pham, V. T. H., Al Kobaisi, M., Bhadra, C., Orlowska, A., Ghanaati, S., et al. (2016). Adsorption of human plasma albumin and fibronectin onto nanostructured black silicon surfaces. *Langmuir* 32, 10744–10751. doi: 10.1021/acs.langmuir.6b02601

Rothamel, D., Schwarz, F., Sager, M., Herten, M., Sculean, A., and Becker, J. (2005). Biodegradation of differently cross-linked collagen membranes: an experimental study in the rat. *Clin. Oral Implants Res.* 16, 369–378. doi: 10.1111/j.1600-0501.2005.01108.x

Schlee, M., Ghanaati, S., Willershausen, I., Stimmlmayr, M., Sculean, A., and Sader, R. A. (2012). Bovine pericardium based non-cross linked collagen matrix for successful root coverage, a clinical study in human. *Head Face Med*. 8:6. doi: 10.1186/1746-160X-8-6

Wend, S., Kubesch, A., Orlowska, A., Al-Maawi, S., Zender, N., Dias, A., et al. (2017). Reduction of the relative centrifugal force influences cell number and growth factor release within injectable PRF-based matrices. *J. Mater. Sci. Mater. Med*. 28:188. doi: 10.1007/s10856-017-5992-6

Xia, Z., and Triffitt, J. T. (2006). A review on macrophage responses to biomaterials. *Biomed. Mater*. 1, R1–R9. doi: 10.1088/1748-6041/1/1/R01

Conflict of Interest Statement: The authors declare that the research was conducted in the absence of any commercial or financial relationships that could be construed as a potential conflict of interest.

frontiers in Bioengineering and Biotechnology

ORIGINAL RESEARCH
published: 20 August 2018
doi: 10.3389/fbioe.2018.00108

Immune Assisted Tissue Engineering via Incorporation of Macrophages in Cell-Laden Hydrogels Under Cytokine Stimulation

Julien Barthes[1,2†], *Camille Dollinger*[1†], *Celine B. Muller*[1], *Urmas Liivas*[3], *Agnes Dupret-Bories*[4], *Helena Knopf-Marques*[2,5] *and Nihal E. Vrana*[1,2*]

[1] PROTiP Medical, Strasbourg, France, [2] INSERM UMR 1121, Strasbourg, France, [3] Protobios LLC, Tallinn, Estonia, [4] Institut Claudius Regaud, Institut Universitaire du Cancer Toulouse-Oncopole, Toulouse, France, [5] Faculté de Chirurgie Dentaire, Université de Strasbourg, Strasbourg, France

OPEN ACCESS

Edited by:
May Griffith,
Université de Montréal, Canada

Reviewed by:
Monica Neagu,
Institutul National Victor Babes, Romania
Christopher Darrell McTiernan, University of Ottawa Heart Institute, Canada

***Correspondence:**
Nihal E. Vrana
e.vrana@protipmedical.com

[†] These authors have contributed equally to this work

Specialty section:
This article was submitted to Biomaterials, a section of the journal Frontiers in Bioengineering and Biotechnology

Received: *25 May 2018*
Accepted: *13 July 2018*
Published: *20 August 2018*

Citation:
Barthes J, Dollinger C, Muller CB, Liivas U, Dupret-Bories A, Knopf-Marques H and Vrana NE (2018) Immune Assisted Tissue Engineering via Incorporation of Macrophages in Cell-Laden Hydrogels Under Cytokine Stimulation. Front. Bioeng. Biotechnol. 6:108. doi: 10.3389/fbioe.2018.00108

The function of soft tissues is intricately linked to their connections with the other systems of the body such as circulation, nervous system, and immune system. The presence of resident macrophages in tissues provides a means to control tissue homeostasis and also a way to react to the physical/biological insults and tissue damage. Thus, incorporation of resident macrophage like phenotype-controlled macrophages in engineered tissues can improve their fidelity as model tissues and also improve their rate of integration and facilitate the resolution of inflammation for regenerative medicine applications. Herein, we demonstrate two potential ways to immunoassist the remodeling process of engineered soft tissues in three-dimensional (3-D) gelatin based hydrogels containing fibroblasts and/or endothelial cells: (i) with supplementation of interleukin-4 (IL-4) in the presence of macrophages and (ii) in tri-culture via naive monocytes or differentiated macrophages. The presence of IL-4 had a proliferative effect on fibroblasts, with a significant boosting effect on proliferation and cytokine secretion in the presence of differentiated macrophages with an upregulation of activin, interleukin-1 receptor antagonist (IL-1RA), tumor necrosis factor alpha (TNF-α), and interleukin-1 beta (IL-1β), creating a more stimulating microenvironment. The addition of IL-4 in endothelial cell/macrophage co-culture configuration improved the organization of the sprout-like structures, with a boost in proliferation at day 1 and with an upregulation of IL-6 and IL-1RA at the earliest stage in the presence of differentiated macrophages creating a favorable microenvironment for angiogenesis. In tri-culture conditions, the presence of monocytes or macrophages resulted in a denser tissue-like structure with highly remodeled hydrogels. The presence of differentiated macrophages had a boosting effect on the angiogenic secretory microenvironment, such as IL-6 and IL-8, without any additional cytokine supplementation. The presence of fibroblasts in combination with endothelial cells also had a significant effect on the secretion of angiopoietin.

Our results demonstrate that incorporation of macrophages in a resident macrophage function and their phenotype control have significant effects on the maturation and cytokine microenvironment of 3-D multiple cell type-laden hydrogels, which can be harnessed for better integration of implantable systems and for more physiologically relevant *in vitro* tissue models with an immune component.

Keywords: macrophage, encapsulation, hydrogels, tissue engineering, cytokines, co-culture

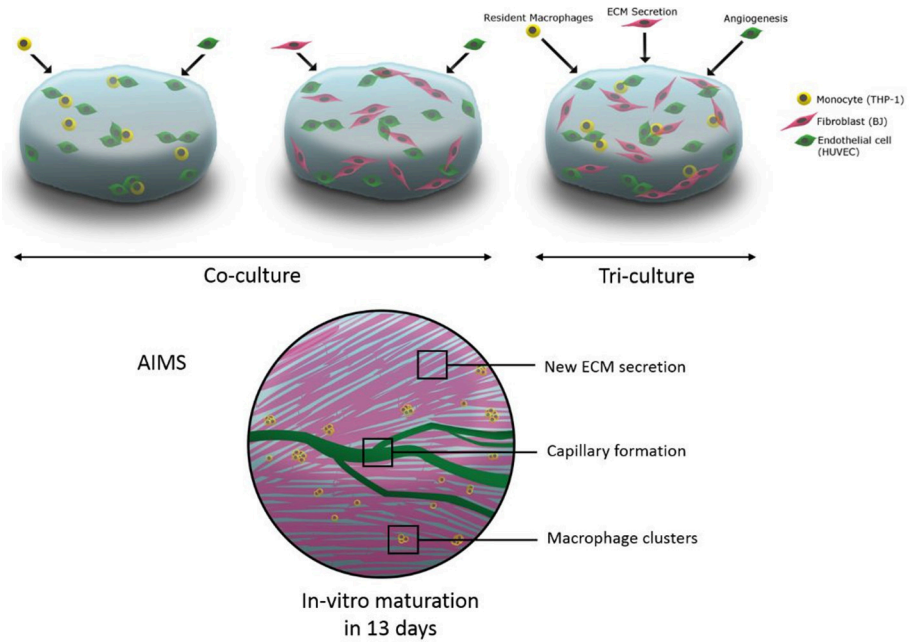

Graphical Abstract | The schematic representation of utilisation of tri-culture systems including macrophages in hydrogels for immune assisted tissue engineering.

INTRODUCTION

Macrophages possess an important role in regulating multiple tissue repair processes because of their direct relation to all stages of tissue healing through their phenotypic plasticity (Spiller and Koh, 2017). Thus, for regenerative medicine and tissue engineering applications, harnessing the pro-healing properties of macrophages has a strong potential for facilitated *in vitro* tissue maturation or improved *in vivo* integration and vascularization.

In a multifactorial n-dimension polarization space, the macrophage polarization has been generally described in a simplified spectrum of M1 (pro-inflammatory) and M2 (anti-inflammatory) macrophages with subgroups (M2a, M2c, etc.) (Mantovani et al., 2005). A recent study on the gene expression and protein secretion profiles of different macrophage phenotypes for angiogenesis *in vitro* has shown that all phenotypes support angiogenesis in different ways. M1 and M2c induced endothelial cell sprouting, whereas M2a macrophages promoted anastomosis (Spiller et al., 2014). In tissue repair, the chronological appearance of M1 and M2 macrophage phenotypes correspond to inflammation or initiation of healing process and stabilization and tissue maturation, respectively (Porcheray et al., 2005; Rostam et al., 2016; Cha et al., 2017). A recent co-culture study with a three-dimensional (3-D) polyethylene glycol (PEG)-based system has shown the influence of macrophages on angiogenesis and vasculogenesis. The macrophages were capable of influencing vessel formation within this system. Furthermore, macrophages can also enhance tubule formation by altering the morphology of endothelial cells and by associating with them in a bridging and pericyte-like manner (Moore et al., 2017).

In regard to wound healing and regeneration, harnessing the host macrophages to enhance the differentiation of delivered cells has become a good strategy for regenerative medicine. Niu et al. (2017) recently designed a new acetyl *Bletilla striata* polysaccharide (acBSP) polymer coating, which was able to promote the activation of tissue macrophages at the host-scaffold interface to secrete pro-regenerative cytokines that can enhance the osteogenesis of the mesenchymal stem cells inside the scaffold (Niu et al., 2017).

Macrophage polarization is a strong component in many biological events such as bacterial clearance, wound healing, tumor development, and foreign body response. The phenotypic

plasticity of macrophages and their fast reversion between different polarization states enable them to react to adverse events in a timely and effective manner. One of the most common inducers of M2 differentiation is interleukin-4 (IL-4) stimulation (Martinez et al., 2009). A product of T-cells and mast cells, IL-4, has been shown to induce M2 related cellular behavior *in vitro* [high CD206 expression, low levels of tumor necrosis factor alpha (TNF-α), IL-1 beta (IL-1β) release with high levels of IL-1 receptor antagonist (IL-1RA), and chemokine (C-C motif) ligand 18 (CCL18) release] (Martinez-Santibañez and Lumeng, 2014). Moreover, IL-4 is known to induce collagen secretion by fibroblasts (Fertin et al., 1991) and has been shown to induce angiogenesis by upregulating vascular cell adhesion molecule-1 (VCAM-1) expression *in vitro* (Fukushi et al., 2000). Even though IL-4 is not a cytokine produced by macrophages, it has been recognized as one of the main inducers of M2 macrophage polarization. Beyond its role in M2 macrophage polarization, IL-4 has also been known to induce collagen secretion by fibroblasts and angiogenesis, which makes it a good candidate to develop immunoassisted engineered tissues. In fact, this cytokine has an effect on the three relevant cell types that are used to develop immunoassisted tissues: immune cells (monocytes and macrophages), fibroblasts, and endothelial cells. Nevertheless, this effect needs to be tightly controlled as IL-4 is also active in fibrosis, tumor formation via tumor-associated macrophages, and also in atherosclerosis. Thus, it is important to provide such potent cytokines in a proper 3-D extracellular matrix (ECM) microenvironment. One potential way of harnessing IL-4 stimulated macrophage activity is their direct incorporation into 3-D hydrogel structures for a given tissue (Vrana, 2016).

Over the last few years, the demand for the development of new strategies for the repair of diseased and damaged tissues has increased (Brodbeck et al., 2002; Anderson et al., 2008; Brown and Badylak, 2013). One potential way is the delivery of cells to the damaged tissue, which involves cell encapsulation in biopolymer gels such as alginate, collagen, fibrin, hyaluronic acid, and gelatin, which are described as promising materials for tissue engineering of cartilage, bone, ligament, tendon, skin, and blood vessels in the presence of growth factors and cytokines (Hunt and Grover, 2010). In particular, gelatin which is formed from hydrolysis of collagen is widely used in medical applications because of its biodegradable nature (Ikada and Tabata, 1996; Tabata and Ikada, 1998; Miyoshi et al., 2005). However, gelatin is soluble in aqueous solution at 37°C and for biomedical applications it must be crosslinked to improve the mechanical and thermal stability. The crosslinking can be done by chemical crosslinkers [glutaraldehyde (Bigi et al., 2001), 1-ethyl-3-(3-dimethylaminopropyl)-carbodiimide/N-hydroxysuccinimide (EDC/NHS) (Liang et al., 2004), or genipin (Bigi et al., 2002)], photocrosslinking [methacrylated gelatin by UV irradiation (Nichol et al., 2010)], or by enzymatically catalyzed reactions [transglutaminase (TGA) (De Carvalho and Grosso, 2004; McDermott et al., 2004) or tyrosinase (Jus et al., 2012)]. Studies conducted with endothelial cells demonstrated that, once they were encapsulated in gelatin methacryloyl (GelMA) hydrogels, the cells readily bind to, proliferate, elongate, and migrate in the matrix (Nichol et al., 2010). These results revealed that gelatin based materials, such as GelMA, act as an attractive material for creating cell-laden microtissues (Ngo and Harley, 2017; Prakash Parthiban et al., 2017). Among the different crosslinking methods discussed, using TGA crosslinking reaction has the most advantages because of the absence of toxic components, such as crosslinking agents or photoinitiators. Transglutaminase catalyzes the formation of amide crosslink between carboxamide (RCONH2) from glutamine and primary amine functionalities from lysine (Orban et al., 2004).

Vascularization of the engineered constructs with the creation of functional blood vessels is one of the key parameters of tissue engineering and regenerative medicine. Blood vessels provide nutrients, oxygen, and also eliminate the waste, which are crucial for tissue maturation (Jain et al., 2005). It has been shown that an engineered tissue construct without vascularization is limited to about 100–200 μm thickness, and this is the reason why a vascularization strategy must be considered with all thick engineered tissues. Different strategies have been envisioned to vascularize tissue constructs, such as introduction of cellular components (endothelial cells as main components), to assist the remodeling of tissues necessary for the creation of blood vessels or introduction of channels in the scaffold using, for example, 3-D printing techniques with sacrificial network which will accelerate blood vessel formation (Kolesky et al., 2016). In all these strategies, one of the main components is the cellular component, and to achieve fully functional vascular network many cell types present in soft tissues are required. This necessitates a co-culture system and the study of interactions between all these cells is necessary to better understand this process. Moreover, the major limitation with all these strategies is the time required to achieve the vascularization. To solve this problem, the introduction of immune components in the construct, such as macrophages, could harness the inflammation and promote the healing process with a faster vascularization, even for thick engineered tissue constructs (Spiller et al., 2014; Tattersall et al., 2016; Moore et al., 2017).

Recently, we have demonstrated the effect of encapsulated macrophages on incoming cells in an *in vitro* model, where the cytokine microenvironment had a significant effect on cell behavior and subsequent cytokine secretion profiles (Dollinger et al., 2017). However, the co-encapsulation of naive or activated macrophages in a 3-D environment with connective tissue cells has not been widely studied. Some recent work, demonstrating the ability of macrophages to take part in a pericyte-like manner for capillary sprouting *in vitro* (Moore et al., 2017), suggests that such an approach can be potentially beneficial for tissue maturation in regenerative medicine applications.

Our aim is to incorporate inflammation related signals into the engineered tissues in the form of different cell types co-encapsulated in hydrogels with the presence of cytokines (IL-4, selected to induce a resident macrophage like phenotype) and monocytes and macrophages (to contribute to the remodeling and an artificial homeostasis in the hydrogel via paracrine and cell-cell contact effects). As a proof of concept, the effects of immune cell inclusion and IL-4 presence were tested in a model containing a connective tissue cell type (fibroblasts) and vascular endothelial cells for potential vascularization in

gelatin hydrogels crosslinked with TGA. In a previous study, co-culture and tri-culture experiments have been performed with primary osteoblasts, endothelial cells, and THP-1 derived macrophages using a ratio of 1/10 (macrophages/osteoblasts) and 1/6 (macrophages/endothelial cells); in order to get sufficient number of macrophages to remodel our cell-laden hydrogel, we have decided to perform all our experiments using a single ratio of 1/6 (fibroblasts or endothelial cells/macrophages) (Dohle et al., 2014).

MATERIALS AND METHODS

Materials

Gelatin type A from porcine skin (Mw = 5–10 × 10^4 Da, G-1890) was purchased from Sigma-Aldrich (Saint-Quentin-Fallavier, France). Interleukin-4 (recombinant human interleukin-4, *E. coli*-derived, C-61421), human umbilical vein endothelial cells (HUVEC) (Promocell® C-12200), endothelial cell growth medium (C-22010), apoptotic/necrotic/healthy cells detection kit (PK-CA707-30018), fluorimetric cell viability kit I (Resazurin, PK-CA707-30025-1), and 4′,6-diamidino-2-phenylindole (DAPI) (PK-CA707-40009) were purchased from Promocell (Heidelberg, Germany). Human monocytic cell line (THP-1, ATCC® TIB-202) and human fibroblast cells (BJ2, ATCC® CRL-2522) were purchased from ATCC (Manassas, US) in frozen form. RPMI-1640 and DMEM media, Dulbecco's phosphate buffered saline (DPBS), fetal bovine serum (FBS), 0.05% trypsin/0.02% EDTA, TripLE™ Express (1x), β-mercaptoethanol, Cell tracker™ (C-2925), and Vybrant cell adhesion assay kit (V-13181) were obtained from Life Technologies (Carlsbad, USA). Microbial TGA (Mw = 3.8 × 10^4 Da) was kindly provided by Ajinomoto Inc. (Tokyo, Japan).

Methods

Cell Lines

The THP-1 cells were cultured in RPMI 1640 GlutaMAX supplemented with 10% FBS, 1% penicillin/streptomycin, 0.2% fungizone, and 0.05 mM 2-mercaptoethanol. To differentiate from monocytes to macrophages, cells were treated with 50 ng of phorbol myristate acetate (PMA), dissolved in medium (RPMI 1640 without 2-mercaptoethanol), for 24 h at 37°C and 5% CO_2. Unattached cells were removed after washing with DPBS. Phorbol myristate acetate activated THP-1 cells were detached using TripLE ™ Express (1x), centrifuged, and resuspended in medium (without 2-mercaptoethanol).

The BJ2 cells were cultured in RPMI 1640 (Gibco Life Technologies, USA) supplemented with 10% FBS, 1% penicillin/streptomycin, 0.2% fungizone at 37°C in a 5% CO_2 atmosphere. Prior to seeding, cells were harvested using 0.05% trypsin/0.02% EDTA, centrifuged, and resuspended in medium.

Human umbilical vein endothelial cells were used from passages between 4 and 8. The culture media used were endothelial cell growth medium supplemented with Supplement Mix C-39215 (mainly composed of heparin, hydrocortisone, fetal calf serum, basic fibroblast growth factor, epithelial growth factor, and endothelial cell growth supplement) and 1% penicillin/streptomycin. Prior to seeding, cells were harvested using 0.05% trypsin/0.02% EDTA, centrifuged, and resuspended in medium.

Cell Encapsulation in Gelatin Hydrogel

For the encapsulation experiments, the gelatin solution was prepared in a 6% w/v gelatin type A/ MilliQ water at 37°C until complete dissolution; microbial TGA solution was prepared in a 20% w/v in PBS. The cell encapsulation was done with different cell types: monocytes (naive THP-1), human fibroblasts (BJ2), HUVECs, and macrophages (activated THP-1) cells. The cells were encapsulated in gelatin solution with a concentration of 1 × 10^6 cells mL^{-1} for naive and activated THP-1 and 6 × 10^6 cells mL^{-1} for HUVEC and fibroblasts cells. A 50 μL aliquot of cells encapsulated in gelatin solution was mixed with 10 μL TGA solution to get homogeneous crosslinking effect, and the hydrogel was then kept in incubator at 37°C for at least 15 min.

For the conditions with IL-4 supplementation, supernatant was supplemented with 10 ng mL^{-1} IL-4 each time the medium was changed (days 3, 7, and 10). The concentration of IL-4 (10 ng mL^{-1}) was chosen according to our previous study, where macrophages were successfully polarized into M2 phenotype using this concentration (Riabov et al., 2017).

The experiments were done with encapsulated cells in gelatin hydrogel under different conditions, as shown in **Scheme 1**:

(I) *In EMEM medium (supplemented with 10% FBS) with or without IL-4 (10 ng mL^{-1}):* Fibroblasts alone, **BJ2** (**Scheme Ia**); Fibroblasts alone + IL-4 supplementation, **BJ2 + IL-4** (**Scheme Ib**); Fibroblasts + Monocytes, **BJ2 + Monocytes** (**Scheme Ic**); Fibroblasts + Monocytes + IL-4 supplementation, **BJ2 + Monocytes + IL-4** (**Scheme Id**); Fibroblasts + Macrophages, **BJ2 + Macrophages** (**Scheme Ie**); Fibroblasts + Macrophages, **BJ2 + Macrophages + IL-4** (**Scheme If**).

(II) *In ECG medium (supplemented with endothelial supplement mix) with or without IL-4 (10 ng mL^{-1}):* Endothelial cells alone, **HUVECs** (**Scheme IIa**); Endothelial cells alone + IL-4 supplementation, **HUVECs + IL-4** (**Scheme IIb**); Endothelial cells + Monocytes, **HUVECs + Monocytes** (**Scheme IIc**); Endothelial cells + Monocytes + IL-4 supplementation, **HUVECs + Monocytes + IL-4** (**Scheme IId**); Endothelial cells + Macrophages, **HUVECs + Macrophages** (**Scheme IIe**); and Endothelial cells + Macrophages, **HUVECs + Macrophages + IL-4** (**Scheme IIf**).

(III) *In ECG medium (supplemented with endothelial supplement mix + 10% FBS):* Fibroblasts + Endothelial cells, **BJ2 + HUVECs** (**Scheme IIIa**); Fibroblasts + Endothelial cells + Monocytes, **BJ2 + HUVECs + Monocytes** (**Scheme IIIb**); Fibroblasts + Endothelial cells + Monocytes, **BJ2 + HUVECs + Macrophages** (**Scheme IIIc**).

Metabolic Activity

To assess metabolic activity, samples were incubated with 10% v/v Resazurin (Fluorometric cell viability kit I, PromoKine, Germany) in cell culture medium for 2 h. The substrate becomes

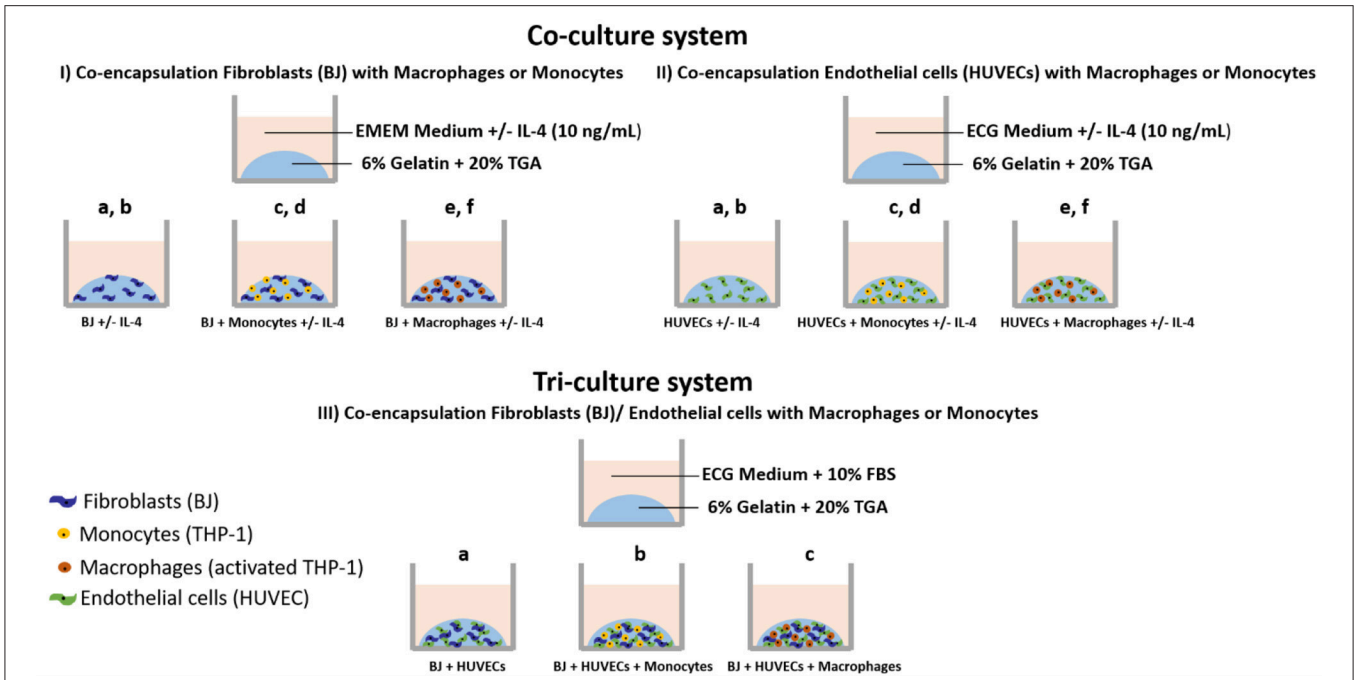

SCHEME 1 | Cell encapsulation conditions. **(I)** Co-culture experiments with fibroblasts: **(Ia)** Fibroblasts alone **(BJ2)**; **(Ib)** Fibroblasts alone + IL-4 supplementation **(BJ2 + IL-4)**; **(Ic)** Fibroblasts + Monocytes **(BJ2 + Monocytes)**; **(Id)** Fibroblasts + Monocytes + IL-4 supplementation **(BJ2 + Monocytes + IL-4)**; **(Ie)** Fibroblasts + Macrophages **(BJ2 + Macrophages)**; and **(If)** Fibroblasts + Macrophages + IL-4 supplementation **(BJ2 + Macrophages + IL-4)**. **(II)** Co-culture experiments with endothelial cells: **(IIa)** Endothelial cells alone **(HUVECs)**; **(IIb)** Endothelial cells alone + IL-4 supplementation **(HUVECs + IL-4)**; **(IIc)** Endothelial cells + Monocytes **(HUVECs + Monocytes)**; **(IId)** Endothelial cells + Monocytes + IL-4 supplementation **(HUVECs + Monocytes + IL-4)**; **(IIe)** Endothelial cells + Macrophages **(HUVECs + Macrophages)**; and **(IIf)** Endothelial cells + Macrophages + IL-4 supplementation **(HUVECs + Macrophages + IL-4)**. **(III)** Tri-culture experiments: **(IIIa)** Fibroblasts + Endothelial cells **(BJ + HUVECs)**; **(IIIb)** Fibroblasts + Endothelial cells + Monocytes **(BJ2 + HUVECs + Monocytes)**; and **(IIIc)** Fibroblasts + Endothelial cells + Macrophages **(BJ2 + HUVECs + Macrophages)**.

fluorescent (red) when incubated with viable cells due to reduction. The amount of fluorescence was monitored with a SAFAS Xenius XML fluorescence reader (SAFAS, Monaco) at excitation wavelength of 560 nm and emission wavelength of 590 nm [in AU (Arbitrary Unit)].

Cytokine Detection by ELISA

Cell culture media were collected at days 1, 3, 6, 10, and 13 and the cytokine amounts in the media were quantified by ELISA developer kits. Absorbance measurements were done at 450 nm. The cytokine amounts were calculated using the standard curves. Optical density (OD) cutoff is set as the OD value for standard concentration of 0 ng mL^{-1}. The following cytokines were quantified: transforming growth factor beta (TGF-β), activin, hepatocyte growth factor (HGF), platelet-derived growth factor (PDGF), angiopoietin 1, IL-4, IL-6, IL-8, IL-1β, TNF-α, IL-1RA. The references for all ELISA tests performed are presented here: TGF-β (R&D Systems DY240); activin (R&D Systems DY338); HGF (R&D Systems DY294); PDGF (PeproTech 900-K04); angiopoietin 1 (R&D Systems DY923); IL-6 (PeproTech 900 K-16); IL-8 (R&D Systems DY208); IL-1β (Capture: Antobody Solutions AS56-P, Standard protein: PeproTech 200-01B, Detection-Antibody Solutions AS57-B); TNF-α (R&D Systems DY394); and IL-1RA (PeproTech 900-K474).

TABLE 1 | Quantification of cytokines by ELISA tests as a function of the cell culture condition.

Conditions	Quantified cytokines	
BJ2 +/- IL-4	TGF-β	
BJ2 + Monocytes +/- IL-4	Activin	IL-1β
BJ2 + Macrophages +/- IL-4		TNF- α
		IL-1RA
HUVECs + IL-4	HGF	
HUVECs + Macrophage +/- IL-4	IL-6	IL-1β
HUVECs + Monocytes +/-IL-4	PDGF	TNF- α
		IL-1RA
HUVECs + BJ2	HGF	
HUVECs + BJ2 + Monocytes	Activin	IL-1β
HUVEC + BJ2 + Macrophages	Angiopoietin 1	TNF-α
		IL-1RA
	IL-6	
	IL-8	

The cytokines were quantified as a function of the cell culture condition, as shown in **Table 1**.

Cell Pre-labeling With Calcein

For co-culture experiments fibroblasts, HUVECs, and THP-1 cells were pre-labeled with calcein before the encapsulation in gelatin. Fibroblasts and HUVECs were stained with green calcein

(Vybrant Cell Adhesion Assay Kit (V-13181), ThermoFisher Scientific), whereas THP-1 cells were stained with red-orange calcein [CellTrace™ Calcein Red-Orange, AM (C34851) ThermoFisher Scientific].

The fluorescent indicators, green and red calcein, were prepared as 1 mM stock in DMSO and stored at −20°C until use. Cells were centrifuged to get cell pellet and were resuspended in staining solution. Cells were labeled at a concentration of 1×10^6 cells mL^{-1} and a dye concentration of 5 μM (in serum free medium) of calcein for 30 min at 37°C in the dark and subsequently washed twice in PBS. Cells were resuspended in gelatin for encapsulation.

Cell Labeling With Vimentin/Phalloïdin/PECAM-1/DAPI

Before labeling, encapsulated cells were fixed with a 3.7% (v/v) solution of paraformaldehyde (PFA) in PBS for 15 min and then washed three times with PBS.

For morphological characterization of HUVECs, cells were then incubated in a Triton X solution (0.1% in PBS) for 5 min. Then two rinsing steps with PBS were performed, and the samples were incubated for 20 min with bovine serum albumin (BSA) solution (1% v/v) in PBS. After incubation with Triton X and BSA solution, samples were incubated for 90 min with primary antibody (0.938 mg mL^{-1}, mAb mouse anti-human, Thermo Scientific) against PECAM-1 (CD31, cell-cell contact related cell membrane protein) at a dilution of 1/150 in PBS. Then the samples were incubated for 30 min with secondary antibody (2 mg mL^{-1} Oregon green 488 conjugate, goat anti-mouse IgG, Thermo Scientific) at a dilution of 1/200 in PBS and two rinsing steps with PBS were performed.

F-actin filaments for fibroblasts, HUVECs, and THP-1 cells were labeled with phalloïdin. The samples were incubated for 1 h with phalloïdin (6.6 μM Alexa Fluor 568 phalloïdin, Molecular Probes Life Technologies) at a dilution of 1/40 in BSA solution (1% v/v in PBS) and two rinsing steps in PBS were performed.

After treatment with a blocking solution (10% goat serum) for 20 min, fibroblast cells were stained with primary anti-vimentin (Vimentin V9, mouse IgG1, Santa Cruz) for 1 h at a dilution of 1/100 in 5% goat serum solution. The samples were rinsed three times for 5 min with PBS and treated with the appropriate fluorophore-conjugated secondary antibodies (goat anti-mouse, Oregon Green) for 1 h at a dilution of 1/200 in 5% goat serum solution.

Finally, at the end of each staining, the samples were incubated for 5 min in DAPI (1 mg mL^{-1}, Promokine) at a dilution of 1/100 in PBS and two rinsing steps were performed.

Microscopy Characterization

Fluorescence images were captured using Nikon Eclipse Ti-S with a 10× PL Fluor (0.30 NA) objective equipped with Nikon Digital Camera (with NIS-Elements software) and processed with ImageJ. For 3-D images, the labeled cells were analyzed with confocal laser scanning microscope (Zeiss LSM 710, Germany). Excitation/emission wavelength for green calcein was 489/556 nm, 577/599 nm for red calcein, 578/600 nm for Alexa Fluor® 568 Phalloïdin, 489/556 nm for vimentin, and 358/461 nm for DAPI.

For scanning electron microscopy (SEM), the samples were fixed with 4% glutaraldehyde. The specimens were washed with DPBS, prior to a dehydration protocol using an alcohol series of increasing concentrations (70, 95, and 2× 100%), with incubation periods of 5 min each. Subsequently, samples were incubated in 100% ethanol/hexamethyldisilazane (HMDS) (1:1) for 5 min, then only in HMDS for 2× 5 min and were dried overnight. Samples were made to adhere onto titanium discs using a carbon tape and were coated with gold/palladium in a sputter coater. The samples were sputtered at 7.5 mA for 3 min under argon atmosphere. Analysis with SEM was performed with a Quanta 400 ESEM (FEI Company, Eindhoven, the Netherlands) at an accelerating voltage of 10 kV.

Histology

Before histological analysis, encapsulated cells were fixed with a 3.7% (v/v) solution of PFA in PBS for 15 min and then washed three times with PBS. Then, samples were embedded in paraffin and cut into sections of 4–5 μM and stained with hematoxylin and eosin (H&E). Slides were scanned with Hamamatsu Nanozoomer 2.0 HT Scanner.

Statistical Analysis

The statistical significance of the obtained data was assessed using the *t*-test, Kruskal–Wallis, Shapiro–Wilk, or Mann–Whitney tests ($n \geq 3$). The error bars were representative of standard deviation (SD). Differences at $p \geq 0.05$ were considered statistically insignificant.

RESULTS AND DISCUSSION

Co-encapsulation of Fibroblasts With Macrophages or Monocytes (Co-culture System)

We first studied the co-encapsulation of human fibroblasts (BJ2) with either monocytes (naive THP-1 cells) or macrophages (PMA activated THP-1 cell). The first step was to check if macrophages or monocytes were still persistent in the hydrogel after 13 days of experimentation. Different cell types were distinguished by pre-labeling BJ2 cells with green calcein and monocytes or macrophages with red calcein (**Figure 1A**) (Ratio of the cells were 6:1 BJ2/THP-1). In **Figure 1A**, we could observe that macrophages or monocytes were still persistent after 13 days of experimentation. Moreover, the number of remaining immune cells was higher in the case of BJ2/monocyte co-culture condition. This result can be explained by the fact that once activated with PMA macrophages can no longer proliferate. The presence of macrophages and monocytes had a boosting effect on the metabolic activity of the overall system (**Figure 1B**). At day 1, the metabolic activity was the same among all conditions (BJ2, BJ2 + Monocyte, and BJ2 + Macrophage), but after 3 days the increase in the metabolic activity became significant for BJ2 + Macrophage and after 6 days for BJ2 + Monocyte. These results indicate that the boosting effect on the proliferation cannot be

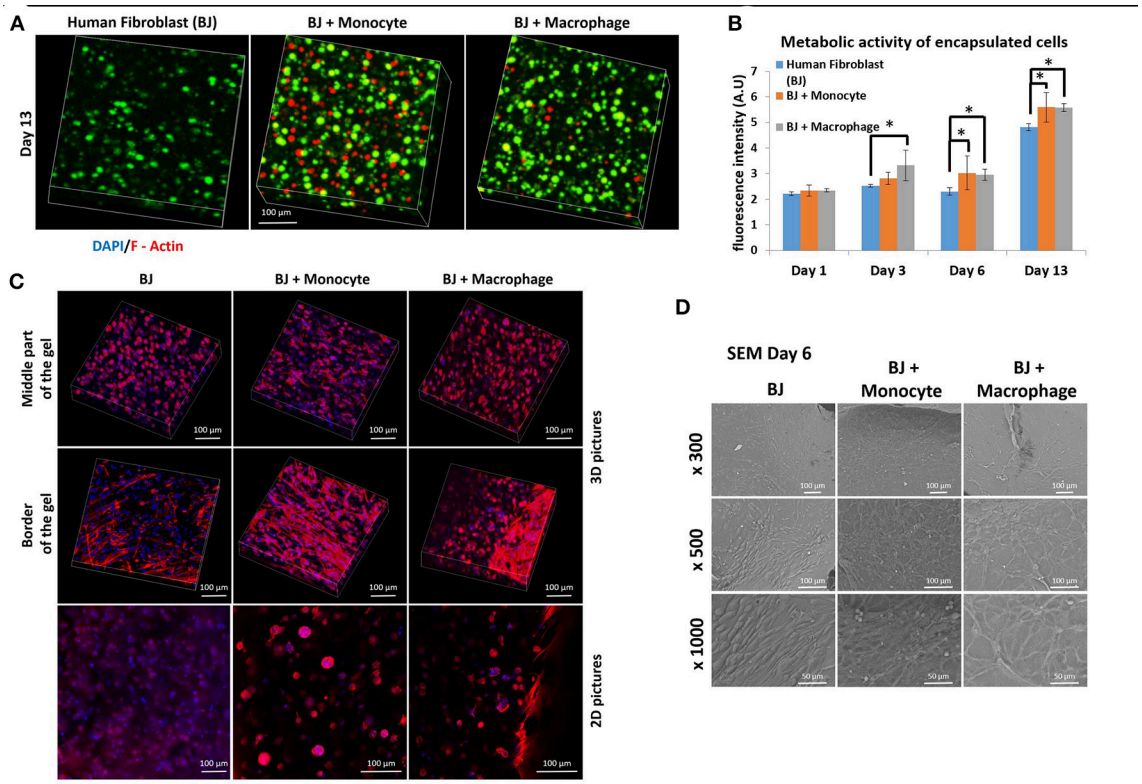

FIGURE 1 | Co-encapsulation of Human fibroblasts (BJ2) in gelatin hydrogel in co-culture condition with either monocyte or macrophage without IL-4 supplementation. **(A)** Confocal pictures of encapsulated cells labeled with green calcein (BJ2) or red calcein (monocyte or macrophage) after 13 days of experiment. **(B)** Follow up of metabolic activity of the different co-culture systems for 13 days ($n = 3$) (*$p < 0.05$). **(C)** Confocal pictures of DAPI/ Phalloidin (F-actin) stainings and **(D)** SEM pictures of the different co-culture systems after 6 days of experiment.

attributed to the higher number of cells present in the beginning of the experiment alone.

Cellular organization in the hydrogel was also checked by performing DAPI/F-Actin staining (**Figure 1C**). With confocal 3-D reconstructions, when we looked at the center of the hydrogel, we could see a different level of cellular organization between BJ2 alone and BJ2 + Macrophage or BJ2 + Monocyte. In the case of co-culture condition, we observed more spreading of the cells, whereas in BJ2 alone condition cells assumed a more spherical morphology. At the border of the gel, areas with extensive cellular organization were observed with co-culture conditions, especially in the condition with monocyte, indicating denser structure with well extended F-Actin filaments. This might indicate that the presence of macrophages enables faster outward movement of the cells from the hydrogels. In co-culture conditions, the presence of monocytes or macrophages resulted in the formation of clusters, which was not seen in conditions where BJ2 cells were encapsulated alone in the hydrogel.

In order to better characterize the interactions of cells with the surrounding hydrogel, SEM pictures were taken after 6 days of experimentation (**Figure 1D**). Extensive cellular coverage of cells with lamellipodia was apparent on both macrophage and monocyte systems, whereas in monocyte condition individual spherical monocytes were also seen. Moreover, in both monocyte and macrophage systems, zones with fibrillary components resembling ECM secretion were also observed on the SEM pictures. In the case of monocytes, spherical monocytes in contact with fibroblasts were clearly observed. The co-culture conditions increased cell-cell contact and resulted in denser web-like cellular clusters within and on top of the hydrogels.

The next step was to investigate the effect of IL-4 supplementation in the supernatant on the overall co-culture system. Supernatant was supplemented with 10 ng mL^{-1} IL-4 each time the medium was changed (day 3, 7, and 10). As previously explained, IL-4 was chosen to induce resident macrophage like phenotype and to promote tissue remodeling and inflammation resolution. For all the conditions, IL-4 supplementation seemed to have a boosting effect on the metabolic activity of the overall system. Without IL-4, the metabolic activity reached values around 6 AU, and with IL-4, we reached values around 12–13 AU (**Figure 2B**). The presence of macrophages had a significant effect on metabolic activity until day 6, whereas on day 13 in BJ2 alone condition with IL-4 supplementation the metabolic activity was significantly high when compared to no IL-4 conditions. This means that IL-4

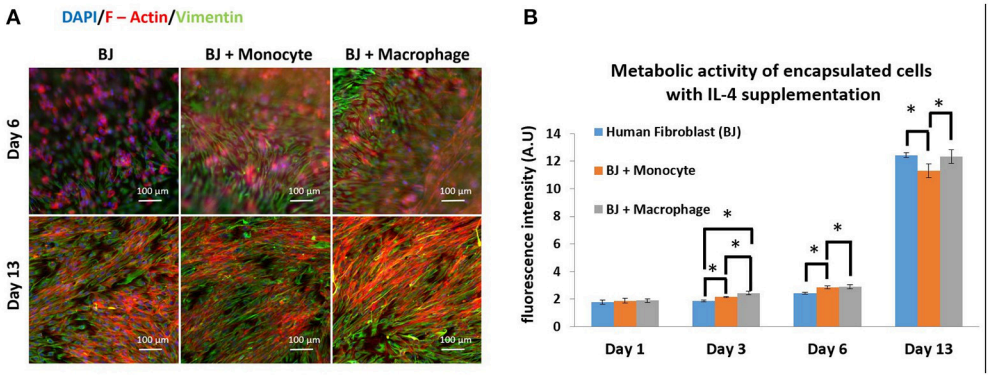

FIGURE 2 | Co-encapsulation of Human fibroblasts (BJ2) in gelatin hydrogel in co-culture condition with either monocyte or macrophage with IL-4 supplementation. **(A)** Pictures obtained with epifluorescence microscope of encapsulated cells stained with DAPI/Phalloidin (red)/Vimentin (green). **(B)** Follow up of metabolic activity of the different co-culture systems for 13 days ($n = 3$) (*$p < 0.05$).

has particularly induced fibroblast proliferation even without immune cells. Vimentin is an intermediate filament protein with important roles in cell integrity, migration, and stability. It has been shown that vimentin deficiency decreases the fibroblast's ability to migrate (Eckes et al., 1998). Moreover, it has been shown that during monocyte to macrophage differentiation there is an increase in vimentin expression (Benes et al., 2006). In order to observe the potential effect of IL-4 and monocyte/macrophage presence on vimentin expression, the system was immunostained with vimentin (**Figure 2A**). On day 6, a denser cellular body was apparent with both monocyte and macrophage containing conditions, where the staining is stronger for macrophage samples. By day 13, the difference in staining between monocytes and macrophages was less obvious with more overlap in actin filaments in the case of macrophage containing structures. High level of actin/vimentin co-localization has been observed with macrophages previously consistent with our observations (Correia et al., 1999). Moreover, the addition of IL-4 did not have an effect on the clusters (**Supplementary Figure 1**). With or without IL-4 supplementation, we can always observe the formation of clusters for co-culture conditions of BJ2 with monocyte or macrophage.

In all co-culture conditions, cytokine/growth factor analyses were done with three goals: (i) detection of the effect of created microenvironment on the secretion of cytokines/growth factors related to the function of the non-immune component, (ii) the presence and the stability of the supplemented cytokine (IL-4), and (iii) the effect of created microenvironment on the secretion of pro-/anti-inflammatory cytokines. As shown in **Figure 3**, the stability of the supplemented IL-4 was demonstrated with its quantification in the supernatant at different time points during the cell culture. The possible secretion of IL-4 from the different cell types could not be evaluated since this interleukin was also supplemented in the medium. In the case of fibroblasts, the most important effect is a significant boost of activin, IL1-β, TNF-α, and IL-1RA secretion at day 1 in the presence of activated macrophages and IL-4 (**Figure 3**). The presence of IL-4 resulted in an increase in secretion creating a cytokine enriched environment, regardless of the pro- or anti-inflammatory nature of the cytokines. Activin is a potent growth factor involved in proliferation of fibroblasts; the initial boost in activin expression at day 1 time point might also be related to the significant increase in IL-1β and TNF-α presence, which have been previously shown to induce activin secretion (Hübner and Werner, 1996). IL-1β and TNF-α are pro-inflammatory cytokines secreted by M1 macrophages, whereas IL-1 receptor antagonist is a M2 marker for cytokine stimulated macrophage polarization. However, the presence of 3-D proteinaceous microenvironment available to monocytes and macrophages under encapsulation conditions creates intermediate phenotypes that would be difficult to define in M1/M2 paradigm. Previously, in animal studies, it had been shown that the overexpression of IL-1β and TNF-α significantly increased collagen deposition and also fibronectin expression (Margetts et al., 2002). Prolonged expression of pro-inflammatory markers might have pathological outcomes (such as fibrosis), but an initial boost in cytokines in the context of *in vitro* tissue maturation can be highly beneficial for faster proliferation, ECM secretion, and organization of the cells within the artificial tissue.

The cytokine boosting effect in the presence of IL-4 and macrophage was seen with all the conditions, except TGF-β. For the three conditions (BJ2, BJ2 + Monocytes, and BJ2 + Macrophages) the production of TGF-β increases with cell culture time (from day 1 to 13). Previously a similar effect was demonstrated by Dardalhon et al. (2008) where the presence of IL-4 decreased TGF-β expression in T cells, which in turn resulted in inhibition of TGF-β induced T-reg cell differentiation (Dardalhon et al., 2008). In co-encapsulation conditions, the presence of IL-4 in medium has an important effect on downregulating the TGF-β production at day 6 for both conditions. This downregulation becomes significant at day 13 for all co-encapsulation conditions, even without IL-4 after 13 days of experimentation, so the presence of monocyte or macrophages seems to have an effect on TGF-β secretion.

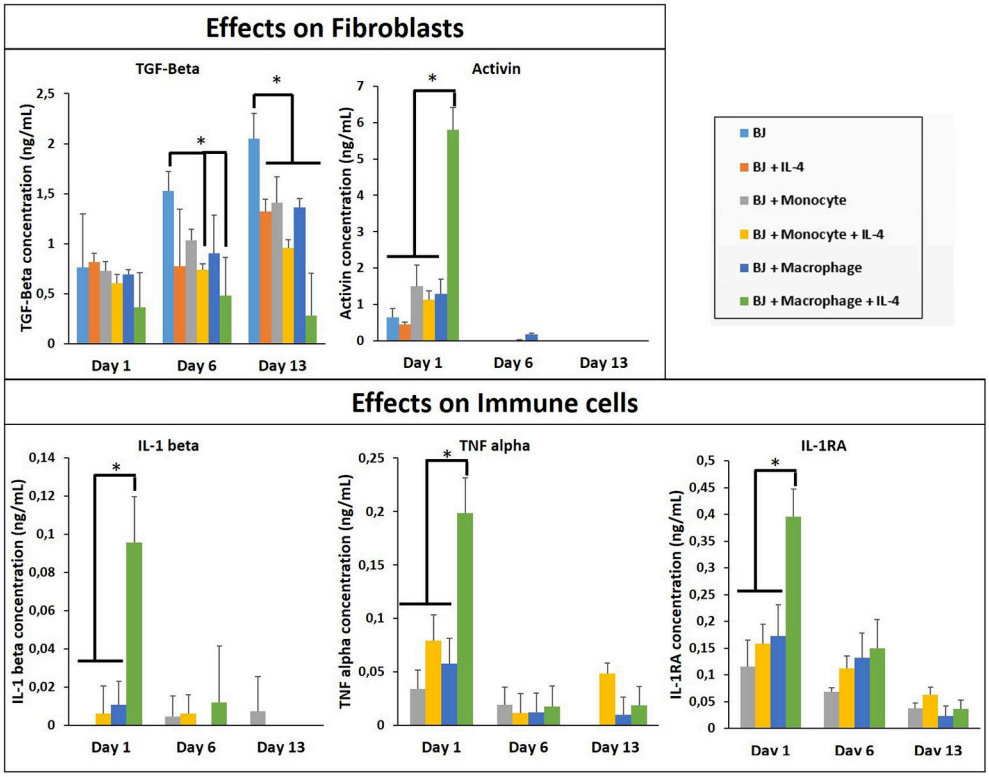

FIGURE 3 | Cytokine quantification (TGF-β, Activin, IL-1β, 1I-1R1, and TNF-α) in the supernatant at different time point for the co-culture experiments with and without IL-4 supplementation ($n = 3$) (*$p < 0.05$).

Co-encapsulation of Endothelial Cells/Macrophages or Monocytes (Co-culture System)

After the investigation of the effect of co-encapsulation of fibroblasts with immune cells (macrophages or monocytes), we have continued the monocyte/macrophage co-encapsulation with another cell type critical for tissue engineering and regenerative medicine, that is, vascular endothelial cells. For tissue regeneration, obtaining a mature vascular network is crucial to provide nutrient and evacuate waste, and we hypothesize that the presence of macrophages can aid in the formation of capillary networks in hydrogels, and thus the interaction of endothelial cells and immune cells in a co-encapsulation system has been studied. We have used the same protocol as previously described with fibroblasts. Cells were encapsulated in a gelatin hydrogel (6% w/v) at a density of six million HUVECs and one million monocytes or macrophages per mL of hydrogel. We have also checked if macrophages or monocytes were still persistent after 13 days of co-encapsulation experiment with HUVECs by using the same strategy to pre-label the cells with green calcein (HUVECs) and red calcein (macrophages or monocytes). In **Figure 4A**, we have shown that macrophages or monocytes were still persistent after 13 days of experimentation, with higher number of remaining monocytes when compared to macrophages for the same reasons explained previously (once activated, macrophages can no longer proliferate).

The metabolic activity of the system was also followed for 13 days (**Figure 4B**) and the effect was similar to the case of fibroblasts. The presence of macrophages and monocytes in the co-encapsulation system with HUVECs had a boosting effect on the metabolic activity of the overall system, which cannot be attributed to the higher number of cells at the beginning of the experiment alone since the metabolic activity of all conditions were equivalent at day 1. Our primary findings have shown that the addition of macrophage or monocyte in a co-encapsulation system with connective tissue cells such as fibroblasts or endothelial cells has a boosting effect on the proliferation of these cells. The effect cannot be attributed only to the proliferation of monocytes either, as there was no significant difference between the conditions with monocyte and macrophage (non-proliferative) co-encapsulation; both conditions had higher metabolic activity when compared to HUVECs alone condition.

We have performed DAPI/phalloïdin (F-actin) staining and observed the formation of large clusters after 6 days of experimentation for the condition HUVECs + Macrophages (**Supplementary Figure 2**). These clusters were still present after 13 days of experimentation. For the condition HUVECs + Monocytes, these clusters were much smaller and easier to observe after 13 days of culture. So there is a correlation

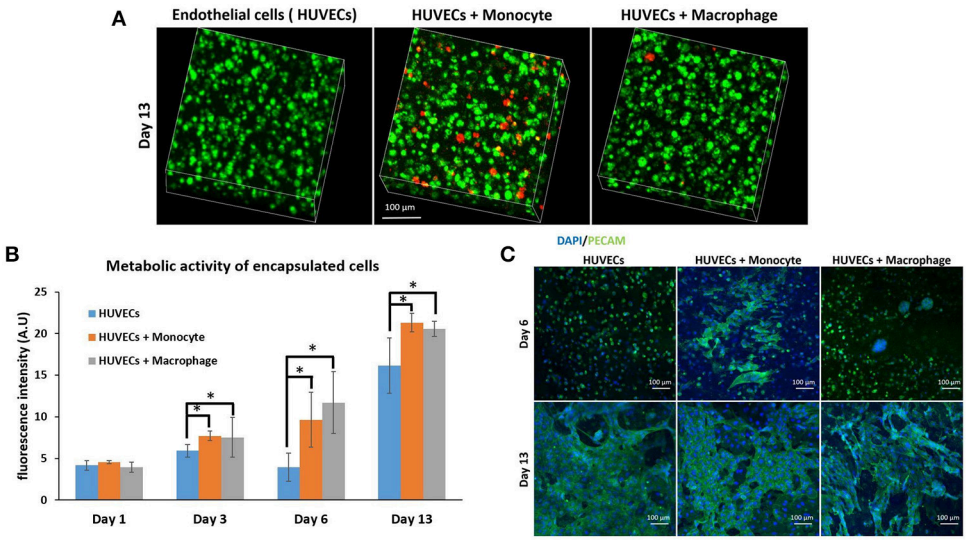

FIGURE 4 | Co-encapsulation of endothelial cells (HUVECs) in gelatin hydrogel in co-culture condition with either monocyte or macrophage without IL-4 supplementation. **(A)** Confocal pictures of encapsulated cells labeled with calcein green (HUVECs) or calcein red (monocyte or macrophage) after 13 days of experiment. **(B)** Follow up of metabolic activity of the different co-culture systems for 13 days ($n = 3$) (*$p < 0.05$). **(C)** Confocal pictures of DAPI/ PECAM stainings after 6 and 13 days of experiment.

between HUVECs and fibroblasts when co-encapsulated with macrophages or monocytes, which can be attributed to the behavior of monocytes/macrophages within the hydrogel. In both cases, we can see the formation of clusters which cannot be seen when fibroblasts or HUVECs are encapsulated alone in the hydrogel.

PECAM CD31 staining was also performed after 6 and 13 days of experimentation (**Figure 4C**) to check endothelial cell organization within the hydrogel. This a membrane protein found on the surface of an endothelial cell, which is a marker of endothelial intercellular junctions. It is a well-known endothelial marker that establishes at cell-cell junctions (Ford et al., 2006). PECAM is expressed at the earliest stage of angiogenesis and this is why its expression is relevant in tissue engineering (Pinter et al., 1999). After 6 days of culture, there was limited organization in the case of HUVECs alone and co-culture HUVECs + Macrophages, except for the presence of large clusters in the case of co-culture. For HUVECs + Monocytes condition after 6 days of experimentation, we could see increased PECAM staining indicating that the cells were more interconnected. After 13 days of culture, for all conditions, CD31 marker was well expressed and the cells were interconnected. With this experiment, we could conclude that the presence of monocyte seemed to have a positive effect on HUVEC organization at the early stage, since HUVECs expressed more cell-cell connections.

We have also investigated the effect of IL-4 supplementation in the supernatant on the overall co-culture system. Supernatant was supplemented with 10 ng mL^{-1} IL-4 each time the medium was changed. As presented in **Figure 5B**, IL-4 supplementation had a boosting effect on the metabolic activity of the overall system for all conditions, especially for the first day. Indeed, without IL-4 the metabolic activity reached values around 4–5 AU for all conditions on the first day, whereas with IL-4 the metabolic activity reached values around 15 AU. After that we could notice a small decrease at days 3 and 6, and then the metabolic activity increased again to reach values around 16–17 AU for all conditions. The analysis of metabolic activity of the overall co-encapsulation system with endothelial cells have shown that IL-4 induced the proliferation of endothelial cells at the early stage, but then the proliferation seemed to stop and most probably in the benefit of cell organization in this 3-D microenvironment.

Moreover, DAPI/phalloïdin staining performed at days 6 and 13 has also shown that the addition of IL-4 did not have an effect in the presence of clusters (**Supplementary Figure 3**). After 6 days, we were able to see larger clusters in the case of HUVECs + Macrophages when compared to HUVECs + Monocytes. Over time, it seemed that the clusters became even bigger for these two conditions.

PECAM CD31 staining was also performed to check the cellular organization in this hydrogel (**Figure 5A**). After 6 days of experimentation, we could see more organization for HUVECs alone in the hydrogel when compared to HUVEC alone samples without IL-4. For the two co-encapsulation conditions (HUVECs + Monocytes and HUVECs + Macrophages), the effect was more striking since we could observe that the HUVECs started to organize in a vessel-like structure with more sprouting. In the presence of monocytes/macrophages, the macroscopic organization resembled that of sprouting capillaries on day 6. After 13 days, most of the cells were interconnected and we could observe almost the same organization for all the conditions except for HUVECs + Macrophages where some tubular structures could be seen.

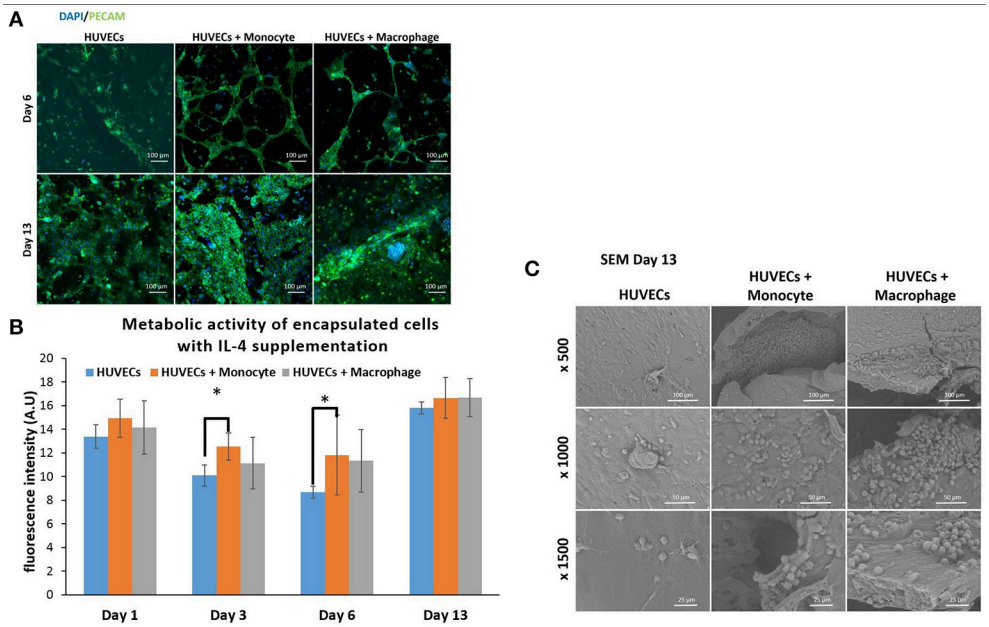

FIGURE 5 | Co-encapsulation of endothelial cells (HUVECs) in gelatin hydrogel in co-culture condition with either monocyte or macrophage with IL-4 supplementation. **(A)** Confocal pictures of DAPI/ PECAM stainings after 6 and 13 days of experiment. **(B)** Follow up of metabolic activity of the different co-culture systems for 13 days ($n = 3$) ($^*p < 0{,}05$). **(C)** SEM pictures of the different co-culture systems after 13 days of experiment.

With this experiment we have seen that even though IL-4 did not affect the presence of clusters, it seemed to have an effect on their size over time by promoting their growth. Moreover, in the presence of IL-4, we could see faster organization of HUVECs and higher intercellular junctions especially on the first day of the experiment. The positive effect of macrophages on angiogenesis have already been demonstrated with capillary sprouting assay using beads (Tattersall et al., 2016). In this study, it was shown that IL-4 stimulation resulted in less developed sprouts, but in our case, IL-4 stimulation triggered the sprouting of vessel in the earliest stage. The difference can be attributed to the change in cell microenvironment (3-D cell culture in degradable hydrogel) together with the proliferation boosting effect of IL-4. In the earliest stage, the proliferation of HUVECs under IL-4 stimulation was higher and as a consequence they were able to easily remodel the hydrogel to organize themselves into a vessel like structure.

In order to see the cell-cell interactions between monocytes/macrophages with HUVECs at higher magnifications, we carried out SEM. In the case of HUVECs only condition, connected layers of well-spread endothelial cells were visible with occasional cellular clusters (**Figure 5C**), and with the addition of monocytes and macrophages, the two cell populations could be distinguished as the well-spread endothelial cells interacting with spherical monocytes/macrophages (**Figure 5C**). The clusters which were also observed in confocal microscopy images seemed to be mostly formed from the immune component (**Figure 5C**).

In **Figure 6**, we first checked and demonstrated the stability of the supplemented IL-4 with its quantification in the supernatant at different time point during the cell culture. The possible secretion of IL-4 from the different cell types could not be evaluated since this IL was also supplemented in the medium. The presence of IL-4 resulted in a production boost of IL-6 and IL-1RA in the presence of macrophages in a similar manner as in the case of fibroblasts (**Figure 6**). However, in the presence of HUVECs the boosting effect was not observed for TNF-α, showing that the cytokine release profiles were culture condition dependent and could not be explained based on the effect of IL-4 and encapsulation conditions on monocytes and macrophages. In a similar vein, the upregulation of HGF was the most prominent for the case of HUVEC + Monocyte condition after 10 days of culture, with the difference being significant after day 10 and day 13. Hepatocyte growth factor is a potent growth factor active in angiogenesis and shown to be mostly effective on endothelial and epithelial cells. Previously, HGF has been shown to induce a regulatory phenotype for monocytes (Rutella et al., 2006), and thus the cross talk between HUVECs and monocytes seems to induce an increase in its secretion. It is possible to see that HGF was also released from HUVEC + Macrophage in presence of IL-4. In the case of PDGF, a growth factor which is implicated in cell proliferation and late stages of angiogenesis, there was a steady increase until day 13 for all culture conditions; but its highest expression was observed in HUVECs only conditions (**Figure 6**). This can be related to the fact that endothelial cells secrete PDGF for recruitment of pericytes for establishing the stability of the newly formed vessel structures (Saik et al., 2011); in the presence of monocytes and macrophages such a support component is readily available which can result in the downregulation of PDGF secretion,

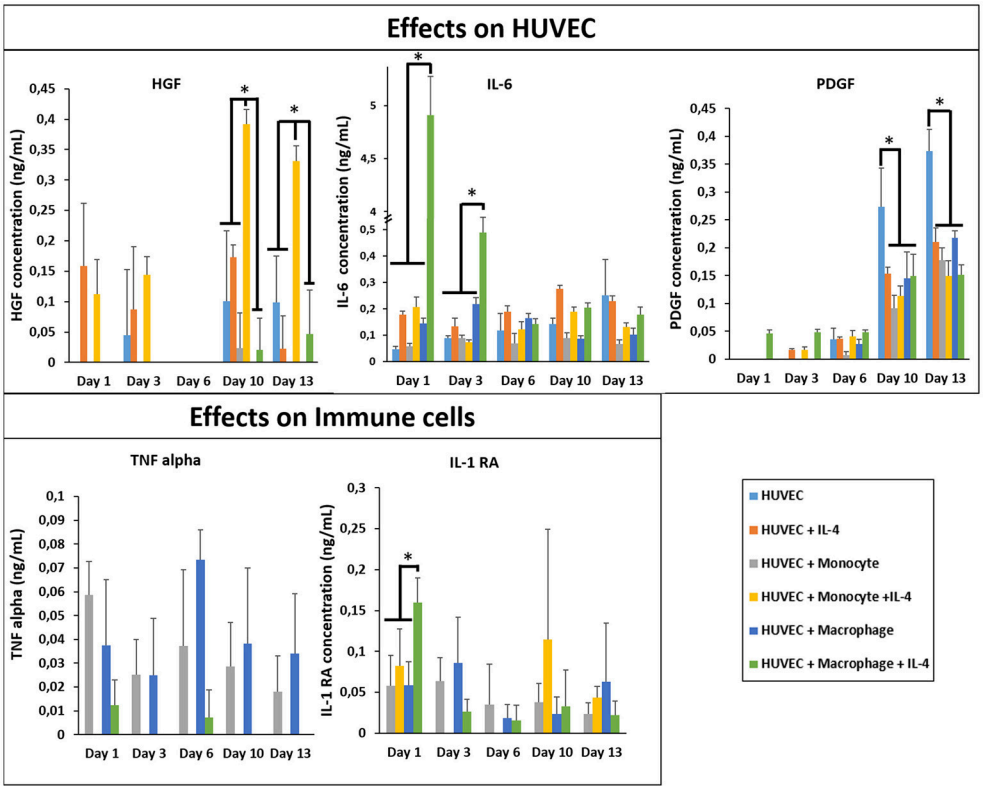

FIGURE 6 | Cytokine quantification (HGF, PDGF, IL-1RA, IL-6, and TNF-α) in the supernatant at different time point for the co-culture experiments with and without IL-4 supplementation ($n = 3$) (*$p < 0.05$).

whereas in the case of HUVECs only no such support is forthcoming so the secretion continues steadily as a function of increasing number of endothelial cells. The downregulation of PDGF in the case of IL-4 presence for HUVEC only conditions can be related to its induction by cell-cell contact proteins in HUVECs (Iademarco et al., 1995), which might have a negative feedback effect on recruitment via PDGF thus resulting in a decrease in secretion.

Co-encapsulation of Fibroblasts/Endothelial Cells/Macrophages or Monocytes (Tri-Culture System)

Finally, we studied the co-encapsulation of both fibroblasts and endothelial cells with monocytes or macrophages to recreate the *in vivo* microenvironment with immune and connective tissue cells. We checked the metabolic activity of the different systems (**Figure 7B**). The metabolic activity remained constant and at the same level for all conditions (BJ2 + HUVECs and BJ2 + HUVECs with monocytes or macrophages).

Moreover, the level was close to what we found for co-encapsulation of HUVECs with immune cells with IL-4 supplementation. In this configuration, we promoted cellular organization instead of proliferation without cytokine supplementation. In **Figure 7A**, we can see well defined intercellular junctions after 13 days of experimentation (PECAM staining), which was denser in the presence of macrophages or monocytes. The staining of F-actin filaments (**Figure 7A**) confirmed these findings by showing denser tissue-like structure after 13 days of experimentation in the presence of macrophages or monocytes. We could also see the presence of clusters for these two conditions. H&E staining was performed for all conditions to check cellular organization and tissue remodeling (**Figure 7C**). After 13 days of experimentation, we observed more cellular migration, especially more hydrogel degradation and remodeling in the presence of macrophages or monocytes. We were still able to observe the clusters.

The co-culture of fibroblasts and HUVECs tri-culture conditions resulted in more remodeled gel structures at higher magnification in SEM compared to other single or co-culture conditions. The fibroblast/HUVEC culture alone by day 6 resulted in more contracted hydrogel structures with pleated surface features by day 6, indicating contraction of the 3-D microenvironment by the activities of the encapsulated cells (**Figure 8A**). The monocytes and macrophages could be distinguished as separate spherical cells interacting with other cells by day 6. The difference with the previous conditions was more evident by day 13 as the hydrogel substrate has highly organized collagen-like structures, particularly in the case of macrophage containing tri-culture system (**Figure 8B**). Moreover, unlike previous cases, the clusters of macrophages

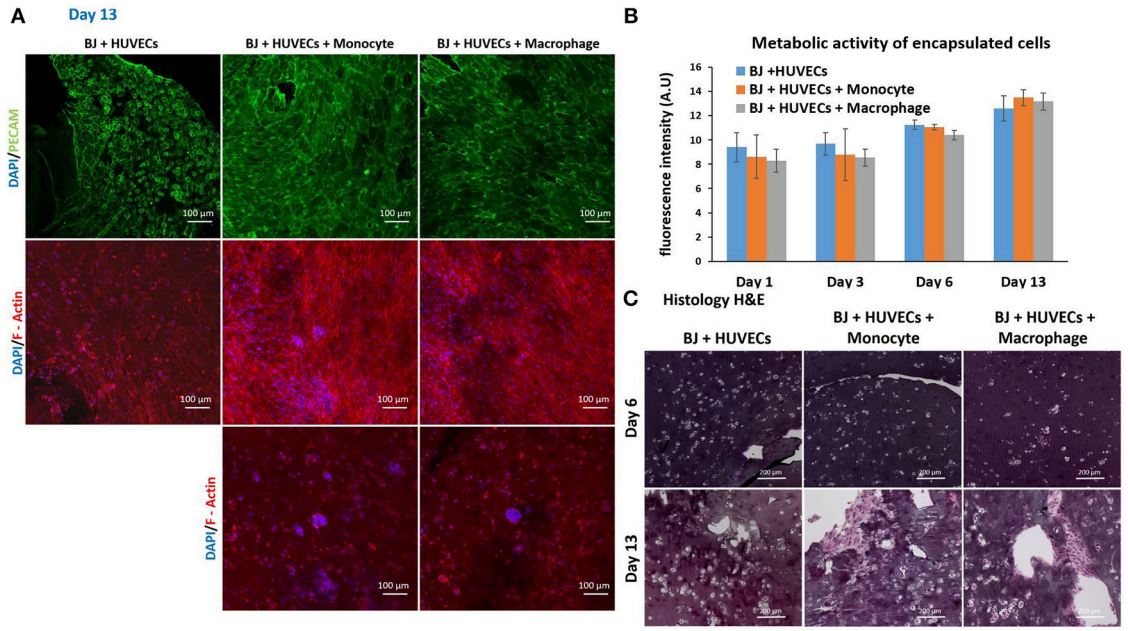

FIGURE 7 | Co-encapsulation of endothelial cells (HUVECs)/ Fibroblast (BJ2) in gelatin hydrogel in tri-culture condition with either monocytes or macrophages without IL-4 supplementation. **(A)** Confocal pictures of DAPI/PECAM/Phalloidin stainings after 13 days of experiment. **(B)** Follow up of metabolic activity of the different tri-culture systems for 13 days ($n = 3$). **(C)** Histology pictures (Hematoxylin/Eosin stainings) of the different co-culture systems after 6 and 13 days of experiment.

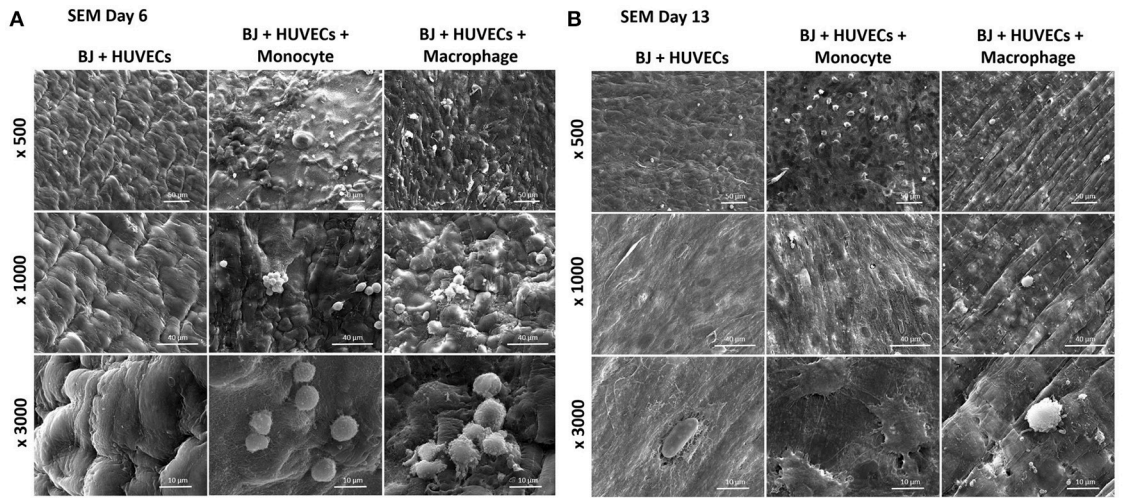

FIGURE 8 | Co-encapsulation of endothelial cells (HUVECs)/Fibroblast (BJ2) in gelatin hydrogel in tri-culture condition with either monocyte or macrophage without IL-4 supplementation. SEM pictures of the different co-culture systems after 6 **(A)** and 13 **(B)** days of experiment.

were less prominent at high magnifications and dense highly remodeled structures were observed (**Figure 8B**). Together with confocal microscopy images showing dense cellular layers, histology images showing higher hydrogel degradation, and cellular movement and SEM images showing highly organized ECM like structures with cellular components; it can be concluded that the presence of the monocytes and macrophages has a distinct synergistic effect on remodeling and integration of gelatin hydrogel based scaffolds.

In order to see the effect of tri-culture conditions on cytokine secretion, cytokine screening similar to that of co-culture conditions was carried out. The presence of macrophages resulted in a significant boost in the secretion of activin, IL-6, and IL-8, which are important in connective tissue cell proliferation and angiogenesis (**Figure 9**), previously obtained in a similar manner from co-culture conditions in the presence of IL-4 and macrophages. However, one additional advantage of tri-culture conditions was the longer period of the boost

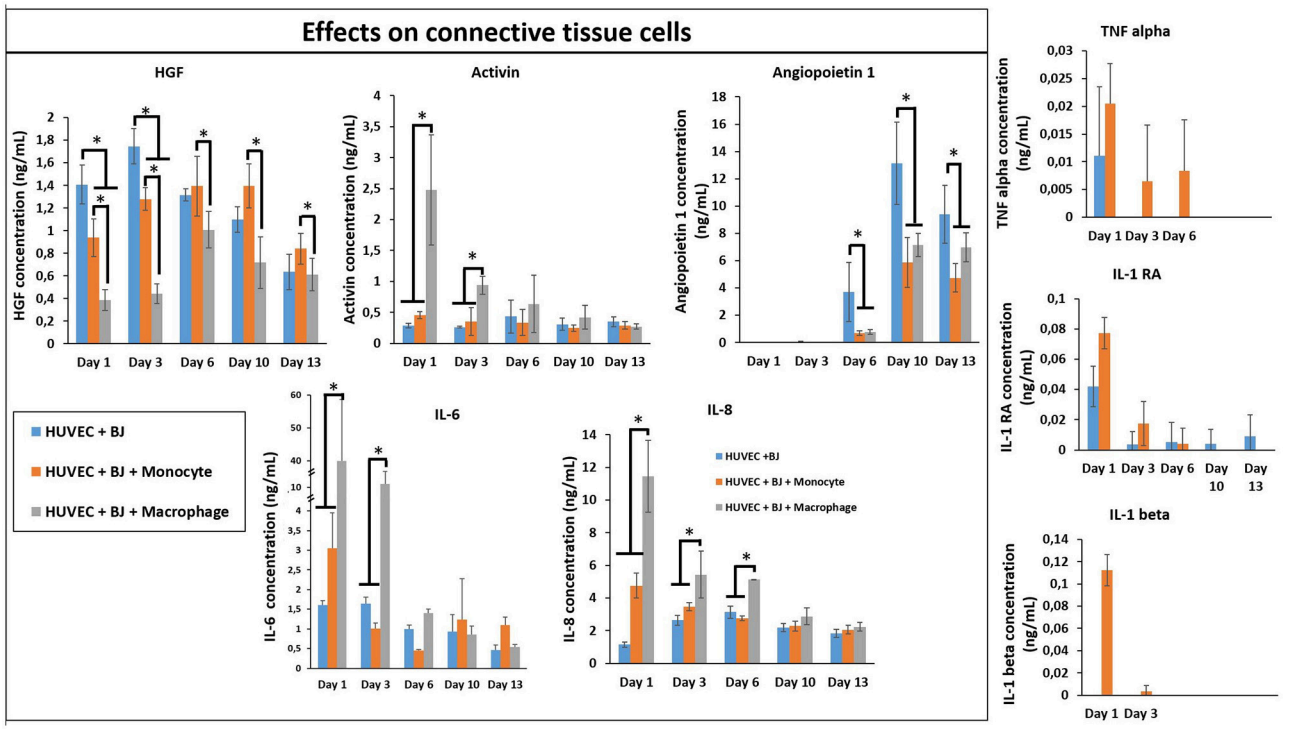

FIGURE 9 | Cytokine quantification (Angiopoetin-1, Activin, HGF, IL-1β, IL-1RA, IL-6, IL-8, and TNF-α) in the supernatant at different time point for the tri-culture experiments ($n = 3$) (*$p < 0.05$).

observed; in IL-4/macrophage case the boost was generally limited to the first day of culture, whereas in tri-culture conditions the effect was sustained at a significant level for at least 3 days (6 days for IL-6 and IL-8). Similar to the case of HUVEC/monocyte/macrophage encapsulation conditions (but in the presence of IL-4), HGF secretion was lower in the presence of macrophages. For the case of monocytes, it steadily increased and became significantly higher when compared to macrophage containing tri-culture conditions, suggesting that the presence of the fibroblasts provides additional cues resulting in effects similar to that of biochemical stimulation. Angiopoeitin-1, is one of the ligands of TIE receptors expressed by endothelial cells and macrophages and is highly implicated in angiogenesis (Fagiani and Christofori, 2013). Similar to PDGF, it is more active in the maturation and stability of blood vessels. The secretion of angiopoetin became detectable after day 6 for all conditions and significantly increased at day 10. For both timepoints the secretion was higher for HUVEC/fibroblast co-culture when compared to the monocyte/macrophage containing tri-cultures. This can be related to the presence of more cells with physical support potential in the capillaries formed. The presence of macrophages resulted in higher amount of both pro- and anti-inflammatory cytokine secretion for day 1 (TNF-α, IL-1β, and IL-1RA, respectively), with concentrations similar to that of previous co-culture conditions.

In our model, in the presence of fibroblasts there was a clear increase in the secretion of IL-1β, IL-1RA, and TNF-α between monocytes and differentiated macrophages. When only HUVEC component was present this effect was confounded; however in tri-culture conditions the secretion in the presence of macrophages increased several times, demonstrating the potential effect of macrophages on the biochemical microenvironment.

Previously, interactions between three cell types have been studied in other contexts, with synergistic and antagonistic effects. For example, a hydrogel-based 3-D culture system has been used by several groups in order to allow live cell retrieval to investigate the interaction between different cell types under co- or tri-culture configurations. One example is the research done by Rinker et al. (2014), in which the interactions between mesenchymal stem cells, adipocytes, and osteoblasts were studied in a 3-D tri-culture model of hyperglycemic conditions in the bone marrow microenvironment (Rinker et al., 2014). Another example of tri-culture in a hydrogel encapsulation system is the recent work described by Bray et al. (2017), in which a 3-D tri-culture model was developed for the *ex vivo* study of acute myeloid leukemia (Bray et al., 2017). As a hydrogel, they used the matrix metalloproteinase-sensitive hydrogels prepared from PEG and heparin, functionalized with adhesion ligands and pro-angiogenic factors, allowing for the analysis of acute myeloid leukemia development and response to treatment. Furthermore, endothelial cells and mesenchymal stromal cells were co-seeded to mimic the vascular niche for acute myeloid leukemia cells. However, these studies were more related to *in vitro* disease

models and not for harnessing its effects for potential therapeutic applications. In this work, we have chosen gelatin as an ECM based hydrogel that can be used in implantable configurations to encapsulate the co- and tri-culture system to better understand the signals of inflammation into the engineered tissues in the form of different cell types (HUVEC, fibroblasts, and macrophages) co-encapsulated in hydrogels with the presence of IL-4.

For the maturation of engineered tissue, cell-cell interactions, growth factors, and morphogens have been widely utilized. However, these maturations are generally done in the form of single culture systems without involving all the cell types present in a given tissue because of the difficulties in establishing such cultures while ensuring the viability and phenotypic stability of all cell types involved. One potential way of circumventing this problem would be to establish a specific microenvironment in the co-culture environment that would mimic a given event during the timeline of healing, so that the cellular interactions can make up for the missing components in the culture medium. In this study, we tried to use the inflammatory components both differentiated macrophages (to mimic the first group of immune cells that are in place) or monocytes (to mimic incoming cells at a later time point and also having a resident macrophage-like phenotype induced by the process of encapsulation as previous studies suggested) (Cha et al., 2017). In order to deconvolute the basis of interactions, co-culture systems with each component was also developed.

An interesting study done by Kirkpatrick and group previously, demonstrated that PMA treated THP-1 cells expressed macrophage markers such as CD68 and showed increased expression of macrophage related markers such as IL-1β, IL-8, and IL-10 secretion (Dohle et al., 2014). Previous transcriptomics studies also demonstrated that, under PMA activation THP-1 cells have a gene expression pattern similar to differentiated macrophages (Daigneault et al., 2010). Dohle et al. (2014) demonstrated that in three culture conditions (co-culture of osteoblasts, endothelial cells, and macrophages) the addition of THP-1 derived macrophages significantly increased the secretion of IL-6, IL-8, and TNF-α, which is in line with our observations. The main difference is that, in our model the 3-D ECM microenvironment was also mimicked by a crosslinked gelatin hydrogel based co-encapsulation of the cells which further guided the cell-cell interactions and provided sequestration of the secreted cytokines and their longer retention in a manner similar to the ECM.

CONCLUSION

Macrophages are important actors in the host's reaction to implantable materials. In cell-based therapies, particularly in tissue engineering applications, their activities in the form of cytokine secretion, cell-cell contacts, and cross-talk with other cell types can be harnessed for faster maturation and better vascularization of artificial tissues with less pro-inflammatory responses. The effect can be pronounced by inducing further phenotypic control by incorporating specific stimulations for controlling macrophage phenotype. In this study, we have demonstrated that a combination of anti-inflammatory cytokines and macrophages can be used for improving the remodeling of hydrogels. The presence of IL-4 induced fibroblast proliferation in fibroblast/macrophage co-cultures resulted in the boost of cytokine secretion. The presence of monocytes/macrophages with IL-4 in co-culture conditions with endothelial cells resulted in more sprout-like organization within the hydrogel. When all three cell types were incorporated, the remodeling and population of the hydrogel structure together with the release of cytokines were improved. These results demonstrated the potential advantages of immune cells and immunomodulatory cytokines within tissue engineering context for better remodeling and vascularization. The presence of the immune component in this manner can also improve the fidelity of model organs for organ-on-a-chip applications. Our future work will focus on the demonstration of the effect of macrophage incorporation in specific organs and determination of the optimal macrophage phenotypes for different organ maturation.

AUTHOR CONTRIBUTIONS

JB, CD, CM, and UL did the experiments. JB and NV designed the experiment. JB, NV, HK-M, and AD-B contributed to the interpretation of the results and the writing of the paper.

FUNDING

This project received funding from the European Union's Seventh Framework Programme for research, technological development, and demonstration under grant agreement no. 602694 (IMMODGEL) and from the European Union's Horizon 2020 research and innovation program under grant agreement No 760921 (PANBioRA).

ACKNOWLEDGMENTS

We would like to thank Althisia for histological analyses.

SUPPLEMENTARY MATERIAL

The Supplementary Material for this article can be found online at: https://www.frontiersin.org/articles/10.3389/fbioe.2018.00108/full#supplementary-material

REFERENCES

Anderson, J. M., Rodriguez, A., and Chang, D. T. (2008). Foreign body reaction to biomaterials. *Semin. Immunol.* 20, 86–100. doi: 10.1016/j.smim.2007.11.004

Benes, P., Macečková, V., Zdráhal, Z., Konečná, H., Zahradníčková, E., MuŽík, J., et al. (2006). Role of vimentin in regulation of monocyte/macrophage differentiation. *Differentiation* 74, 265–276. doi: 10.1111/j.1432-0436.2006.00077.x

Bigi, A., Cojazzi, G., Panzavolta, S., Roveri, N., and Rubini, K. (2002). Stabilization of gelatin films by crosslinking with genipin. *Biomaterials* 23, 4827–4832. doi: 10.1016/S0142-9612(02)00235-1

Bigi, A., Cojazzi, G., Panzavolta, S., Rubini, K., and Roveri, N. (2001). Mechanical and thermal properties of gelatin films at different degrees of glutaraldehyde crosslinking. *Biomaterials* 22, 763–768. doi: 10.1016/S0142-9612(00)00236-2

Bray, L. J., Binner, M., Korner, Y., Von Bonin, M., Bornhauser, M., and Werner, C. (2017). A three-dimensional tri-culture model for the *ex vivo* study of acute myeloid leukaemia. *Haematologica* 102, 1215–1226. doi: 10.3324/haematol.2016.157883

Brodbeck, W. G., Patel, J., Voskerician, G., Christenson, E., Shive, M. S., Nakayama, Y., et al. (2002). Biomaterial adherent macrophage apoptosis is increased by hydrophilic and anionic substrates *in vivo*. *Proc. Natl. Acad. Sci. U.S.A.* 99, 10287–10292. doi: 10.1073/pnas.162124199

Brown, B. N., and Badylak, S. F. (2013). Expanded applications, shifting paradigms and an improved understanding of host–biomaterial interactions. *Acta Biomater.* 9, 4948–4955. doi: 10.1016/j.actbio.2012.10.025

Cha, B. H., Shin, S. R., Leijten, J., Li, Y. C., Singh, S., Liu, J. C., et al. (2017). Integrin-mediated interactions control macrophage polarization in 3D hydrogels. *Adv. Healthcare Mater.* 6:1700289. doi: 10.1002/adhm.201700289

Correia, I., Chu, D., Chou, Y.-H., Goldman, R. D., and Matsudaira, P. (1999). Integrating the actin and vimentin cytoskeletons. *J. Cell Biol.* 146:831. doi: 10.1083/jcb.146.4.831

Daigneault, M., Preston, J. A., Marriott, H. M., Whyte, M. K., and Dockrell, D. H. (2010). The identification of markers of macrophage differentiation in PMA-stimulated THP-1 cells and monocyte-derived macrophages. *PLoS ONE* 5:e8668. doi: 10.1371/journal.pone.0008668

Dardalhon, V., Awasthi, A., Kwon, H., Galileos, G., Gao, W., Sobel, R. A., et al. (2008). IL-4 inhibits TGF-β-induced Foxp3+ T cells and, together with TGF-β, generates IL-9+ IL-10+ Foxp3– effector T cells. *Nat. Immunol.* 9:1347. doi: 10.1038/ni.1677

De Carvalho, R., and Grosso, C. (2004). Characterization of gelatin based films modified with transglutaminase, glyoxal and formaldehyde. *Food Hydrocoll.* 18, 717–726. doi: 10.1016/j.foodhyd.2003.10.005

Dohle, E., Bischoff, I., Böse, T., Marsano, A., Banfi, A., Unger, R., et al. (2014). Macrophage-mediated angiogenic activation of outgrowth endothelial cells in co-culture with primary osteoblasts. *Eur. Cell. Mater.* 27:149. doi: 10.22203/eCM.v027a12

Dollinger, C., Ciftci, S., Knopf-Marques, H., Guner, R., Ghaemmaghami, A. M., Debry, C., et al. (2017). Incorporation of resident macrophages in engineered tissues: multiple cell type response to microenvironment controlled macrophage-laden gelatine hydrogels. *J. Tissue Eng. Regen. Med.* 12, 330–340. doi: 10.1002/term.2458

Eckes, B., Dogic, D., Colucci-Guyon, E., Wang, N., Maniotis, A., Ingber, D., et al. (1998). Impaired mechanical stability, migration and contractile capacity in vimentin-deficient fibroblasts. *J. Cell Sci.* 111, 1897–1907.

Fagiani, E., and Christofori, G. (2013). Angiopoietins in angiogenesis. *Cancer Lett.* 328, 18–26. doi: 10.1016/j.canlet.2012.08.018

Fertin, C., Nicolas, J. F., Gillery, P., Kalis, B., Banchereau, J., and Maquart, F. X. (1991). Interleukin-4 stimulates collagen synthesis by normal and scleroderma fibroblasts in dermal equivalents. *Cell. Mol. Biol.* 37, 823–829.

Ford, M. C., Bertram, J. P., Hynes, S. R., Michaud, M., Li, Q., Young, M., et al. (2006). A macroporous hydrogel for the coculture of neural progenitor and endothelial cells to form functional vascular networks *in vivo*. *Proc. Natl. Acad. Sci. U.S.A.* 103, 2512–2517. doi: 10.1073/pnas.0506020102

Fukushi, J., Ono, M., Morikawa, W., Iwamoto, Y., and Kuwano, M. (2000). The activity of soluble VCAM-1 in angiogenesis stimulated by IL-4 and IL-13. *J. Immunol.* 165, 2818–2823. doi: 10.4049/jimmunol.165.5.2818

Hübner, G., and Werner, S. (1996). Serum growth factors and proinflammatory cytokines are potent inducers of activin expression in cultured fibroblasts and keratinocytes. *Exp. Cell Res.* 228, 106–113. doi: 10.1006/excr.1996.0305

Hunt, N. C., and Grover, L. M. (2010). Cell encapsulation using biopolymer gels for regenerative medicine. *Biotechnol. Lett.* 32, 733–742. doi: 10.1007/s10529-010-0221-0

Iademarco, M. F., Barks, J. L., and Dean, D. C. (1995). Regulation of vascular cell adhesion molecule-1 expression by IL-4 and TNF-alpha in cultured endothelial cells. *J. Clin. Invest.* 95, 264–271. doi: 10.1172/JCI117650

Ikada, Y., and Tabata, Y. (1996). "Gelatin hydrogel as a matrix to release protein drugs," in *Abstracts of Papers of the American Chemical Society* (Washington, DC).

Jain, R. K., Au, P., Tam, J., Duda, D. G., and Fukumura, D. (2005). Engineering vascularized tissue. *Nat. Biotechnol.* 23, 821–823. doi: 10.1038/nbt0705-821

Jus, S., Stachel, I., Fairhead, M., Meyer, M., Thoeny-Meyer, L., and Guebitz, G. M. (2012). Enzymatic cross-linking of gelatine with laccase and tyrosinase. *Biocatal. Biotransformation* 30, 86–95. doi: 10.3109/10242422.2012.646036

Kolesky, D. B., Homan, K. A., Skylar-Scott, M. A., and Lewis, J. A. (2016). Three-dimensional bioprinting of thick vascularized tissues. *Proc. Natl. Acad. Sci. U.S.A.* 113, 3179–3184. doi: 10.1073/pnas.1521342113

Liang, H. C., Chang, W. H., Liang, H. F., Lee, M. H., and Sung, H. W. (2004). Crosslinking structures of gelatin hydrogels crosslinked with genipin or a water-soluble carbodiimide. *J. Appl. Polym. Sci.* 91, 4017–4026. doi: 10.1002/app.13563

Mantovani, A., Sica, A., and Locati, M. (2005). Macrophage polarization comes of age. *Immunity* 23, 344–346. doi: 10.1016/j.immuni.2005.10.001

Margetts, P. J., Kolb, M., Yu, L., Hoff, C. M., Holmes, C. J., Anthony, D. C., et al. (2002). Inflammatory cytokines, angiogenesis, and fibrosis in the rat peritoneum. *Am. J. Pathol.* 160, 2285–2294. doi: 10.1016/S0002-9440(10)61176-5

Martinez, F. O., Helming, L., and Gordon, S. (2009). Alternative activation of macrophages: an immunologic functional perspective. *Annu. Rev. Immunol.* 27, 451–483. doi: 10.1146/annurev.immunol.021908.132532

Martinez-Santibañez, G., and Lumeng, C. N. (2014). Macrophages and the regulation of adipose tissue remodeling. *Annu. Rev. Nutr.* 34, 57–76. doi: 10.1146/annurev-nutr-071812-161113

McDermott, M. K., Chen, T., Williams, C. M., Markley, K. M., and Payne, G. F. (2004). Mechanical properties of biomimetic tissue adhesive based on the microbial transglutaminase-catalyzed crosslinking of gelatin. *Biomacromolecules* 5, 1270–1279. doi: 10.1021/bm034529a

Miyoshi, M., Kawazoe, T., Igawa, H. H., Tabata, Y., Ikada, Y., and Suzuki, S. (2005). Effects of bFGF incorporated into a gelatin sheet on wound healing. *J. Biomater. Sci.* 16, 893–907. doi: 10.1163/1568562054255709

Moore, E. M., Ying, G., and West, J. L. (2017). Macrophages influence vessel formation in 3D bioactive hydrogels. *Adv. Biosyst.* 1:1600021. doi: 10.1002/adbi.201600021

Ngo, M. T., and Harley, B. A. (2017). The influence of hyaluronic acid and glioblastoma cell coculture on the formation of endothelial cell networks in gelatin hydrogels. *Adv. Healthc. Mater.* 6:1700687. doi: 10.1002/adhm.201700687

Nichol, J. W., Koshy, S. T., Bae, H., Hwang, C. M., Yamanlar, S., and Khademhosseini, A. (2010). Cell-laden microengineered gelatin methacrylate hydrogels. *Biomaterials* 31, 5536–5544. doi: 10.1016/j.biomaterials.2010.03.064

Niu, Y., Li, Q., Xie, R., Liu, S., Wang, R., Xing, P., et al. (2017). Modulating the phenotype of host macrophages to enhance osteogenesis in MSC-laden hydrogels: design of a glucomannan coating material. *Biomaterials* 139, 39–55. doi: 10.1016/j.biomaterials.2017.05.042

Orban, J. M., Wilson, L. B., Kofroth, J. A., El-Kurdi, M. S., Maul, T. M., and Vorp, D. A. (2004). Crosslinking of collagen gels by transglutaminase. *J. Biomed. Mater. Res. Part A* 68, 756–762. doi: 10.1002/jbm.a.20110

Pinter, E., Mahooti, S., Wang, Y., Imhof, B. A., and Madri, J. A. (1999). Hyperglycemia-induced vasculopathy in the murine vitelline vasculature: correlation with PECAM-1/CD31 tyrosine phosphorylation state. *Am. J. Pathol.* 154, 1367–1379. doi: 10.1016/S0002-9440(10)65391-6

Porcheray, F., Viaud, S., Rimaniol, A. C., Léone, C., Samah, B., Dereuddre-Bosquet, N., et al. (2005). Macrophage activation switching: an asset for the resolution of inflammation. *Clin. Exp. Immunol.* 142, 481–489. doi: 10.1111/j.1365-2249.2005.02934.x

Prakash Parthiban, S., Rana, D., Jabbari, E., Benkirane-Jessel, N., and Ramalingam, M. (2017). Covalently immobilized VEGF-mimicking peptide with gelatin methacrylate enhances microvascularization of endothelial cells. *Acta Biomater.* 51, 330–340. doi: 10.1016/j.actbio.2017.01.046

Riabov, V., Salazar, F., Htwe, S. S., Gudima, A., Schmuttermaier, C., Barthes, J., et al. (2017). Generation of anti-inflammatory macrophages for implants

and regenerative medicine using self-standing release systems with a phenotype-fixing cytokine cocktail formulation. *Acta Biomater.* 53, 389–398. doi: 10.1016/j.actbio.2017.01.071

Rinker, T. E., Hammoudi, T. M., Kemp, M. L., Lu, H., and Temenoff, J. S. (2014). Interactions between mesenchymal stem cells, adipocytes, and osteoblasts in a 3D tri-culture model of hyperglycemic conditions in the bone marrow microenvironment. *Integr. Biol.* 6, 324–337. doi: 10.1039/c3ib40194d

Rostam, H. M., Singh, S., Salazar, F., Magennis, P., Hook, A., Singh, T., et al. (2016). The impact of surface chemistry modification on macrophage polarisation. *Immunobiology* 221, 1237–1246. doi: 10.1016/j.imbio.2016.06.010

Rutella, S., Bonanno, G., Procoli, A., Mariotti, A., De Ritis, D. G., Curti, A., et al. (2006). Hepatocyte growth factor favors monocyte differentiation into regulatory interleukin (IL)-10⁺⁺IL-12^{low/neg} accessory cells with dendritic-cell features. *Blood* 108, 218–227. doi: 10.1182/blood-2005-08-3141

Saik, J. E., Gould, D. J., Watkins, E. M., Dickinson, M. E., and West, J. L. (2011). Covalently immobilized platelet-derived growth factor-BB promotes angiogenesis in biomimetic poly(ethylene glycol) hydrogels. *Acta Biomater.* 7, 133–143. doi: 10.1016/j.actbio.2010.08.018

Spiller, K. L., Anfang, R. R., Spiller, K. J., Ng, J., Nakazawa, K. R., Daulton, J. W., et al. (2014). The role of macrophage phenotype in vascularization of tissue engineering scaffolds. *Biomaterials* 35, 4477–4488. doi: 10.1016/j.biomaterials.2014.02.012

Spiller, K. L., and Koh, T. J. (2017). Macrophage-based therapeutic strategies in regenerative medicine. *Adv. Drug Deliv. Rev.* 122, 74–83. doi: 10.1016/j.addr.2017.05.010

Tabata, Y., and Ikada, Y. (1998). Protein release from gelatin matrices. *Adv. Drug Deliv. Rev.* 31, 287–301. doi: 10.1016/S0169-409X(97)00125-7

Tattersall, I. W., Du, J., Cong, Z., Cho, B. S., Klein, A. M., Dieck, C. L., et al. (2016). *In vitro* modeling of endothelial interaction with macrophages and pericytes demonstrates Notch signaling function in the vascular microenvironment. *Angiogenesis* 19, 201–215. doi: 10.1007/s10456-016-9501-1

Vrana, N. E. (2016). Immunomodulatory biomaterials and regenerative immunology. *Future Sci.* 2:FSO146. doi: 10.4155/fsoa-2016-0060

Conflict of Interest Statement: JB, CM, and NV are full-time employees of Protip Medical. CD is an ex-employee of Protip Medical. NV is a shareholder of Protip Medical. UL is a full-time employee of Protobios. The collection, analysis, and interpretation of results presented was not influenced by the aforementioned companies.

The remaining authors declare that the research was conducted in the absence of any commercial or financial relationships that could be construed as a potential conflict of interest.

frontiers in Bioengineering and Biotechnology

REVIEW
published: 03 September 2018
doi: 10.3389/fbioe.2018.00120

In vitro Models and On-Chip Systems: Biomaterial Interaction Studies With Tissues Generated Using Lung Epithelial and Liver Metabolic Cell Lines

Milica Nikolic [1,2]*, *Tijana Sustersic* [1,2,3] *and Nenad Filipovic* [1,2,3]

[1] Faculty of Engineering, University of Kragujevac, Kragujevac, Serbia, [2] Steinbeis Advanced Risk Technologies Institute doo Kragujevac, Kragujevac, Serbia, [3] Bioengineering Research and Development Center, Kragujevac, Serbia

OPEN ACCESS

Edited by:
Pinar Zorlutuna,
University of Notre Dame,
United States

Reviewed by:
Ahmed El-Fiqi,
Dankook University, South Korea
Meltem Avci-Adali,
Universitätsklinikum Tübingen,
Universität Tübingen, Germany

***Correspondence:**
Milica Nikolic
mnikolic@risk-technologies.com

Specialty section:
This article was submitted to Biomaterials, a section of the journal Frontiers in Bioengineering and Biotechnology

Received: 31 May 2018
Accepted: 13 August 2018
Published: 03 September 2018

Citation:
Nikolic M, Sustersic T and Filipovic N (2018) In vitro Models and On-Chip Systems: Biomaterial Interaction Studies With Tissues Generated Using Lung Epithelial and Liver Metabolic Cell Lines. Front. Bioeng. Biotechnol. 6:120. doi: 10.3389/fbioe.2018.00120

In vitro models are very important in medicine and biology, because they provide an insight into cells' and microorganisms' behavior. Since these cells and microorganisms are isolated from their natural environment, these models may not completely or precisely predict the effects on the entire organism. Improvement in this area is secured by organ-on-a-chip development. The organ-on-a-chip assumes cells cultured in a microfluidic chip. The chip simulates bioactivities, mechanics and physiological behavior of organs or organ systems, generating artificial organs in that way. There are several cell lines used so far for each tested artificial organ. For lungs, mostly used cell lines are 16HBE, A549, Calu-3, NHBE, while mostly used cell lines for liver are HepG2, Hep 3B, TPH1, etc. In this paper, state of the art for lung and liver organ-on-a-chip is presented, together with the established *in vitro* testing on lung and liver cell lines, with the emphasis on Calu-3 (for lung cell lines) and Hep-G2 (for liver cell lines). Primary focus in this review is to discuss different researches on the topics of lung and liver cell line models, approaches in determining fate and transport, cell partitioning, cell growth and division, as well as cell dynamics, meaning toxicity and effects. The review is finalized with current research gaps and problems, stating potential future developments in the field.

Keywords: Calu-3, HepG2, *in vitro* models, organ-on-a-chip, epithelial barrier, toxicology

INTRODUCTION

In vitro models are the starting point in biological and medical research. With scientific progress and emergence of different *in vitro* models, knowledge of the entire organism behavior is growing. Together with experimental *in vitro* models, computer *in silico* models are being developed. Different types of models are developed, at different scales—macro, meso, micro, nano, depending on whether they explain the behavior of the whole system (macro; finite element models), behavior at the level of molecular clusters (meso; dissipative particle dynamics models) or behavior at the

molecular level (micro, nano; molecular dynamics models). Results obtained from *in vitro* and *in silico* models should be compared and verified. The final goal is to develop adequate *in silico* models, which reduce costs and time of experimental measurements and provide satisfactory results. However, first we need the results of *in vitro* models. *In vitro* models were used for many segments of the human organism—for blood-brain barrier (Ogunshola, 2011), the study of osteoarthritis (Johnson et al., 2016), psoriasis (Jean and Pouliot, 2010), myocardial tissue (Vunjak Novakovic et al., 2014) and myocardial ischemic injury (Tumiati et al., 1994) and paroxysmal supraventricular tachycardia (Wit et al., 1971), murine middle ear epithelium (Mulay et al., 2016), Alzheimer's disease (Stoppelkamp et al., 2011), thrombosis (Zhang et al., 2017) and vascular inflammation (Ahluwalia et al., 2018), as well as for different models of cancer (Katt et al., 2016), etc.

Calu-3 cell line was established in 1975 from a metastatic site (pleural effusion) in a 25-year-old Caucasian male with lung adenocarcinoma (Memorial Sloan Kettering Cancer Center, 2018). Current research shows that this cell line possesses characteristics similar to primary epithelial cells and can be used for investigation of the airway epithelial barrier to evaluate the regularity and irregularity of the barrier functions. Formed epithelial barrier can be used for investigation of diseases and for testing novel therapies and medicaments.

Although known for being part of the digestive tract and for the role of metabolizing xenobiotics and nutrients (carbohydrates and lipids), the liver is involved in more than 300 vital functions (Angier, 2017). When it comes to toxicological studies, chemical of interest is often tested on the liver. In recent years, new *in vitro* and *in silico* technologies have enabled insight into toxic mechanisms in order to replace or reduce the use of animals in tissue examinations (Gubbels-van Hal et al., 2005; Jie et al., 2016; Comenges et al., 2017). This is done at the molecular level to understand how changes at lower levels influence higher levels of biological organization (e.g., tissue, organs, etc.; EPA, 2003). One of the cell lines that has recently gained considerable attention is human hepatocarcinoma cell line, HepG2, that is used in *in vitro* studies on liver tissue (Gonzales et al., 2015). It has one nucleus and the epithelial-like morphology (Wilkening et al., 2003). HepG2 cell line is originally extracted from a 15-year-old Caucasian boy in the form of hepatocellular carcinoma (Gonzales et al., 2015). However, many of the mechanisms associated with the normal human hepatocytes are to be found in HepG2 cells, some of which are plasma proteins secretion, bile acids production, as well as detoxification processes. It is also reported that hepatoma cells possess receptors for insulin, transferrin, estrogen and low-density lipoproteins (Bouma et al., 1989; Gonzales et al., 2015), which means that they have the detoxification mechanisms, performed by rendering biotransformation reactions (Dehn et al., 2004).

The following section presents *in vitro* models for lung and liver cell lines. After that, data processing and available models of lung and liver cell lines are discussed. The fourth section contains on-chip review related to the previously mentioned cell lines, and, finally, the conclusion section provides a summary of the state-of-the-art and critically observes possible future steps in this field.

RETROSPECTIVE OF *IN VITRO* MODELS OF LUNG AND LIVER CELLS

Modeling of Lung Using Calu-3 Epithelial Cell Lines

Even though Calu-3 cells represent immortalized cells, they still possess many characteristics of primary airway cells and can be used for observation of transport, metabolism and testing novel medicament approach (Zhu et al., 2010).

Differentiated human bronchial epithelial cell culture systems were evaluated for asthma research —primary cells (human bronchial epithelial cells, HBEC) and non-primary cells, cell lines [Calu-3, BEAS-2B, BEAS-2B R1; (Stewart et al., 2012)] (**Figure 1**). More physiological models can be obtained with HBECs cultured at air-liquid interface with specifically determined medium which differentiates appropriate phenotype. Cells possess the ability to differentiate into goblet (MUC5AC+), to form ciliated layer (β-tubulin IV+) and to develop high transepithelial electric resistance (TEER), which serves as an indirect measure of occurrence of tight junctions (ZO-1 protein) and as a marker of disruption of the epithelial layer. Calu-3 cells grow up to confluence within 5 days and form tight epithelial monolayer over 21 days in culture. Cell layer tightness is confirmed with TEER measurements. Permeability can be observed using flu-Na uptake and the current results show that there is connection between TEER parameter and flu-Na uptake and membrane permeability (Haghi et al., 2010). Cell surface P-gp expression on Calu-3 is time dependent and does not depend on the cell passages. It was concluded that mucous secretion increases with time in culture. Determination of mucous quantity can be done with alcian blue. Cells differentiation can be evaluated by confocal imaging and qPCR (Stewart et al., 2012). Calu-3 cells take the greatest amount of time to become fully confluent, but more homogenous with increased mucus secretion. Grainger et al. (2006) in their research also concluded that Calu-3 cell line could be used to model the function and behavior of airway epithelial barrier. They cultured cells as air-interfaced culture (AIC) and as liquid-covered culture (LCC). In comparison to environmental conditions AIC provided greater quantity of mucus covering the cell surface, pseudostratified layer with more columnar cells (LCC creates monolayer)and more permeable cells. By comparing AIC and LCC, authors concluded that Calu-3 cell line cultured with AIC produced cell layer more similar to real airway epithelial morphology and electrical resistance *in vivo*, than cells cultured using LCC (**Figure 1**). Kreft et al. came to similar conclusion (Kreft et al., 2015) by investigating Calu-3 cell line under different culture conditions to ensure optimized *in vitro* model to investigate bronchial epithelial function. Calu-3 cells were tested in A-MEM media at air-liquid interface (A-L) and at liquid-liquid interface (L-L). A-L interface showed to be more natural in physiological way, forming pseudostratified columnar epithelium with more microvilli and secretory vesicles, showing higher TEER values and lower

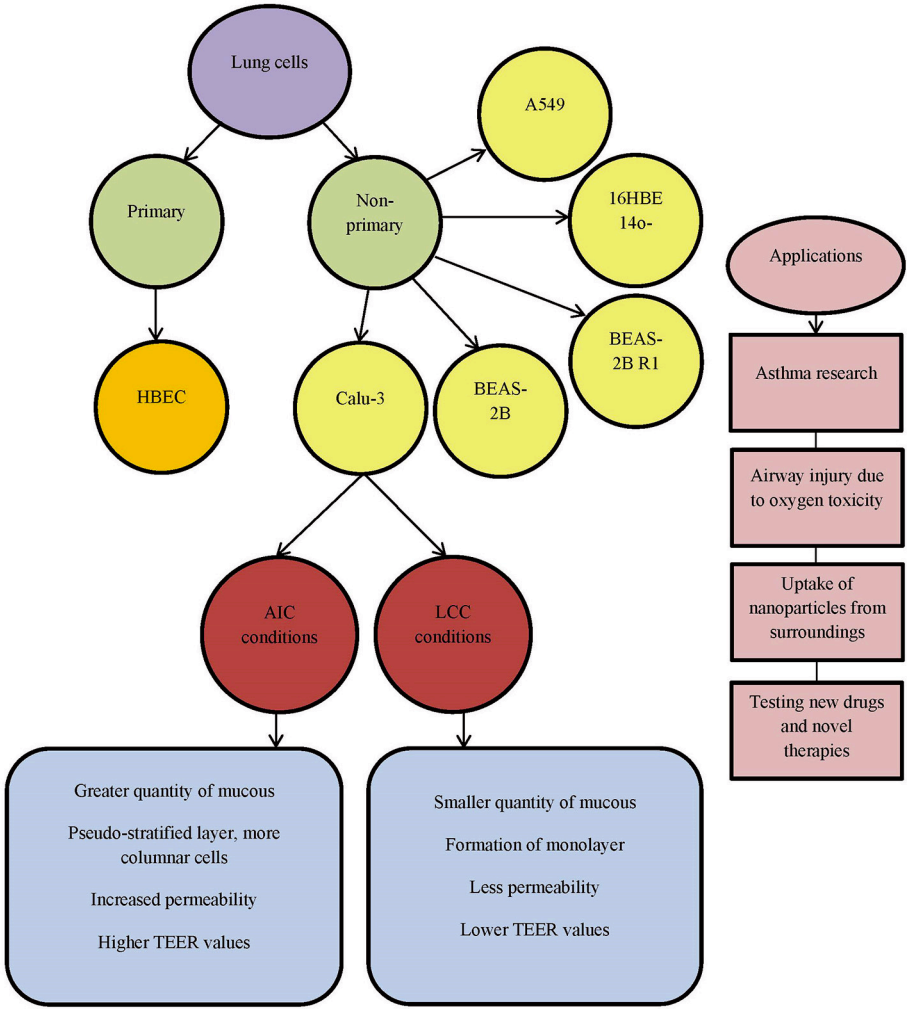

FIGURE 1 | List of commonly used lung cell lines. AIC, air-interfaced culture; LCC, liquid-covered culture.

permeability of dextran. Longer time in culture significantly decreased dextran permeability and increased expression of drug transporter. Major conclusion from this investigation was that cell culture conditions as well as time in culture affect cell differentiation, barrier function, permeability values and drug transporter expression. All these should be standardized for Calu-3 cell line as an *in vitro* model for drug delivery system and lung diseases.

Zhu et al. gave a review on human cultured airway epithelial cells, Calu-3 (Zhu et al., 2010). They used a model for assessing the effects of oxygen concentration, positive airway pressure and certain pharmacological agents. This cell line proved to be useful for studying the respiratory diseases, airway injury related to oxygen toxicity and evaluation of novel therapies (**Figure 1**). Isolated Calu-3 cells can mainly mimic airway epithelial cells, but absence of systematic inflammation should not be neglected in certain investigations. Another important characteristic in studying lung diseases is the uptake of nanoparticles from the surroundings, polluted air and water. Especially dangerous are carbon nanoparticles (CNP, beads). CNP uptake in the body can occur through inhalation of nanoparticles from air and can cause lung disease or further enter into circulatory system and even brain (Banga et al., 2012). Carbon nanoparticles affect barrier function of the airway epithelial Calu-3 monolayer by reducing it. Loss of cells viability decreases TEER, measured on the cellular monolayer, which is related to cytokine release. Calu-3 cell line can be used for observing respiratory irritation and testing toxicity of drugs and their medium by using MTT assay (Ihekwereme et al., 2014). Epithelial cell lines, like Calu-3, can be used for testing new drugs and novel therapies. Ong et al. focused on pharmaceutical applications of the Calu-3 cell line (Ong et al., 2013), but analyzed the use of other cell lines, such as bronchial cell lines 16HBE14o-, BEAS-2B and alveolar cell line A549. Their conclusion based upon the literature is that AIC has advantage over LCC surroundings and that TEER can be used as a measurement of integrity of the formed monolayer. Drug transport is based on layer permeability. Calu-3 cells show expression and functional activity of P-glycoprotein (P-gp),

the multidrug resistance associated proteins (MRPs), as well as breast cancer resistance protein (BCRP). These transporters are detectable in human lungs, *in vivo*, and in Calu-3 cell line. Drug-drug interactions could result in increased toxicity and side effects to diverse therapeutic outcomes. For example, Mamlouk et al. showed that nonsteroidal anti-inflammatory drugs (aspirin, ibuprofen, etc.) reduced the uptake of salbutamol across Calu-3 cells (Mamlouk et al., 2013). Calu-3 cell line is also used in investigation of anticancer therapeutics for growth inhibition, due to its cancer origin (Ong et al., 2013).

Modeling of Liver Using HepG2 Metabolic Cell Lines

Human hepatic cell lines, no matter if they are cancer-derived or immortalized hepatocytes, can be effectively cultured and used for different purposes. Some of the widely used hepatic cell lines are HepG2, Huh7, Hep3B, and SK-Hep-1, which are derived from hepatocellular carcinoma (HCC), and HepaRG, which is an HCC cell line that includes both hepatocytes and biliary-like cells (Guo et al., 2011; Gerets et al., 2012) (**Figure 2**). However, human hepatic cell lines have some limitations such as lower and variable cytochrome P450 enzymes (CYP450) expression presence which is not the case in primary human hepatocytes (Guo et al., 2011). In that sense, the results obtained with induction of CYP450 enzymes are more promising, meaning that drug transporter MDR1 is better in a novel hepatic cell line, Fa2N-4 (Mills et al., 2004). Another cell line, HepaRG cell line, is a promising substitute for primary human hepatocytes. It was noticed that in the case of low density seeding, HepaRG cells proliferate and differentiate to confluence, only to form colonies of hepatocytes. These colonies are than surrounded by biliary epithelial cells that show CYP450 expression levels, which is the result comparable to primary human hepatocytes (Guillouzo et al., 2007). What is more interesting, regarding drug delivery, is the ability of HepaRG cells to identify drugs that are likely to induce liver injury (Tomida et al., 2015). Additionally, HepaRG cells also show a response that is more robust to the inflammatory stimuli (e.g., IL-6, TNFα), in comparison to the primary human hepatocytes, which could be a result of the genetic variation (Klein et al., 2015) (**Figure 2**).

In recent years, lot of advancements have been made in the area of culture systems, which have enhanced functionality and stability of liver cells *in vitro* (Zeilinger et al., 2016). In order to describe the behavior of the native organ *in vivo*, cell types used in hepatic *in vitro* research have to fulfill some of those functions, depending on the study aim (Zeilinger et al., 2016). Many different *in vitro* liver models have been designed in order to accurately describe chemical treatment that will be able to be translated to *in vivo* responses. Out of the proposed methods, those that remain applicable for *in vitro* liver toxicity testing are liver slices, cell lines, and primary hepatocytes (Soldatow et al., 2013). Liver tissue slices are used because they retain liver structure, have good correlation *in vitro*/*in vivo* (because they contain cell types found *in vivo*) and maintain zone-specific cytochrome activity and mechanisms of toxicity (Lerche-Langrand and Toutain, 2000).

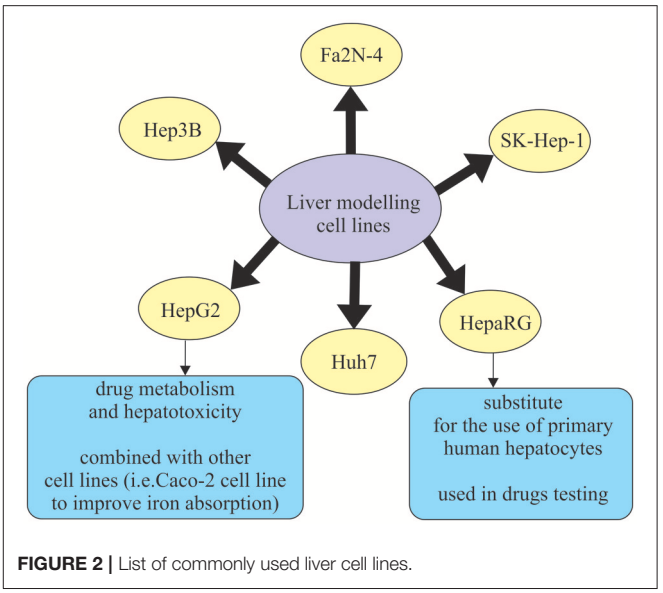

FIGURE 2 | List of commonly used liver cell lines.

Studies using tissue slices are typically in culture length that ranges from 30 min to 5 days and follow the parameters like oxygen tension, media and supplements, and culture system (i.e., shaken flasks, multiwall plates, stirred wells, etc.). They are usually modified to increase cell viability and reduce degenerative changes that are present in the tissue during the examination (Soldatow et al., 2013). Immortalized cell lines derived from the liver mostly do not possess phenotypic characteristics of the liver tissue (Yu et al., 2001). Most commonly used immortalized liver-derived cell lines are Fa2N-4, HepG2, Hep3B, PLc/PRFs Huh7, HBG, and HepaRG (Guguen-Guillouzo and Guillouzo, 2010; Guguen-Guillouzo et al., 2010) (**Figure 2**). Primary hepatocytes and hepatocyte-like cells have restricted application using standard culture conditions for some types of toxicity testing due to the problems in long-term maintenance of their functionality, lack of proper absorption, distribution, metabolism, and excretion (ADME) properties (Soldatow et al., 2013). Primary hepatocytes suspensions are also widely used in moderately high-throughput toxicity studies (Soldatow et al., 2013). Previous studies demonstrated that suspensions also keep high levels of functionality, which enables better correlation to *in vivo* toxicity studies (O'Brien and Siraki, 2005; Hewitt et al., 2007). For example, Griffin and Houston (2005) concluded that suspensions of hepatocytes allow for better and more accurate prediction of internal clearance rate in comparison to the conventional monolayer cultures. However, in *in vitro* testing, primary hepatocyte cultures have been mostly used, as they are able to maintain functional activities for 24–72 h. Therefore they can be applied not only in studies for enzyme induction and inhibition, allowing for medium-throughput monitoring of compounds, but are also ideal for studying interspecies and inter-individual differences in metabolism (LeCluyse, 2001; Hewitt et al., 2007). Primary hepatocyte cultures are often combined with inflammatory mediators. The reason for this is that traditional 2D hepatocyte cultures are not well applicable

in high-throughput screening (Soldatow et al., 2013). An *in vitro* combination—drug/inflammatory cytokine/inflammatory mediator co-treatment was used in the study by Cosgrove et al. (2009) to reproduce clinical drug hepatotoxicity. It was performed especially for idiosyncratic drugs, not only in cultured primary human and rat hepatocytes, but also in HepG2 cells.

Additionally, *in vitro* studies often combine two cell lines. For example, one study by Scheers et al. (2014) combined well established Caco-2 cell line with human liver cells HepG2 in order to improve iron absorption. The results show that this approach is a possible alternative to the traditional Caco-2 *in vitro* model for iron absorption (Scheers et al., 2014).

Main applications of liver cell lines used in *in vitro* research are in cancer development studies and therapy (Zeilinger et al., 2016). Cell line HepG2, as tumor cell line, has been investigated for the purposes of examining specific metabolic pathways that are related to liver tumors or testing development of drugs for cancer therapy. It should be emphasized that usually different sensitivities in various tumor cell lines from different origins are examined in parallel, in order to cover different types of cancer. For example, HepG2 cells were used in a research that analyzed the expression and regulation of cancer-related transcription factors (Samatiwat et al., 2016). HepG2 cell line can also be used to examine drug metabolism and hepatotoxicity. This is the case in the study by Palabiyik et al. (2016), who investigated the drug metabolism and hepatotoxicity, more specifically acetaminophen toxicity and prevention. HepaRG cell line also shows a promising alternative for the use of primary human hepatocytes (PHH) for the studies on drug metabolism, disposition, and toxicity (Lübberstedt et al., 2011; Andersson et al., 2012). They showed that HepaRG cells have the ability to highly differentiate and express typical hepatic functions. It means they could be used in studies including CYP-dependent metabolism, CYP induction, and drug transporter expression (Andersson et al., 2012). HepaRG cells, when used in drug toxicity tests, demonstrate similar response to the effects of acetaminophen as PHH and higher activation of genes related to liver damage in comparison to HepG2 cells. On the other hand, they show reduced sensitivity to the detection of hepatotoxic drugs (Gerets et al., 2012). As a result, it can be concluded that HepaRG cells can be an alternative to PHH in screening studies for CYP induction (Zeilinger et al., 2016).

DEVELOPED METHODS FOR LIVER AND LUNG CELLS ANALYSIS—TOXICOLOGY ASSESSMENT, CELL GROWTH AND DIVISION

Computer models and mathematical models of the lungs are rare. There are no many reports in literature related to this subject. Most of the developed models for lung-on-a-chip microfluidic device include imaging methods for 3D cell biology, like confocal laser scanning microscopy, two-photon and multiphoton microscopy, transmission and scanning electron microscopy, time-lapse imaging (Konar et al., 2016). Konar et al. analyzed applications of lung organoid, which assumes 3D tissue-engineered culture system that accurately replicates the histological and functional aspects of the *in vivo* tissue. Application of such system can be divided into several areas: cancer research, inflammations and infections of lungs, drug toxicity testing and drug development and finally personalized medicine.

A model of the lung-on-a-chip was developed by Hancock and Elabbasi (2018) with COMSOL Multiphysics software, according to the model presented by Huh (2015). COMSOL ensures methods for simulating fluid-structure interaction, nonlinear structural materials, laminar fluid flow, dilute species transport and particle tracing capability. The PDMS membrane and the walls can be modeled as neo-Hookean, Mooney-Rivlin or Ogden nonlinear material models. Additional features may be added, such as simulation of drug and nutrient transport, uptake by cells on the porous membrane, etc. COMSOL model provides insight into device functioning in dependence on the manufacturing and chosen material.

Savla et al. (2004) mathematically modeled airway epithelial wound closure during mechanical cycling strain. Modeling part was based upon *in vitro* model of human and cat airway epithelial cells (AEC) cultured cells, used for studying the repair mechanisms of wounded airway epithelial monolayer subjected to cyclic strain. Mathematical representation of the model included extended diffusion equation, combining parameters such as diffusion coefficient, spreading coefficient, and proliferation coefficient. These parameters influence wound closure and concentration of the cells to a large extent.

One of the goals in the future will be improvement of the mathematical and computer models of lung-on-a-chip device, as well as automation of the imaging techniques.

On the other hand, computer liver models were developed mainly with the goal to analyse toxicity of drug metabolites. Some studies used multi-scale approaches, such as physiologically-based kinetic/dynamic (PBK/D) models that describe the transportation of the chemicals in the body (Sala Benito et al., 2017). These models were often combined with some refinements (Gubbels-van Hal et al., 2005) to estimate the bioavailability and partitioning of the chemical in the assay in order to improve the estimations of concentrations *in vivo*, by using extrapolations of *in vitro* obtained concentrations (Sala Benito et al., 2017). This modeling approach is useful in the chemical risk assessment, when prioritization of chemical testing is important (Kramer et al., 2015; Bell et al., 2017). Whenever possible, *in vitro* studies were combined with *in vivo* studies in order to validate the proposed approach (Comenges et al., 2017).

Although *in vitro* assays are convenient to estimate toxic mechanisms, there are still some limitations of *in vitro* assays that make it impossible to completely replace *in vivo* studies (Comenges et al., 2017). These limitations mainly concern differences found between *in vitro* and *in vivo* experiments (false positives and negatives, large inter-assay variability, the low sensitivity etc.) (Höfer et al., 2004; Lilienblum et al., 2008). Because of that, mathematical models that comprise the fate of a compound in the cell-based assay combined with a cell growth model are developed (Comenges et al., 2017). Virtual Cell Based Assay (VCBA) was developed from HTS laboratory

data (Zaldívar et al., 2010; Zaldívar and Baraibar, 2011) with the aim to describe dynamic effects, since the kinetics is already described by PBK models (Sala Benito et al., 2017). The VCBA can be described as a process-based model or mathematical representation of an *in vitro* assay to simulate the effects and a fate of a chemical (Comenges et al., 2017). The VCBA model (Comenges et al., 2017; Sala Benito et al., 2017) consists of many parameters dependent on the physicochemical, experimental, as well as cell line characteristics, but can be divided into four sub models that describe:

1. Fate and transport model,
2. Cell partitioning model,
3. Cell growth and division model,
4. Cell dynamics including toxicity and effects model (**Figure 3**).

Fate and transport sub-model calculates time-dependent chemical concentration in the assay, by using dynamic mass balance equations. This means that several phenomena are included (evaporation, absorption onto the plastic, degeneration, partitioning of the chemicals etc.) Further on, cell partitioning sub-model includes extrapolation of the cell model equation, assuming that the total concentration of the compound can be partitioned into the concentrations of the compartments. Cell growth and division sub-model examines four stages G1, S, G2, M of cell cycle, while cell dynamics including toxicity and effects sub-model includes the influence effects of the chemical concentration on the survival rate (by taking into account the mortality rate) (Sala Benito et al., 2017).

Initially, the VCBA was built in Matlab with the aim to examine the toxicological effects of chemicals on cells (Zaldívar et al., 2010; Zaldívar and Baraibar, 2011; Comenges et al., 2012). It was later adapted to R Language, to make it freely available to end-users. Comenges et al. integrated the code into the Knime environment through an R-KNIME node (Comenges et al., 2017). The KNIME Analytics Platform[1] (Berthold et al., 2009) was developed as a user friendly and free graphical workbench that supports data analytics which includes data management and transformation, investigation, as well as visualization and reporting. In that sense, Benito et al. used the KNIME Analytics Platform, as a user-friendly tool in automation of generating the key input parameters in biokinetic models (Sala Benito et al., 2017).

It should be stated that VCBA models were also used in examining HepG2 cell lines. Paini et al. examined repeated exposure from human liver cell lines HepG2 (and also HepaRG) in order to optimize the VCBA (Paini et al., 2017). The main advantage of this research is that the repeated dose toxicity is not convenient in *in vivo* studies and VCBA models can help reduce and optimize the time spent in the assessment of human safety when it comes to similar research. Additionally, it should be emphasized that the entire projects were dedicated to the development of computational tools and predictive models to estimate the safety of the chemicals. EU COSMOS project[2] was one of them. Within this project 11 chemical specific PBK models were developed (Bois et al., 2017; Sala Benito et al., 2017). The COSMOS models were inserted in previously mentioned KNIME versions, with two possibilities for execution—locally, on a desktop computer, or remotely, using web browser and KNIME WebPortal[3].

ON-CHIP SYSTEMS

Organ-on-a-chip stands for the microfluidic device that mimics the behavior of a certain organ or system on a microchip. In the past few years, several different organs were developed with on-chip technology (**Figure 4**).

The major advantage of organ-on-a-chip technology is its capability to represent structural and functional complexity of living tissues and organs, unlike *in vitro* cell culture techniques, which fail in reproduction of dynamic mechanical and biochemical microenvironment. Organ-on-a-chip micro device mimics microsystems and possesses tremendous potential as an innovative and predictive screening platform.

Lung-on-a-Chip

Lung-on-a-chip, initially developed at Wyss Institute for Biologically Inspired Engineering at Harvard University, stands for microfluidic device that mimics breathing human lungs on a microchip[4]. The design includes two layers of lung cells separated by porous membrane and covered with two canals—upper and lower. The upper canal represents the airways and permits airflow. The lower canal represents the blood vessels and permits blood flow. Mimicking breathing is achieved with vacuum applied to the chambers, which creates cyclic mechanical stretching. Design of the lung-on-a-chip is presented in **Figure 5**.

The main purpose of generation of organ-on-chips, including lung, is to reduce and ultimately replace experiments on the animals.

Lung-on-a-chip device can be used to simulate the breathing of a healthy lung and to analyse the interaction of nanoparticles, which derive from air and water pollution and can lead to inflammatory processes. Furthermore, new drugs and therapies for certain lung diseases can be tested, the toxicity of novel drugs can be measured and lung cancer can be simulated.

Huh is one of the founders of lung-on-a-chip technology (Huh, 2015). He also created lung model, focusing on the alveolar-capillary interface—microfluidic device as a unit of living human lung. The model consists of two chambers, separated by porous membrane. The upper chamber contains alveolar epithelial cells and the lower chamber contains pulmonary microvascular endothelial cells. The upper chamber is filled with air and the lower one with blood. Side chambers are used for cyclic vacuum suction to induce cyclic stretching in order to simulate breathing motions and deformation of the alveolar-capillary barrier (**Figure 5**).

[1] Available online at http://www.knime.org

[2] Available online at http://www.cosmostox.eu/home/welcome

[3] Available online at https://knimewebportal.cosmostox.eu/com.knime.enterprise.server

[4] Wyss Institute. (November 07, 2012). Available online at: https://wyss.harvard.edu/wyss-institute-models-a-human-disease-in-an-organ-on-a-chip.

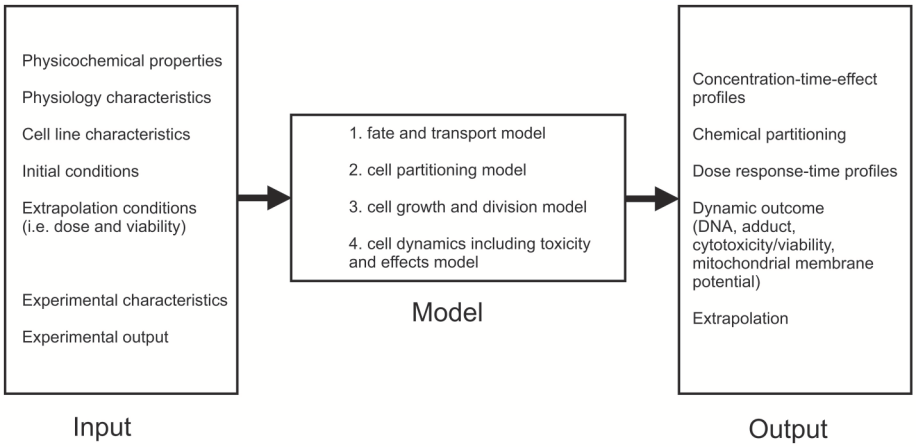

FIGURE 3 | Schematic representation of VCBA model.

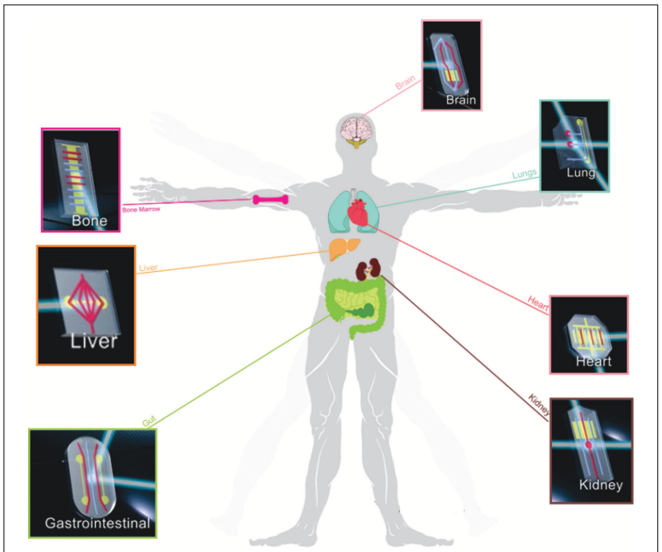

FIGURE 4 | Organs-on-a-chip.

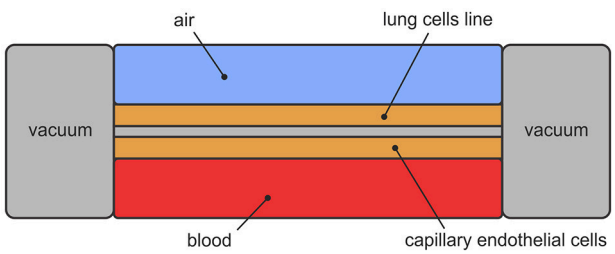

FIGURE 5 | Schematic view of lung-on-a-chip.

The micro-device has the ability to reproduce lungs' properties. It can be used for better understanding of lungs' function and simulation of pulmonary diseases (Metzger, 2018). Essential processes in breathing lungs are gas exchanges between alveolus and capillary. After established function of gas exchanges, the micro-device can be used for toxicity analysis as well as for analysis of certain pulmonary diseases. This model can be used for analysis of silica nanoparticles absorption and acute toxic response to the nanoparticle absorption due to stretching of alveolar-capillary barrier. This leads to conclusion that breathing increases nanoparticles absorption[5]

[5]Wyss Institute. (June 24, 2010). Available online at https://wyss.harvard.edu/living-breathing-human-lung-on-a-chip-a-potential-drug-testing-alternative/.

In the Wyss laboratory[4], alveolus-on-a-chip model was developed for reproducing pulmonary thrombosis. To simulate an intravascular thrombosis, the tumor necrosis factor (TNF-α) was added to the upper chamber. The aim was to provoke inflammation involving cytokines, which alert leukocytes and platelets blood particles. These blood particles further trigger thrombi formation. It was confirmed at the Wyss institute that permeability of the lung was related to the TNF-α concentration (Jain et al., 2018). The use of LPS (lipopolysaccharides) induced thrombosis and caused inflammation by interactions between alveolar epithelial and vascular endothelial cells. In conclusion, drug Parmodulins reduced vascular inflammation without endothelial injury. Therefore, one of the potential applications of lung-on-a-chip technology is the analysis of thrombosis. Another one can be the analysis of the physiological reactions during acute asthmatic crisis (Benam et al., 2015). Different types of pulmonary diseases can be analyzed using the micro-device. Novel drug testing for observed disease can be produced without using animals and with reduced costs. Pulmonary edema can be analyzed as well. It is the condition where blood clots and fluid are filling the lung, caused by heart failure or cancer drug side effects. Huh (2015) tested the model presented in **Figure 5** to pulmonary edema and the cancer drug was injected into the lower chamber for that purpose.

Migration of the fluid and plasma protein into the upper air chamber was noticed, similar to the drug's side effect. The immune system is not involved in leakage side effects, as it was thought. In fact, breathing increases leakage (Rojahn, 2012). Usage of different drug candidates, such as GlaxoSmithKline drug, is found to be able to prevent the leakage in the chip system (Rojahn, 2012). Small airway-on-a-chip was developed for the analysis of lung inflammation and drug responses (Benam et al., 2015). Airway-on-a-chip was created by seeding primary human airway epithelial cells (hAECs) and primary human lung microvascular endothelial cells on the opposite sides of the porous membrane. Epithelial cells formed a barrier by creation of tight junctions, which were detected by ZO1 expression, while endothelial cells junctions were observed by PECAM-1 expression. Measurements of airway-on-a-chip were compared with *in vivo* measurements, in order to validate the usage of micro device. Electron microscopic analysis confirmed that the cilia at the apical side had the same structure as healthy cilia found in living human lung *in vivo* (9 + 2 microtubule organization). Cilia beat actively at a frequency range [9–20 Hz]. Mucociliary transport was measured and it was observed that the particle velocity was nearly identical to the one observed in healthy human lungs' airway. The conclusion is that airway-on-a-chip can be used as a representation of the human living healthy lung and further for asthma and chronic obstructive pulmonary disease (COPD). IL-13 has an important role in asthma evolving and it is sufficient and necessary for induction of allergic asthma in animal models. It participates in airway inflammation, goblet cell hyperplasia and mucus hypersecretion, as well as in creation of subepithelial fibrosis and airway hyper-responsiveness. Increase in the number of goblet cells was noticed after 8 days when small airway-on-a-chip was treated with IL-3, like in other *in vitro* models. Higher production of inflammatory cytokines G-CSF and GM-CSF into vascular channel and decrease in cilia beating frequency were also noticed. Pathogenic infections are major cause of COPD exacerbation in patients. Airways-on-a-chip epithelial cells were lined up with either normal or COPD epithelial cells and treated with the viral mimic poly (I:C) or lipopolysaccharide endotoxin (LPS). Bacterial wall derived component that simulates cytokine production and has been widely used for that purpose. M-CSF cytokine secretion was analyzed, because it promotes differentiation and survival of macrophages. On the other hand, production of the IL-8 was monitored, because IL-8 attracts neutrophils. Stimulation with poly(I:C) promoted secretion of the cytokines IP-10 and RANTES in both healthy and COPD chips. Besides IP-10, which is an excellent clinical marker, level of M-CSF was increased in poly(I:C) treated airway chip. For this reason, it could be used as a new biomarker for COPD exacerbations induced by respiratory viruses. The developed microfluidics models of human asthmatic and COPD airways can be further used for testing the efficacy of new experimental drugs and also for dissection of the mechanism of drug action at the molecular level.

Cells from lung-on-chip micro device can be monitored with microimpedance tomography system, which can provide useful information about the cells and culture conditions (Mermoud et al., 2018). Novel microimpedance tomography (MITO) can be integrated in a lung-on-chip and can allow the real-time monitoring of the integrity of an epithelial barrier located 1 mm away from the electrodes. This system successfully monitored in real-time resistivity changes occurring on the lung epithelial barrier.

Yang et al. developed tumors-on-a-chip with PLGA electrospinning nanofiber membrane, which thickness is about 3 μm and that is porous and permeable to molecules (Yang et al., 2018). Gefitinib drug, an EGFR-targeted anti-tumor drug, was evaluated and A549 cell resistance in the co-culture with HFL1 was analyzed. One of the reasons could be secretion of IGF-1 by HFL1 cells which activated PI3K/Akt signal pathway after inhibition and led to low response of the tumor cells to the chemotherapeutic drugs. Also, A549 cells cause apoptosis and death of the endothelial cells and this can further lead to tumor spreading. The final goal of the authors (Yang et al., 2018) is to apply model in personalized treatment of the lung tumor, which can be important in future clinical research.

Liver on-a-Chip

The main reason for the failure of possible treatments after testing on animals is the hepatotoxicity (Ho et al., 2006; Lee et al., 2015). The possibility of using livers-on-chips enables us to avoid this stage. "Organ-on-a-chip" concept started as a way of mimicking tissues and organs by constructing the networks composed of several connectional functional units connected by multi-channels (Baker, 2011; Bhatia and Ingber, 2014; Esch et al., 2015). However, liver cells are said to be some of the most difficult cell lines for keeping alive in a Petri dish (Domansky et al., 2013) and a way of mimicking their normal environment is of crucial importance in order to increase their lifespan. Parker et al. (2008) showed that liver cells multiplied and their metabolic activity was increased when mesenchymal cells from human placenta were placed together with liver cells. The most important parameter in this process is the ratio between the two aforementioned types of cells. The microfluidic cell line devices are given full attention due to the advantage of small length scale and flow control (Sia and Whitesides, 2003). Some initial attempts toward real life applications of on-chip systems in tissue engineering included examination of impedance measurements in order to determine where certain cell aggregates are placed in a biologically relevant 3D environment (Canali et al., 2015). In normal biological environment, cells are surrounded by hydrogel-like extracellular matrix (ECM) made out of proteins (Canali et al., 2015). When alternating electric field is induced, cells and tissues exhibit complex behavior, which is mainly dependent on the frequency (Yang et al., 1999). This was the main assumption behind the research by Canali et al. (2015) who performed finite element (FE) simulations to examine 4T impedance sensing. They introduced high density of human HepG2 cells encapsulated in gelatine through artificial 3D cell constructs and wanted to determine the sensitivity field distribution depending on the combinations of current carrying (CC) and voltage pick-up (PU) electrodes. Simulations were performed in COMSOL Multiphysics software and showed that this method is suitable for impedance-based sensing with the

application on formation of bio artificial organs (Canali et al., 2015).

Micro fabricated devices have been examined with various silicon and poly-dimethylsiloxane (PDMS) substrates in order to use it for hepatocyte culture in membrane-based bioreactors (De Bartolo et al., 2000; Ostrovidov et al., 2004), multi-layer polymer structures (Leclerc et al., 2004), and devices that include oxygen and nutrient delivery systems accompanied by online monitoring (Powers et al., 2002; Lee et al., 2006). Ho et al. (2006) have managed to recreate a liver lobule (functional unit of the liver) on a microfluidic chip using dielectrophoresis. Weng et al. (2017) managed to design a device without a scaffold, primarily because scaffold-based technologies have serious limitations (e.g., inherent stability of a scaffold or unpredictable effects on signaling pathways).

A very important already mentioned aspect of on-chip systems is the appropriate distribution of nutrients where non-uniform distribution and shear stresses throughout the scaffold region can decrease cell colonization and influence the quality of the regenerated tissue (Podichetty et al., 2015). For that purpose, axial-flow bioreactors (also named perfusion bioreactors) have been examined to determine optimal flow rates (Gardel et al., 2013), inlet and outlet diameters, as well as scaffold surface for hepatocyte cultivation (Leclerc et al., 2004). The purposes of aforementioned researches were said to be found in bone regeneration (Azuaje, 2010), cardiac patch (Dvir et al., 2006), and abdominal wall (Pu et al., 2010). Some modeling studies used computational fluid dynamics (CFD) to gain insight into fluid dynamics and nutrient distribution in bioreactors (Cioffi et al., 2006; Wendt et al., 2008; Patrachari et al., 2012). They used either a multi-scale continuum modeling approach (Causin et al., 2013) or Boltzmann-Lattice model (Spencer et al., 2013). Their approach using modeling is useful, but the main drawback in the research is the lack of experimental validation (Podichetty et al., 2015). They examined nutrient distribution characteristics because of the influence of the non-ideal flow on tissue regeneration (Podichetty et al., 2015). The results of the CFD simulation and dispersion model were validated with experiments of nutrient consumption (Podichetty et al., 2015). Metabolically very active HepG2 cells were seeded on chitosan-gelatin (CG) scaffolds and the results showed that *in vitro* tissue regeneration monitoring is possible with this kind of simulation. This represents a step forward toward the understanding the mechanical stimulus effect on 3D cell culture (Podichetty et al., 2015).

A research group at the Universitätsklinikum Jena, Germany, developed liver-on-chip[6]. They examined the activation patterns of macrophages in inflammatory responses, in order to control bacterial infections. A liver-on-chip model with microfluidic perfusions was made to examine liver infections. With all essential cell types of the human liver on this chip and emulation of a microphysiological environment, this chip can be used to examine inflammation-associated molecular processes of hepatic function disorder and macrophage-associated processes of tissue repair that is subjected to the inflammatory conditions. Particularly, this research group used the described liver-on-chip system to investigate the pathogenesis of *Staphylococcus aureus* infections and infections with *Candida albicans*, as well as in treatment of sepsis-associated hepatic disorders by using functionalized nanoparticles. A schematic view of a liver-on-a-chip is given in **Figure 6**.

A multi-type cell on-hip model was made by Jie et al. (2016) to reconstruct physiological drug kinetics by seeding Caco-2, HepG2, and U251 cells (they were used to mimic the intestine, liver, and glioblastoma, respectively). A full description of the microfluidic on-chip was given by Jie et al. (2016), where Caco-2 cells served as intestine tissue for oral drug absorption. HepG2 cells, as a liver equivalent, were placed below the Caco-2 cell line. U251 cells, as a glioblastoma compartment, were connected with HepG2 cells unit by narrow channels array (Jie et al., 2016). All this could be said to mimic *in vivo* 3D microenvironment and examine the functions of drug absorption, metabolism and response in a produced microenvironment, with the possible application in personalized cancer therapy (Jie et al., 2016). Other researchers also examined microfluidic chips (Huh et al., 2012; Ramadan et al., 2013). Imura et al. (2013) simulated distribution of drugs and excretion processes in a dynamical microfluidic system, while Maschmeyer et al. (2015) established a microphysiological multi-organ system for long-time co-cultivation. The study by Zhang et al. (2008) also needs to be mentioned, as this research specifically deals with microfluidic environment, designed for improved hepatocyte liver cell culture *in vitro*. Finite element simulations modeled using COMSOL were performed in order to examine the effect of continuous perfusion on glucose consumption by HepG2 cell (Zhang et al., 2008). The results show that the suggested method is appropriate for production of microfluidic devices with mass transport conditions, as well as discuss the effects on maintenance of biological function and differentiated phenotype (Zhang et al., 2008).

Additionally, designs that consist of interconnected compartments allow research on how different cell types and organs communicate and interact in the sense of interdependent cellular responses. Theobald et al. examined simplified liver-kidney-on-chip model and concluded that the combined liver-kidney model is adequate for initial determination of liver mediated toxic effects. They showed that hepatic cells, growing in large amounts in microfluidic conditions, expressed metabolism-related biomarkers (Theobald et al., 2017). Investigation of toxicity of Aflatoxin B1 (AFB1) and Benzoalphapyrene (BαP) showed the importance of examining multi-organs

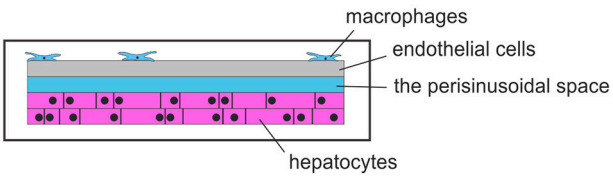

FIGURE 6 | Schematic view of liver-on-a-chip.

[6]Available online at https://www.uniklinikum-jena.de/cscc/mosig.html (Accessed May 05, 2018)

in microfluidic devices for the purposes of *in vitro* toxicity testing and drug screening (Theobald et al., 2017). Chang et al. developed an integrated liver-kidney microphysiological (MPS) system to identify nephrotoxic liver-metabolized chemicals using the connected liver-on-a-chip and kidney-on-a-chip (Chang et al., 2016). Their results show the important specific purpose of hepatic biotransformation in toxicity research and validation of *in vitro* and *in vivo* model comparisons (Chang et al., 2016).

CONCLUSIONS

Many scientists are skeptical when it comes to further improvement of the organ-on-a-chip systems and replacement of animal experiments because human organism is very complex by structure and function, and they do not believe that organ-on-a-chip can include all the environmental parameters. That is true—lung-on-a-chip is not a real lung, but there can be certain benefits from finding more details related to specific lung diseases. There can be benefits from testing the novel drugs before trying them on animals. Experiments on animals should fill ethical requirements and cannot be related to the human lungs in every aspect (Benam et al., 2015). For example, mouse and rat lungs have less frequent mucin-producing cells, which are important for asthma developing. Lung inflammation involves complex tissue-tissue interactions between lung airway epithelium cells and microvascular endothelium cells that activate the immune system—recruit immune cells, such as neutrophils. These processes can be simulated by using lung-on-a-chip microfluidic device. Besides regular behavior of the lung, these microfluidic devices can be used for collecting information and new knowledge about lung diseases, as well as for testing novel drugs approaches and treatments.

As far as liver cell line studies are concerned, it was reported that drug-induced hepatic injury in liver (liver hepatotoxicity) is the most common reason for delays in the clinical phase in drug development and even withdrawal of an approved drug (Bies et al., 2006). Contrary to other human organs, liver has a remarkable capacity to regenerate. Along with the physiological importance and plasticity of this organ, a better understanding of human physiology, disease and response to exogenous compounds is enabled through the examination of the liver. Additionally, the main challenge for the construction of microfluidic liver devices is the complexity of the liver itself. Due to its complexity and numerous functions combined with different types of cells and a specific construction, the liver is very hard to model. Therefore, the main convenience of the liver-on-a-chip is its ability to replicate microscopic details, which is important in future examination (Lee et al., 2015). Once the improvements in liver-on-a-chips are made, curing a lot of diseases (e.g., hepatitis B, hepatocellular carcinoma) will become easier.

AUTHOR CONTRIBUTIONS

All authors listed have made a substantial, direct and intellectual contribution to the work, and approved it for publication.

FUNDING

This study was funded by the European Project H2020 PANBioRA [grant number 760921-2] and grants from the Serbian Ministry of Education, Science, and Technological Development [grant number III41007 and grant number OI174028].

REFERENCES

Ahluwalia, A., Misto, A., Vozzi, F., Magliaro, C., Mattei, G., Marescotti, M. C., et al. (2018). Systemic and vascular inflammation in an *in-vitro* model of central obesity. *PLoS ONE*. 13:e0192824. doi: 10.1371/journal.pone.0192824

Andersson, T. B., Kanebratt, K. P., and Kenna, J. G. (2012). The HepaRG cell line: a unique *in vitro* tool for understanding drug metabolism and toxicology in human. *Expert Opin. Drug Metab. Toxicol.* 8, 909–920. doi: 10.1517/17425255.2012.685159

Angier, N. (2017). Physiologie. Le foie, cet organe à tout faire. *Courrier International* (The New York Times).

Azuaje, F. (2010). Computational discrete models of tissue growth and regeneration. *Briefings Bioinform.* 12, 64–77. doi: 10.1093/bib/bbq017

Baker, M. (2011). Tissue models: a living system on a chip. *Nature* 471, 661–665. doi: 10.1038/471661a

Banga, A., Witzmann, F. A., Horia, I. P., and Blazer-Yost, B. L. (2012). Functional effects of nanoparticle exposure on Calu-3 airway epithelial celss. *Cell. Physiol. Biochem.* 29, 197–212. doi: 10.1159/000337601

Bell, S. M., Chang, X., Wambaugh, J. F., Allen, D. G., Bartels, M., Brouwer, K. L., et al. (2017). *In vitro* to *in vivo* extrapolation for high throughput prioritization and decision making. *Toxicol. In Vitro*. 47, 213–227. doi: 10.1016/j.tiv.2017.11.016

Benam, K. H., Villenave, R., Lucchesi, C., Varone, A., Hubeau, C., Lee, H. H., et al. (2015). Small airway-on-a-chip enables analysis of human lung inflammatory and drug responses *in vitro*. *Nat. Methods* 13, 151–157. doi: 10.1038/nmeth.3697

Berthold, M. R., Cebron, N., Dill, F., Gabriel, T. R., Kötter, T., Meinl, T., et al. (2009). KNIME-the Konstanz information miner: version 2.0 and beyond. *AcM SIGKDD Explorations Newsletter* 11, 26–31. doi: 10.1145/1656274.1656280

Bhatia, S. N., and Ingber, D. E. (2014). Microfluidic organs-on-chips. *Nat. Biotechnol.* 32, 760–762. doi: 10.1038/nbt.2989

Bies, R. R., Navarro, V. J., and Senior, J. R. (2006). Drug-related hepatotoxicity. *J. Clin. Pharmacol.* 46, 1052–1053. doi: 10.1177/0091270006292979

Bois, F. Y., Ochoa, J. G. D., Gajewska, M., Kovarich, S., Mauch, K., Paini, A., et al. (2017). Multiscale modelling approaches for assessing cosmetic ingredients safety. *Toxicology* 392, 130–139. doi: 10.1016/j.tox.2016.05.026

Bouma, M. E., Rogier, E., Verthier, N., Labarre, C., and Feldmann, G. (1989). Further cellular investigation of the human hepatoblastoma-derived cell line HepG2: morphology and immunocytochemical studies of hepatic-secreted proteins. *In Vitro Cell. Devel. Biol.* 25, 267–275. doi: 10.1007/BF02628465

Canali, C., Mazzoni, C., Larsen, L. B., Heiskanen, A., Martinsen, Ø. G., Wolff, A., et al. (2015). An impedance method for spatial sensing of 3D cell constructs–towards applications in tissue engineering. *Analyst* 140, 6079–6088. doi: 10.1039/C5AN00987A

Causin, P., Sacco, R., and Verri, M. (2013). A multiscale approach in the computational modeling of the biophysical environment in artificial cartilage tissue regeneration. *Biomech. Model. Mechanobiol.* 12, 763–780. doi: 10.1007/s10237-012-0440-5

Chang, S. Y., Weber, E. J., Ness, K. V., Eaton, D. L., and Kelly, E. J. (2016). Liver and kidney on chips: microphysiological models to understand transporter function. *Clin. Pharmacol. Therap.* 100, 464–478. doi: 10.1002/cpt.436

Cioffi, M., Boschetti, F., Raimondi, M. T., and Dubini, G. (2006). Modeling evaluation of the fluid-dynamic microenvironment in tissue-engineered constructs: a micro-CT based model. *Biotechnol. Bioeng.* 93, 500–510. doi: 10.1002/bit.20740

Comenges, J. M. Z., Joossens, E., Benito, J. V. S., Worth, A., and Paini, A. (2017). Theoretical and mathematical foundation of the virtual cell based assay–a review. *Toxicol. In Vitro* 45, 209–221. doi: 10.1016/j.tiv.2016.07.013

Comenges, J. M. Z., Wambaugh, J., and Judson, R. (2012). Modeling *in vitro* cell-based assays experiments: cell population dynamics. *Dev. Environ. Modell.* 25, 51–71. doi: 10.1016/B978-0-444-59396-2.00004-3

Cosgrove, B. D., King, B. M., Hasan, M. A., Alexopoulos, L. G., Farazi, P. A., Hendriks, B. S., et al. (2009). Synergistic drug–cytokine induction of hepatocellular death as an *in vitro* approach for the study of inflammation-associated idiosyncratic drug hepatotoxicity. *Toxicol. Appl. Pharmacol.* 237, 317–330. doi: 10.1016/j.taap.2009.04.002

De Bartolo, L., Jarosch-Von Schweder, G., Haverich, A., and Bader, A. (2000). A novel full-scale flat membrane bioreactor utilizing porcine hepatocytes: cell viability and tissue-specific functions. *Biotechnol. Prog.* 16, 102–108. doi: 10.1021/bp990128o

Dehn, P. F., White, C. M., Conners, D. E., Shipkey, G., and Cumbo, T. A. (2004). Characterization of the human hepatocellular carcinoma (hepg2) cell line as an *in vitro* model for cadmium toxicity studies. *In Vitro Cell. Dev. Biol. Animal* 40, 172–182. doi: 10.1290/1543-706X(2004)40<172:COTHHC>2.0.CO;2

Domansky, K., Leslie, D. C., McKinney, J, Fraser, J. P., Sliz, J. D., Hamkins-Indik, T., et al. (2013). Clear castable polyurethane elastomer for fabrication of microfluidic devices. *Lab On A Chip* 13, 3956–3964. doi: 10.1039/c3lc50558h

Dvir, T., Benishti, N., Shachar, M., and Cohen, S. (2006). A novel perfusion bioreactor providing a homogenous milieu for tissue regeneration. *Tissue Eng.* 12, 2843–2852. doi: 10.1089/ten.2006.12.2843

EPA US. (2003). *A Framework for a Computational Toxicology Research Program.* Washington, DC: United States Environmental Protection Agency (EPA600/R-03/65).

Esch, E. W., Bahinski, A., and Huh, D. (2015). Organs-on-chips at the frontiers of drug discovery. *Nat. Rev. Drug Disc.* 14, 248–260. doi: 10.1038/nrd4539

Gardel, L. S., Serra, L. A., Reis, R. L., and Gomes, M. E. (2013). Use of perfusion bioreactors and large animal models for long bone tissue engineering. *Tissue Eng. Rev.* 20, 126–146. doi: 10.1089/ten.teb.2013.0010

Gerets, H. H., Tilmant, K., Gerin, B., Chanteux, H., Depelchin, B. O., Dhalluin, S., et al. (2012). Characterization of primary human hepatocytes, HepG2 cells, and HepaRG cells at the mRNA level and CYP activity in response to inducers and their predictivity for the detection of human hepatotoxins. *Cell Biol. Toxicol.* 28, 69–87. doi: 10.1007/s10565-011-9208-4

Gonzales, G. B., Van Camp, J., Vissenaekens, H., Raes, K., Smagghe, G., and Grootaert, C. (2015). Review on the use of cell cultures to study metabolism, transport, and accumulation of flavonoids: from mono-cultures to co-culture systems. *Comprehensive Rev. Food Sci. Food Safety* 14, 741–754. doi: 10.1111/1541-4337.12158

Grainger, C. I., Greenwell, L. L., Lockley, D. J., Martin, G. P., and Forbes, B. (2006). Calture of Calu-3 cells at the air interface provides a representative model of airway epithelial barrier. *Pharmaceut. Res.* 23, 1482–1490. doi: 10.1007/s11095-006-0255-0

Griffin, S. J., and Houston, J. B. (2005). Prediction of *in vitro* intrinsic clearance from hepatocytes: comparison of suspensions and monolayer cultures. *Drug Metab. Disposition* 33, 115–120. doi: 10.1124/dmd.33.1.

Gubbels-van Hal, W. M., Blaauboer, B. J., Barentsen, H. M., Hoitink, M. A., Meerts, I. A. T. M., and Van Der Hoeven, J. C. M. (2005). An alternative approach for the safety evaluation of new and existing chemicals, an exercise in integrated testing. *Regul. Toxicol. Pharmacol.* 42, 284–295. doi: 10.1016/j.yrtph.2005.05.002

Guguen-Guillouzo, C., Corlu, A., and Guillouzo, A. (2010). Stem cell-derived hepatocytes and their use in toxicology. *Toxicology* 270, 3–9. doi: 10.1016/j.tox.2009.09.019

Guguen-Guillouzo, C., and Guillouzo, A. (2010). "General review on *in vitro* hepatocyte models and their applications," in *Hepatocytes,* eds P. Maurel (New York, NY: Humana Press), 1–40. doi: 10.1007/978-1-60761-688-7_1

Guillouzo, A., Corlu, A., Aninat, C., Glaise, D., Morel, F., and Guguen-Guillouzo, C. (2007). The human hepatoma HepaRG cells: a highly differentiated model for studies of liver metabolism and toxicity of xenobiotics. *Chem. Biol. Interact.* 168, 66–73. doi: 10.1016/j.cbi.2006.12.003

Guo, L., Dial, S., Shi, L., Branham, W., Liu, J., Fang, J. L., et al. (2011). Similarities and differences in the expression of drug metabolizing enzymes between human hepatic cell lines and primary human hepatocytes. *Drug Metab. Dispos.* 39, 528–538. doi: 10.1124/dmd.110.035873

Haghi, M., Young, P. M., Traini, D., Jaiswal, R., Gong, J., and Bebawy, M. (2010). Time- and passage-dependent characteristics of a Calu-3 respiratory epithelial cell model. *Drug Devel Industrial Pharmacy* 36, 1207–1214. doi: 10.3109/03639041003695113

Hancock, M. J., and Elabbasi, N. (2018). *Modeling a Lung-On-A-Chip Microdevice*. COMSOL. Available online at: https://www.comsol.com/paper/download/257421/hancock_abstract.pdf

Hewitt, N. J., Gómez Lechón, M. J., Houston, J. B., Hallifax, D., Brown, H. S., Maurel, P., et al. (2007). Primary hepatocytes: current understanding of the regulation of metabolic enzymes and transporter proteins, and pharmaceutical practice for the use of hepatocytes in metabolism, enzyme induction, transporter, clearance, and hepatotoxicity studies. *Drug Metab. Rev.* 39, 159–234. doi: 10.1080/03602530601093489

Ho, C. T., Lin, R. Z., Chang, W. Y., Chang, H. Y., and Liu, C. H. (2006). Rapid heterogeneous liver-cell on-chip patterning via the enhanced field-induced dielectrophoresis trap. *Lab Chip* 6, 724–734. doi: 10.1039/b602036d

Höfer, T., Gerner, I., Gundert-Remy, U., Liebsch, M., Schulte, A., Spielmann, H., et al. (2004). Animal testing and alternative approaches for the human health risk assessment under the proposed new European chemicals regulation. *Arch. Toxicol.* 78, 549–564. doi: 10.1007/s00204-004-0577-9

Huh, D., Leslie, D. C., Matthews, B. D., Fraser, J. P., Jurek, S., Hamilton, G. A., et al. (2012). A human disease model of drug toxicity–induced pulmonary edema in a lung-on-a-chip microdevice. *Sci. Transl. Med.* 4:159ra147 doi: 10.1126/scitranslmed.3004249

Huh, D. D. (2015). A human breating lung-on-a-chip. *Ann. Am. Thoracic Soc.* 12, S42–S44. doi: 10.1513/AnnalsATS.201410-442MG

Ihekwereme, C., Esimone, C., Shao, D., and Agu, R. U. (2014). Preliminary studies on validation of Calu-3 cell line as a model for screening respiratory mucosa irritation and toxicity. *Pharmaceutics* 6, 268–280. doi: 10.3390/pharmaceutics6020268

Imura, Y., Yoshimura, E., and Sato, K. (2013). Microcirculation system with a dialysis part for bioassays evaluating anticancer activity and retention. *Analytical Chem.* 85, 1683–1688. doi: 10.1021/ac302938q

Jain, A., Barrile, R., van der Meer, A. D., Mammoto, A., Mammoto, T., De Ceunynck, K., et al. (2018). Primary human lung alveolus-on-a-chip model of intravascular thrombosis for assessment of therapeutics. *Clin. Pharmacol. Ther.* 103, 332–340. doi: 10.1002/cpt.742

Jean, J., and Pouliot, R. (2010). "*In vivo* and *in vitro* models of psoriasis," in *Tissue Engineering,* ed D. Eberli (Rijeka), 359–382.

Jie, M., Li, H. F., Lin, L., Zhang, J., and Lin, J. M. (2016). Integrated microfluidic system for cell co-culture and simulation of drug metabolism. *RSC Adv.* 6, 54564–54572. doi: 10.1039/C6RA10407J

Johnson, C. I., Argyle, D. J., and Clements, D. N. (2016). *In vitro* models for the study of osteoarthritis. *Vet. J.* 209, 40–49. doi: 10.1016/j.tvjl.2015.07.011

Katt, M. E., Placone, A. L., Wong, A. D., Xu, Z. S., and Searson, P. C. (2016). *In vitro* tumor models: advantages, disadvantages, variables, and selecting the right platform. *Front. Bioeng. Biotechnol.* 4:12. doi: 10.3389/fbioe.2016.00012

Klein, M., Thomas, M., Hofmann, U., Seehofer, D., Damm, G., and Zanger, U. M. (2015). A systematic comparison of the impact of inflammatory signaling on absorption, distribution, metabolism, and excretion gene expression and activity in primary human hepatocytes and HepaRG cells. *Drug Metab. Disposition* 43, 273–283. doi: 10.1124/dmd.114.060962

Konar, D., Devarasetty, M., Yildiz, D. V., Atala, A., and Murphy, S. V. (2016). Lung-on-a-chip technologies for disease modeling and drug development. *Biomed. Eng. Comput. Biol.* 7, 17–27. doi: 10.4137/BECB.S34252

Kramer, N. I., Di Consiglio, E., Blaauboer, B. J., and Testai, E. (2015). Biokinetics in repeated-dosing *in vitro* drug toxicity studies. *Toxicol. In Vitro* 30, 217–224. doi: 10.1016/j.tiv.2015.09.005

Kreft, M. E., Jerman, U. D., Lasic, E., Hevir-Kene, N., Lanisnik RiŽner, T., Peternel, L., et al. (2015). The characterization of the human cell line Calu-3 under different culture conditions and its use as an optimized *in vitro* model

to investigate bronchial epithelial function. *Eur. J. Pharmaceut. Sci.* 69, 1–9. doi: 10.1016/j.ejps.2014.12.017

Leclerc, E., Sakai, Y., and Fujii, T. (2004). Microfluidic PDMS (polydimethylsiloxane) bioreactor for large-scale culture of hepatocytes. *Biotechnol. Prog.* 20, 750–755. doi: 10.1021/bp0300568

LeCluyse, E. L. (2001). Human hepatocyte culture systems for the *in vitro* evaluation of cytochrome P450 expression and regulation. *Eur. J. Pharmaceut. Sci.* 13, 343–368. doi: 10.1016/S0928-0987(01)00135-X

Lee, H. L., Boccazzi, P., Ram, R. J., and Sinskey, A. J. (2006). Microbioreactor arrays with integrated mixers and fluid injectors for high-throughput experimentation with pH and dissolved oxygen control. *Lab on a Chip* 6, 1229–1235. doi: 10.1039/b608014f

Lee, K. H., Lee, J., and Lee, S. H. (2015). 3D liver models on a microplatform: well-defined culture, engineering of liver tissue and liver-on-a-chip. *Lab On A Chip* 15, 3822–3837. doi: 10.1039/C5LC00611B

Lerche-Langrand, C., and Toutain, H. J. (2000). Precision-cut liver slices: characteristics and use for *in vitro* pharmaco-toxicology. *Toxicology* 153, 221–253. doi: 10.1016/S0300-483X(00)00316-4

Lilienblum, W., Dekant, W., Foth, H., Gebel, T., Hengstler, J. G., Kahl, R., et al. (2008). Alternative methods to safety studies in experimental animals: role in the risk assessment of chemicals under the new European Chemicals Legislation (REACH). *Arch. Toxicol.* 82, 211–236. doi: 10.1007/s00204-008-0279-9

Lübberstedt, M., Müller-Vieira, U., Mayer, M., Biemel, K. M., Knöspel, F., Knobeloch, D., et al. (2011). HepaRG human hepatic cell line utility as a surrogate for primary human hepatocytes in drug metabolism assessment *in vitro*. *J. pharmacol. Toxicol. Methods* 63, 59–68. doi: 10.1016/j.vascn.2010.04.013

Mamlouk, M., Young, P. M., Bebawy, M., Haghi, M., Mamlouk, S., Mulay, V., et al. (2013). Salbutamol sulfate absorption across Calu-3 bronchial epithelia cell monolayer is inhibited in the presence of common anionic NSAIDs. *J. Asthma* 50, 334–341. doi: 10.3109/02770903.2013.773518

Maschmeyer, I., Lorenz, A. K., Schimek, K., Hasenberg, T., Ramme, A. P., Hübner, J., et al. (2015). A four-organ-chip for interconnected long-term co-culture of human intestine, liver, skin and kidney equivalents. *Lab Chip* 15, 2688–2699. doi: 10.1039/C5LC00392J

Memorial Sloan Kettering Cancer Center (2018). *Calu-3: Human Lung Cancer Cell Line*. Available online at https://www.mskcc.org/research-advantage/support/technology/tangible-material/calu-3-human-lung-cell-line (Accessed March 10, 2018).

Mermoud, Y., Felder, M., Stucki, A. O., and Guenat, O. T. (2018). Microimpedance tomography system to monitor cell activity and membrane movements in a breathing lung-on-chip. *Sensors Actuators B* 255, 3647–3653. doi: 10.1016/j.snb.2017.09.192

Metzger, M. (2018). *Recent Research Breakthroughs in Lung-on-Chip Technology*. Elveflow. Available online at https://www.elveflow.com/organs-on-chip/organs-chip-review/microfluidic-lung-on-chip/

Mills, J. B., Rose, K. A., Sadagopan, N., Sahi, J., and de Morais, S. M. (2004). Induction of drug metabolism enzymes and MDR1 using a novel human hepatocyte cell line. *J. Pharmacol. Exp. Therapeut.* 309, 303–309. doi: 10.1124/jpet.103.061713

Mulay, A., Akram, K. M., Williams, D., Armes, H., Russell, C., Hood, D., et al. (2016). An *in vitro* model of murine middle ear epithelium. *Dis. Models Mech.* 9, 1405–1417. doi: 10.1242/dmm.026658

O'Brien, P. J., and Siraki, A. G. (2005). Accelerated cytotoxicity mechanism screening using drug metabolising enzyme modulators. *Curr. Drug Metab.* 6, 101–109. doi: 10.2174/1389200053586082

Ogunshola, O. O. (2011). *In vitro* modeling of the blood-brain barrier: simplicity versus complexity. *Curr. Pharmaceut. Design* 17, 2755–2761. doi: 10.2174/138161211797440159

Ong, H. X., Traini, D., and Young, P. M. (2013). Pharmaceutical applications of the Calu-3 lung epithelia cell line. *Expert Opin. Drug Delivery* 10, 1287–1302. doi: 10.1517/17425247.2013.805743

Ostrovidov, S., Jiang, J., Sakai, Y., and Fujii, T. (2004). Membrane-based PDMS microbioreactor for perfused 3D primary rat hepatocyte cultures. *Biomed. Microdevices* 6, 279–287. doi: 10.1023/B:BMMD.0000048560.96140.ca

Paini, A., Mennecozzi, M., Horvat, T., Gerloff, K., Palosaari, T., Sala Benito, J. V., et al. (2017). Practical use of the virtual cell based assay: simulation of repeated exposure experiments in liver cell lines. *Toxicol In Vitro* 45, 233–240. doi: 10.1016/j.tiv.2016.10.007

Palabiyik, S. S., Karakus, E., Halici, Z., Cadirci, E., Bayir, Y., Ayaz, G., et al. (2016). The protective effects of carvacrol and thymol against paracetamol–induced toxicity on human hepatocellular carcinoma cell lines (HepG2). *Hum. Exp. Toxicol.* 35, 1252–1263. doi: 10.1177/0960327115627688

Parker, K. K., Tan, J., Chen, C. S., and Tung, L. (2008). Myofibrillar architecture in engineered cardiac myocytes. *Circul. Res.* 103, 340–342. doi: 10.1161/CIRCRESAHA.108.182469

Patrachari, A. R., Podichetty, J. T., and Madihally, S. V. (2012). Application of computational fluid dynamics in tissue engineering. *J. Biosci. Bioeng.* 114, 123–132. doi: 10.1016/j.jbiosc.2012.03.010

Podichetty, J. T., Bhaskar, P. R., Singarapu, K., and Madihally, S. V. (2015). Multiple approaches to predicting oxygen and glucose consumptions by HepG2 cells on porous scaffolds in an axial-flow bioreactor. *Biotechnol. Bioeng.* 112, 393–404. doi: 10.1002/bit.25355

Powers, M. J., Domansky, K., Kaazempur-Mofrad, M. R., Kalezi, A., Capitano, A., Upadhyaya, A., et al. (2002). A microfabricated array bioreactor for perfused 3D liver culture. *Biotechnol. Bioeng.* 78, 257–269. doi: 10.1002/bit.10143

Pu, F., Rhodes, N. P., Bayon, Y., Chen, R., Brans, G., Benne, R., et al. (2010). The use of flow perfusion culture and subcutaneous implantation with fibroblast-seeded PLLA-collagen 3D scaffolds for abdominal wall repair. *Biomaterials* 31, 4330–4340. doi: 10.1016/j.biomaterials.2010.02.010

Ramadan, Q., Jafarpoorchekab, H., Huang, C., Silacci, P., Carrara, S., Koklü, G., et al. (2013). NutriChip: nutrition analysis meets microfluidics. *Lab Chip* 13, 196–203. doi: 10.1039/C2LC40845G

Rojahn, S. Y. (2012). *Organ-on-A-Chip Mimics Deadly Lung Condition*. Cambridge, MA: MIT Technology Review.

Sala Benito, J. V. , Paini, A., Richarz, A. N., Meinl, T., Berthold, M. R., Cronin, M. T. D., et al. (2017). Automated workflows for modelling chemical fate, kinetics and toxicity. *Toxicol. In Vitro* 45, 249–257. doi: 10.1016/j.tiv.2017.03.004

Samatiwat, P., Takeda, K., Satarug, S., Ohba, K., Kukongviriyapan, V., and Shibahara, S. (2016). Induction of MITF expression in human cholangiocarcinoma cells and hepatocellular carcinoma cells by cyclopamine, an inhibitor of the Hedgehog signaling. *Biochem. Biophys. Res. Commun.* 470, 144–149. doi: 10.1016/j.bbrc.2016.01.010

Savla, U., Olson, L. E., and Waters, C. M. (2004). Mathematical modeling of airway epithelial wound closure during cyclic mechanical strain. *J. Appl. Physiol.* 96, 566–574. doi: 10.1152/japplphysiol.00510.2003

Scheers, N. M., Almgren, A. B., and Sandberg, A. S. (2014). Proposing a Caco-2/HepG2 cell model for *in vitro* iron absorption studies. *J. Nutr. Biochem.* 25, 710–715. doi: 10.1016/j.jnutbio.2014.02.013

Sia, S. K., and Whitesides, G. M. (2003). Microfluidic devices fabricated in poly (dimethylsiloxane) for biological studies. *Electrophoresis* 24, 3563–3576. doi: 10.1002/elps.200305584

Soldatow, V. Y., LeCluyse, E. L., Griffith, L. G., and Rusyn, I. (2013). *In vitro* models for liver toxicity testing. *Toxicol. Res.* 2, 23–39. doi: 10.1039/C2TX20051A

Spencer, T. J., Hidalgo-Bastida, L. A., Cartmell, S. H., Halliday, I., and Care, C. M. (2013). *In silico* multi-scale model of transport and dynamic seeding in a bone tissue engineering perfusion bioreactor. *Biotechnol. Bioeng.* 110, 1221–1230. doi: 10.1002/bit.24777

Stewart, C. E., Torr, E. E., Mohd Jamili, N. H., Bosquillon, C., and Sayers, I. (2012). Evaluation of differentiated human bronchial epithelial cell culture systems for asthma research. *J. Allergy* 2012:943982. doi: 10.1155/2012/943982

Stoppelkamp, S., Bell, H. S., Palacios-Filardo, J., Shewan, D. A., Riedel, G., and Platt, B. (2011). *In vitro* modelling of Alzheimer's disease: degeneration and cell death induced by viral delivery of amyloid and tau. *Exp. Neurol.* 229, 226–237. doi: 10.1016/j.expneurol.2011.01.018

Theobald, J., Ghanem, A., Wallisch, P., Banaeiyan, A. A., Andrade-Navarro, M. A., Taskova, K., et al. (2017). Liver-kidney-on-chip to study toxicity of drug metabolites. *ACS Biomaterials Sci. Eng.* 4, 78–89. doi: 10.1021/acsbiomaterials.7b00417

Tomida, T., Okamura, H., Satsukawa, M., Yokoi, T., and Konno, Y. (2015). Multiparametric assay using HepaRG cells for predicting drug-induced liver injury. *Toxicol. Lett.* 236, 16–24. doi: 10.1016/j.toxlet.2015.04.014

Tumiati, L. C., Mickle, D. A. G., Weisel, R. D., Williams, W. G., and Li, R.K. (1994). An *in vitro* model to study myocardial ischemic injury. *J. Tissue Cult. Methods* 16, 1–9. doi: 10.1007/BF01404830

Vunjak Novakovic, G., Eschenhagen, T., and Mummery, C. (2014). Myocardial tissue enginreeing: *in vitro* models. *Cold Spring Harb. Perspect. Med.* 4:a014076. doi: 10.1101/cshperspect.a014076

Wendt, D., Riboldi, S. A., Cioffi, M., and Martin, I. (2008). *Bioreactors in Tissue Engineering: Scientific Challenges and Clinical Perspectives*. Berlin; Heidelberg: Springer. doi: 10.1016/B978-0-12-370869-4.00016-1

Weng, Y. S., Chang, S. F., Shih, M. C., Tseng, S. H., and Lai, C. H. (2017). Scaffold-free liver-on-a-chip with multiscale organotypic cultures. *Adv. Materials* 29:1701545. doi: 10.1002/adma.201701545

Wilkening, S., Stahl, F., and Bader, A. (2003). Comparison of primary human hepatocytes and hepatoma cell line Hepg2 with regard to their biotransformation properties. *Drug Metab. Dispos.* 31, 1035–1042. doi: 10.1124/dmd.31.8.1035

Wit, A. L., Bruce, N. G., and Damato, A. N. (1971). An *in vitro* model of paroxymal supraventricular tachycardia. *Circulation* 43, 862–875. doi: 10.1161/01.CIR.43.6.862

Yang, J., Huang, Y., Wang, X. B., Becker, F. F., and Gascoyne, P. R. (1999). Cell separation on microfabricated electrodes using dielectrophoretic/gravitational field-flow fractionation. *Anal. Chem.* 71, 911–918. doi: 10.1021/ac981250p

Yang, X., Li, K., Zang, X., Liu, C., Guo, B., Wen, W., et al. (2018). Nanofiber membrane supported lung-on-a-chip microdevice for anti-cancer drug testing. *Lab Chip* 18, 486–495. doi: 10.1039/c7lc01224a

Yu, L. J., Matias, J., Scudiero, D. A., Hite, K. M., Monks, A., Sausville, E. A., et al. (2001). P450 enzyme expression patterns in the NCI human tumor cell line panel. *Drug Metab. Disposition* 29, 304–312.

Zaldívar, J. M., and Baraibar, J. (2011). A biology-based dynamic approach for the reconciliation of acute and chronic toxicity tests: application to *Daphnia magna*. *Chemosphere* 82, 1547–1555. doi: 10.1016/j.chemosphere.2010.11.062

Zaldívar, J. M., Mennecozzi, M., Marcelino Rodrigues, R., and Bouhifd, M. (2010). *A Biology-Based Dynamic Approach for the Modelling of Toxicity in Cell-Based Assays. Part I: Fate Modelling*. Luxembourg: European Commission.

Zeilinger, K., Freyer, N., Damm, G., Seehofer, D., and Knöspel, F. (2016). Cell sources for *in vitro* human liver cell culture models. *Exp. Biol. Med.* 241, 1684–1698. doi: 10.1177/1535370216657448

Zhang, M. Y., Lee, P. J., Hung, P. J., Johnson, T., Lee, L. P., and Mofrad, M. R. (2008). Microfluidic environment for high density hepatocyte culture. *Biomed. Microdevices* 10, 117–121. doi: 10.1007/s10544-007-9116-9

Zhang, Y. S., Oklu, R., and Albadawi, H. (2017). Bioengineered *in vitro* models of thrombosis: methods and techniques. *Cardiovasc. Diagn. Ther.* 7:3. doi: 10.21037/cdt.2017.08.08

Zhu, Y., Chidekel, A., and Shaffer, T. H. (2010). Cultured human airway epithelial cells (Calu-3): a model of human respiratory function, structure, and inflammatory responses. *Crit. Care Res.* 2010:394578. *Pract.* doi: 10.1155/2010/394578

Conflict of Interest Statement: The authors declare that the research was conducted in the absence of any commercial or financial relationships that could be construed as a potential conflict of interest.

frontiers in Bioengineering and Biotechnology

ORIGINAL RESEARCH
published: 09 May 2018
doi: 10.3389/fbioe.2018.00060

Zeta Potential Measurements on Solid Surfaces for *in Vitro* Biomaterials Testing: Surface Charge, Reactivity Upon Contact With Fluids and Protein Absorption

Sara Ferraris[1], *Martina Cazzola*[1], *Veronica Peretti*[1], *Barbara Stella*[2] *and Silvia Spriano*[1]*

[1] *Department of Applied Science and Technology, Institute of Materials Physics and Engineering, Politecnico di Torino, Turin, Italy,* [2] *Dipartimento di Scienza e Tecnologia del Farmaco, Università degli Studi di Torino, Turin, Italy*

Surface properties of biomaterials (e.g., roughness, chemical composition, charge, wettability, and hydroxylation degree) are key features to understand and control the complex interface phenomena that happens upon contact with physiological fluids. Numerous physico-chemical techniques can be used in order to investigate in depth these crucial material features. Among them, zeta potential measurements are widely used for the characterization of colloidal suspensions, but actually poorly explored in the study of solid surfaces, even if they can give significant information about surface charge in function of pH and indirectly about surface functional groups and reactivity. The aim of the present research is application of zeta potential measurements of solid surfaces for the *in vitro* testing of biomaterials. In particular, bare and surface modified Ti6Al4V samples have been compared in order to evaluate their isoelectric points (IEPs), surface charge at physiological pH, *in vitro* bioactivity [in simulated body fluid (SBF)] and protein absorption. Zeta potential titration was demonstrated as a suitable technique for the surface characterization of surface treated Ti6Al4V substrates. Significant shift of the isoelectric point was recorded after a chemical surface treatment (because of the exposition of hydroxyl groups), SBF soaking (because of apatite precipitation IEP moves close to apatite one) and protein absorption (IEP moves close to protein ones). Moreover, the shape of the curve gives information about exposed functional groups (e.g., a plateau in the basic range appears due to the exposition of acidic OH groups and in the acidic range due to exposition of basic NH_2 groups).

Keywords: zeta potential, biomaterials, *in vitro* testing, surface charge, reactivity, protein absorption

OPEN ACCESS

Edited by:
Nihal Engin Vrana,
Protip Medical, France

Reviewed by:
Alina Vladescu,
National Institute for Research and Development in Optoelectronics, Romania
Eda Ayse Aksoy,
Hacettepe University, Turkey

***Correspondence:**
Silvia Spriano
silvia.spriano@polito.it

Specialty section:
This article was submitted to Biomaterials, a section of the journal Frontiers in Bioengineering and Biotechnology

Received: *28 February 2018*
Accepted: *25 April 2018*
Published: *09 May 2018*

Citation:
Ferraris S, Cazzola M, Peretti V, Stella B and Spriano S (2018) Zeta Potential Measurements on Solid Surfaces for in Vitro Biomaterials Testing: Surface Charge, Reactivity Upon Contact With Fluids and Protein Absorption. Front. Bioeng. Biotechnol. 6:60. doi: 10.3389/fbioe.2018.00060

INTRODUCTION

The biological response to implanted biomaterials strongly depends on their surface properties, such as roughness, chemical composition, charge, wettability and hydroxylation degree. These features drive the absorption of water molecules, ions and proteins, immediately after implantation and consequently affect the ability of materials to interact with cells and also with bacteria, eventually present at the implant site (Kasemo, 2002).

Numerous techniques can be employed for surface characterization of biomaterials (Voros et al., 2001): Field Emission Scanning Electron Microscopy (FESEM) is often used for morphological evaluation together with Atomic Force Microscopy (AFM). X-ray Photoelectron Spectroscopy (XPS) is applied for the investigation of chemical composition and chemical functional groups, as well as Fourier Transformed Infrared (FTIR) and Raman Spectroscopies. The same techniques can be employed for the investigation of protein absorption phenomena, together with ellipsometry, quartz crystal microbalance, circular dichroism, bicichroninic acid assay (BCA) and fluorescent o radiolabeling techniques (Tengvall, 2001; Rabe et al., 2011; Silva-Bermudez and Rodil, 2013).

Among them, zeta potential measurements are widely applied in the field of colloidal suspensions (for the investigation of their stability, Bhattacharjee, 2016), but they are still poorly considered in the case of solid surfaces and almost unexplored for the investigation of protein absorption on biomaterials. To this regard, zeta potential describes the surface charging behavior in contact with water based electrolytes and gives information about the isoelectric point, the surface charge in function of pH, but also (indirectly) of the functional groups exposed at the solid-liquid interface, the reactivity of the surface in the test solution and absorption processes (Luxbacher, 2014).

When a material comes into contact with water-based media (such as physiological fluids) a surface charge is developed at the interface. This phenomenon has different causes depending on the surface characteristics: in case of hydrophobic surfaces with no functional groups, the exposed surface charge is due to replacement of the adsorbed water molecules with ions (OH^-, H_3O^+); on the other hand, in case of specific functional groups exposed on the surface, acid-basic reactions between the liquid medium and these groups can take part (e.g., dissociation of the hydroxyl groups or protonation of the amine groups) with consequent development of charges (Luxbacher, 2014).

The development of a charge at the solid-liquid interface is consequent to counterions distribution in the liquid. The surface potential decays increasing the distance from the surface. This phenomenon can be described by means of the Electrochemical Double Layer (EDL) model which defines a "*stationary layer*" (stationary immobile layer) and a "*diffuse layer*" (diffuse mobile layer) of counterions that compensate the surface charge. The zeta potential is defined as the potential at the outside of the stationary layer (Luxbacher, 2014). A schematization of the surface charge development at the solid-liquid interface and of the EDL model as well as of the surface and zeta potential definitions is reported in **Figure 1A**.

Considering the solid-liquid interface with the above described development of a surface charge, if the water based medium moves, its flow will cause the motion of the counterions, that compensate the surface charge, in the direction of the flow itself. The consequent charge separation causes a difference in the electrical potential called streaming potential. This physical entity can be used for the determination of the zeta potential of solid surfaces by means of the so called streaming potential technique (Luxbacher, 2014) (**Figure 1B**). This method has been employed in the present research for the characterization of bulk biomaterials.

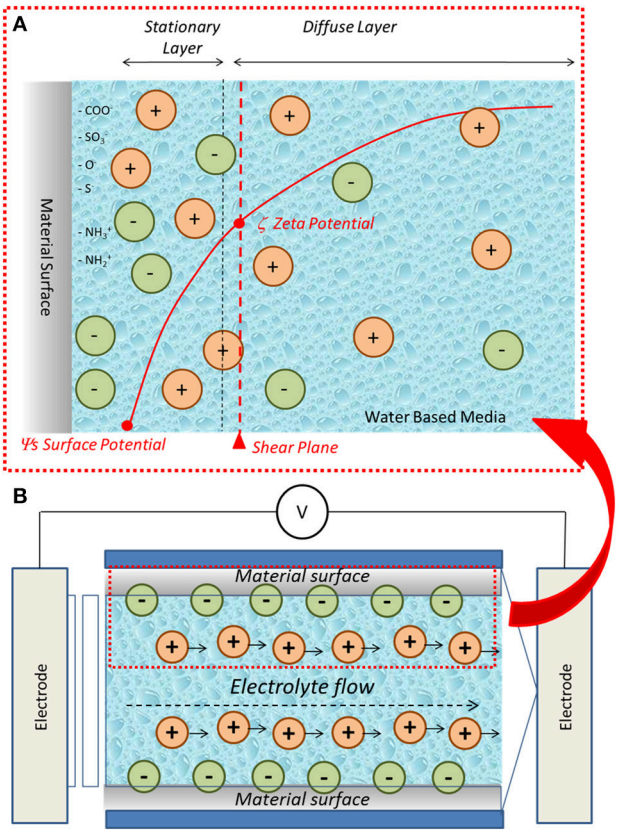

FIGURE 1 | (A) Schematic representation of charge development at biomaterial-water based medium interface and zeta potential, **(B)** schematic representation of the streaming potential technique for the measurement of solid surface zeta potential.

In particular, the study of different surface modifications, of *in vitro* bioactivity and of protein absorption have been carried out in the present research by means of zeta potential titrations on solid surfaces. At the best of author knowledge, this is the first time in which this technique is employed for the investigation of surface modifications, bioactivity and protein absorption. The obtained results suggest that zeta potential measurements can be extremely sensitive and useful in the in depth understanding of surface properties of biomaterials.

MATERIALS AND METHODS

Samples Preparation

Ti6Al4V disks (2 mm thick, 10 mm in diameter) were obtained from cylindrical bars (ASTM B348, gr5, Titanium Consulting and Trading) by automatic cutting (Brillant 220, ATM GmbH, Mammelzen, Germany, provided with an alumina blade) and employed as substrate in the experimental study. Specimens were manually polished with SiC abrasive papers (120–4,000 grit) and

colloidal silica suspension in order to obtain mirror polished Ti6Al4V (Ti6Al4V – MP).

Two different surface modification processes were examined in the present study.

The first one is a chemical treatment aimed at the obtainment of bioactive titanium surfaces for bone integration (Ti6Al4V – CT). It is a patented process which foresees a first etching in hydrofluoric acid followed by controlled oxidation in hydrogen peroxide (Spriano et al., 2007; Ferraris et al., 2011, 2015).

The second one is a coating of titanium boride finalized to better fretting, corrosion and wear resistance (Ti6Al4V – B-coat). The coating is obtained by means of a thermal diffusion process from a boriding powder mixture (50wt% B, 15wt% Na2B4O7, and 35wt% C) in Ar atmosphere for 3.5 h at 800°C, following the protocol of Sarman et al. (2012).

In Vitro Bioactivity Evaluation

In order to evaluate inorganic bioactivity, modified samples (only Ti6Al4V – CT were tested because are intended for bone integration) were soaked in Simulated Body Fluid at pH 7.4 (SBF) (Kokubo and Takadama, 2006) up to 28 days in order to induce apatite precipitation. Refresh of the solution was performed every 2 days. Samples were gently washed at the end of soaking period and dried under a laminar flow cabinet in order to avoid contaminations. In order to compare Ti6Al4V – CT with a surface completely covered by hydroxyapatite, only the sample after 28 days soaking was analyzed in the present research work. Two samples per type were used for *in vitro* bioactivity tests.

Protein Absorption

Bovine Serum Albumin (BSA) (Sigma Aldrich, Saint Louis, USA) was used as model protein for absorption studies. A 20 mg/ml solution of the protein in PBS was prepared in order to mimic the concentration of bovine serum. Each sample (Ti6Al4V – MP, Ti6Al4V – CT, and Ti6Al4V – B-coat) was introduced in a multi well plate and covered with 1ml of BSA solution. The plate was then sealed with parafilm, wrapped in an aluminum foil and stored at 37°C for 2 h in an incubator. At the end of soaking, samples were removed from plates, rinsed in ultrapure water and dried under laminar flow cabinet. Five samples per type were used for protein absorption studies.

Zeta Potential Measurements

The zeta potential was measured by means of an electrokinetic analyzer (SurPASS, Anton Paar) equipped with an adjustable gap cell. The surface zeta potential was determined in function of pH in a 0.001 M KCl electrolyte solution varying the solution pH by addition of 0.05M HCl or 0.05M NaOH through the instrument automatic titration unit. Separate couples of samples were used for the acidic and basic titrations in order to avoid artifacts due to surface reactions during the measurement. Four measurements were carried out for each pH point.

XPS Measurements

The surface chemical composition and the presence of specific functional groups were investigated by means of XPS analyses (XPS, XPS, PHI 5000 VERSA PROBE, PHYSICAL ELECTRONICS), in survey and high resolution (C, Ti, O) modes respectively. The high resolution spectra were referenced by setting the hydrocarbon C1s peak to 284.80 eV in order to guarantee the charging effect compensation.

RESULTS

Evaluation of the Surface Modifications

The graphs of zeta potential vs. pH of Ti6Al4V – MP and Ti6Al4V – CT are reported in **Figure 2**, together with a schematic representation of the surface and its XPS high resolution spectrum of the oxygen region.

The comparison between the two zeta potential titration curves (**Figure 2C**) highlights an acidic shift of the IEP (from 4.7 to at about 2) after CT treatment. Moreover, a plateau appears in the basic region.

The graphs of zeta potential vs. pH on Ti6Al4V – MP and Ti6al4V – B-coat are reported in **Figure 3** together with a schematic representation of the surface and its XPS high resolution spectrum of the oxygen region.

Similarly to Ti6Al4V – CT sample, the B-coating induces an acidic shift of the IEP (from 4.7 to 3) and the appearance of a plateau in the basic region.

Investigation of *in Vitro* Bioactivity

The graphs of zeta potential vs. pH of Ti6Al4V – CT and Ti6Al4V – CT after 28 days in SBF are reported in **Figure 4**, together with the FESEM image of the surface before and after soaking, with a well-developed apatite layer after 28 days in SBF.

The result shows a shift of the IEP of Ti6Al4V – CT surface to more basic values (4.5), close to the ones reported in literature for hydroxyapatite (Botelho et al., 2002).

Investigation of Protein Absorption

Zeta potential measurements vs. pH of Ti6Al4V – MP, Ti6Al4V – CT, and Ti6Al4V – B-coat after BSA absorption are reported in **Figure 5**, together with the zeta potential titration curve of an albumin solution obtained by electrophoretic measurements (insert).

The IEP of all the tested surface is similar after BSA absorption, even if with some small variations, and close to the one of the BSA solution measured by the electrophoretic technique.

The presence of two plateaus (in the basic and acidic regions) can be noticed for Ti6Al4V – MP, while only the basic plateau is visible on Ti6Al4V – CT and Ti6Al4V – B-coat samples.

DISCUSSION

Zeta potential measurements (based on the electrophoretic mobility of particles) are widely employed for the characterization of colloidal suspensions (Bhattacharjee, 2016). On the other hand, zeta potential measurements on solid surfaces are less usual. Contact angle titatration has been proposed for the evaluation of the isoelectric point of solid samples (Chedov and Logan, 2004), but the result is limited to the IEP value and measurements are quite complex with

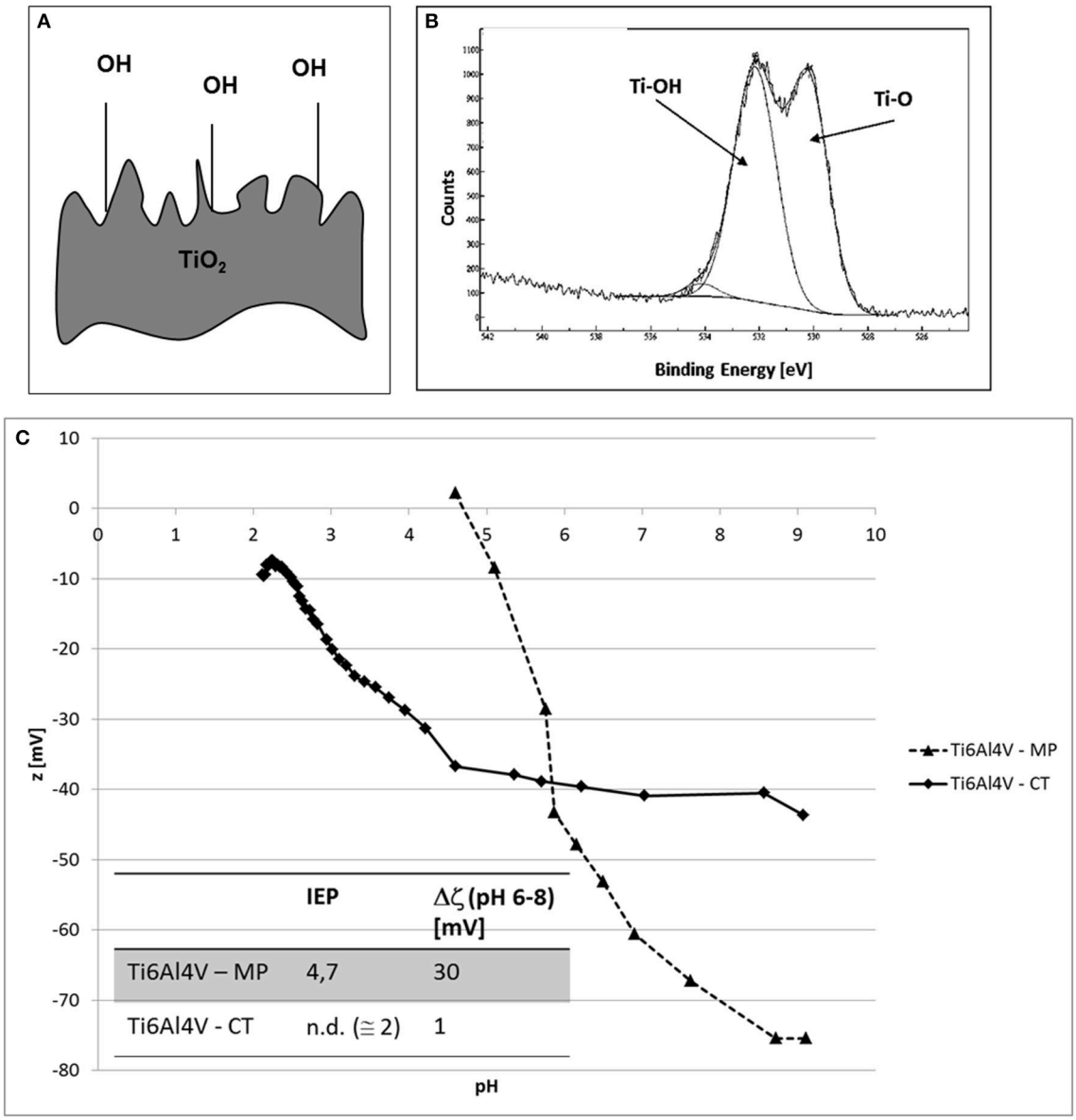

FIGURE 2 | (A) Schematic representation of Ti6Al4V – CT surface, **(B)** XPS high resolution spectrum of the oxygen region for Ti6Al4V – CT and **(C)** zeta potential vs. pH measurements of Ti6Al4V – MP and Ti6Al4V – CT samples.

consequent difficulties in the obtainment of reliable results (Spriano et al., 2017). Electrokinetic measurements of the zeta potential of solid surfaces can be more interesting for the determination of both the IEP value and also of the zeta potential in function of pH, making possible a more in depth understanding of surface properties (Cai et al., 2006; Luxbacher, 2014; Spriano et al., 2017).

Characterization of different surfaces by means of the streaming potential technique for the determination of zeta potential of solid surfaces can give interesting and useful information about surface chemistry, as here discussed. The IEP of Ti6Al4V – MP sample is 4.7, according to the values reported in literature for titanium surfaces (Bal and Rahaman, 2012). For both the considered treatments (Ti6Al4V – CT and Ti6Al4V – B-coat), a shift of the IEP to more acidic values, compared to bare Ti6Al4V, can be noticed, with major evidence in the case of Ti6Al4V – CT. In addition, the appearance of a plateau in the basic region can be noticed. These two results can be associated with the surface enrichment in hydroxyl groups with acidic behavior after the surface modification process, in accordance with XPS results (**Figures 1B**, **2B**). The plateau starts around pH 4.5 in the case of Ti6Al4V – CT and around pH6 in the case of Ti6Al4V – B-coat: this evidence can be related to a different acidic strength of the OH groups on the two

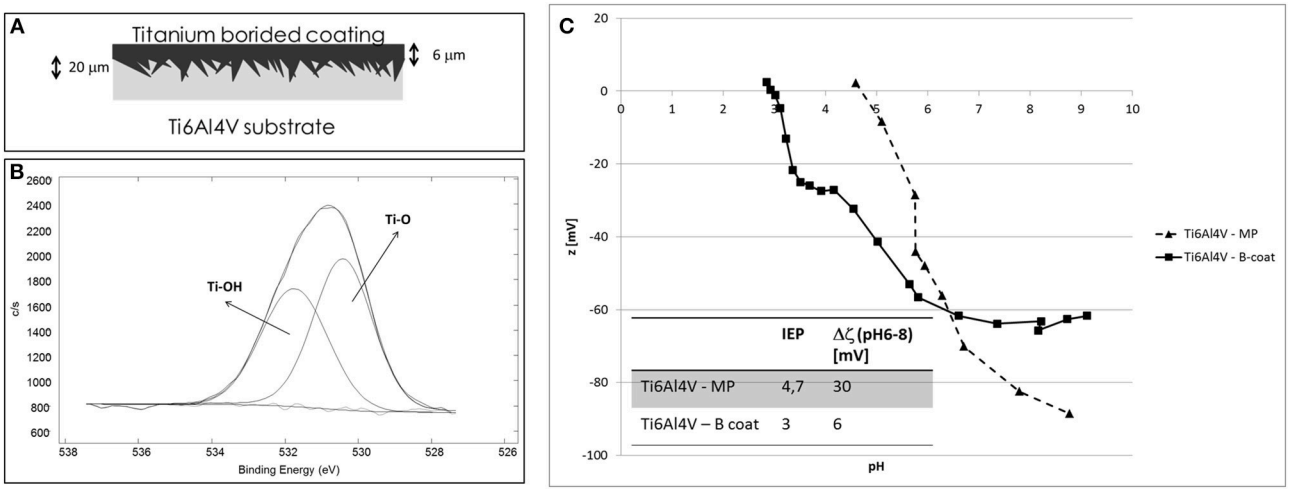

FIGURE 3 | (A) Schematic representation of Ti6Al4V – B-coat surface, **(B)** XPS high resolution spectrum of the oxygen region for Ti6Al4V – B-coat, and **(C)** zeta potential vs. pH measurements of Ti6Al4V – MP and Ti6Al4V – B-coat samples.

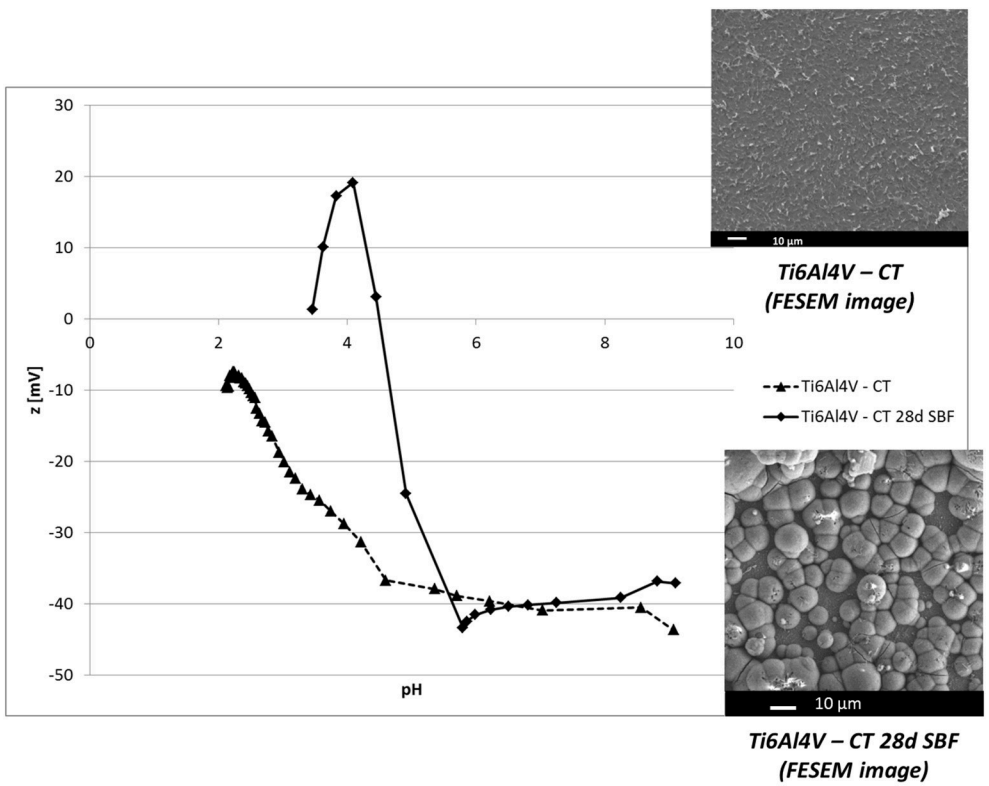

FIGURE 4 | Zeta potential vs. pH of Ti6Al4V – CT and Ti6Al4V – CT after 28 in SBF. Inserts: FESEM image of Ti6Al4V – CT before and after 28 days in SBF (apatite deposition).

different surfaces. They act as a much more strong acid in the first case with a complete deprotonation at a lower pH value. The slope of the curve before the plateau can give information about surface hydrophilicity/hydrophobicity, in fact a hydrophobic surface, which weakly bonds water molecules and easily exchange them with ions from the solution, shows an high slope. In fact, Ti6Al4V – MP shows wettability lower than Ti6Al4V – CT, in accordance with the wettability measurements performed by the sessile drop method using ultrapure water as wetting fluid (81.4° for Ti6Al4V – MP and 76.0° for Ti6Al4V – CT, as reported

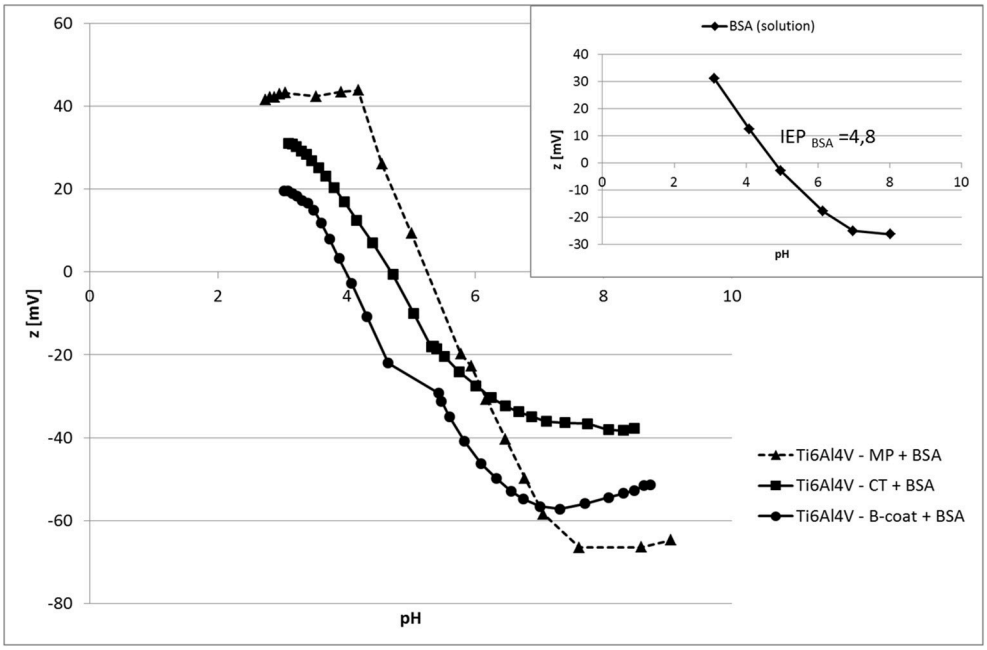

FIGURE 5 | Zeta potential measurements vs. pH of Ti6Al4V – MP, Ti6Al4V – CT, and Ti6Al4V – B-coat after BSA absorption. Insert: zeta potential of an albumin solution (electrophoretic measurements).

in Ferraris et al., 2011). Both hydrophilicity/hydrophobicity and acidic/basic behavior of surface functional groups have a great effect on bioactivity and surface reactions of a bio-surface with physiological fluid, that is why this kind of measurement is of great relevance.

After SBF soaking for 28 days, the surface of Ti6Al4V – CT is completely covered by a hydroxyapatite layer (FESEM observation in the insert of **Figure 4**). Apatite deposition on Ti6Al4V – CT surfaces was demonstrated by the authors starting from 14 days soaking (Ferraris et al., 2011).

Zeta potential measurements in function of pH revealed a significant change on the surface, in fact the IEP results shifted close to the one of apatite (Botelho et al., 2002) and the shape of the curve changes, as indication of a different surface chemistry. A plateau persists in the basic region in accordance with the high density of acidic OH groups in hydroxyapatite. In the acid range, chemical stability of HA can be estimated by the maximum at pH 4, at this pH in fact the z value becomes unstable, that is related to its reaction with the solution: this information can be related to "maturation" and chemical stability of the apatite layer. All things considered, zeta potential titration curve can be an interesting tool in order to characterize the mechanism, kinetic and type of HA formed on bioactive materials.

Zeta potential measurement can be also a technique for evaluate protein absorption on bio-surfaces. The IEP moves in the tested materials close to the one measured with pure albumin by electrophoretic technique (**Figure 5**, insert) confirming the effective absorption of BSA on all the tested materials. The shape of the curves, however, is different among the tested surfaces. In fact, while two plateau (one in the basic region and one in the acidic one) are observable on Ti6Al4V – MP +BSA, there is only the acidic one on Ti6Al4V – CT + BSA and Ti6Al4V – B-coat+BSA. The acidic plateau can be associated with the presence of basic functional groups (NH_2 groups of the BSA molecule), while the basic one with acidic functional groups (COOH of BSA molecule). The here reported results suggest a different disposition of BSA on Ti6Al4V – MP compared to Ti6Al4V – CT and Ti6Al4V – B-coat. This difference can be associated with the presence of OH groups on both Ti6Al4V – CT and Ti6Al4V – B-coat, as underlined by XPS and zeta potential measurements, previously discussed, while the Ti6Al4V – MP surface is a hydrophobic surface without specific functional groups. Moreover, the slope of the curve before the plateau is higher for Ti6Al4V – MP than for Ti6Al4V – CT and Ti6Al4V – B-coat, suggesting that BSA is adsorbed in a highly hydrophilic configuration onto Ti6Al4V – CT and Ti6Al4V – B-coat surfaces. The amount and configuration of protein adsorption on bio-surfaces is of great relevance in determining their biological response and zeta potential titration curves can give a contribution to understand these issues.

In conclusion, zeta potential titration curves of bulk biomaterials, linked to XPS, wettability and other chemical surface analyses, can be of great interest in order to understand the behavior of bio-surfaces in contact with SBF or protein solutions, to design novel biomaterials and to explain their *in vivo* behavior. The technique is extremely sensitive and, in combination with other measurements (e.g., XPS) can support an in depth understanding of surface modifications after chemical treatments or interface reactions with fluids of biological interest. In the present study the possibility to detect changes in the

isoelectric point of the surface after chemical treatments, apatite precipitation or protein absorption has been demonstrated for the first time on solid titanium surfaces. Moreover it was observed that the technique is suitable for the investigation of surface functional groups exposed on the surfaces in different media and at different pH. In order to identify these groups the combination of zeta potential measurements and XPS analyses result crucial.

AUTHOR CONTRIBUTIONS

SF, MC, and VP: performed the experiments, discussed the results and wrote the first draft of the work; BS: participate to experimental activity, discussion, and paper drafting; SS: coordinated the work, discussed the results, participated to the first draft of the paper, and performed its final revision.

REFERENCES

Bal, B. S., and Rahaman, M. N. (2012). Orthopedic applications of silicon nitride ceramics. *Acta Biomater.* 8, 2889–2898. doi: 10.1016/j.actbio.2012.04.031

Bhattacharjee, S. (2016). DLS and zeta potential – what they are and what they are not? *J. Control Release* 235, 337–351. doi: 10.1016/j.jconrel.2016.06.017

Botelho, C. M., Lopes, M. A., Gibson, I. R., Best, S. M., and Santos, J. D. (2002). Structural analysis of Si-substituted hydroxyapatite: zeta potential and X-ray photoelectron spectroscopy. *J. Mater. Sci. Mater. Med.* 13, 1123–1127. doi: 10.1023/A:1021177601899

Cai, K., Frant, M., Bossert, J., Hildebrand, G., Liefeith, K., and Jandt, K. D. (2006). Surface functionalized titanium thin films: zeta-potential, protein adsorption and cell proliferation. *Colloids Surf. B Biointerfaces* 50, 1–8. doi: 10.1016/j.colsurfb.2006.03.016

Chedov, D., and Logan, E. L. B. (2004). Surface charge properties of oxides and hydroxides formed on metal substrates determined by contact angle titration. *Colloids Surf. A Physicochem. Eng. Asp.* 240, 211–223. doi: 10.1016/j.colsurfa.2004.03.022

Ferraris, S., Bobbio, A., Miola, M., and Spriano, S. (2015). Micro and nano-textured, hydrophilic and bioactive titanium dental implants. *Surf. Coat. Tech.* 276, 374–383. doi: 10.1016/j.surfcoat.2015.06.042

Ferraris, S., Spriano, S., Pan, G., Venturello, A., Bianchi, C. L., Chiesa, R., et al. (2011). Surface modification of Ti-6Al-4V alloy for biomineralization and specific biological response: part I, inorganic modification. *J. Mater. Sci. Mater. Med.* 22, 533–545. doi: 10.1007/s10856-011-4246-2

Kasemo, B. (2002). Biological surface science. *Surf. Sci.* 500, 656–677. doi: 10.1016/S0039-6028(01)01809-X

Kokubo, T., and Takadama, H. (2006). How useful is SBF in predicting *in vivo* bone bioactivity. *Biomaterials* 27, 2907–2915 doi: 10.1016/j.biomaterials.2006.01.017

Luxbacher, T. (2014). *The ZETA Guide Principles of the Streaming Potential Technique*. Graz: Anton Paar.

Rabe, M., Verdes, D., and Seeger, S. (2011). Understanding protein adsorption phenomena at solid surfaces. *Adv. Colloid Interface Sci.* 162, 87–106. doi: 10.1016/j.cis.2010.12.007

Sarman, B., Tikekar, N. M., and Ravi Chandran, K. S. (2012). Kinetics of growth of superhard boride layers during solid state diffusion of boron into titanium. *Ceram. Int.* 38, 6795–6805. doi: 10.1016/j.ceramint.2012.05.077

Silva-Bermudez, P., and Rodil, S. E. (2013). An overview of protein adsorption on metal oxide coatings for biomedical implants. *Surf. Coat. Tech.* 233, 147–158. doi: 10.1016/j.surfcoat.2013.04.028

Spriano, S., Sarath Chandra, V., Cochis, A., Uberti, F., Rimondini, L., Bertone, E., et al. (2017). How do wettability, zeta potential and hydroxylation degree affect the biological response of biomaterials? *Mat. Sci. Eng. C Mater. Biol. Appl.* 74, 542–555. doi: 10.1016/j.msec.2016.12.107

Spriano, S., Verne', E., and Ferraris, S. (2007). *Multifunctional Titanium Surfaces for Bone Integration*. European Patent 2214732.

Tengvall, P. (2001). *Proteins at Titanium Interfaces in Titanium in Medicine.* New York, NY: Springler-Verlag, Berlin Heidelberg.

Voros, J., Wieland, M., Ruiz-Taylor, L., Textor, M., and Brunette, D. M. (2001). *Characterization of Titanium Surfaces in Titanium in Medicine*. New York, NY: Springler-Verlag, Berlin Heidelberg.

Conflict of Interest Statement: The authors declare that the research was conducted in the absence of any commercial or financial relationships that could be construed as a potential conflict of interest.

frontiers in Bioengineering and Biotechnology

ORIGINAL RESEARCH
published: 30 November 2018
doi: 10.3389/fbioe.2018.00187

The Importance of Controlled Mismatch of Biomechanical Compliances of Implantable Scaffolds and Native Tissue for Articular Cartilage Regeneration

Michael Gasik[1,2], Alexandra Zühlke[1], Anne-Marie Haaparanta[3], Virpi Muhonen[4], Kaisa Laine[3], Yevgen Bilotsky[2], Minna Kellomäki[3,5] and Ilkka Kiviranta[4]*

[1] School of Chemical Engineering, Aalto University Foundation, Espoo, Finland, [2] Seqvera Ltd., Helsinki, Finland, [3] BioMediTech and Faculty of Biomedical Sciences and Engineering, Tampere University of Technology, Tampere, Finland, [4] Department of Orthopaedics and Traumatology, University of Helsinki, and Helsinki University Hospital, Helsinki, Finland, [5] BioMediTech and Faculty of Life Sciences and Medicine, University of Tampere, Tampere, Finland

OPEN ACCESS

Edited by:
Pinar Zorlutuna, University of Notre Dame, United States

Reviewed by:
Piergiorgio Gentile, Newcastle University, United Kingdom
Pinar Yilgor Huri, Ankara University, Turkey
Justin Lee Brown, Pennsylvania State University, United States

***Correspondence:**
Michael Gasik
michael.gasik@aalto.fi

Specialty section:
This article was submitted to Biomaterials, a section of the journal Frontiers in Bioengineering and Biotechnology

Received: *16 June 2018*
Accepted: *16 November 2018*
Published: *30 November 2018*

Citation:
Gasik M, Zühlke A, Haaparanta A-M, Muhonen V, Laine K, Bilotsky Y, Kellomäki M and Kiviranta I (2018) The Importance of Controlled Mismatch of Biomechanical Compliances of Implantable Scaffolds and Native Tissue for Articular Cartilage Regeneration. Front. Bioeng. Biotechnol. 6:187. doi: 10.3389/fbioe.2018.00187

Scaffolds for articular cartilage repair have to be optimally biodegradable with simultaneous promotion of hyaline cartilage formation under rather complex biomechanical and physiological conditions. It has been generally accepted that scaffold structure and composition would be the best when it mimics the structure of native cartilage. However, a reparative construct mimicking the mature native tissue in a healing tissue site presents a biological mismatch of reparative stimuli. In this work, we studied a new recombinant human type III collagen-polylactide (rhCol-PLA) scaffolds. The rhCol-PLA scaffolds were assessed for their relative performance in simulated synovial fluids of 1 and 4 mg/mL sodium hyaluronate with application of model-free analysis with Biomaterials Enhanced Simulation Test (BEST). Pure PLA scaffold was used as a control. The BEST results were compared to the results of a prior *in vivo* study with rhCol-PLA. Collectively the data indicated that a successful articular cartilage repair require lower stiffness of the scaffold compared to surrounding cartilage yet matching the strain compliance both in static and dynamic conditions. This ensures an optimal combination of load transfer and effective oscillatory nutrients supply to the cells. The results encourage further development of intelligent scaffold structures for optimal articular cartilage repair rather than simply trying to imitate the respective original tissue.

Keywords: articular cartilage, scaffold, PLA, collagen, biomechanics, testing, synovial fluid

INTRODUCTION

The need to develop tissue substitutes and regeneration platforms is one of the most demanding and challenging applications in modern tissue engineering (Hubbell, 1995; Burdick and Mauck, 2011). Three-dimensional biomaterial structures (scaffolds) are highly desirable matching the biomechanical properties of the tissue (Gomes and Reis, 2004) and closely mimicking *in vivo* behavior [facilitating cell adhesion, growth, and tissue formation (Volfson et al., 2008)]. Such biomaterials assist the body to rebuild the damaged tissue and eventually they minimize associated

pain and healing time (Wong and Bronzino, 2007; Chung and Burdick, 2008). The combined static and dynamic biomechanical properties of these scaffolds are crucial for the final success of the treatment. Any progress in the development of scaffolds should ensure a high correlation between *in vitro* conditions and expected *in vivo* tissue regeneration (Frost, 2004; Wilson et al., 2006; Mollon et al., 2013). The non-toxic biodegradation of the scaffold should gradually transfer the stress to the new growing tissue over an appropriate time period. As pointed out recently (Panadero et al., 2016), the synergetic effect of correct mechanical stimulation is greatly dependent on the scaffolding material, its environment and the cell presence. This shows the needs for consistent simultaneous analysis to compare different biomaterials and to get conclusions about these features.

One of the most challenging applications of biomedical scaffolds is the articular cartilage (AC) repair. The damage and degradation of AC are not only progressing with age, obesity, or systemic diseases, but also in the young and active population due to physical causes, such as injury. If untreated, these defects may progress toward osteoarthritis (OA), affecting over 150 million people worldwide, mainly by degeneration of the hyaline cartilage in synovial joint lacking the ability of self-regeneration (Armstrong and Mow, 1982). Natural wound healing, in full-thickness defects of cartilage, often leads to the formation of fibrocartilage (Armstrong and Mow, 1982; Wilson et al., 2006; Mollon et al., 2013; Panadero et al., 2016), which is functionally and biomechanically inferior to the original hyaline cartilage making the tissue more prone to further deterioration and osteoarthritic changes of the joint. Initiated vicious cycle (Benders et al., 2012) ultimately will call for a total or partial joint replacement. Therefore, chondro-conductive and -inductive biomaterials are highly desirable to treat cartilage lesions at early stages before manifestation of OA.

Clinically used biomaterials include various naturally derived and synthetic materials (von Recum, 1998; Agrawal and Parr JE, 2000). The advantage of natural materials is their intrinsic bioactivity for the purpose, although application of animal-derived materials (xenografts) contains certain risks, such as contamination and undesired immune response. This could be avoided by using bioabsorbable synthetic materials not causing foreign body or hypersensitivity reactions themselves. Synthetic materials can be made biologically more advantageous and biocompatible. On the other hand, compared to the naturally derived materials, synthetic polymers are usually lacking the desired intrinsic biological cues that promote cell adhesion, proliferation and tissue recovery. However, any biomaterial is always challenging to evaluate and optimize for clinical use and for the purpose aiming on "precise medicine" solutions. It is now widely anticipated that the present level to evaluate the mechanical function of biomaterial and tissue engineering constructs is highly insufficient. For example, of 205 analyzed articles on cartilage tissue engineering, mentioning of applied mechanical stimulation, only 29% shows some quantified material properties (Lujan et al., 2011). Correct and detailed biomaterial testing is rather time-consuming and expertise to properly quantify non-elastic material behavior of tissue is also scarce in many dedicated biology labs (Lujan et al., 2011).

Synthetic materials with fibrous origin are often used for AC repair applications. These scaffolds have 75–85% porosity and they are exposed to synovial fluid with sodium hyaluronate (NaHA). Animal studies are needed to ensure the biological functionality of the scaffolds before clinical use. However, the relationship between the natural tissue and the scaffold is challenging to measure. The regulations and the worldwide trends impose more pressure to move from animal models into *in vitro* evaluation (Directive 2010/63/EC for Alternative Methods, 2015). Therefore, in order to develop and optimize biomaterials, one must establish protocols for reliable comparison of different materials before *in vivo* tests can be ethically justified and their results truly extrapolated toward safe and effective human use.

The structure, functions and biomechanical behavior of AC are very complex, highly anisotropic and time- and loading history-dependent (Wilson et al., 2005). The articular cartilage consists of a relatively small number of chondrocytes surrounded by a multi-component matrix, which can be imaged as a composite with 70–85% water and remaining proteoglycans (proteins with glycosaminoglycans attached as a bottlebrush-like structure) and collagen (Hayes, 1972). Proteoglycans and water concentration vary through the depth of the cartilage tissue. Proteoglycans can bind or aggregate to a backbone of sodium hyaluronate (NaHA) of molecular weight of 2–4 MDa to form a macromolecule weighting up to 200 MDa (Kobayashi et al., 1994).

The biomechanics of AC and synovial fluid is also complex and essentially non-linear (Hayes and Mockros, 1971; Hayes and Bodine, 1978). Not some many studies have coherently and systematically analyzed AC properties (Ahsan and Sah, 1999; Korhonen et al., 2006) due to variability of the samples, local inhomogeneity and applied biomechanical methods. Complex loading schemes are associated with significant variations of interstitial fluid pressure and fluid flow, complicating the results interpretation (Ahsan and Sah, 1999). The collagen-rich matrix behavior is highly non-linear and requires rather sophisticated models to be described as a composite material, whether with theories (Mäkelä and Korhonen, 2016). Synovial fluid is well-known to have non-Newtonian viscosity vs. its composition, shear rate, mode of loading and the presence of other factors (King, 1966). Most of the biomechanical properties of AC tissue reported experimentally are obtained with either confined compression (Mow et al., 1980) or indentation (Kempson et al., 1971). These measurements data are commonly approximated with biphasic (Mak et al., 1987) or triphasic (Lai et al., 1991) theories, or even more simplified viscoelastic models. However, due to peculiarities of the AC tissue properties (Lai et al., 1981), it is difficult to compare results published with different studies, using various specimen types, methods and testing devices. It was also reported (Hosseini et al., 2014) that fluid flow and flow-dependent phenomena may dominate the AC behavior in different testing regimes and thus it is impossible to determine in general required recovery time. Aggregate modulus in range of 50–120 kPa was reported for human, bovine and canine tissues by different sources (Hayes and Mockros, 1971; Kempson et al., 1971; Hayes, 1972; Mow et al., 1980; Lai et al., 1981; Armstrong and Mow, 1982; Wilson et al., 2006), but often full test data

were not available to compare these data [indentation usually produces much larger values (Ahsan and Sah, 1999; Korhonen et al., 2006)]. Formal models of AC are missing essential features which limit their practical application only to specimens analyzed in that studies. Therefore, it is a great oversimplification to characterize AC or scaffolds for AC repair by set of one or two numbers without exact data on the test method and data analysis.

In this study we used highly porous PLA mesh manufactured from fine PLA fibers. Even though PLA itself is a stiff material, this studied PLA mesh was optimized to have a relatively soft nature to suit better as cartilage repair matrix. The hypothesis was that a scaffold which is less stiff than surrounding tissue and which is acting in compression under the requirement of strain compliance will have less stress and therefore fluid pressure which would cause fluid to flow into the scaffold to bring more nutrients to chondrocytes. The collagen component was added to the PLA mesh to increase the hydrophilic nature of the scaffolds and to promote cell proliferation (Muhonen et al., 2016; Gasik et al., 2017). Here we report results of this new xeno-free, recombinant human collagen-laden (rhCol) polylactide (PLA) mesh scaffolds (rhCol-PLA) developed for repair of early cartilage lesions to avoid osteoarthritic changes, which have been designed, produced, and biomechanically optimized *in vitro* and *in vivo* validated in equine (unpublished data) and porcine models (Muhonen et al., 2016; Gasik et al., 2017). The rhCol-PLA scaffolds were assessed for their relative performance in simulated synovial fluids for mimicking both human and veterinary conditions with application of model-free analysis with Biomaterials Enhanced Simulation Test (BEST). The results of the scaffold materials selection were also correlated with *in vivo* tests, carried out in a separate study (Haaparanta et al., 2014; Muhonen et al., 2016), where this material combination was found to work better than the previously studied plain PLA scaffolds with stiffer structure (Pulliainen et al., 2007).

MATERIALS AND METHODS

Materials Analyzed

The scaffolds tested were made of synthetic polymer fibers. The polylactide scaffold (PLA) was processed of medical grade poly-(L/D)-lactide PLA96/4 (Corbion Purac, Gorinchem, NED), manufactured to melt spun fibers and afterwards carded and needle punched into meshes (porosity ∼90–93%) in Tampere University of Technology (Tampere, Finland). The used PLA was a highly purified, medical grade polymer (Länsman et al., 2006) with a residual monomer content of <0.5%. The PLA meshes were washed with ethanol, dried, packed and sterilized by gamma irradiation 25 kGy. A part of PLA scaffolds was aseptically doped (Haaparanta et al., 2014) with a recombinant human collagen III (FibroGen, Inc., San Francisco, USA) solution and the structure was freeze-dried (marked as rhCol-PLA). The rhCol-PLA scaffolds were further crosslinked with 14 mM 1-ethyl-3-(3-dimethylaminopropyl)-carbodiimide hydrochloride (EDC) + 6 mM N-hydroxysuccinimide (NHS) (Sigma-Aldrich, Helsinki, Finland) in 95% ethanol, washed and subsequently freeze-dried again. The ratio between the PLA and collagen components in the rhCol-PLA scaffolds was 86/14 vol. % of PLA and collagen, respectively.

All the specimens of PLA and rhCol-PLA scaffolds were cut into rectangular pieces ∼5 × 5 mm (±1 mm) in size with the thickness of the original materials as supplied. The exact size of the specimens was measured with a non-contact method using a laser micrometer (MetraLight, CA, USA) with ±1 μm resolution and the samples were weighted with a balance before and after the test. The measuring and weighing process was repeated three times; on the dry sample, on the immersed sample and on the sample after the measurement. The samples were immersed in distilled water to ensure that the sample was completely wet before inserting to the sample holder as possible trapped air bubbles may alter the test results improperly.

The media-simulated synovial fluid (SSF)—for the tests was prepared as two solutions with different concentrations of sodium hyaluronate (NaHA). Sodium hyaluronate of molecular weight 1.68 MDa (Nutrihyl®, Contipro Biotech, Czech Republic) was dissolved in 200 mL of cold distilled water to mimic "normal" (4 mg/mL) and "osteoarthritic" (1 mg/mL) solutions (Fam et al., 2007).

Experimental Methods

The viscosity of the SSF solutions was determined using SV-10 vibro-viscosimeter (A&D Co. Ltd., JAP) consisted of two vibrating gold plates immersed in the solution. About 45 mL of the SSF solution was poured in a cuvette and heated to 40°C. The cuvette was then placed at the viscometer and the viscosity with temperature was measured simultaneously upon free cooling. Viscosity curves were well-fitted for every composition with the Arrhenius equation.

The biomechanical analysis was carried out using two dynamic mechanical analysis (DMA) 242C and 242E machines (Netzsch Gerätebau GmbH, Germany) with a specially developed biomaterials enhanced simulation test (BEST; Seqvera Ltd., Finland) protocol (Gasik, 2014, 2017a,b), adjusted for simulated cartilage conditions (Hayes and Bodine, 1978; Mow et al., 1980; Lai et al., 1981). The compressive mode sample holder and the specimen were fully immersed in the thermally controlled bath with media (∼30 mL). This resembles the gradients of deformation, pore pressure and fluid flow similar to tibial cartilage conditions as has been shown with other experiments and computer simulations (Korhonen et al, 2002; Milan et al., 2010). Three different protocols were applied for immersion tests: creep ($n = 38$ for PLA and $n = 40$ for rhCol-PLA), frequency scans (0.01–20 Hz) as $n = 38$ for PLA and $n = 28$ for rhCol-PLA, and strain sweeps up to 25–50 μm at 1 Hz) as $n = 20$ for PLA and $n = 30$ for rhCol-PLA.

A preconditioning step was applied (Pioletti and Rakotomanana, 2000) to all specimens by an axial confinement by ∼5 μm of initial deformation (offset), following the 15 min equilibration under a small force of 0.05 N to stabilize the dimensions and temperature. This was found to suppress initial swelling (where present; as explained below) thus all the creep deformation and compliance are originated from zero. At these conditions it was observed that deformation of the porous, fully saturated fibrous structures proceeded without excessive

deformation of the fibers themselves and without substantial decrease in porosity. Whereas, *in vivo* pressures expressed on healthy articular cartilage may reach 1–10 MPa at peak, here the fluid flow is unconfined but the scaffold as AC tissue undergoes deformation similar to one in clinical conditions (Lai et al., 1981, 1991; Milan et al., 2010).

Data Analysis

Experimental data has been converted into biomechanical values and analyzed with an application of idempotent type analysis without use of a material model (Gunawardena, 1996; Pioletti and Rakotomanana, 2000; Litvinov et al., 2001). This gives an advantage over commonly reported moduli functional dependence as it allows extraction of the time-invariant data suitable for future prediction of the material behavior. The data quality reported for the same material might be also confusing, as no exact information is given for conditioning changes, and usually no solid proof shown, e.g., about suitability of the small strain theory or material linearity (Norris, 2008; Lujan et al., 2011). Such conditions are often assumed by default, despite it is of common knowledge that "elastic modulus" cannot be uniquely defined for material which does not follow linear elasticity model.

Idempotent processing, common in computer technology (Gunawardena, 1996) preserves the data structure and original variables without demand of explicit knowledge of their functional dependencies. It obeys causality principle (response always comes after the stimulus applied) and respects the boundaries of thermodynamics (no violation of conservation laws). One essential advantage in testing of biomaterials with this method is in taking into account non-local effects—on the contrary to conventional mathematical analysis, where the derivative of a function is always local. Hence, the predictors can be used in *in silico* simulations to calculate, for example, mechano-regulative index without necessity of explicit local fluid flow determination (Maslov, 1970; Gasik, 2017b).

Stress was calculated as Piola–Kirchhoff stress, from the ratio of acting force to the original surface area A_0 of the specimen, $\sigma = F/A_0$. The strain was calculated as Lagrange (true logarithmic) strain, related to the initial thickness H_0 at the beginning of the creep: $\varepsilon(t) = ln(1 + \Delta L(t)/H_0)$, where $\Delta L(t)$ is the observed change in the specimen thickness with experiment time t. Whereas, other strain definitions can be also used, this one has a rigorous thermodynamic rationale (Xiao, 1995; Lubarda and Chen, 2008). The ratio of the strain $\varepsilon(t)$, to constant stress, σ_0, is the creep compliance $C(t) = \varepsilon(t)/\sigma_0$, which is the main readout from the creep experiments. For dynamic loading, the strain amplitude is from a harmonic signal waveform extreme, taking into account load history:

$$\varepsilon_\omega(t) = \frac{1}{2}\ln\left(\frac{H_0 + \Delta L(t) + a_0}{H_0 + \Delta L(t) - a_0}\right) \quad (1)$$

where a_0 is the applied deformation amplitude at some instant frequency ω. In this format, the irreversible creep or similar deformation is taken into account for long experiment times (t). All experiments were preformed in triplicate and for every frequency or strain test 10 cycles were used within every run. Hence for time dependencies one should consider both long time (real time of the test—minutes and hours) and short time (time span within one or few dynamic cycles—seconds).

Test readouts from DMA experiments have been processed with model-free idempotent methods (Gasik and Bilotsky, 2018). In general, there is no explicit mathematical formula written as the calculation is iteratively progressing for every data point collected. This allows inclusion of specimen history without a need of assumption of time kernels (hereditary integrals). In this work the approach was used to find for instance aggregate modulus, material memory, static and dynamic permeability.

RESULTS

Materials Preparation and Preliminary Analysis

The viscosity of SSF compositions was approximated as function of temperature with Arrhenius equation, leading to $8.14 \cdot 10^{-4} \cdot \exp(3022.2/T)$ and $1.746 \cdot \exp(1143/T)$ in mPa·s, for 1 and 4 mg/mL NaHA, respectively (correlation $r^2 = 0.9869$–0.9953). At 25°C this gives 20.5 and 80.9 mPa·s values for these SSF (for comparison, water viscosity is 0.89 mPa·s). The exact values are not explicitly required because the DMA device and sample holder dynamics have been recalibrated for every type of SSF, and thus media viscosity changes have been automatically included in the test data.

At the beginning of the tests it was discovered that PLA materials exhibit very high swelling ratios even if they were completely soaked in liquid before the tests. This is usually faced in hydrophobic materials at free swelling due to repulsive forces and pressure variations (Bennethum and Weinstein, 2004). It was formulated (Bennethum and Cushman, 1996) that the macroscopic solid stress tensor (related to visible bulk swelling) is combined of a thermodynamic solid pressure, a solid stress tensor, a stress due to the interaction of the solid and liquid phases, and a stress due to the interaction of the interface with the solid phase as well as kinetic component of constituents. By changing the conditioning pressure, it was found that the force of ∼50 mN (equivalent to applied ∼1 kPa stress) is required to suppress the swelling but not to cause pre-compression of the sample, **Figure 1**. This conditioning pressure was used in all these experiments to get consistent results.

Pseudo-Static Experiments

The results of one set of creep measurements at 0.2 N (∼4 kPa applied stress) are shown in **Figure 2**. The level of applied stress of 4 kPa (∼30 mmHg) was considered to be a limit which does not cause cartilage-adjacent soft tissues necrosis (Goode and Shinn, 1977). The nature of a creep test is pseudo-static (change of strain in time at constant applied stress) and it is often used to evaluate viscoelastic nature of materials and to approximate it with some models (Bilotsky and Gasik, 2015). Here one may see that addition of NaHA to media does not affect compliance of PLA much, but has a great effect on rhCol-PLA. It is notable that compliance of rhCol-PLA in 1 mg/mL SSF is the highest, and in 4 mg/mL is average between 1 mg/mL and water (0

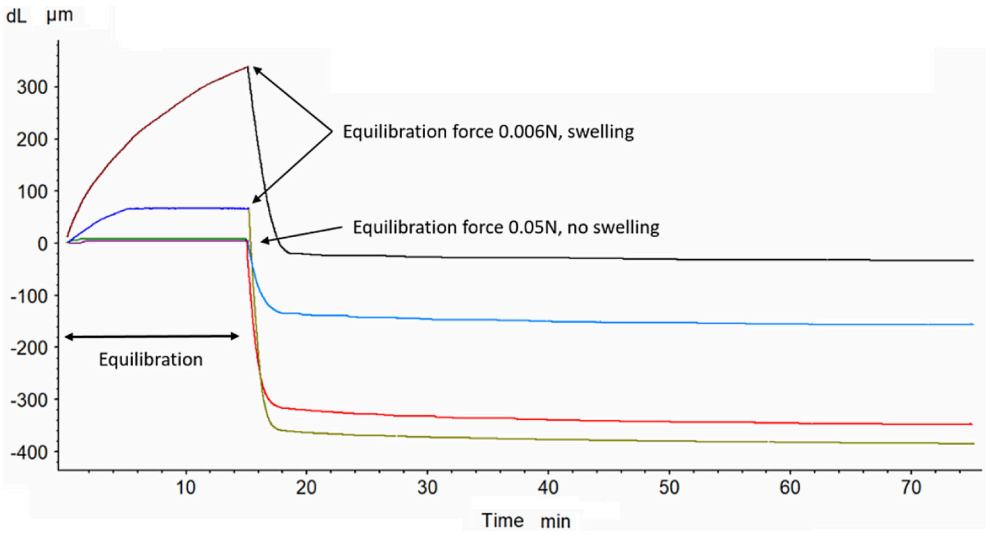

FIGURE 1 | The effect of conditioning force (0.006 and 0.05 N) on swelling and compaction (at 0.2 N) of PLA scaffold (two experimental curves for either forces combination).

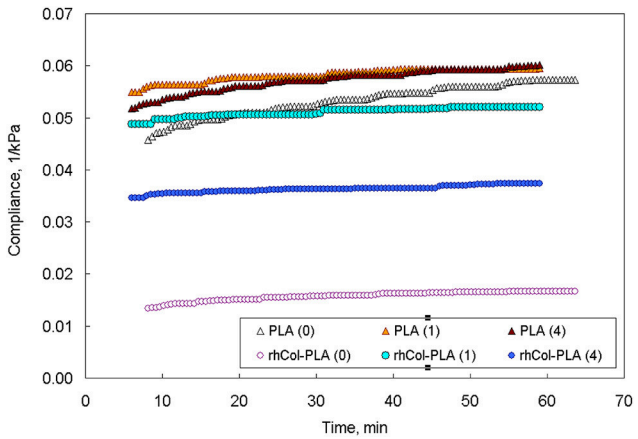

FIGURE 2 | Creep compliance at 0.2 N for P LA and rhCol-PLA in different media (numbers in parentheses show NaHA concentration in SSF, mg/mL).

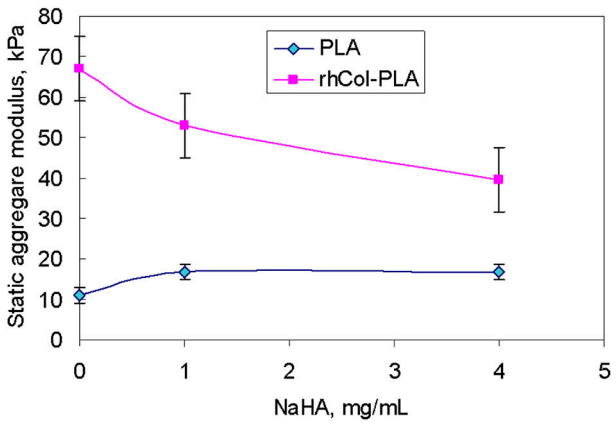

FIGURE 3 | Static aggregate modulus (kPa) of the scaffolds vs. NaHA concentration in SSF. Bars here and further indicate standard error unless stated otherwise.

mg/mL NaHA). The higher is the compliance, the more easily the material deforms under constant load. Hence an observation can be drawn that addition of cross-linked collagen to PLA makes it "stiffer" when tested in water but makes little difference when testing in 1 mg/mL SSF.

The comparison of the data from pseudo-static (creep) analysis (**Figure 3**) shows that stiffness of the rhCol-PLA scaffolds is increased by several times when compared to PLA, and this effect is independent on the type of SSF used. Also rhCol-PLA material in static conditions has lower permeability (**Figure 4**), which in combination supports a vision that synovial fluid will likely be kept in rhCol-PLA better than in PLA—at the same loading, within the same time span PLA will lose fluid to a greater extent.

Frequency Experiments

Behavior of materials under constant deformation but varied frequency is different from pseudo-static one. These differences in the case of fibrous porous materials are due: (1) oscillating mobility of fluid within a fibrous structure, (2) inertia effects associated with hysteresis between incoming and outgoing fluid flow, and (3) non-linearity in fluid viscous properties and possible non-linearity in coupled deformation of the fibrous skeleton of the scaffold.

One of the experimental criteria to observe the differences is the loss tangent [tan(δ)], which is defined as the ratio of imaginary to real part of elastic moduli or stiffness. Higher loss tangent of rhCol-PLA vs. PLA (**Figure 5**) was observed for all frequencies. **Figure 6** shows a 3D plot of these dependencies of

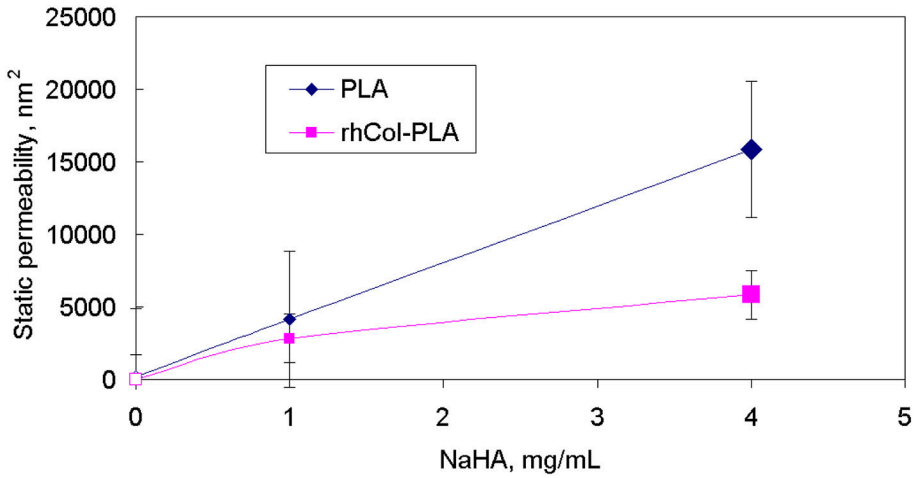

FIGURE 4 | Static (creep) permeability of scaffolds vs. NaHA concentration in SSF, indicating that static permeability increases at higher NaHA concentration.

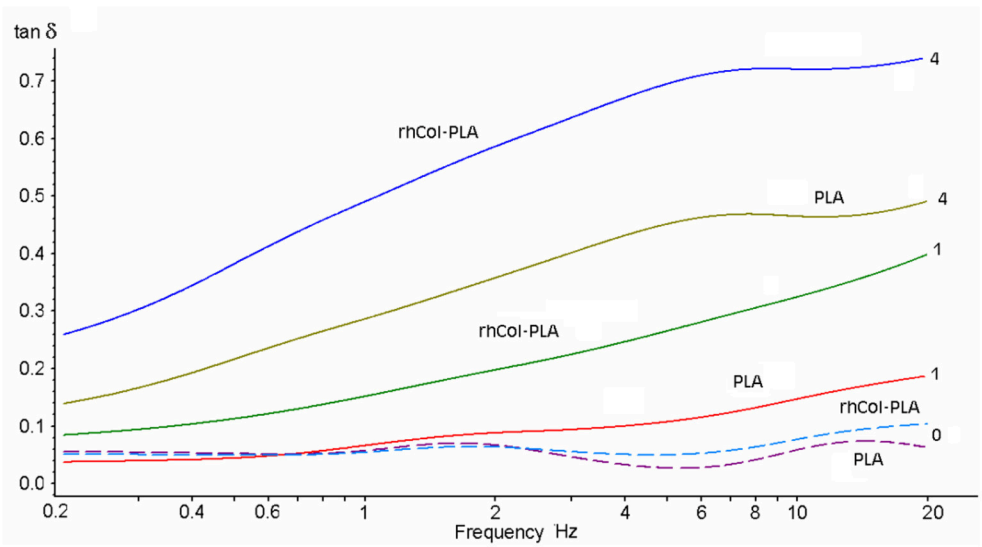

FIGURE 5 | Loss tangent of the scaffolds in different SSF (NaHA concentration as numbers, mg/mL) vs. frequency at 25 μm deformation amplitude.

tan(δ) vs. applied frequency at 25 μm deformation amplitude along with experiment time (note the tangent is practically constant with the time and depends essentially on frequency only).

It is seen that addition of NaHA to the media and respective increase in viscosity also leads to increase in the loss tangent (the more, the higher is the NaHA concentration). For rhCol-PLA loss tangent is roughly 2–3 times higher than for PLA in all SSF (**Figure 6**). This indicates more active interaction of fluid flow with rhCol-PLA than PLA and is likely associated with a finest collagen fibrils network between the PLA-based fibers in rhCol-PLA (Länsman et al., 2006; Muhonen et al., 2016; Gasik et al., 2017). Notable is that this interaction is only due to presence of NaHA, as such differences are not seen when only water is used (**Figure 6**).

Strain Sweep Experiments

One of the more physiologically relevant dynamic conditions is application of variable deformation under constant frequency. This can be depicted as change of the gait loads keeping normal walking conditions (∼1 Hz) (Hayes and Mockros, 1971; Hayes, 1972; Mow et al., 1980; Armstrong and Mow, 1982). Thus, the last test sequence was applied to simulate changes in properties of scaffolds up to 50 μm of dynamic deformation with repeating of the load cycles. At constant frequency, loss tangent is not

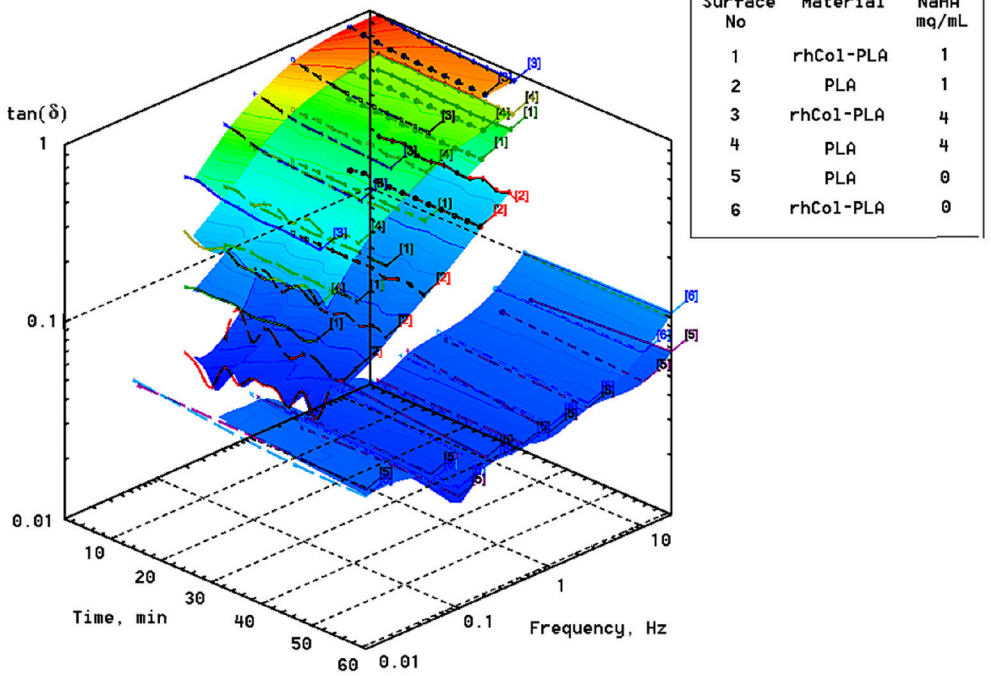

FIGURE 6 | Loss factor [tan(δ)] of scaffolds in different SSF vs. applied frequency at 25 μm displacement amplitude. Note plots for water (0 mg/mL NaHA; surfaces No. 5 and 6) are shifted ahead of time scale to improve visual readability of the plots.

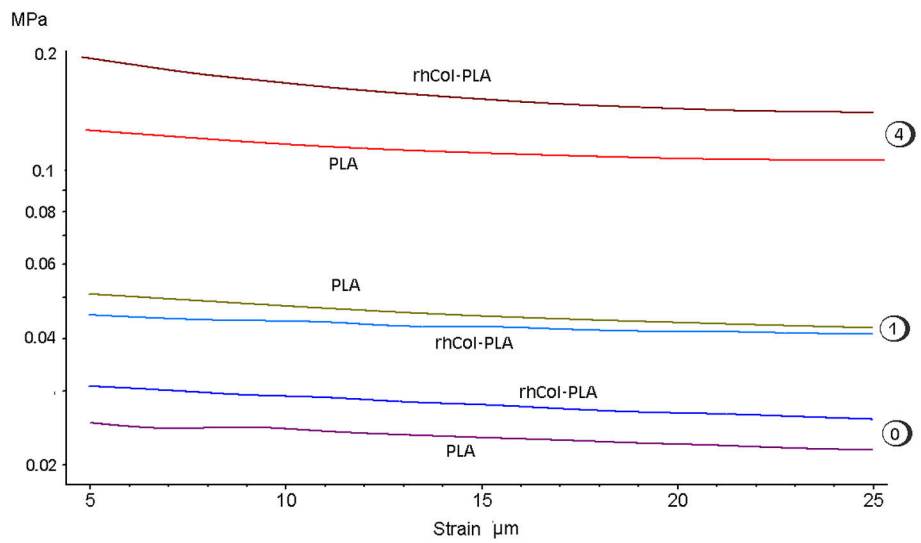

FIGURE 7 | Average dynamic modulus of scaffolds at 1 Hz vs. applied deformation ad different SSF (numbers indicating NaHA concentration, mg/mL). Note log scale for modulus.

significantly deformation- or stress-dependent so here major performance comes from dynamic stiffness and fluid exchange.

The absolute value of average dynamic elastic modulus at 1 Hz is shown in **Figure 7** as directly obtained from the DMA signal. It is seen that this modulus slightly decreases with deformation. However, with increased number of loading cycles and true strain variations due to changes in geometry, true (corrected) elastic modulus slightly increases. Also, higher NaHA concentration shows higher stiffness of all materials but it is noteworthy this stiffness incorporated fluid movement under dynamic load and therefore unavoidably includes some viscous and inertia contribution, as shown about for loss tangent (**Figures 5**, **6**).

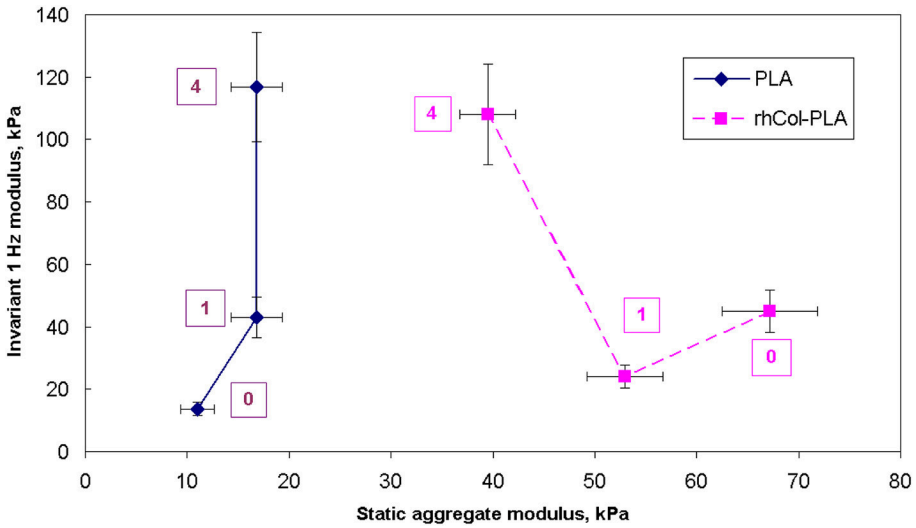

FIGURE 8 | Comparison of static aggregate modulus (**Figure 3**) with invariant dynamic modulus at 1 Hz. Numbers indicate concentration of NaHA in SSF, mg/mL.

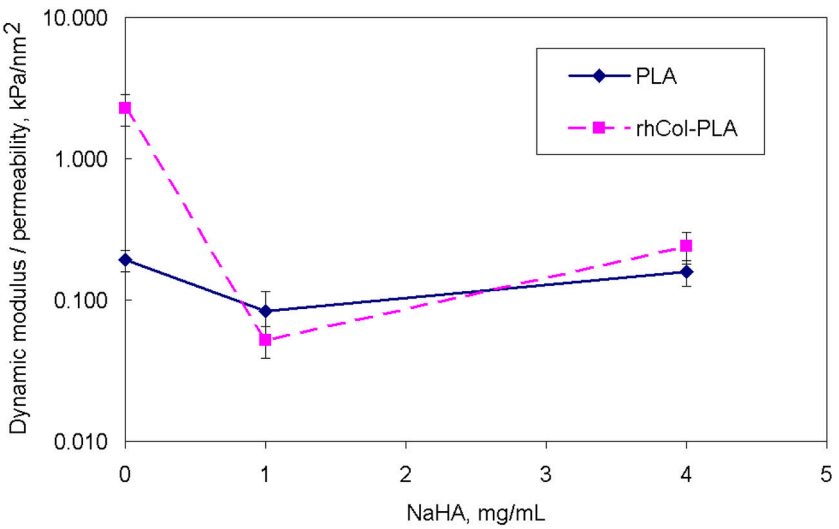

FIGURE 9 | Comparison of ratio of dynamic invariant modulus to dynamic permeability vs. NaHA concentration (note log scale).

Analyzed invariant modulus at 1 Hz is shown in **Figure 8** vs. respective static aggregate modulus (**Figure 3**) for respective NaHA concentration. The ratio of dynamic modulus to dynamic permeability is shown in **Figure 9** for 1 Hz condition. Here rhCol-PLA is at least similar or better (at 1 mg/mL NaHA) than PLA scaffolds.

DISCUSSION

The two studied scaffolds contained the same kind of PLA mesh structures. The PLA scaffolds were studied as such and in the rhCol-PLA scaffolds the collagen component was added into the structure to give the highly porous PLA scaffold increased hydrophilic nature and to promote cell proliferation. From the post-processing of the experimental data, many additional values have been obtained without assumption of a material model (a proprietary patent-pending method). Here data for aggregate modulus (in static and dynamics) and permeability are shown as an example.

The relevancy of static conditions results for clinical conditions is that rhCol-PLA scaffolds are better supportive for weight-bearing and undergo smaller deformation than pure PLA. In combination of lower permeability this suggests synovial fluid to stay likely rhCol-PLA more than in PLA, whereas the latter will lose more fluid at the same loading. As a simple decision-aiding criterion, one might consider the ratio of aggregate modulus to

permeability: the higher it is, the better the scaffold withstands static loads. **Figure 10** shows that in this respect rhCol-PLA material is by 1–2 orders of magnitude superior to PLA at all tested SSF compositions.

At dynamic conditions, such as walking, the situation reverses: under dynamic loading one has to aim on more active fluid exchange to provide biomechanical stimulus to chondrocytes, to ensure fluid and nutrients supply and removal of metabolic products, promoting tissue regeneration (Gerisch and Chaplain, 2006; Sittichokechaiwut et al., 2010). Cartilage tissue is avascular and its extracellular matrix creates further barriers for nutrient/waste exchange by diffusion. Thus, lower dynamic modulus (**Figure 8**) and better fluid diffusivities are desired. These features have to be, however, compatible to the above requirements for static conditions as cartilage must work well in both these extremes.

The viscosities of SSF are substantially higher than water: about 20 and 100 times for 1 and 4 mg/mL, respectively. This means that even small changes in permeability, i.e., a feature of the material structure, will affect changes in permittivity, a feature of a specific fluid flow thought the material structure. High loss tangent (**Figures 5**, **6**) means more dissipation of applied mechanical energy (inelastic losses) which is important to keep high damping properties of articular cartilage (Mow et al., 1980; Lai et al., 1981; Armstrong and Mow, 1982). Therefore, rhCol-PLA is superior to PLA also in this property, whether for "arthritic" (1 mg/mL NaHA) or "normal" (4 mg/mL NaHA) synovial fluids.

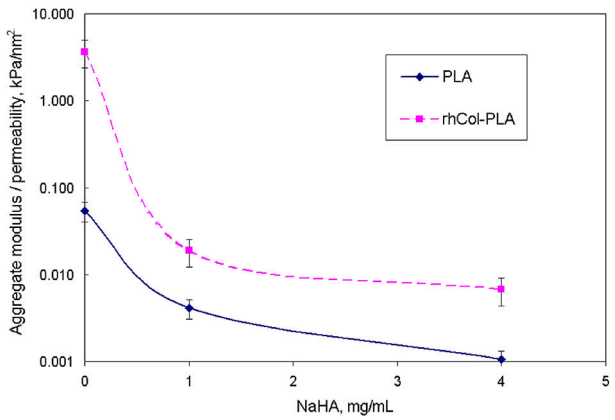

FIGURE 10 | Comparison of ratio of static aggregate modulus (**Figure 3**) to permeability (**Figure 4**) vs. NaHA concentration (note log scale).

A proof-of-concept animal study was performed in domestic pigs (*Sus scrofa domestica*, 4-months-old, $n = 20$) in a separate study, reported elsewhere (Muhonen et al., 2016). Briefly, the animals were randomized into three groups: (1) rhCol-PLA scaffold treatment, (2) commercial scaffold treatment and (3) spontaneous repair. A circular full-thickness chondral lesion with a diameter of 8 mm was created in the right medial femoral condyle. The removed cartilage tissue was collected and further processed for chondrocyte isolation and subsequent proliferation. After 3 weeks, the lesion was approached again, cleaned and repaired with one of the constructs, i.e., rhCol-PLA or commercial scaffold with chondrocytes, or left untreated. Only one lesion per animal was performed and the animals were allowed free weight-bearing and unrestricted movement after the operations. The repair tissue was evaluated after 4 months. Hyaline cartilage was reported to be formed most frequently in the rhCol-PLA treatment group. Here the analysis of the cartilage repair scores (Haaparanta et al., 2014; Muhonen et al., 2016) was additionally performed using BUGS—Bayesian inference Using Gibbs Sampling (US FDA, 2010), a form of a Markov Chain Monte Carlo sampling. The results of using normal or Poisson distributions of the total normalized ICRS (International Cartilage Repair Society) scores show rhCol-PLA having statistically significant higher average score (0.515) vs. 0.38 for commercial scaffold and 0.288 for spontaneous healing control group (Muhonen et al., 2016).

A schematic of the advantage of lower dynamic stiffness scaffold for AC repair is depicted in **Figure 11.** There a scaffold implanted into a cartilage defect should exhibit the same strain compliance (no tears, twisting or buckling). For the same strain, material with a higher apparent stiffness will generate more internal stresses and hence higher fluid pressure (Hayes, 1972; Mow et al., 1980; Lai et al., 1991). This will lead to preferential fluid movement out of cartilage which will not allow cells and tissue regeneration ("dry-out"). For an opposite, lower

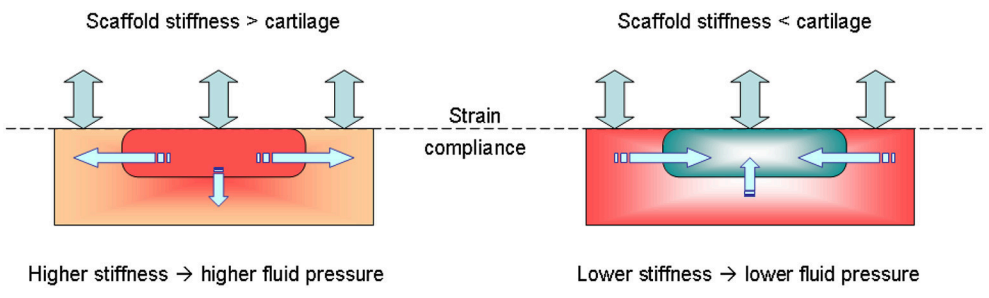

FIGURE 11 | Possible mechanism of beneficial compliance mismatch of scaffolds vs. native tissue when submitted to a mechanical load: when a scaffold with fluid is too stiff, higher generated fluid pressure leads to fluid flow out of scaffold (**left**), whereas for the same deformation conditions of lower stiffness system **(right)** fluid is driven into the scaffold.

apparent stiffness (material system with fluid) will have lower fluid pressure which will promote external fluid supply into the scaffold (Bilotsky and Gasik, 2015; Gasik, 2017b; Gasik et al., 2017). The exact values depend on the tissue and scaffold systems differences, fluid properties and loading conditions. Here it is important to note that static and dynamic properties need to be evaluated coherently in a single test to ensure that fluid flow and mechanical compliances are measured linked under proper boundary conditions, and not evaluated separately.

CONCLUSIONS

The results of biomechanical comparison of rhCol-PLA and PLA scaffolds for articular cartilage repair show how both collagen addition and media composition (NaHA concentration) change elastic, viscoelastic and inelastic properties of the scaffolds. Using model-free idempotent analysis methods, it was for the first time possible to extract data on scaffold permeability and invariant moduli in a coherent way, without use of separate experiments. These values make easier design, *in silico* simulation and optimization of such materials.

It might be expressed that for a successful tissue regeneration with scaffolds the properties of the scaffold should not be too close to expected tissue properties, as in this case there will be less stimuli acting on the scaffold for repair. Furthermore, one should consider static and dynamic behavior of the material in the physiologically relevant conditions—the material matching both simultaneously will be the best option to implant.

The studies performed for articular cartilage repair materials could be extended to other cartilage tissues repair implants, as most of these tissues are also subjected to different static and dynamic loading, tightly coupled with fluid supply and exchange as well as interaction with body systems (intervertebral disk, cartilageous end plate, larynx, etc.). Proper test conditions and data processing can assist the development of better scaffolds for cartilage repair.

AUTHOR CONTRIBUTIONS

The manuscript has been written and composed by MG and AZ, with the assistance of all other authors. Materials preparation and description were done by A-MH and KL under guidance of MK. Medical relevance has been analyzed by IK and VM, and data from parallel animal studies were obtained and processed by VM. Advanced data processing was performed by YB based on experiments made by AZ. All authors have reviewed the manuscript.

FUNDING

The funding support for biomaterials processing and experimental testing provided by Finnish Agency of Innovation (Tekes) is acknowledged (Grants No. 40190/13, 40113/13, 40171/14, and 40172/14). The part of studies related to experimental data analysis has been also partially supported by funding from the European Union's Horizon 2020 research and innovation programme under grant agreement No. 760921 PANBioRA.

ACKNOWLEDGMENTS

MG and AZ would like to express thanks to M.Sc. Ines Hiropoulos (Synoste Ltd.) for making extensive preliminary experiments with PLA in water.

REFERENCES

Agrawal, C. M., Parr, J. E., and Lin, S. T. (2000). *Synthetic Biodegradable Polymers for Implants*. West Conshohocken, PA: ASTM STP1936.

Ahsan, T., and Sah, R. L. (1999). Biomechanics of integrative cartilage repair. *Osteoarthr. Cartil.* 7, 29–40. doi: 10.1053/joca.1998.0160

Armstrong, C. G., and Mow, V. C. (1982). Variations in the intrinsic mechanical properties of human articular cartilage with age, degeneration, and water content. *J. Bone Joint Surg.* 64, 88–94. doi: 10.2106/00004623-198264010-00013

Benders, K. E., van Weeren, P. R., Badylak, S. F., Saris, D. B., Dhert, W. J., and Malda, J. (2012). Extracellular matrix scaffolds for cartilage and bone regeneration. *Trends Biotechnol.* 31, 169–176. doi: 10.1016/j.tibtech.2012.12.004

Bennethum, L. S., and Cushman, J. H. (1996). Multiscale, hybrid mixture theory for swelling systems–II: constitutive theory. *Int. J. Eng. Sci.* 34, 147–169.

Bennethum, L. S., and Weinstein, T. (2004). Three pressures in porous media. *Transp. Porous Media* 54, 1–34. doi: 10.1023/A:1025701922798

Bilotsky, Y., and Gasik, M. (2015). Modelling of poro-visco-elastic biological systems. *J. Phys. Conf. Series* 633:021234. doi: 10.1088/1742-6596/633/1/012134

Burdick, J. A., and Mauck, R. L. (2011). *Biomaterials for Tissue Engineering Applications: A Review of the Past and Future Trends*. New York, NY: Springer, 564. doi: 10.1007/978-3-7091-0385-2

Chung, C., and Burdick, J. A. (2008). Engineering cartilage tissue. *Adv. Drug Deliv. Rev.* 60, 243–262. doi: 10.1016/j.addr.2007.08.027

Directive 2010/63/EC for Alternative Methods (2015). *Directive 2010/63/EC for Alternative Methods "3R" = Replacement, Reduction, Refinement, Complemented With 'Stop Vivisection' The European Citizens'*. Initiative submitted to the European Commission (C(2015)3773 final).

Fam, H., Bryant, J. T., and Kontopoulou, M. (2007). Rheological properties of synovial fluids. *Biorheology* 44, 59–74.

Frost, H. M. (2004). A 2003 update of bone physiology and Wolff's law for clinicians. *Angle Orthodont.* 74, 3–15. doi: 10.1043/0003-3219(2004)074<0003:AUOBPA>2.0.CO;2

Gasik, M. (2014). New BEST – biomaterials enhanced simulation test. *J. Tissue Sci. Eng.* 5:66. doi: 10.4172/2157-7552.S1.014

Gasik, M. (2017a). *In vitro Test Method for Implant Materials.* Patent US 9683267B2.

Gasik, M. (2017b). Understanding biomaterial-tissue interface quality: combined *in vitro* evaluation. *Sci. Techn. Adv. Mater.* 18, 550–562. doi: 10.1080/14686996.2017.1348872

Gasik, M., and Bilotsky, Y. (2018). High-output screening and biomechanical optimization of biomaterials for orthopaedic applications. *Orthopaed. Proc.* 100B:S44S3.

Gasik, M., Hiropoulos, I., Zühlke, A., Muhonen, V., Haaparanta, A.-M., Laine, K., et al. (2017). Biomechanical comparison for commercial and novel scaffolds for articular cartilage repair. *Orthopaed. Proc.* 99B(Suppl. 1), 79.

Gerisch, A., and Chaplain, M. A. J. (2006). Robust numerical methods for taxis-diffusion-reaction systems: applications to biomedical problems. *Mathem. Comput. Model.* 43, 49–75. doi: 10.1016/j.mcm.2004.05.016

Gomes, M. E., and Reis, R. L. (2004). Biodegradable polymers and composites in biomedical applications: from catgut to tissue engineering. *Intern. Mater. Rev.* 49, 261–273. doi: 10.1179/095066004225021918

Goode, R. L., and Shinn, J. B. (1977). Long-term stenting in the treatment of subglottic stenosis. *Ann. Otol. Rhinol. Laryngol.* 86(6 Pt 1), 795–8.

Gunawardena, J. (1996). *An Introduction to Idempotency*. Bristol, UK: HP Laboratories Bristol, Publication HPL-BRIMS-96-24. p. 50.

Haaparanta, A. M., Järvinen, E., Cengiz, I. F., Ellä, V., Kokkonen, H. T., Kiviranta, I., et al. (2014). Preparation and characterization of collagen/PLA, chitosan/PLA, and collagen/chitosan/PLA hybrid scaffolds for cartilage tissue engineering. *J. Mater. Sci. Mater. Med.* 25, 1129–1136. doi: 10.1007/s10856-013-5129-5

Hayes, W. (1972). Some viscoelastic properties of human articular cartilage. *Acta Orthop. Belg.* 38, 23–31.

Hayes, W. C., and Bodine, A. J. (1978). Flow-independent viscoelastic properties of articular cartilage matrix. *J. Biomech.* 11, 407–419. doi: 10.1016/0021-9290(78)90075-1

Hayes, W. C., and Mockros, L. F. (1971). Viscoelastic properties of human articular cartilage. *J. Appl. Physiol.* 31, 562–568. doi: 10.1152/jappl.1971.31.4.562

Hosseini, S. M., Wilson, W., Ito, K., and van Donkelaar, C. C. (2014). How preconditioning affects the measurement of poro-viscoelastic mechanical properties in biological tissues. *Biomech. Model. Mechanobiol.* 13, 503–513. doi: 10.1007/s10237-013-0511-2

Hubbell, J. A. (1995). Biomaterials in tissue engineering. *Nat. Biotechnol.* 13, 565–576. doi: 10.1038/nbt0695-565

Kempson, G. E., Freeman, M. A., and Swanson, S. A. (1971). The determination of a creep modulus for articular cartilage from indentation tests of the human femoral head. *J. Biomech.* 4, 239–250. doi: 10.1016/0021-9290(71)90030-3

King, R. G. (1966). A rheological measurement of three synovial fluids. *Rheol Acta* 5, 41–44. doi: 10.1007/BF01973577

Kobayashi, Y., Okamoto, A., and Nishinari, K. (1994). Viscoelasticity of hyaluronic acid with different molecular weights. *Biorheology* 31, 235–244. doi: 10.3233/BIR-1994-31302

Korhonen, R. K., Julkunen, P., Rieppo, J., Lappalainen, R., Konttinen, Y. T., and Jurvelin, J. S. (2006). Collagen network of articular cartilage modulates fluid flow and mechanical stresses in chondrocyte. *Biomech. Model. Mechanobiol.* 5, 150–159. doi: 10.1007/s10237-006-0021-6

Korhonen, R. K., Laasanen, M. S., Töyräs, J., Rieppo, J., Hirvonen, J., Helminen, H. J., et al., (2002). Comparison of the equilibrium response of articular cartilage in unconfined compression, confined compression and indentation. *J. Biomech.* 35, 903–909. doi: 10.1016/S0021-9290(02)00052-0

Lai, W. M., Hou, J. S., and Mow, V. C. (1991). A triphasic theory for the swelling and deformation behaviors of articular cartilage. *J. Biomech. Eng.* 113, 245–258. doi: 10.1115/1.2894880

Lai, W. M., Mow, V. C., and Roth, V. (1981). Effects of nonlinear strain-dependent permeability and rate of compression on the stress behavior of articular cartilage. *J. Biomech. Eng.* 103, 61–66. doi: 10.1115/1.3138261

Länsman, S., Pääkkö, P., Ryhänen, J., Kellomäki, M., Waris, E., Törmälä, P., et al. (2006). Poly-L/D-lactide (PLDLA) 96/4 fibrous implants: histological evaluation in the subcutis of experimental design. *J. Craniofac. Surg.* 17, 1121–1128. doi: 10.1097/01.scs.0000231627.33382.85

Litvinov, G. L., Maslov, V. P., and Shpiz, G. B. H. (2001). Idempotent functional analysis: an algebraic approac. *Mathem. Notes* 69, 696–729. doi: 10.1023/A:1010266012029

Lubarda, V. A., and Chen, M. C. (2008). On the elastic moduli and compliances of transversely isotropic and orthotropic materials. *J. Mech. Mater. Struct.* 3, 153–171. doi: 10.2140/jomms.2008.3.153

Lujan, T. J., Wirtz, K. M., Bahney, C. S., Madey, S. M., Johnstone, B., and Bottlang, M. (2011). A novel bioreactor for the dynamic stimulation and mechanical evaluation of multiple tissue-engineered constructs. *Tissue Eng. C* 17, 367–374. doi: 10.1089/ten.tec.2010.0381

Mak, A. F., Lai, W. M., and Mow, V. C. (1987). Biphasic indentation of articular cartilage—I. Theoretical analysis. *J. Biomech.* 20, 703–714. doi: 10.1016/0021-9290(87)90036-4

Mäkelä, J. T. A., and Korhonen, R. K. (2016). Highly non-linear stress-relaxation response of articular cartilage in indentation: importance of collagen nonlinearity. *J. Biomech.* 49, 1734–1741. doi: 10.1016/j.jbiomech.2016.04.00

Maslov, V. P. (1970). The characteristics of pseudo-differential operators and difference schemes. *Actes Congrès. Intern. Math.* 2, 755–769.

Milan, J. L., Planell, J. A., and Lacroix, D. (2010). Simulation of bone tissue formation within a porous scaffold under dynamic compression. *Biomech. Model. Mechanobiol.* 9, 583–596. doi: 10.1007/s10237-010-0199-5

Mollon, B., Kandel, R., Chahal, J., and Theodoropoulos, J. (2013). The clinical status of cartilage tissue regeneration in humans. *Osteoarthr. Cartil.* 21, 1824–1833. doi: 10.1016/j.joca.2013.08.024

Mow, V. C., Kuei, S. C., Lai, W. M., and Armstrong, C. G. (1980). Biphasic creep and stress relaxation of articular cartilage in compression: theory and experiments. *J. Biomech. Eng.* 102, 73–84. doi: 10.1115/1.3138202

Muhonen, V., Salonius, E., Haaparanta, A. M., Järvinen, E., Paatela, T., Meller, A., et al. (2016). Articular cartilage repair with recombinant human type II collagen/polylactide scaffold in a preliminary porcine study. *J. Orthopaed. Res.* 34, 745–753. doi: 10.1002/jor.23099

Norris, A. (2008). Eulerian conjugate stress and strain. *J. Mech. Mater. Struct.* 3, 243–260. doi: 10.2140/jomms.2008.3.243

Panadero, J. A., Lanceros-Mendez, S., and Gomez Ribelles, J. L. (2016). Differentiation of mesenchymal stem cells for cartilage tissue engineering: individual and synergetic effects of three-dimensional environment and mechanical loading. *Acta Biomater.* 33, 1–12. doi: 10.1016/j.actbio.2016.01.037

Pioletti, D. P., and Rakotomanana, L. R. (2000). Non-linear viscoelastic laws for soft biological tissues. *Eur. J. Mech. A Solids* 19, 749–759. doi: 10.1016/S0997-7538(00)00202-3

Pulliainen, O., Vasara, A. I., Hyttinen, M. M., Tiitu, V., Valonen, P., Kellomäki, M., et al. (2007). Poly-L-D-lactic acid scaffold in the repair of porcine knee cartilage lesions. *Tissue Eng.* 13, 1347–1355. doi: 10.1089/ten.2006.0347

Sittichokechaiwut, A., Edwards, J. H., Scutt, A. M., and Reilly, G. C. (2010). Short bouts of mechanical loading are as effective as dexamethasone at inducing matrix production by human bone marrow mesenchymal stem cells. *Eur. Cells Mater.* 20, 45–57. doi: 10.22203/eCM.v020a05

US FDA (2010). *Guidance for the Use of Bayesian Statistics in Medical Device Clinical Trials*. Guidance for industry and FDA staff. US FDA Docket No.2006D-0191, 50.

Volfson, D., Cookson, S., Hasty, J., and Tsimring, L. S. (2008). Biomechanical ordering of dense cell populations. *PNAS* 105, 15346–15351. doi: 10.1073/pnas.0706805105

von Recum, A. (1998). *Handbook of Biomaterials Evaluation, ed.* (New York, NY: Taylor-Francis), 916.

Wilson, W., Huyghe, J. M., and van Donkelaar, C. C. (2006). A composition-based cartilage model for the assessment of compositional changes during cartilage damage and adaptation. *Osteoarthr. Cartil.* 14, 554–560. doi: 10.1016/j.joca.2005.12.006

Wilson, W., van Donkelaar, C. C., and Huyghe, J. M. (2005). A comparison between mechano-electrochemical and biphasic swelling theories for soft hydrated tissues. *J. Biomech. Eng. Trans. ASME* 127, 158–165. doi: 10.1115/1.1835361

Wong, J. Y., and Bronzino, J. D. (2007). *Biomaterials* (Boca Raton, FL: CRC Press; Taylor & Francis), 296. doi: 10.1201/9780849378898

Xiao, H. (1995). Invariant characteristic representations for classical and micropolar anisotropic elasticity tensors. *J. Elasticity* 40, 239–265.

Conflict of Interest Statement: MG is a shareholder of company Seqvera Ltd.

The remaining authors declare that the research was conducted in the absence of any commercial or financial relationships that could be construed as a potential conflict of interest.

Advantages of publishing in Frontiers

OPEN ACCESS
Articles are free to read for greatest visibility and readership

FAST PUBLICATION
Around 90 days from submission to decision

HIGH QUALITY PEER-REVIEW
Rigorous, collaborative, and constructive peer-review

TRANSPARENT PEER-REVIEW
Editors and reviewers acknowledged by name on published articles

Frontiers
Avenue du Tribunal-Fédéral 34
1005 Lausanne | Switzerland

Visit us: www.frontiersin.org
Contact us: info@frontiersin.org | +41 21 510 17 00

REPRODUCIBILITY OF RESEARCH
Support open data and methods to enhance research reproducibility

DIGITAL PUBLISHING
Articles designed for optimal readership across devices

FOLLOW US
@frontiersin

IMPACT METRICS
Advanced article metrics track visibility across digital media

EXTENSIVE PROMOTION
Marketing and promotion of impactful research

LOOP RESEARCH NETWORK
Our network increases your article's readership